ONTOGENY, DISPARITY, AND FUNCTION OF THE ENIGMATIC CASQUES OF CASSOWARIES (*CASUARIUS*): A CASE STUDY OF CRANIAL ORNAMENTATION IN ARCHOSAURS

By

TODD LANDON GREEN

Bachelor of Science in Biology; Zoology
Colorado State University
Fort Collins, Colorado
2008

Master of Science in Zoology
Colorado State University
Fort Collins, Colorado
2012

Submitted to the Faculty of the
Graduate College of the
Oklahoma State University
in partial fulfillment of
the requirements for
the Degree of
DOCTOR OF PHILOSOPHY
December, 2020

ONTOGENY, DISPARITY, AND FUNCTION OF THE ENIGMATIC CASQUES OF CASSOWARIES (*CASUARIUS*): A CASE STUDY OF CRANIAL ORNAMENTATION IN ARCHOSAURS

Dissertation Approved:

Paul M. Gignac, PhD

Dissertation Adviser

Haley D. O'Brien, PhD

Holly N. Ballard, PhD

Jennifer L. Volberding, PhD

ACKNOWLEDGEMENTS

This project has been fueled by lifelong interests in flightless birds and paleontology. My parents, Richard and Jane Green, helped cultivate my early passions for the natural world, and they have been an unwavering source of encouragement and inspiration. I am proud to be their son. To my partner Amie McCarthy, I thank you for your love, strength, and patience, particularly during the stressful periods of my doctoral program, as well as accompanying me to cassowary territory in Australia despite your demanding schedule. I express the sincerest gratitude to my advisor, Paul Gignac, whose generosity, compassion, and ravenous pursuit of knowledge exemplify the characters I aspire to attain as a professional scientist. I thank the other members of my committee, Haley O'Brien, Holly Ballard, and Jennifer Volberding, for their emotional support, feedback, and excitement for my project. Haley has taught me how to always strive to be better, and simultaneously kind to myself along the way. My lab mate, David Kay, has become a trustworthy and loyal colleague and friend, and there is no one I would have rather fought in the graduate student trenches with. I additionally thank all of the other paleontology faculty, biomedical faculty, staff, postdocs, graduate students, medical students, undergraduate researchers, and OKStars students at Oklahoma State University Center for Health Sciences that have helped me through this journey.

This project would not have been possible without the constant support and generous cassowary access from R. Glenn Hood and Scott Snedecker (Cassowary Conservation Project; Fort Pierce, FL, USA). We are bonded by birds. Linn and Terry Turner (Rabbit Creek Emu Ranch; Livermore, CO, USA) have donated specimens over the course of my graduate career, and in the process have become an invaluable support system. We lost Linn during my time in this program, but I will always remember him standing beside the emus he loved. Other specimen access, data files, or regional information were provided by the considerate assistance of: Bentley Bird, Paul Sweet, Thomas Trombone (American Museum of Natural History; New York, NY, USA), Mark Balman (BirdLife International; Cambridge, UK), Leslie Boucher, Tony Boucher, Madison Boucher, Thomas Grazier (Boucher Family Farms, Longmont, CO, USA), M. David Quavillon, Michelle Ferguson, Ellen Dreyer, Michelle Smurl (Brevard Zoo; Melbourne, FL, USA), Jay Young (Colorado Gators; Mosca, CO, USA), Peter Rowles (Community for Coastal and Cassowary Conservation, Mission Beach, QLD, AU), Mark Corbridge, Tish Corbridge (Dream Acres Emu Ranch; Cheyenne, WY, USA), Garth Spellman, Jeff Stephenson, Andrew Doll (Denver Museum of Nature and Science; Denver, CO, USA), Thomas deMaar, Natalie Lindholm (Gladys Porter Zoo; Brownsville, TX,

USA), Yulia Brockdorf, Rich McClure (Hillsboro, OR, USA), Jeff Krehbiel (Krehbiels Specialty Meats; McPherson, KS, USA), Stan Barenberg, Samantha Potts (Longneck Ranch; Rose Hill, KS, USA), Ricky-Lee Erickson, Kylea Clarke (Melbourne Museum - Museums Victoria; Melbourne, VIC, AU), Jay Villemarette, Michelle Hayer (Museum of Osteology; Oklahoma City, OK, USA), Hein Van Grouw, Mark Adams, Paul Kitching. Joanne Cooper, Judith White, Pete Key, Claire Walsh (Natural History Museum; Tring, UK), Lawrence Witmer (Ohio University Vertebrate Collection; Athens, OH, USA), Eddie Witte, Rebecca Snyder, Jennifer D'Agostino (Oklahoma City Zoo, Oklahoma City, OK, USA), Ashley Bowen, Kathy Wolyn, Katie Glatfelter (Pueblo Zoo; Pueblo, CO, USA), Heather Janetzki, Kristen Spring, Alison Douglas (Queensland Museum; Brisbane, QLD, AU), John De Campo (Queensland Parks and Wildlife Service and Partnerships; Cairns, QLD, AU), Scott Newland, Heather Arens, Phillip Horvey (Sedgwick County Zoo; Wichita, KS, USA), Joylene Reavis (Sugar Maple Emus; Monroe, WI, USA), Josef Lindholm, Richard Kotarsky, Tom Mortimer (Tulsa Zoo; Tulsa, OK, USA), University of New England Natural History Museum (Armidale, NSW, AU), Betty Lou Cauffman (Valley View Emus; Fennimore, WI, USA), Steve Sarno, Adam Sarno (Wellington, CO, USA), Terry Carmichael (Wet Tropics Management Authority; Cairns, QLD, AU), and Jean A. Paré, Charlotte Hollinger (Wildlife Conservation Society at Bronx Zoo; Bronx, NY, USA).

For believing in me, and always stepping up to assist in my research or foolhardy pursuits when I need them, I am grateful for my close relationships with Nicholas Mahler, Sue Ware, Maria Bailey, Jennifer Campbell-Smith, Tim Carlton, Laura Rosen, and AJ Dodd. For colleagues and mentors that have helped me get to where I am today, and have probably done more for me than they realize, I additionally thank Akinobu Watanabe, Shane Kanatous, Brent Breithaupt, Joseph Sertich, Malcolm Bedell, Louis Taylor, Gregory McDonald, Larry Witmer, Danny Martin, Kirk Johnson, Chris Weege, Ryan Felice, Alan Turner, Peter Larson, Mike Getty, Gregory Erickson, Philip Currie, Mark Norell, Patrick O'Connor, Scott Sampson, Nathan Kley, Amy Balanoff, Gabe Bever, and James Kirkland.

I appreciate the assistance in specimen µCT imaging from: Morgan Hill, Andrew Smith (Microscopy and Imaging Facility of the AMNH; New York, NY, USA), Steven Rigsby (Dentsply Research and Development Office; Tulsa, OK, USA), Manon Wilson, Claire Terhune, Lyndon Colvin (MicroCT Imaging Consortium for Research and Outreach; Fayetteville, AR, USA), and Ryan Ridgely (Ohio University MicroCT Scanning Facility; Athens, OH, USA). The author also thanks Jeremy Delcambre, Robert Lee (Colorado State University; Fort Collins, CO, USA) for their kind use of dissection and processing facilities.

Research funding and conference travel assistance for this study was provided by the following organizations: National Science Foundation (1450850, 1457180, 1725925, & 1754659; to P. M. G.), Oklahoma State University Center for Health Sciences (Department of Anatomy and Cell Biology, Graduate and Professional Student Government Association Travel Reimbursement), Western Interior Paleontological Society (Karl Hirsh Memorial Grants; to T. L. G.), The Company of Biologists and

sponsoring journal, Experimental Biology (Visiting Fellowship, JEBTF1903122; to T. L. G.), American Association for Anatomy (Visiting Scholarship, travel awards; to T. L. G.), Society of Vertebrate Paleontology (Jackson School of Geosciences Travel Grant; to T. L. G.), Society of Integrative and Comparative Biology (Charlotte Mangum Student Support Travel Awards; to T. L. G.), and American Emu Association (Travel Assistance; to T. L. G.).

Name: TODD LANDON GREEN

Date of Degree: DECEMBER, 2020

Title of Study: ONTOGENY, DISPARITY, AND FUNCTION OF THE ENIGMATIC CASQUES OF CASSOWARIES (*CASUARIUS*): A CASE STUDY OF CRANIAL ORNAMENTATION IN ARCHOSAURS

Major Field: BIOMEDICAL SCIENCES

Abstract:

Modern cassowaries (*Casuarius* spp.) are flightless birds best known for their elaborate cranial casques, keratin and bone headgear located above the orbit and neurocranium. Because cassowaries are rare, seclusive, and potentially dangerous, there have been few in-depth studies regarding headgear biology despite functional speculations and suggestions of the casque as a modern analog for the ornaments of extinct taxa, which they resemble. Without baseline anatomical, ontogenetic, disparity, and functional studies, the casque's position in comparative and evolutionary studies remains uncertain. I address this uncertainty by elucidating the biological role(s) of the casque through micro-computed tomography imaging (μCT), evaluation of allometric scaling, two-dimensional shape analyses, and testing for similarities and differences in the comparative anatomy of osseous headgear across extant and extinct casqued archosaurs. I find that southern cassowary (*C. casuarius*) casques are comprised of eight distinct cranial bones and are far more complex than previously realized. Additionally, the central, dorsal element appears to be neomorphic and unique to cassowaries. The keratinous and osseous portions of *C. casuarius* casques scale with strong positive allometry, reaching the majority of their maximum size by sexual maturity. Casques of *C. casuarius* do not appear to be sexually dimorphic in ontogenetic trajectory nor adult shape. However, I find that casque shape may differ between certain *C. casuarius* regional populations and that casques are shaped significantly differently between the three extant species of cassowaries (*C. bennetti, C. casuarius, C. unappendiculatus*). Taken together, ontogenetic scaling of *C. casuarius* casques implicates their potential roles in signaling maturity or status, and shape analysis supports casques functioning in species differentiation. Because cassowary casque composition differs substantially from those of most other archosaurs (including neognathous birds), I find that the casques of modern neognaths (e.g., *Macrocephalon maleo, Numida meleagris*) may represent more appropriate anatomical analogs for ornament patterning and homology studies in extinct, non-avian dinosaurs with comparably simple cranial ornaments. Nonetheless, cassowary casques appear to be particularly important for our understanding of elemental elongation, developmental timing with whole-body indicators of maturity (e.g., feather and apteria coloration), multi-functionality, and ornament disparity among archosaurs.

TABLE OF CONTENTS

Chapter Page

Chapter Page

LIST OF TABLES

Table Page

LIST OF FIGURES

Figure Page

Figure Page

CHAPTER I

INTRODUCTION: PHENOTYPIC COMPLEXITY AND AVIAN ORNAMENTATION

The association between the form of an anatomical structure, its specific function(s), and how an organism utilizes these to acquire/maintain resources or stay alive is referred to as its biological role (Bock, 1980). The interrelationships between form and function have long been studied (Darwin, 1871; Russell, 1916; Bock & Von Wahlert, 1965) in living organisms as a means to explain the biological role of anatomical structures, particularly unexpected or seemingly bizarre morphological traits. A deep understanding of both how organisms use their anatomical features and how those features came about in the first place, requires the study of evolutionary and potentially developmental changes in anatomical complexity. Cranial anatomy, for example, is particularly intricate and difficult to meaningfully reduce to individual integrants, thus, comprehensive insight about its biological role is best gained by addressing morphology, behavior, ecological utility, structure-function relationships, and fitness in tandem whenever possible (Arnold, 1983).

Unusual cranial structures are common in extinct and extant archosaurs (e.g., Bubenik & Bubenik, 1990; Bickel & Losos, 2002; Jared et al., 2005; Molnar, 2005; Hone et al., 2012; Mayr, 2018). Examples include the crests of lambeosaurine hadrosaurs that have been suggested to be used in vocalizations (Weishampel, 1981), the casques of *Rhinoplax vigil* that are used in aerial

jousting (Kinnaird et al., 2003), and the feather crests of *Aethia cristatella* that are thought to be used in inter- and intra-sexual selection (Jones & Hunter, 1999). Archosaur cranial ornaments are often grouped into the wide category of "display" for functionality, and these are thought to allow for status assessment (i.e., *Callipepla gambelii*; Hagelin, 2002), sexual displays (e.g., *Pteridophora*, *Parotia*; Diamond, 1986), and species recognition (e.g., putatively in non-avian dinosaurs, Padian & Horner, 2011). Due in part to subtleties of how visual displays are presented and perceived, it can be elusive for scientists to observe or decipher their context-specific meanings (Gill, 2007). This has contributed to a phenomenon of "default" explanations for cranial-elaborations-as-display anatomy that stand as clear hypotheses but often remain untested (see Padian & Horner, 2011). For example, the ornaments of non-avian theropod dinosaurs are often referred to as having socio-sexual functions (e.g., Gates et al., 2016; Hone et al., 2016; Lü et al., 2017), even though these inferences are routinely drawn without ground-truthing via comparison to specific examples that have been thoroughly studied in modern taxa. Over time, these hypotheses can become stand-ins for actual understanding of presumptive display structures. This has become somewhat common within the paleontological literature, leading to deeper speculation regarding biological roles (e.g., physiological, mechanical, or display) as a result of the difficulty or impossibility of rigorous testing (e.g., Dodson, 1975; Molnar, 2005; Horner & Goodwin, 2006; Evans, 2010; Knell & Sampson, 2011; Padian & Horner, 2011; Schott et al., 2011; Hone at al., 2012; Peterson & Vittore, 2012; Farke et al., 2013; Hone & Naish, 2013; Farke, 2014; Gates et al., 2016; Lü et al., 2017).

To overcome barriers to testing functional and evolutionary hypotheses of display structures that include extinct groups, a deep understanding of how extant organisms can be related to their precursors is required. To this end, I investigate cranial ornament anatomy in living birds to gain a better understanding of the ontogenetic arrangement, adult variation, and potential functionalities that caused these structures to arise in the first place and persist through evolutionary time. I focus my efforts on the cranial anatomy of cassowaries (*Casuarius*; Fig. 1), which includes a commonly cited, but poorly understood, ornamented avian system. Because cassowaries are living dinosaurs with

headgear, the cranial casques in these animals have been implicated as sufficient analogs for superficially comparable ornaments in extinct dinosaurs (Dodson, 1975; Padian & Horner 2011, Hone at al., 2012; Farke et al., 2013; Naish & Perron, 2016; Lü et al., 2017; Eastick et al., 2019). However, cassowaries themselves are little-studied members of the poorly-understood paleognathous lineage that includes ratites (i.e., cassowaries, emus, rheas, ostriches, kiwis, moas, and elephant birds), tinamous (a modern flighted group), and a number of fossil forms with uncertain taxonomic placements and curious anatomies (e.g., Lithornithids, *Remiornis*, *Palaeotis*). As a result, the strength of our inferences about partially preserved fossil forms has tended to derive from exemplars of their living relatives that we do not yet clearly understand—but could.

As paleognathous birds, cassowaries are not unique in harboring unusual morphologies. Potentially due to an evolutionary release resulting from the loss of flight along multiple independent evolutionary events (Maderspacher, 2017), rather than sharing a flightless common ancestor (Harshman et al., 2008; Phillips et al., 2010, Baker et al., 2014, Mitchell et al., 2014), each ratite lineage has shown an individual propensity to evolve atypical (for birds) structures and morphologies. These include the gigantic eggs of elephant birds, didactyl feet of ostriches, and facial mechanoreceptors of kiwis, as well as the cranial casques of cassowaries. The cassowary casque (Fig. 2) has remained particularly enigmatic, even after over a century and a half of study, however (Parker, 1866; Flower, 1871; Marshall, 1872; Pycraft, 1900; Rothschild, 1900; Dodson, 1975; Crome & Moore, 1988; Richardson, 1991; Phillips & Sanborn, 1994; Starck, 1995; Mack & Jones, 2003; Hone at al., 2012; Farke et al., 2013; Naish & Perron, 2016; Perron, 2016; Lü et al., 2017; Mayr, 2018; Eastick et al., 2019). During that period, it has been implicated in several potential biological roles. These include visual social display, vocalization, and thermoregulation (Crome & Moore, 1988; Phillips & Sanborn, 1994; Mack & Jones, 2003; Naish & Perron, 2016), among others. In this dissertation I aim to establish an anatomical baseline for southern cassowary (*C. casuarius*) cranial morphology in order to address proposed display functions of the cassowary casque.

The proposition that the biological role of the casque is for display has been suggested passively in numerous studies. The Rothchild (1900) monograph that serves as a nucleus of the cassowary biology literature includes brief references to potential sexual dimorphism in casque shape and size among *Casuarius* taxa. These observations were not tested, however. Crome and Moore (1988) hypothesized casque use in physical ramming as well as advocated for a potential secondary display function also related to casque dimorphism. Despite this being one of the first direct propositions of a visually focused biological role, the authors go on to clarify that they had not observed the casque being used during mating displays (Crome & Moore, 1988). The display role of the casque was also listed as a potential secondary function in another study (Mack & Jones, 2003) concerned primarily with the casque as a feature for vocalization or sound reception. More recent studies discuss cassowary casques in a predominantly display biological role, specifically in sexual displays versus species recognition, suggesting the potential for multifunctionality (Hone et al., 2012; Naish & Perron, 2016). In all cases, prior efforts to ascertain potential roles of the casque in display have focused on a few focal individuals only, taken descriptive and non-quantitative approaches to studying the casque, and erected but not tested hypotheses concerning how the casque may be used for visual displays.

Comprehensive documentation of cassowary casque anatomy, ontogeny (Fig. 3), and variation (Figs. 1, 2), along with conceptual tests for function are imperative to gain the understanding necessary for cassowaries to potentially bridge ornament biology to the fossil record. My findings will assist in determining the biological role(s) of the cassowary casque and allow me to evaluate the proposed utility of cassowaries as modern analogs for the development and evolution of cranial ornamentation in archosaurs, including other extant, ornamented avians as well as extinct dinosaurs such as hadrosaurs and oviraptorosaurs. In order to gain this understanding, I will address the following aims:

1. Determine the cranial elements that comprise the casque of *C. casuarius* by tracking the expansion of skull bones during ontogeny, from embryonic development to adult

specimens, using direct visual examination and micro-computed tomography imaging (Chapter II);

2. Ascertain the ontogenetic scaling patterns of the keratinous and bony components *C. casuarius* casques to quantify how growth of these structures relate during development (Chapter III);
3. Assess the type and magnitude of disparity in casque shape within *Casuarius* to detect potential differences in casque morphology between *C. casuarius* sexes, between *C. casuarius* regional populations, and between all three extant *Casuarius* species (Chapter IV);
4. Assess bony casque configuration patterns and timing of growth in *C. casuarius* and outgroup neognathous birds to determine the suitability of casque-bearing avians as analogs for comparative studies of extinct, non-avian dinosaurs with cranial ornamentation (Chapter V).

In the end, I will position *Casuarius* as a model system for addressing the complex evolutionary history of cranial ornaments within Dinosauria, including extant Aves. By spurring a resurgence in cassowary research, I hope to direct a promising community of cassowary-focused ornithologists, paleontologists, physiologists, and comparative evolutionary anatomists (Mack & Jones, 2003; Perron, 2011; Campbell et al., 2012; Hone at al., 2012; Farke et al., 2013; Naish & Perron, 2016; Lü et al., 2017; Mayr, 2018; Angst et al., 2019; Eastick et al., 2019; McInerney et al., 2019; Eliason & Clarke, 2020) to re-examine these enigmatic birds with modern visualization, phylogenetic, and comparative methods tools that stand on the forefront of modern evolutionary biology research (Chapter VI). Finally, by addressing hypotheses that relate to biology and life-history of cassowaries, my research will help inform conservation efforts that are needed (Campbell et al., 2012; IUCN, 2020) to maintain the biodiversity of these rare but amazing flightless birds.

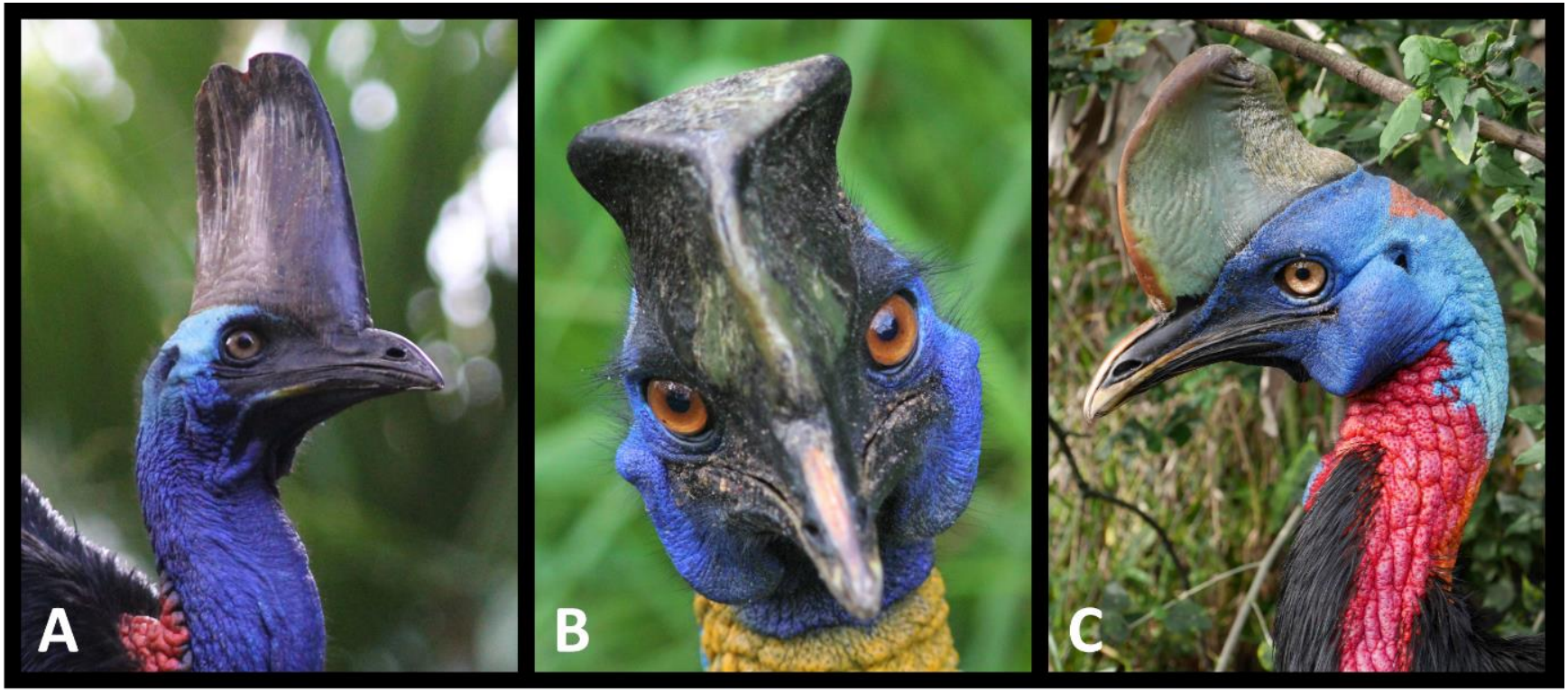

Figure 1. Photographs of living cassowaries demonstrating various casque morphologies across the genus (A = *Casuarius casuarius*; B = *Casuarius unappendiculatus*; C = *Casuarius unappendiculatus*). Morphological differences in color and shape may even appear to exist within the same species (e.g., *C. unappendiculatus*; B–C). Photos by T. L. G.

Figure 2. Micro-computed tomography, three-dimensional digital renderings of osteological cassowary cranial anatomy illustrating osseous casque variations between species (A = *Casuarius bennetti*, AMNH SKEL 7834; B = *Casuarius casuarius*, AMNH SKEL 962; C = *Casuarius unappendiculatus*, AMNH SKEL 3872). The exterior keratinous sheathing (not associated with these specimens) generally follows the contours of the osseous portion, which makes up the majority of the casque's size. Micro-computed tomography image data were collected via a 2010 GE phoenix v|tome|x s240 high-resolution microfocus computed tomography system housed in the Microscopy and Imaging Facility of the AMNH. Scanning parameters were 140 kilovolts (kV), 130 microamps (μA), and 200 millisecond (ms) exposures with isometric voxel size at resolutions ranging from 93.42–100.60 micrometers (μm). The program AvizoLite was used to render three-dimensional (3D) digital skull models by using a combination of automatic and manual segmentation.

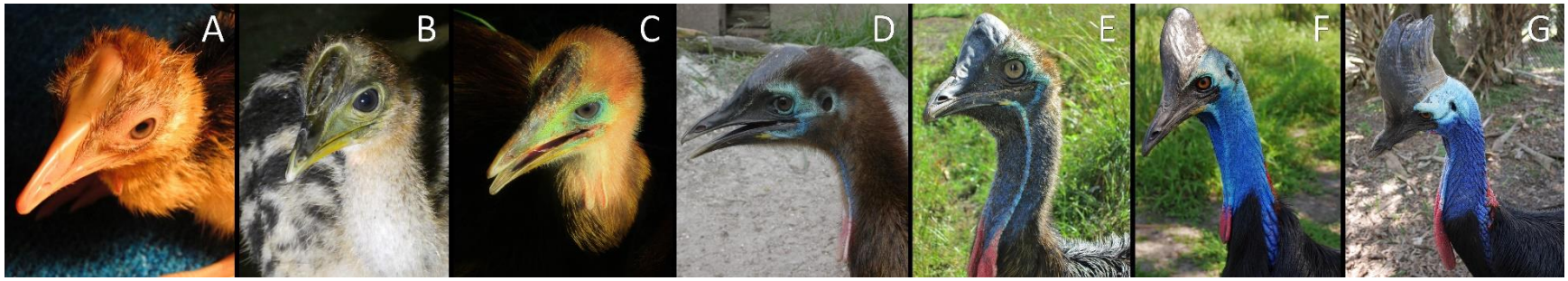

Figure 3. Photographs demonstrating casque ontogeny in C. casuarius: (A) < 24 hour-old immature individual with dorsal keratinous continuation of beak rhamphotheca; (B) ~1.0 month-old immature individual with isolated, dorsal keratinous shield; (C) ~5.0 month-old immature individual incipient casque; (D) ~10 month-old immature individual with a partially developed and dorsally expanded casque; (E) ~1.5 year-old immature individual with a dorsally prominent casque; (F) ~3.5 year-old immature individual with an almost fully developed casque; (G) > 7 year-old mature individual with a fully mature casque. Photos by T. L. G.

CHAPTER II

OSTEOLOGICAL DESCRIPTION OF CASQUE ONTOGENY IN THE SOUTHERN CASSOWARY (*CASUARIUS CASUARIUS*) USING MICRO-CT IMAGING

***** *This chapter has been minimally modified to meet Oklahoma State University dissertation formatting criteria from Green & Gignac (2020), published in* The Anatomical Record.

Abstract

Extant cassowaries (*Casuarius*) are unique flightless birds found in the tropics of Indo-Australia. They have garnered substantial attention from anatomists with focus centered on the bony makeup and function of their conspicuous cranial casques, located dorsally above the orbits and neurocranium. The osteological patterning of the casque has been formally described previously; however, there are differing interpretations between authors. These variable descriptions suggest that an anatomical understanding of casque anatomy and its constituent elements may be enhanced by developmental studies aimed at further elucidating this bizarre structure. In the present study, I clarify casque osteology of the southern cassowary (*C. casuarius*) by detailing casque anatomy across an extensive growth series for the first time. I used micro-computed tomography (μCT) imaging to visualize embryonic development and post-hatching ontogeny through adulthood. I also sampled closely related emus (*Dromaius novaehollandiae*) and

ostriches (*Struthio camelus*) to provide valuable comparative context. I found that southern cassowary casques are comprised of three paired (i.e., nasals, lacrimals, frontals) and two unpaired elements (i.e., mesethmoid, median casque element). Although lacrimals have rarely been considered as casque elements, the contribution to the casque structure was evident in µCT images. The median casque element has often been cited as a portion of the mesethmoid. However, through comparisons between immature *C. casuarius* and *D. novaehollandiae* I document the median casque element as a distinct unit from the mesethmoid.

1. Introduction

Cassowaries (Aves: *Casuarius*) are large-bodied (average of 31.65–45.75 kg as adults; Marchant & Higgins, 1990; Heather & Robertson, 1997; Olson & Turvey, 2013), flightless birds that belong to the extant paleognathous lineage (e.g., also including tinamous, ostriches, rheas, kiwis, and emus). Although well known for their aggressive temperaments (Rothschild, 1900; Kofron, 1999) and ecological importance as seed dispersers (Stocker & Irvine, 1983; Mack, 1995; Webber & Woodrow, 2004; Bradford & Westcott, 2010; Bradford & Westcott, 2011), the hallmark novelties of these paleognath birds are their conspicuous cranial casques (Fig. 1B), which are tall bony and keratinous protrusions that extend dorsally above the orbits and neurocranium. In cassowaries, keratinous outer sheathing generally follows the shape of the bony casque surface, though it may exceed the height of the underlying pneumatized bone (Pycraft, 1900; Richardson, 1991; Naish & Perron, 2016).

Starting in the late nineteenth century (Parker, 1866; Flower, 1871; Marshall, 1872; Pycraft, 1900; Rothschild, 1900) these cranial ornaments have been the subject of numerous hypotheses regarding their composition and function (Dodson, 1975; Crome & Moore, 1988; Richardson, 1991; Phillips & Sanborn, 1994; Starck, 1995; Mack & Jones, 2003; Naish & Perron,

2016; Mayr, 2018; Eastick et al., 2019). Interestingly, previous studies detailing the constitution of cassowary cranial casques have led to several differing interpretations of their contributing bony elements. Such differences likely result from the extensive fusion and remodeling that casques undergo throughout ontogeny, thus, obfuscating clear demarcations between individual skull bones. Clarification of casque composition can, therefore, be gleaned from the use of internal imaging techniques, such as high-resolution micro-computed tomography (μCT), as well as examination of early developmental stages prior to bone fusion. Gaining this understanding would enhance our ability to infer how casque form implicates function and to test hypotheses about the biological role(s) of this unusual structure.

Formal descriptions of cassowary skulls were initially made by Parker (1866), Flower (1871), and Marshall (1872). These works identified the mesethmoid (used interchangeably with "ethmoid" by early authors) as a primary component of the casque. In fact, Parker (1866) described this constituent as the element making up the entirety of the casque. In addition to the mesethmoid, Marshall (1872) included the nasal bones as casque contributors, and Flower (1871) further described potential contributions from the lacrimals, frontals, and parietals. Although variable, each of these descriptions was based on the visual interpretation of a continuous, central bony strut passing superiorly from between the orbits. Building on these works, Pycraft (1900) performed more complete osteological investigations that comparatively sampled cassowary and non-cassowary paleognath cranial osteology. In addition to the mesethmoid, Pycraft (1900) included the nasals and frontals as casque elements based on their characteristic "inflation" (developmental expansion through invasion by adjacent pneumatic passages and extensive growth of thin trabecular bone, internally) as well as direct interfaces with the mesethmoid. Pycraft (1900) also questioned whether the unpaired element at the center of the casque was composed of the mesethmoid only: based on apparent separation between dorsal and ventral components of the bone in early developmental ages (exact ages not specified; see Plate XLIV from Pycraft, 1900), an additional, more dorsal bony element in the midline was identified. This was referred to as a "median element

of the casque" (herein: median casque element), and it was specifically differentiated from the mesethmoid, which was interpreted as having a more inferior position (e.g., contributing to the interorbital septum). The homology of the median casque element was not address by Pycraft at the time (1900), nor has it been formally evaluated since. Together, these historical texts summarize which elements were thought to contribute to which anatomical aspect of the casque: the mesethmoid forming a rostrodorsal portion, a tentatively-labelled median casque element occupying the most dorsal aspect, nasals contributing to the rostrolateral walls, lacrimals marginally involved in the base laterally, and frontals along with parietals supporting the caudolateral base. Expanding on these efforts, more recent osteological descriptions have produced other interpretations of element combinations to casque formation in cassowaries (Richardson, 1991; Naish & Perron, 2016; Mayr, 2018), resulting in the characterization of several casque phenotypes (see Table 1 for historical interpretations).

Cassowary research has been impeded by persistent taxonomic and sampling issues. Namely, multiple species are often grouped by authors into a single *Casuarius* genus complex, which may obscure potential taxonomic differences in casque anatomy as well as our ability to identify homologues for cranial elements between cassowaries and other avians. Additionally, adult cassowary casque shapes and dimensions appear to be taxon-specific, introducing the possibility of variation in the bony elements contributing to the casque. Generally, southern cassowaries (*C. casuarius*) possess tall and laterally compressed casques (Fig. 1B), whereas northern cassowaries (*C. unappendiculatus*) have tall trigonal casques with relatively broad caudal regions and often flattened dorsal surfaces, and dwarf cassowary (*C. bennetti*) casques are less tall trigonal pyramids (Marshall, 1872; Rothschild, 1900; Perron, 2016). Treating the genus *Casuarius* as a monolith subsumes interspecific variation into one taxonomic grouping, and may mask our understanding of how the casque grows, how cranial bones are incorporated in the casque, and how intraspecific (e.g., sexual dimorphism) or interspecific differences (e.g., from reproductive isolation) may relate to casque evolution.

In this study, I expand on prior cassowary cranial anatomical descriptions by sampling cassowary casques across ontogeny using μCT imaging. Although a dorsal keratinous shield is present in neonates where the casque will eventually grow (Fig. 1A), cassowaries begin life without a casque. Therefore, I scanned a comprehensive embryonic and post-hatching growth series of southern cassowaries to track the incipient development of bony casque elements from beneath the initial keratinous shield, through casque initiation and dorsal expansion, and into skeletal maturity and adulthood. High-resolution digital imaging allowed me to identify internal suture boundaries and track patterns of inflation, which were critical for reinterpreting casque constituency. My three aims were to: (1) describe the bony cranial anatomy in *C. casuarius*, specifically, (2) clarify the identity of midline casque constituent(s) through osteological comparison with other extant ratites, and (3) describe the ontogeny of bony casque features by documenting casque inflation and growth. Using these methods, and the largest comparative and ontogenetic dataset of cassowaries to date (n = 54), I found that *C. casuarius* cranial anatomy is unique among major ratite groups and casque composition is more complex than previously described. This comparative and ontogenetically-informed re-description of *C. casuarius* casques provides important osteological context that will enable future studies of casque evolution and function to be more directly characterized.

2. Material and Methods

2.1. Specimen Sampling, Acquisition, & Access

I sampled 54 southern cassowaries: 12 embryonic, 22 immature, and 20 adult individuals (see below for ontogenetic stage criteria). None harbored obvious cranial abnormalities, with the exception of one embryo that possessed a single malformed eye, which was used to assist in embryonic age approximation but was not used to interpret cranial osteology. Twenty-three

individuals ($n_{embryonic}$ = 6, $n_{immature}$ = 12, n_{adult} = 5) were µCT scanned to track bony cranial elements beneath the keratin sheath and within the skull. The remaining 31 (skulls without keratin along with preserved and dissected heads) were used for visual inspection of casque sutural boundaries or aging assessments ($n_{embryonic}$ = 6, $n_{immature}$ = 10, n_{adult} = 15). Data from adult and immature *C. casuarius* specimens were collected from the American Museum of Natural History (AMNH; New York, NY, USA), Cassowary Conservation Project (CCP; Fort Pierce, FL, USA), Denver Museum of Nature and Science (DMNS; Denver, CO, USA), Melbourne Museum (Museums Victoria, MV; Melbourne, VIC, AU), Museum of Osteology (MOO; Oklahoma City, OK, USA), Natural History Museum (NHMUK; Tring, UK), Queensland Museum (QM; Brisbane, QLD, AU), Sedgwick County Zoo (SCZ; Wichita, KS, USA), and T. L. Green Research Collection (TLG; Tulsa, OK, USA). Individuals from the breeding and zoological institutions were collected fresh, whereas museum specimens were fluid-preserved or skeletonized. Institutional care protocol was not required as all specimens were collected as cadaveric after death. No individuals were harmed or sacrificed for the purpose of this study.

In order to describe changes in osteology over development, I also surveyed the literature (e.g., Pycraft 1900, Zusi, 1993; Maxwell, 2009) and sampled non-casqued paleognaths: 19 emus, *Dromaius novaehollandiae* ($n_{embryonic}$ = 5, $n_{immature}$ = 6, n_{adult} = 8) and 13 ostriches, *Struthio camelus* ($n_{embryonic}$ = 1, $n_{immature}$ = 10, n_{adult} = 2). *Dromaius novaehollandiae* specimens were donated by Dream Acres Emu Ranch (DAER; Cheyenne, WY, USA), Rabbit Creek Emu Ranch (RCER; Livermore, CO, USA), S. Sarno (WEL; Wellington, CO, USA), Sugar Maple Emus (SME; Monroe, WI, USA), Valley View Emus (VVE; Fennimore, WI, USA), and Y. Brockdorf (HLB, Hillsboro, OR, USA). *Struthio camelus* specimens were donated from Colorado Gators (CG; Mosca, CO, USA), Krehbiels Specialty Meats (KSM; McPherson, KS, USA), Longneck Ranch (LNR; Rose Hill, KS, USA), and Pueblo Zoo (PBZ; Pueblo, CO, USA). As with the *Casuarius* specimens, no birds were killed or harmed for the purpose of this study, and all specimens were collected opportunistically after death. Samples were frozen on site and shipped frozen to Oklahoma State

University Center for Health Sciences (OSU-CHS; Tulsa, OK, USA); where they were stored in freezers (-20°C). Nine specimens were dissected in laboratories at OSU-CHS and Colorado State University (CSU; Fort Collins, CO, USA) and cleaned through the use dermestid beetles or warm water maceration at CSU in order to view bony cranial surfaces. A full list of adult and immature specimens can be found in Appendix A.

Embryonic specimens were attained from breeding institutions and university collections. Unhatched cassowary eggs (n = 8) were donated by the CCP. Emu eggs (n = 5) were collected from DAER, RCER, and VVE. One ostrich embryo was obtained from LNR. Eggs with embryos that did not develop fully and died in-shell during the incubation process were stored (at -10º C) and then shipped frozen. Eggs were thawed, eggshells were cut carefully away, embryos were removed from yolk and vitelline membrane, and extraneous fluids were removed from carcass surfaces. Extracted embryos were then refrozen or chemically fixed, and four *C. casuarius* and three *D. novaehollandiae* individuals were µCT imaged. Additional embryonic cassowary specimens were provided by the WitmerLab at Ohio University (Ohio University Vertebrate Collection, OUVC; Athens, OH, USA) as µCT datasets (n = 2), by the Gladys Porter Zoo (GPZ; Brownsville, TX, USA) as a fixed specimen (n = 1), and by the CCP as a disarticulated skeleton (n = 1). A full list of embryonic specimens can be found in Appendix A.

2.2. Identification of Southern Cassowary Specimens

All adult specimens were confirmed as *C. casuarius* according to the criteria of Marshall (1872), Rothschild (1900), and Perron (2016), including preserved and/or soft-tissue records that are synapomorphic for the species *C. casuarius* (e.g., two wattles, species-specific coloration patterns). *Casuarius casuarius* maintain distinct casques that appear more similar to conspecifics than to other species (i.e., *C. unappendiculatus*, *C. bennetti*; Marshall, 1872; Rothschild, 1900; Perron, 2016), therefore; skeletal-only adult specimens with little data (n = 7) were categorized as

C. casuarius based specifically on this narrow casque shape. For younger, immature individuals with no or incipient casques, known breeding or detailed collection histories were a prerequisite for inclusion in this study.

2.3. Specimen Preparation

Wet specimens were µCT scanned either as frozen, fixed in 10% neutral buffered formalin, or fixed in 70–95% ethanol. Preparation information can be found in Appendix A. All specimens were packaged in lightweight foam and polyethylene plastic for scanning. Prior to egg processing, embryos were identified within intact eggs via two-dimensional (2D) X-ray imaging. This allowed for targeted dissection of eggs containing embryos across different stages of development.

2.4. µCT Data Collection

Image data were collected on four µCT scanning systems: (1) a 2010 GE phoenix v|tome|x s240 high-resolution microfocus computed tomography system (General Electric, Fairfield, CT, USA) housed in the Microscopy and Imaging Facility of the AMNH; (2) a 2012 Nikon XT H 225 ST µCT system (Nikon Metrology, Brighton, MI, USA) housed at the Dentsply Research and Development Office (Dentsply; Tulsa, OK, USA); (3) a 2018 Nikon XT H 225 ST µCT system housed at the MicroCT Imaging Consortium for Research and Outreach (MICRO; Fayetteville, AR, USA); and (4) a TriFoil Imaging eXplore CT 120 Small Animal X-Ray CT Scanner (TriFoil Imaging, Chatsworth, CA, USA) at the Ohio University MicroCT Scanning Facility (OUµCT; Athens, Ohio, USA). Scanning parameters varied based on system optimizations; see Appendix A for parameter listings.

2.5. Digital Reconstruction of µCT Data

Tagged Image File Format (TIFF) stacks of CT-generated data were cropped of extraneous background pixels to minimize file volumes, and stitched along the Z-axis if necessary (e.g., for "tall" scans), using the program ImageJ (v. 1, US National Institutes of Health, Bethesda, MD). Digital models of bony cranial elements were three-dimensionally (3D) reconstructed in the program Avizo (versions 9–version 9.7; Visualization Science Group, Burlington, MA, USA; Thermo-Fisher Scientific; Waltham, MA, USA) and Avizo Lite (version 2019; Thermo-Fisher Scientific) by automatic and manual segmentation of bone-specific greyscale values. Two-dimensional slices and 3D digital bony models were examined for external and internal anatomy to determine cranial configuration, suture boundaries, bony fusions, and extent of bony inflation.

2.6. Age and Osteological Definitions Utilized in this Study

It is necessary to outline criteria for aging southern cassowary individuals in order to appropriately organize an ontogenetic series from samples spanning multiple sources with differential age indicators available. Similarly, I propose explicit criteria for those traits that constitute participation of cranial bones into the casque as well as how to identify if, or when, such contributions shift across ontogeny.

Because some specimens were unaccompanied by known ages, I develop aging criteria that also enable me to approximate stepwise acquisition of casque element contributions through ontogeny. My criteria for embryonic, immature, and mature classifications are qualitative, such as extent of ossification and integumentary traits. Other criteria include measurements of non-casque skull features to estimate relative ages within each of my three age categories. Osteological specimens were measured with a 300-Millimeter (mm) Stainless Steel Absolute Digital Caliper (Taylor Toolworks, Columbia, MO, USA). Linear measurements were taken for skull length (from

the rostral tip of the premaxilla to the caudalmost extent of the supraoccipital bone) in mm (see Fig. 2 for cranial osteological terms). These measurements were also made for digital samples (in mm) with the "Measurements" functions in Avizo and Avizo Lite. Criteria for embryo, immature, and mature aging follow, along with inclusion/exclusion criteria for elements contributing to the casque.

2.6.1. Embryo Aging Criteria

Embryonic cassowaries are defined herein as individuals that died within an egg, excluding those that died during hatching after the eggshell was perforated. Southern cassowaries have an egg incubation process that ranges from 48–56 days (Romagnano et al., 2012) and emus range from 46–56 days (Minnaar & Minnaar, 1992; 50 days on average, Minnaar & Minnaar, 1998). Exact time of death for embryos was unknown due to opportunistic collection. The embryology of *C. casuarius* has not been described previously although embryology of a sister group, *D. novaehollandiae*, has been (e.g., Minnaar & Minnaar, 1998; Maxwell, 2009; Nagai et al., 2011). Therefore, emus were used as suitable analogs for approximating embryonic developmental stage identification in cassowaries. I assessed relative stages (Hamburger Hamilton Stages, HH; Hamburger & Hamilton, 1951) and ages by documenting embryonic *C. casuarius* anatomies and comparing them to a suite of characters from previous *D. novaehollandiae* studies with known termination ages. These included, (1) external physical characteristics (Nagai et al., 2011), (2) tibiotarsus/embryo length (Minnaar & Minnaar, 1998), and (3) cranial ossification patterns (Maxwell, 2009) (Appendix A). Although the later HH stages (i.e., 40–44) are largely based on bill and digit lengths from embryonic domestic chickens (*Gallus gallus*; Hamburger & Hamilton, 1951), my approximations within this range were made via comparative external morphological characteristics and metrics of emus (Minnaar & Minnaar, 1998; Nagai et al., 2011).

2.6.2. Immature Aging Criteria

Immature individuals include those newly-hatched (neonate; inclusive of egg-bound individuals that perforated the eggshell) through sub-adulthood individuals (described below). None were sexually mature at the time of death. For the purposes of this study, I define sexual maturity as the age at which viable offspring can be produced. Osteological indicators for immature individuals include qualitative features common to neognaths and paleognaths (Pycraft, 1900; Kesteven, 1942; Maxwell, 2008; Maxwell, 2009): incomplete ossification of the interorbital septum with incomplete contributions from the mesethmoid (fused or unfused at this stage), frontals, laterosphenoids, and basiparasphenoid complex (at this stage parasphenoid and basisphenoid may be unfused or fused with one another). Soft-tissue secondary sexual characteristics for immature individuals include: brown feathers and incomplete apteria coloration (e.g., non-contiguous regions of blue, red, and purple; Rothschild, 1900). Subadults, for example, will have begun to transition to adult coloration, but they lack the fully black feathers and well-developed apteria with brightly colored skin of the head and neck, which characterizes adults. If exact age was not known, immature specimens were arranged into an ontogenetic sequence by increasing skull length.

2.6.3. Mature Aging Criteria

This category exclusively includes individuals that were reproductively capable or listed as adults in museum databases. Cranial osteological indicators of maturity are common to neognaths and paleognaths (Parker, 1866; Pycraft, 1900; Zusi, 1993), notably: complete ossification of the interorbital septum with contributions from: the mesethmoid (fully fused), frontals, laterosphenoids, and basiparasphenoid. Soft-tissue secondary sexual characteristics for mature individuals include: completely black feathers and full apteria coloration (e.g., contiguous regions of blue, red, and purple; Rothschild, 1900). The reproductive status of mature individuals

was also confirmed by donating sources when possible (see Appendix A). Mature specimens were arranged first by age (for those known); and then by increasing head length into an ontogenetic sequence. Notably, the most mature male cassowaries do not attain the same body sizes as the most mature females (see Olson & Turvey, 2013), resulting in the largest individuals in the sample represented exclusively by female specimens. Further large-sample studies should be developed to test *C. casuarius* growth trajectories.

2.6.4. Definition of Osteological Traits for Bones Contributing to Casque

Previous studies indicate that bones may contribute fully or partially to osteological ornaments (see Mayr, 2018), therefore; I defined casque participation as bones that exhibit direct physical association with the structural composition of the ornament. Specifically, a bony element can participate partially (e.g., as a single process supporting the base of the casque) or fully (i.e., with the entire element involved in the ornament structure). In cassowaries, the ornament is generally considered as a series of osteological expansions dorsal of the orbit and neurocranium. I utilized non-casqued *D. novaehollandiae* and *S. camelus* as a basis of comparison to identify dorsal expansion beyond that of other paleognathous birds. Birds have highly pneumatized bones generally, and this holds true for casques as well (Starck, 1995; Brassey & O'Mahoney, 2018). However, it is important to note that many other bones within the avian skull can also be pneumatized (Witmer, 1990). Therefore, although the degree of inflation may be used as supporting evidence for casque contribution (e.g., compared to less pneumatized adjacent bones), it was not used as a standalone observation for the purpose of defining casque contribution in this study.

2.6.5. Definition of Osteological Traits for Bones Not Contributing to Casque

Bones that do not exbibit direct physical association with the structural composition of the casque are excluded from my definition of casque composition. Specifically, these are cranial bones which neither fully nor partially provide structure or support to the casque (i.e., no single process or region of the element provides structure to the casque nor its base). Excluded bones are therefore expected to share their relative sizes and shapes with homologous bones in closely related, non-casqued taxa.

3. Results

3.1. Casque Elements in Southern Cassowaries

Due to incomplete bony element fusion, immature specimens proved to be particularly informative for determining casque composition. These individuals capture important stages after casque elements have become well ossified but prior to the point when multi-element fusion begins. Sutures are patent and visible in immature individuals, facilitating identification of individual bony elements and their boundaries (Fig. 2).

I found a total of eight elements that participate in casque composition during ontogeny: three paired (left and right nasals, lacrimals, and frontals) and two unpaired bones (median casque element and mesethmoid; Fig. 3). As exemplified by the immature individual in Figure 3, the rostral and rostrodorsal portions of the casque consist of the nasals laterally and median casque element medially and superiorly. Each extends caudally, dorsal of the orbits. The caudal two-thirds of the nasals (including the frontal processes of the nasals; Baumel & Witmer, 1993) extend to the caudal border of the orbit, contributing to the rostrolateral casque walls. The entirety of the median casque

element continues beyond the caudal orbital margin and forms the most caudal extent of the casque. The orbital processes of the lacrimals (Baumel & Witmer, 1993; Maxwell, 2008) contribute to the lateral bases of the casque, whereas the dorsalmost margins of the frontals form the lateral and caudolateral bases. Both appear to support the more dorsally located elements (Figs. 3, 4A). The frontals contact the lacrimal bones, nasal bones, and median casque element along their dorsalmost margins (Figs. 2E, 3A, D), and they provide the inferior platform for the caudal casque. This occurs as the dorsally projecting and inflated frontal bones grow to "fold" overtop themselves (referred to hereafter as an osteo-developmental fold), forming an acute angle between the projection and the skull table contribution of the frontals (see Fig. 2A, B, E). The mesethmoid occupies an internal-only placement and cannot be seen in dorsal view. However, it becomes inflated like its neighbors, and the dorsalmost portion of the mesethmoid provides support as the central, internal base of the casque (Fig. 4A). Notably, in *C. casuarius*, the mesethmoid is more dorsally expanded compared to *D. novaehollandiae* and *S. camelus* of similar ages, consistent with my interpretation of its inclusion into the casque structure (Fig. 4). The nasals and median casque element comprise the greatest contributions to the casque in mature individuals, whereas those of the lacrimals, frontals, and mesethmoid are less elaborate (Fig. 3).

3.2. Bony Cranial Anatomy in Embryonic Specimens

In the embryonic cassowary samples (e.g., Figs. 5A i–ii, 6, ~HH40, TLG C032; ~HH41, TLG C030; see Appendix A) no cranial ornament was present. None of the eight elements that will eventually make up the casque are fused in embryos, and none are dorsally inflated (Figs. 5A i–ii, 6). Moreover, the mediocaudal portions of the frontals are not fully formed, leaving a relatively large, caudodorsal fontanel in the neurocranium that is present medially between the frontals and parietals (Fig. 6).

The mesethmoid is a T-shaped bone that forms the rostralmost portion of the ossified interorbital septum and contributes to the nasal septum in some avian species (Baumel & Witmer, 1993). The early ontogeny of the mesethmoid has been described previously in emus (Maxwell, 2009) but not in cassowaries. Consistent with emus described in Maxwell (2009), I find that southern cassowaries possess two embryonic ossification centers for the developing mesethmoid (the interorbital septum inferiorly and lamina dorsalis superiorly; Fig. 5), which form a similar T-shaped, midline element when fused. The interorbital septum of the mesethmoid forms first, as seen in TLG C032 (~HH40) and the laminae dorsalis forms second as exemplified in TLG C030 (~HH41). At approximately stage HH41 these mesethmoid ossification centers remain distinct in *C. casuarius* (Fig. 5A ii; TLG C030), while the mesethmoid is fully fused in my comparably staged *D. novaehollandiae* sample (Fig. 5B i; TLG E139). Drawing from my ossification and morphometric data, along with Maxwell (2009), suggests that the appearance of the two separate mesethmoid ossification centers may occur earlier than HH41 in *D. novaehollandiae*. Nonetheless, it has been indicated that the timing of mesethmoid ossification may be highly variable between individuals (Maxwell, 2009), which points toward a need to formally examine this pattern further using additional specimens of known ages. Additionally, the ossifying mesethmoid of *D. novaehollandiae* is perforate, whereas that of *C. casuarius* is not in any of the embryonic stages analyzed in this study (Fig. 5). In *D. novaehollandiae*, this fenestra developmentally closes later in ontogeny (Parker, 1866; Pycraft, 1900; Kesteven, 1942) to more greatly resemble the mesethmoid of *C. casuarius*.

In addition to the mesethmoid, southern cassowaries uniquely possess a second, dorsalmost, and horizontal midline bone, the median casque element (Pycraft, 1900). This bone is distinct from the lamina dorsalis of the of mesethmoid, such that all three ossifications (i.e., both laminae of the mesethmoid and the median casque element) can be identified simultaneously in my cassowary embryos (Figs. 5 ii, 6E). No comparable third bony structure is known for either *D.*

novaehollandiae nor *S. camelus*, and I am not aware that it has ever been identified in embryos of other paleognathous birds.

3.3. Bony Cranial Anatomy in Immature Specimens

Of the three broad age classes, immature individuals characterize the morphological changes important for identifying casque elements and understanding the progression of casque ontogeny. During immaturity, individuals progress from a casque-less skull to one with a rudimentary, incipient casque and ultimately reach a phenotype that includes a moderately raised dome, consisting of several paired and midline elements. For the purposes of clarifying my results, therefore, I subdivided immature individuals into three phases of growth based on osteological traits: phase 1, prior to elemental inflations and fusions; phase 2, after incipient elemental inflation but prior to elemental fusions; and phase 3, after the onset of both elemental inflation and fusion.

3.3.1. Immature: Phase 1

Immature individuals at this phase demonstrate cranial elements that will contribute to the casque in older individuals but are not yet fused or inflated, thus, failing to meet the criteria set for casque formation. Neonate *C. casuarius* skulls (see Fig. 5A iii, TLG C025, seven days old; Fig. 7A–C, TLG C010, one day old; also see Appendix A) are reminiscent of the neonate *D. novaehollandiae* phenotype (see Fig. 5B iii; TLG E093; five days old; also see Appendix A), particularly in lateral view. However, there are exceptions when viewed dorsally, including a more laterally compressed rostrum, frontal processes of the nasals that extend further caudally to the midpoint of the orbit, and the presence of an enlarged, dorsal, and rostro-caudally oriented median casque element visible at the midline surface of the skull (Figs. 5, 6). As ossification of the mesethmoid becomes complete, it also lengthens in a rostro-caudal direction, deep to the median

casque element. The dorsalmost region of the mesethmoid also becomes more pneumatized as compared to an emu of similar age (i.e., 7–24 days old), gaining loosely spaced trabecular bone (Fig. 8A i). Despite this, there is not yet an indication of inflation for any bones dorsal to the orbital margins (Figs. 5A iii, 8A). Because this fails to meet my definition for casque formation at this age, it appears that pneumatization of cranial bones occurs prior to their inflation as an incipient casque. Additionally, ossification of the frontals continues mediocaudally during this period as the caudodorsal fontanel begins to close Fig. 7C.

3.3.2. Immature: Phase 2

Immature individuals at this phase have elements, which have begun inflating (Figs. 5A iv, 7D–F, 8B, 9, 10C–D), but do not show obliteration of sutures between bones comprising the casque. In my ontogenetic series, 1.5 months is the youngest individual (TLG C037; see Appendix A) for which I detected inflation of any casque element (Fig. 8B). The nasals, median casque element, and mesethmoid inflate first (Figs. 5A iv, 8B, 10C). The origin of this inflation appears to derive medially at the median casque element and mesethmoid, which subsequently pneumatize the nasals laterally (Fig. 8B ii). This progression is evident inside these four individual bones as loosely spaced trabeculae proliferate while these elements expand dorsal to the orbit. Externally, the median casque element changes shape from concave to weakly sinusoidal in lateral view (Fig. 5A). In transverse section, the dorsal surface of the median casque element changes from a simple convexity (Fig. 8A) to take on a laterally flared, and dorsally expansive profile (Fig. 8B). In this phase the frontals ossify at their caudomedial margins to fully border the parietals, and no caudodorsal fontanel is present.

The earliest individual for which I observed all casque elements to be at least partially inflated was 10.4 months of age (Figs. 2, 9A–C; TLG C004). In this individual the nasals, median casque element, mesethmoid, lacrimals, and frontals now show at least some degree of inflation

and, as a result, contribution into the casque structure. However, contribution of the orbital processes of the lacrimals is minimal (Figs. 2, 9A–C). As a unit the casque has begun to expand laterally and caudally (Fig. 9A–C). In particular, the lateral pneumatized expansions of the nasals contact and begin to inflate the orbital processes of the lacrimals. The frontal processes of the nasals and median casque element both elongate caudally and contribute to the inflation of the frontals (Figs. 2, 9A–C). In this individual the dorsalmost margins of the frontals that contribute to the caudolateral casque have started to grow in a manner that reflects a flat surface folding onto itself (see Fig. 11A–C iv–vi) over the caudodorsal surface of the frontals (Figs. 3, 9A–C). The loosely spaced trabeculae within the casque now take on a distinctly "honeycombed" appearance.

The individual at 14.0 months of age (Figs. 4A, 9D–F; TLG C031; see Appendix A) clearly illustrates that each of the bony casque components is inflated (Fig. 3). Notably, this is the latest stage in my sample at which sutures are fully to mostly patent between all casque cranial elements (Figs. 3, 4A, 9D–F, 10D). There is some internal remodeling that encompasses the median casque element with the mesethmoid, nasals, and frontals, respectively (Fig. 4A). However, the surface furrows along sutures are deep (Figs. 3, 9D–F), and elements appear to be largely distinct in CT sections (Fig. 4A). The nasals and median casque element are more dorsally protrusive, and the median casque element has widened laterally (Fig. 9) compared to the 10.4-month-old individual (TLG C004). The orbital processes of the lacrimals in this individual have expanded dorsally to further contribute to the overall casque inflation.

3.3.3. Immature: Phase 3

Individuals in this phase have casque elements that are all inflated to some degree, and some elements are fused as indicated by obliterated sutures. By approximately 24.0 months of age (AMNH SKEL 963; see Appendix A) sutures between all bones contributing to the casque are largely obliterated (Fig. 10E). The interior of the casque now appears as a single unit of well-

pneumatized bone (Fig. 11B) with thicker bony margins where suture contacts used to be. The last of the partially patent sutures include superficial aspects of the orbital processes of the lacrimals with the corresponding nasal and frontal as well as the superficial, rostralmost border between the median casque element and mesethmoid (Fig. 10E). Simultaneously, the fused dorsal region (previously of nasals and mesethmoid origin), expands further dorsally, and the internal trabecular bone throughout all casque elements becomes more widely spaced (Fig. 11B). It is also at approximately this point when the orbital processes of the lacrimals and the dorsalmost margins of the frontals have enlarged enough to play a more prominent role as the lateral base of the casque. Finally, the caudodorsal portion of the frontal has osteo-developmentally folded further caudally atop itself (Figs. 10E, 11B v).

3.4. Bony Cranial Anatomy in Adult Specimens

The casques of mature individuals (> 4.0 years of age) are the widest, extend furthest caudally atop the neurocranium, and are most dorsally protrusive. As observed in other studies (e.g., Pycraft, 1900; Flower, 1871; Richardson, 1991; Mayr, 2018), no patent sutures could be visualized on the external surfaces of the casque, nor could I detect internal sutures despite the use of µCT imaging (see Fig. 11C; AMNH SKEL 962; ~4.0–5.0 years; also see Appendix A). This is consistent with a high degree of bone remodeling that occurs during the fast period of casque inflation and expansion in the transitionary period between immaturity and maturity (Fig. 10E–F). Within the internal trabeculae of the casque there are thin, flattened sections of bone that differ from surrounding, sparse honeycombing, and these appear to be remnants of bone-bone interfaces at which internal sutures once occurred. As adults, the internal struts of trabecular bone become so widely spaced that in some areas largely air-filled voids are prominent. This is especially true in the central to caudal regions of the internal casque (Fig. 11C, also see Naish & Perron 2016). These observations contrast with the rostral region of the casque, which shows thicker cortices and larger

struts of trabecular bone in adults. The casque is expanded further caudally via elongation of the nasals and median casque element (Fig. 10F) along with osteo-developmentally folded frontals (Fig. 11C vi). Minor folding also occurs rostrally via inflation of the median casque element atop the caudodorsal process of the premaxilla (Figs. 10F, 11A–C i–iii). Note, the premaxilla is distinct from the casque as it is non-inflated and does not fuse to any casque elements throughout ontogeny. As adults, casques may deviate from the midline, curving laterally to either the right or the left (Rothschild, 1900).

3.5. Summary of Inflations and Fusions of the Casque

It has been proposed that the developmental origin of casque pneumatization in *C. casuarius* is from the tympanic diverticula, through a series of tubes and compartments (Starck, 1995), rather than from the nasal sinuses. These passages appear to travel from the tympanic region through the quadrates, squamosals and caudolateral bones of the cranium and into the frontal bones (Starck, 1995). Witmer (1990) mentions that a caudodorsal diverticulum of the antorbital sinus provides some pneumatization to the mesethmoid, frontals, or both in some birds. This is accompanied by additional pneumatization of the middle ear (Witmer, 1990; Stark, 1995). I do not observe obvious interactions of the antorbital sinus with the multi-element internal casque cavity (endocasque) in *C. casuarius*; however, a more detailed study of this potential mechanism should be completed with cassowaries to provide further clarity. Although the frontals are not the first elements to contribute to the inflation of the casque structure, they do appear to be the first to pneumatize. I hypothesize that pneumatization of the median casque element originates from partial caudal contact with the frontals. Additionally, the tympanic origin of these cranial pneumatic sinuses may supply the basiparasphenoid, passing along its parasphenoid rostrum and traversing dorsally to the inferior aspect of the mesethmoid (Witmer, 1990). Notably, my growth series indicates that the ventral portion of the interorbital septum of the mesethmoid does not contact the

parasphenoid rostrum until *C. casuarius* have reached sub-adulthood (~24.0 months of age; Fig. 10E). Although the mesethmoid appears to begin pneumatization before this contact occurs, I cannot discount the contribution of the basiparasphenoid pneumaticity to subsequent mesethmoid inflation. Immature birds of ages 10.4 and 14.0 months (TLG C004 and TLG C031, respectively) in my study illustrate two small but characteristic dorsal swellings of the casque, which can be seen in lateral profile (Fig. 9B, E). Although it is tempting to interpret this morphology as a result of two sources of pneumatization, it occurs prior to the contact between the parasphenoid rostrum and mesethmoid (see Fig. 10E). Instead, I presume these surficial contours are from inflations of the nasals and median casque element prior to their fusion. Once sutures between the nasals and the median casque element close (between 14.0 and 24.0 months of age), the casque morphology becomes more uniformly convex in appearance. After sutural fusion between all casque elements occurs beyond 24.0 months of age, dorsal expansion of the casque increases relatively rapidly (Figs. 10E–F, 11B–C). Taken as a whole, I propose the sequence of incorporation of individual elements into the casque based on inflations and fusions is: (1) median casque element, (2) mesethmoid, (3) nasals, (4) frontals, and (5) lacrimals (see Fig. 10).

4. Discussion

4.1. Gross Morphology of the Casque

Although several authors have described cassowary casques previously (Parker, 1866; Flower, 1871; Marshall, 1872; Pycraft, 1900; Richardson, 1991; Naish & Perron, 2016; Mayr, 2018; Table 1), a complete understanding of southern cassowary casque osteological composition has been elusive. Cranial µCT data comparing the largest growth series of *C. casuarius* to date (n = 23) allowed me to track bony elements and approximate the timing and sequence by which they

are incorporated into the casque. I determined that the casques of cassowaries are composed of a greater variety of constituent parts than previously reported (Parker, 1866; Flower, 1871; Marshall, 1872; Pycraft, 1900; Richardson, 1991; Naish & Perron, 2016; Mayr, 2018). I find that the casque is comprised from contributions of two midline and three paired bony elements: median casque element, mesethmoid, nasals, lacrimals, and frontals.

Additionally, I found that initiation of incipient casque growth occurs relatively early in development (i.e., by approximately 1.5 months of age; Figs. 5A iv, 8B). Dodson (1975) was the first study to analyze the cranial metrics of an ontogenetic series of cassowaries and provided support for the positive allometry of *Casuarius* casques after approximately two years of age. These data were used by Dodson (1975) to make comparisons of cranial ornament development between cassowaries and hadrosaur dinosaurs. Later, these data were further figured by Farke et al., (2013) in a survey of ornamented archosaurs, showing that *Casuarius* ornaments are present during ontogeny by approximately 65–85% of adult body mass (i.e., roughly two years of age; Dodson, 1975; Farke et al., 2013). These studies provide a framework to compare the developmental timings of cranial ornaments across living and extinct taxa, and I believe my current study can contribute to this understanding by filling in the osteological timespan between neonate and subadult *C. casuarius* in which the dorsal expansion of the incipient casque appears and develops (Figs. 5, 8, 10).

4.2. Reinterpretation of Casque Elements

No previous study has identified the same combination of bony elements within the cassowary casque as I have identified here (Parker, 1866; Flower, 1871; Marshall, 1872; Pycraft, 1900; Richardson, 1991; Naish & Perron, 2016; Mayr, 2018; see Table 1). It is notable that prior examinations of cassowary casques have relied extensively on visual inspection (Parker, 1866; Flower, 1871; Marshall, 1872; Pycraft, 1900; Richardson, 1991; Naish & Perron, 2016; Mayr,

2018), analyzed adult individuals only (Flower, 1871; Richardson, 1991), utilized solitary immature specimens for hallmark species descriptions (*C. bennetti*, Parker, 1866; *C. galetus* (= *C. casuarius*), Marshall, 1872; *C. unappendiculatus* and *C. sclaterii* (= *C. casuarius*), Pycraft, 1900), or sampled from unknown species/subspecies complexes (*C. casuarius* and *Casuarius* sp., Mayr, 2018). Having documented regional, multi-element fusion in the casque within my sample, I suspect that casque growth along with interspecific differences in casque shape (and potentially in configuration or sequence of inflation) may have historically obscured the southern cassowary pattern. These issues likely explain differences in the literature regarding casque composition over the last 150 years.

Regarding midline elements, multiple ossification centers of the mesethmoid (i.e., interorbital septum and lamina dorsalis) have been described previously for ratites (e.g., Maxwell, 2009). My work identifies a similar ossification pattern in *C. casuarius* as has been described in *D. novaehollandiae* (Maxwell, 2009). My data also illustrate that the mesethmoid is a contributor to casque formation (Figs. 4, 10), which was hypothesized in initial interpretations (Parker, 1866; Flower, 1871; Marshall, 1872; Pycraft, 1900) as well as more recent work (Mayr, 2018). I also find, however, that the identity of the dorsalmost structure of the casque is not the lamina dorsalis of the mesethmoid, but rather a separate element (Figs. 3, 4, 5) identified herein as the median casque element (after Pycraft, 1900). The embryonic *C. casuarius* µCT data clearly show the gradual appearance of separate interorbital septum and lamina dorsalis ossification centers of the mesethmoid (Fig. 5A i–ii; TLG C032, ~HH40; TLG C030, ~HH41) from the more dorsal element. Once visible, these centers fuse to one another over a relatively short period of embryogenesis: approximately four days (TLG C030, ~HH41 = two separate mesethmoid elements; TLG C005, ~HH43 = single fused mesethmoid; see Appendix A). As a result, the identities of these elements could be easily missed in post-hatching individuals. My interpretation of the midline casque osteology is most consistent with Pycraft (1900), which includes the mesethmoid internally and the dorsalmost median casque element as an additional, midline contribution. This suggests that the

median casque element may be neomorphic in cassowaries. Additional studies tracing the developmental and evolutionary origin of this bone may help elucidate the coincident appearance of the bone and the casque in exclusively cassowary lineages.

For bilateral casque elements, the lacrimal bones merit discussion. To my knowledge, the lacrimals have only been recognized as potential elements of the casque by a single previous author (Flower, 1871), who described them from an adult specimen with casque sutures developmentally obliterated. I include the lacrimals as casque contributors based on µCT data, which illustrate that, (1) the lacrimals contribute structurally to the lateral base of the casque in *C. casuarius* (Figs. 3, 10), and (2) the orbital processes of the lacrimals become inflated in concert with other casque contributors (Fig. 4). Like the lacrimals, I also find the dorsalmost margins of the frontals contribute to the caudolateral regions of the casque base of southern cassowaries (Figs. 3, 10). Overall, the frontals provide an inferior platform for the caudalmost osteo-developmental folding that occurs (Fig. 11A–C iv–vi). The dorsalmost margins of the frontals first extend dorsally, and as other casque components expand caudodorsally, the frontals osteo-developmentally fold overtop themselves, even as caudal as the parietals, into adulthood (Figs. 10, 11C vi). Some authors have not mentioned the frontals as casque-participating elements (Parker, 1866; Marshall, 1872; Mayr, 2018), which is understandable considering that the adult phenotype obliterates the boundaries between the frontals and adjacent bones. In addition, the bony growth of the folded frontals can appear externally as if it is a remnant suture between the casque and the braincase (Fig. 2). Finally, previous studies have identified the nasals as elements largely contributing to the casque (Pycraft, 1900; Flower, 1871; Marshall, 1872; Mayr, 2018), which generally agrees with my findings for southern cassowaries. The premaxillary processes of the nasals are the only regions of these bones that do not become incorporated into the casque, instead contributing to the dorsal border of the bony nasal aperture (Figs. 3, 10).

4.3. Concluding Remarks

Cassowary casques are osteologically more complex than previously thought. Instead of one or three individual bones, the casque is composed of eight separate bony elements (Fig. 3), including a possibly neomorphic median casque element. Moreover, this configuration appears to be unique among modern birds (see Parker, 1866; Pycraft, 1900; Zusi, 1993; Maxwell, 2008; Maxwell, 2009; Mayr, 2018). I recommend that future studies focus on other cassowary species to determine if the putative neomorphic midline casque element is present throughout the genus, as implied by Pycraft (1900). Notably, the taxonomy of *Casuarius* has been highly speculative, due in part to potential hybridization (e.g., through tribal trading and transport of birds to different ranges; see Perron, 2016). Clearly demonstrating that study specimens are of the same species, and not hybrids, will be critical for addressing potential differences in casque composition across *Casuarius*. I suspect this point will be particularly important not only for tracking homologous bones during embryogenesis and ontogeny in *C. unappendiculatus* and *C. bennetti*, but also for directly comparing cassowary species to other archosaurs. Finally, I anticipate that a newfound understanding of casque osteology will also aid future investigations into the potential biological role(s) of cassowary casques, specifically, as well as for better understanding the phenotypic complexities of osteological ornaments among tetrapods more generally (Bickel & Losos, 2002; Jared et al., 2005; O'Brien et al., 2016; Felice & Goswami, 2018).

Table 1. Terminology by previous authors to describe bony elements contributing to cassowary casques

Publication	Described bony elements	Species
Parker (1866)	"ethmoid" (= mesethmoid)	*C. bennetti*
Flower (1871)	nasals, mesethmoid, lacrimals, frontals, parietals	*C. australis* (= *C. casuarius*)
Marshall (1872)	nasals, "ethmoid" (= mesethmoid)	*C. galetus* (= *C. casuarius*)
Pycraft (1900)	nasals, "median element of the casque" (= median casque element), mesethmoid, frontals	*C. unappendiculatus*, *C. sclaterii* (= *C. casuarius*)
Richardson (1991)	"calcified core" sitting atop cranial bones	*C. casuarius*
Naish & Perron (2016)	frontals	*C.* sp. (= *C. casuarius*)
Mayr (2018)	nasals, mesethmoid	*C. casuarius*, *C.* sp.
Green & Gignac (2020) (*this study*)	nasals, median casque element, mesethmoid, lacrimals, frontals	*C. casuarius*

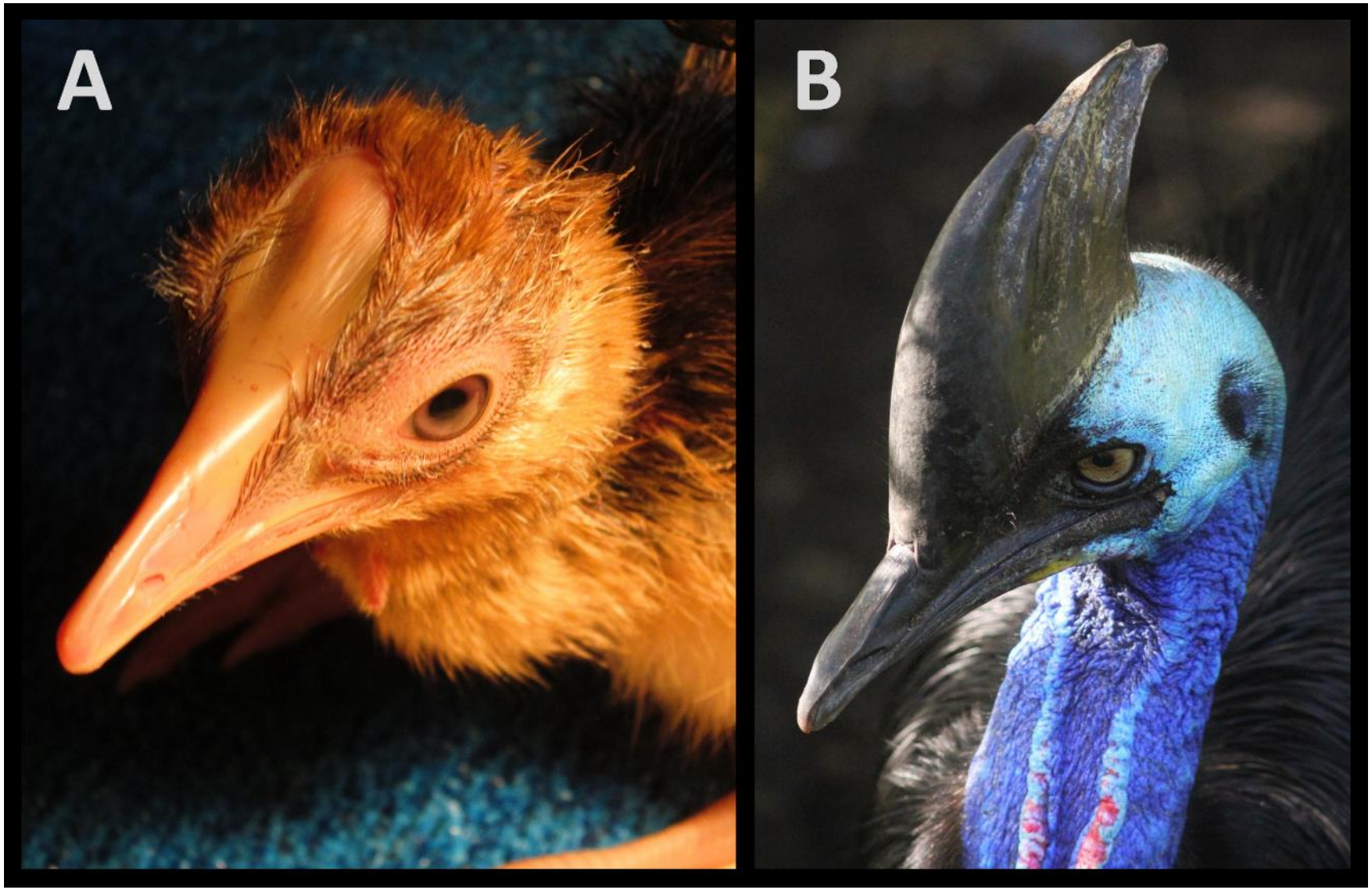
A
B

Figure 1. Photographs depicting the extensive soft- and hard-tissue changes that cassowaries undergo over ontogeny. (A) Southern cassowary (*Casuarius casuarius*) neonate demonstrating cranial anatomy prior to casque growth with a flattened keratinized shield on the dorsal surface of the head, extending caudally from the bill. (B) A mature *C. casuarius* with an enlarged casque, which is a keratinized and bony dorsal expansion of the shield in (A). Photos by T. L. G.

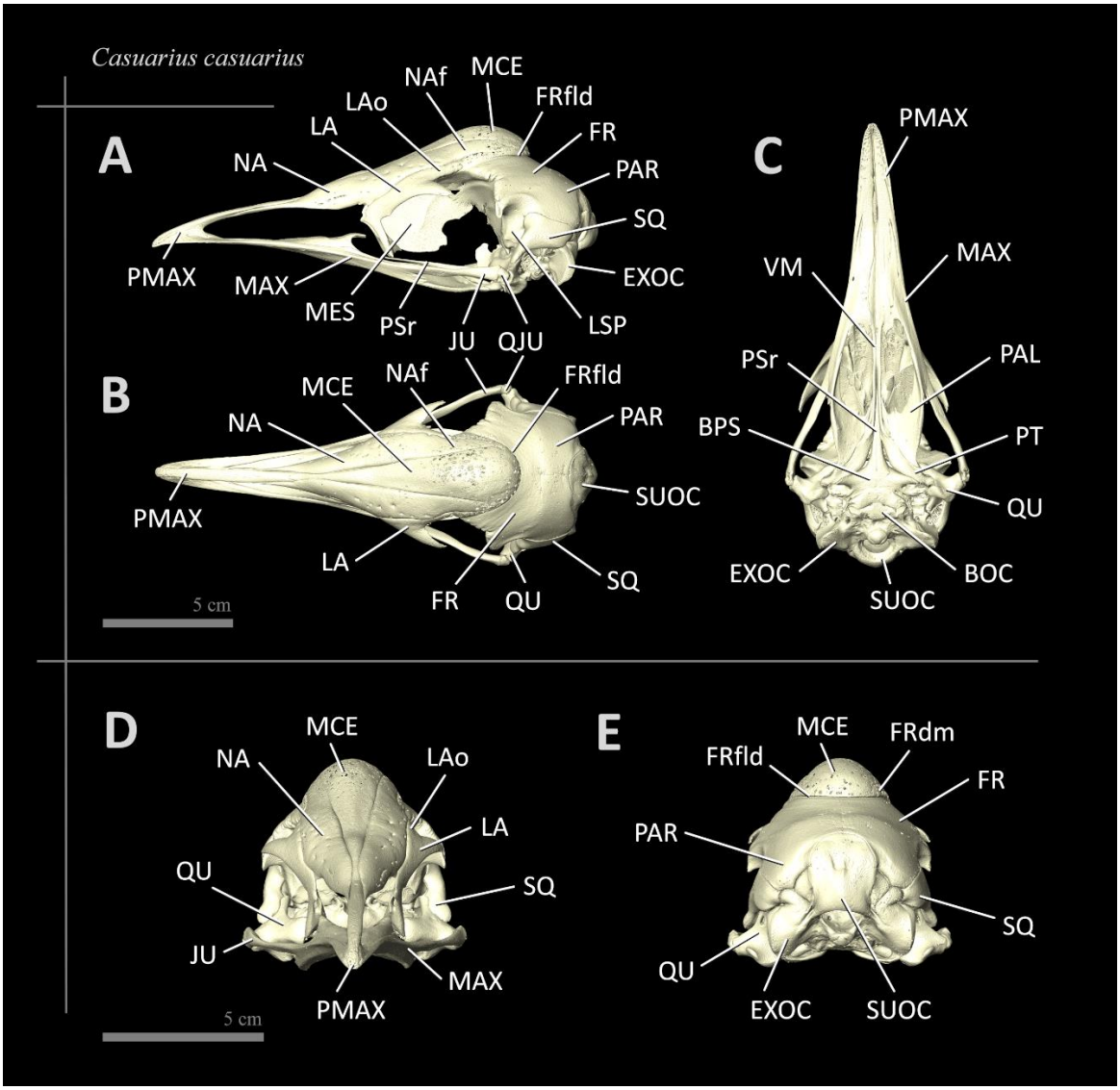
Casuarius casuarius
A
NA
LA
LAo
NAf
MCE
FRfld
FR
PAR
SQ
EXOC
LSP
QJU
JU
PSr
MES
MAX
PMAX
B
NA
MCE
NAf
FRfld
PAR
SUOC
SQ
QU
FR
LA
PMAX
5 cm
C
PMAX
MAX
VM
PAL
PSr
BPS
PT
QU
BOC
SUOC
EXOC
D
NA
MCE
LAo
LA
SQ
QU
JU
MAX
PMAX
5 cm
E
FRfld
MCE
FRdm
FR
PAR
SQ
QU
EXOC
SUOC

Figure 2. Digital rendering of the cranial osteology of an immature 10.4-month-old *Casuarius casuarius* (TLG C004) in (A) left lateral, (B) dorsal, (C) ventral, (D) rostral, and (E) caudal views. Abbreviations: BOC = basioccipital; BPS = basiparasphenoid; EXOC = exoccipital; FR = frontal; FRdm = dorsalmost margin of the frontal; FRfld = frontal fold; JU = jugal; LA = lacrimal; LAo = orbital process of lacrimal; LSP = laterosphenoid; MAX = maxilla; MCE = median casque element; MES = mesethmoid; NA = nasal; NAf = frontal process of nasal; PAL = palatine; PAR = parietal; PMAX = premaxilla; PSr = parasphenoid rostrum; PT = pterygoid; QJU = quadratojugal; QU = quadrate; SQ = squamosal; SUOC = supraoccipital; VM = vomer. See Appendix A for additional specimen information.

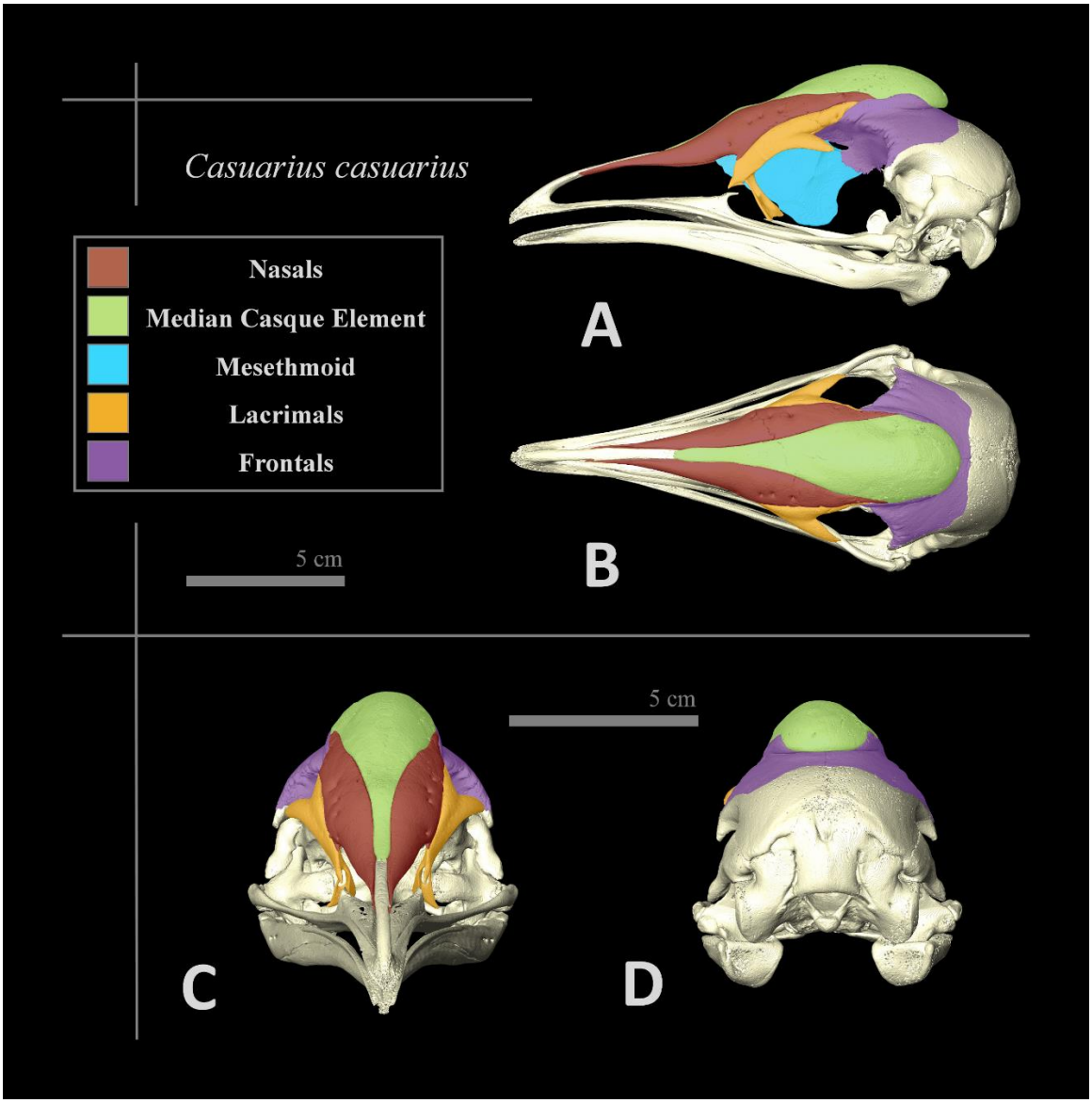

Figure 3. Digital rendering representing the cranial osteology of a 14-month-old immature *Casuarius casuarius* (TLG C031) in (A) left lateral, (B) dorsal, (C) rostral, and (D) caudal views with casque bones false colored (maroon = nasals; green = median casque element; blue = mesethmoid; orange = lacrimals; purple = frontals; see Appendix A for additional specimen information).

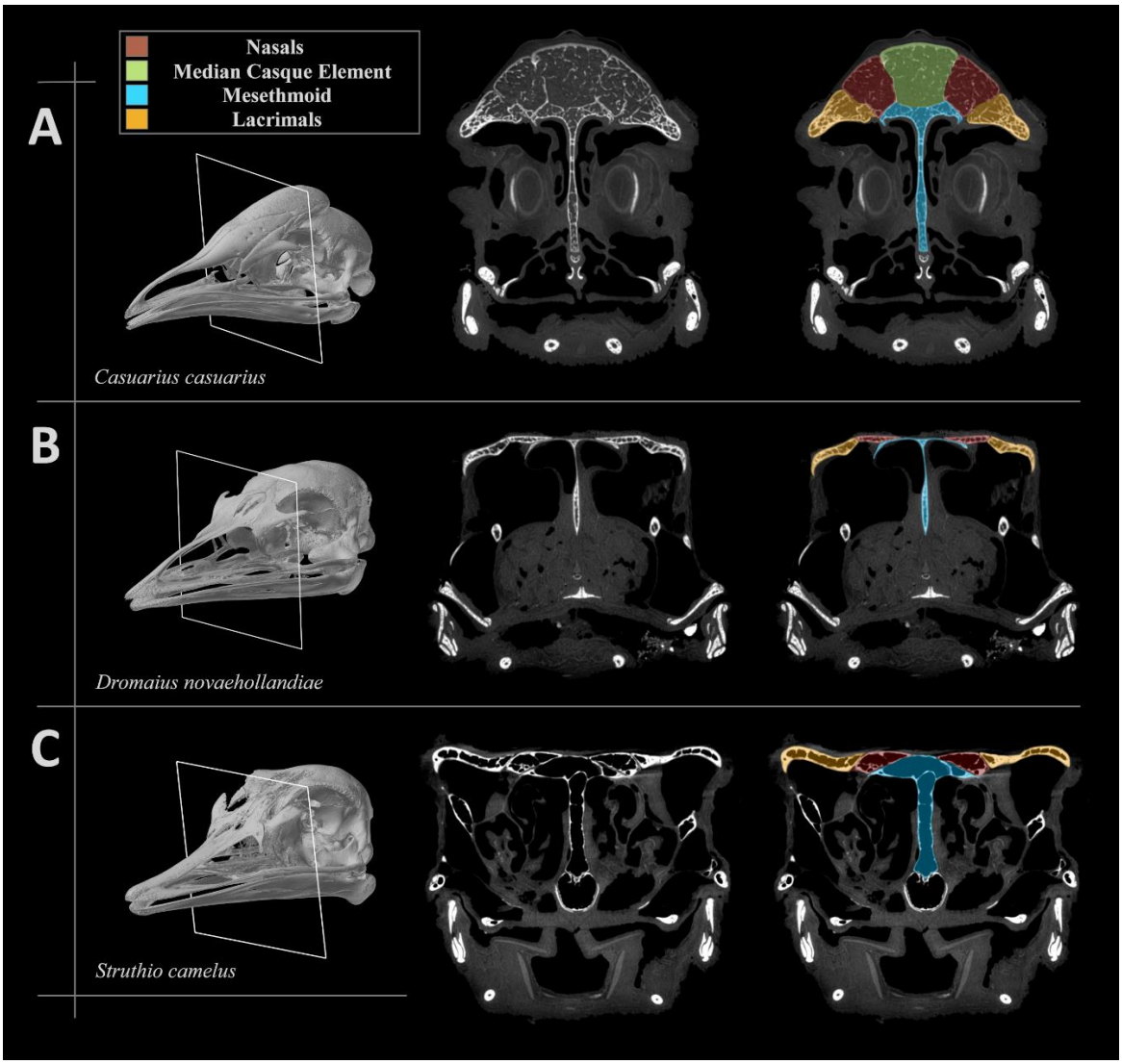

Figure 4. µCT transverse sections through skulls (left column; white squares) of an immature (A) *Casuarius casuarius* (TLG C031; 14.0 months old), (B) *Dromaius novaehollandiae* (TLG E115; 12.0 months old), and (C) *Struthio camelus* (TLG SC063; 15.0 months old). CT sections (middle column) are false-colored (right column) to illustrate the inclusion of the mesethmoid (blue) and lacrimals (orange) as casque components in *C. casuarius* based on increased dorsal expansion compared to non-casqued ratites. (For additional specimen details see Appendix A; maroon = nasals; green = median casque element.)

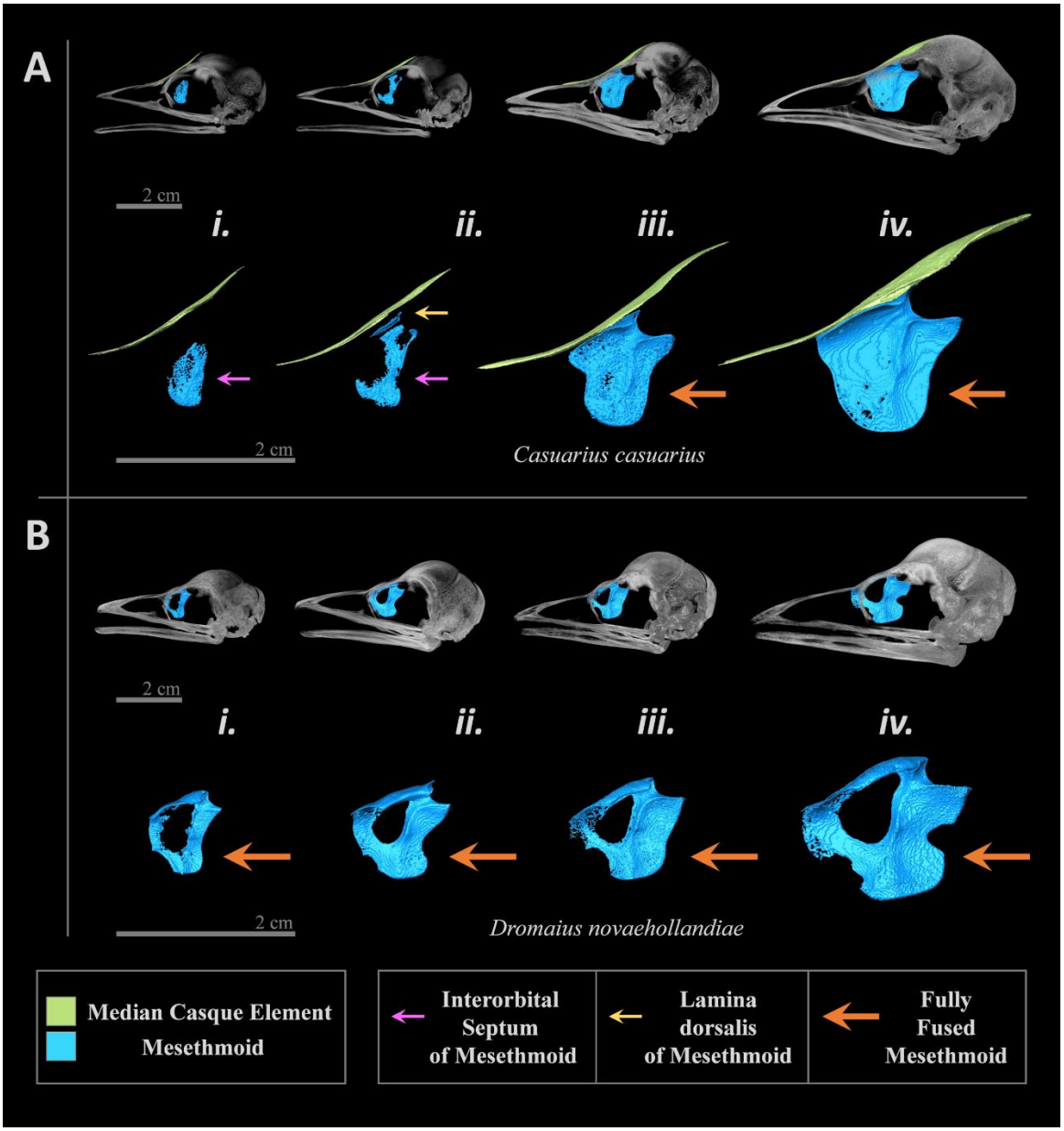
A
2 cm
i.
ii.
iii.
iv.
2 cm
Casuarius casuarius
B
2 cm
i.
ii.
iii.
iv.
2 cm
Dromaius novaehollandiae
Median Casque Element
Mesethmoid
Interorbital Septum of Mesethmoid
Lamina dorsalis of Mesethmoid
Fully Fused Mesethmoid

Figure 5. Left lateral view of digital renderings of select skull elements (green = median casque element; blue = mesethmoid ossifications) from early development in (A) *Casuarius casuarius* (i = embryonic, ~HH40, TLG C032; ii = embryonic, ~HH41, TLG C030; iii = immature, seven days old, TLG C025; iv = immature, 1.5 months old, TLG C037) and (B) *Dromaius novaehollandiae* (i = embryonic, ~HH41, TLG E139; ii = embryonic, ~HH45, TLG E137; iii = immature, five days old, TLG E093; iv = immature, 1.0 month old, TLG E098) with intraspecific samples arranged by skull sizes. Comparisons to *D. novaehollandiae* illustrate that the *C. casuarius* median casque element is a distinct bone from the mesethmoid. Colored arrows indicate specific components of the developing mesethmoid: small purple arrows = interorbital septum ossification center of the mesethmoid; small yellow arrow = lamina dorsalis ossification center of the mesethmoid; large orange arrows = ossification centers joined as a contiguous mesethmoid bone. (See Appendix A for additional specimen information.)

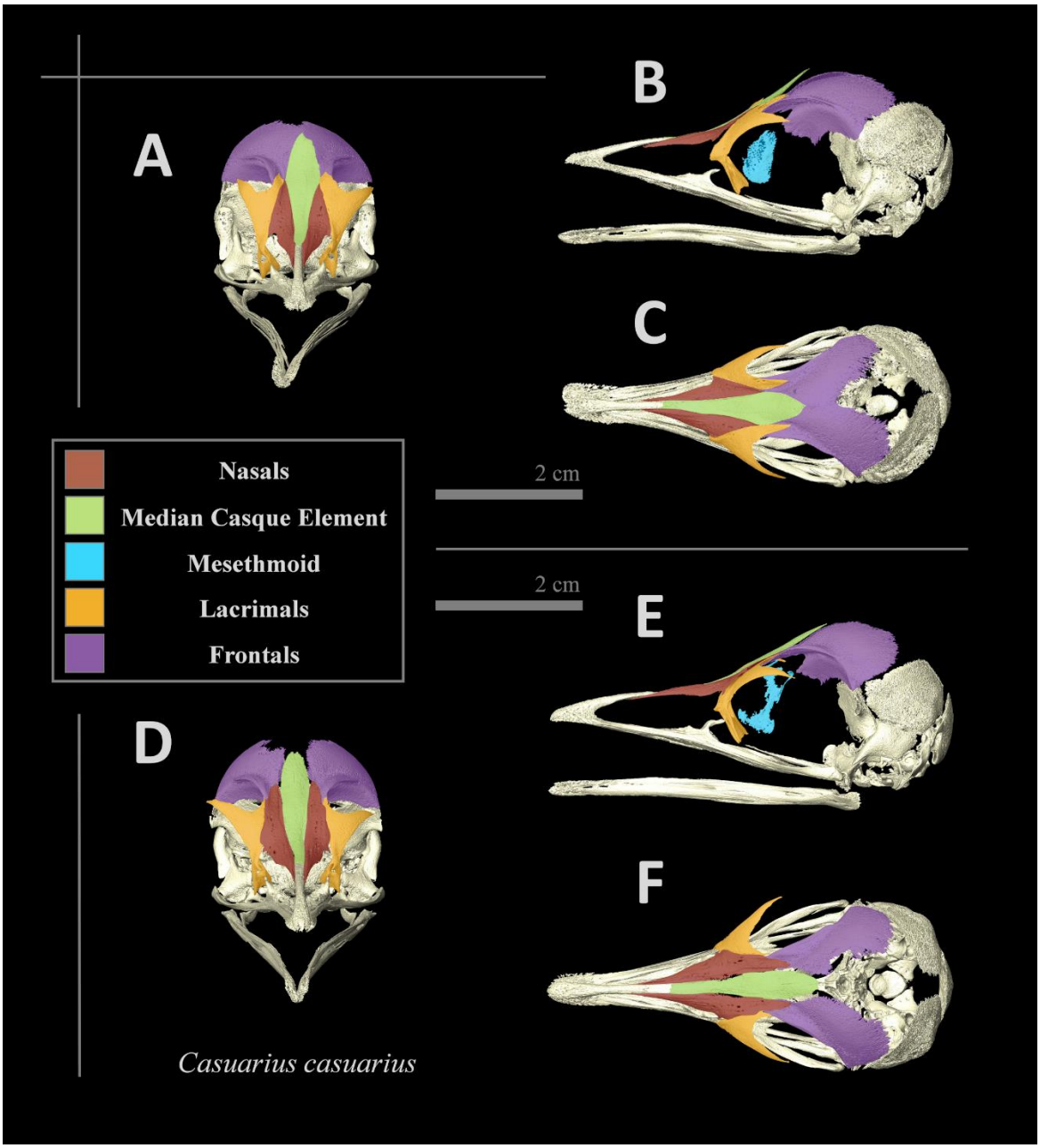
A
B
C
D
E
F
Nasals
Median Casque Element
Mesethmoid
Lacrimals
Frontals
2 cm
2 cm
Casuarius casuarius

Figure 6. Digital rendering of embryonic *Casuarius casuarius* at stages (A–C) ~HH40 (TLG C032) and (D–F) ~HH41 (TLG C030). Skulls are rendered in (A, D) rostral, (B, E) left lateral, and (C, F) dorsal views with elements that will contribute to casque as false colored (maroon = nasals; green = median casque element; blue = mesethmoid and/or mesethmoid ossification centers; orange = lacrimals; purple = frontals; Due to the soft nature of TLG C032, the frontals artificially overlapped at the dorsal midline during μCT imaging; see Appendix A for additional specimen information).

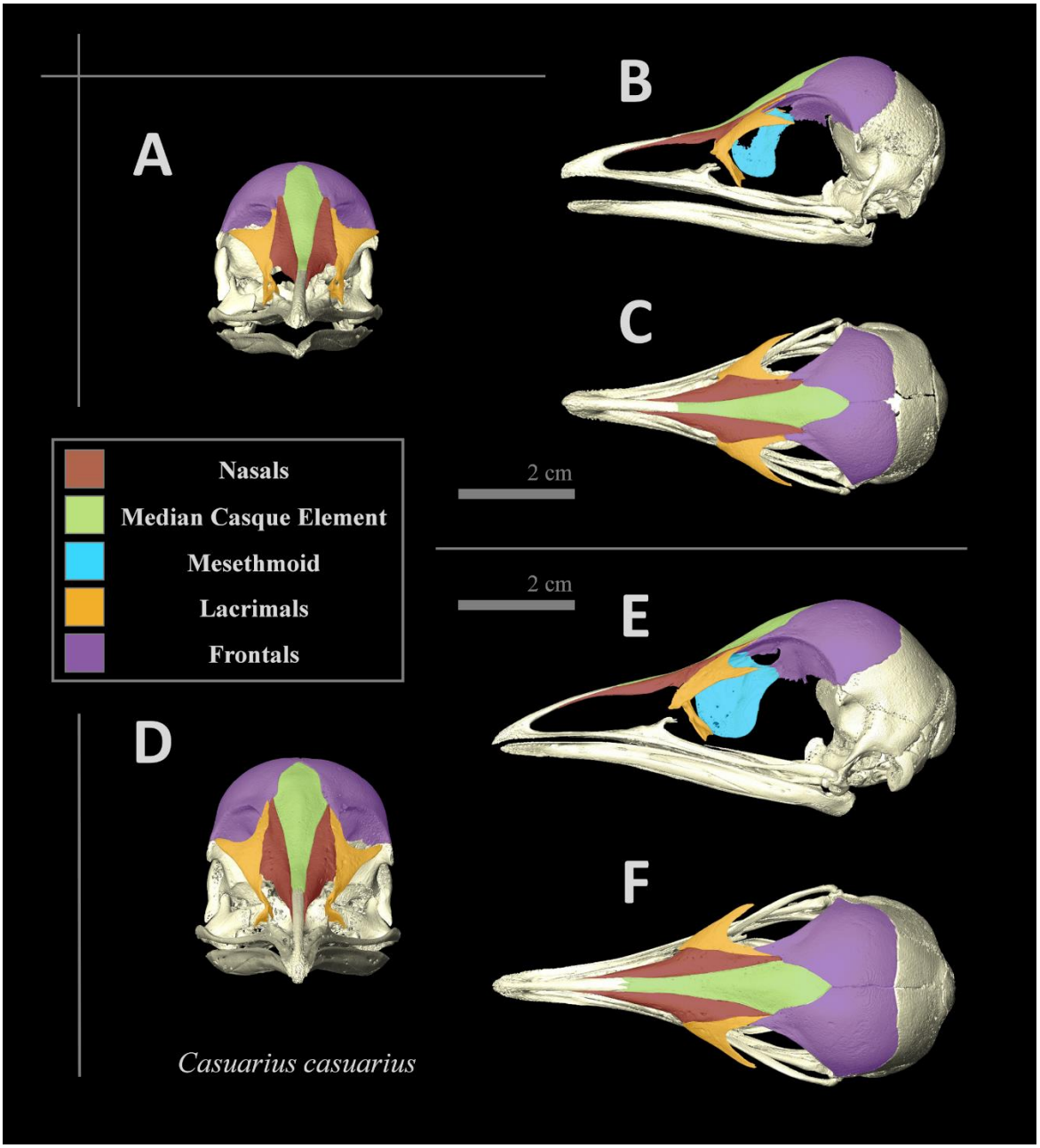

Figure 7. Digital rendering of immature *Casuarius casuarius* skulls at (A–C) one day (TLG C010) and (D–F) 1.5 months of age (= 47 days; TLG C037). Skulls are rendered in (A, D) rostral (B, E) left lateral, and (C, F) dorsal views with elements that will contribute to the adult casque colored (maroon = nasals; green = median casque element; blue = mesethmoid; orange = lacrimals; purple = frontals; see Appendix A for additional specimen information).

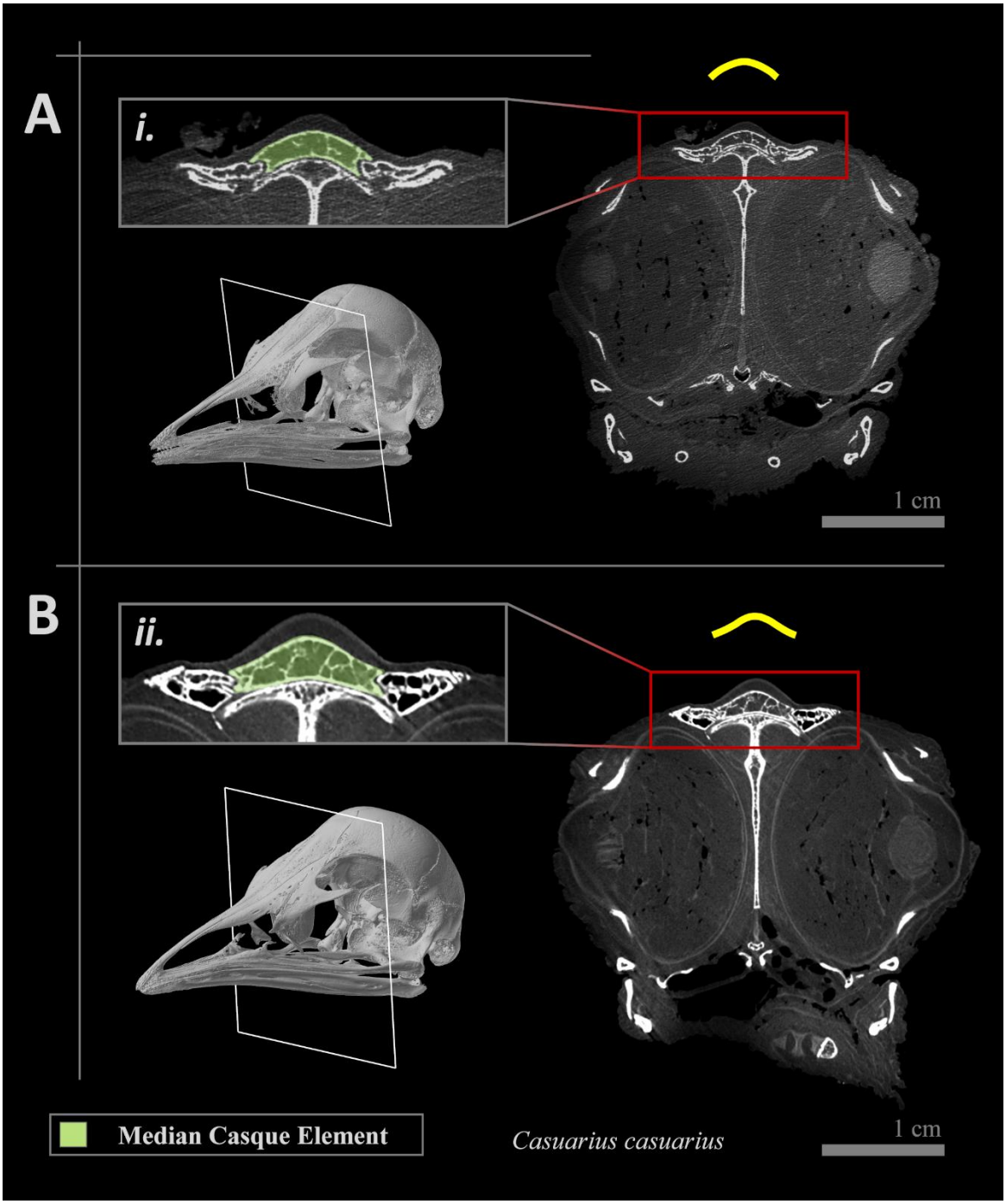
A
i.
1 cm
B
ii.
Median Casque Element
Casuarius casuarius
1 cm

Figure 8. Two- and three-dimensional µCT skull projections of *Casuarius casuarius* specimens (A) (TLG C043; 42 days old) and (B) (TLG C037; 1.5 months old). 3D skulls (left) indicate locations of transverse sections (white squares) that correspond to 2D slices (right, with reticle indicating enhanced view). Small red rectangles contain areas of interest for the initial inflation of the casque, and larger grey rectangles are enlarged views of: (i) a condition that although pneumatized is unelaborated, and (ii) a condition that is both pneumatized and elaborated (indicating an incipient casque). Highlighted osteology (green) represents median casque elements. Yellow lines illustrate the overall shape of the dorsal surface of the median casque element before (top) and during (bottom) initial casque initiation, changing from a simple to a flared convexity in transverse view. (See Appendix A for additional specimen information.)

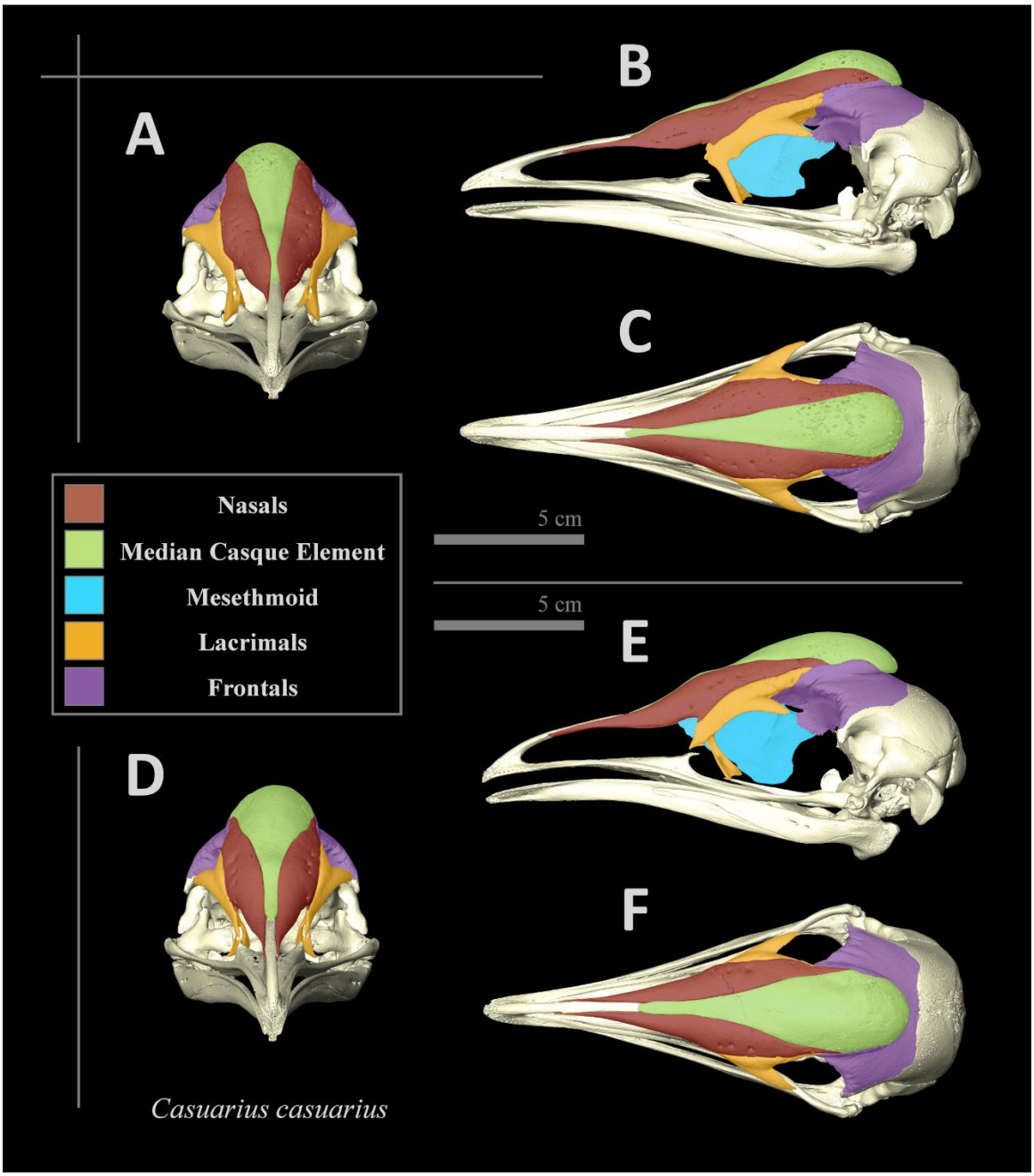

Figure 9. Digital rendering of immature *Casuarius casuarius* at (A–C) 10.4 months (TLG C004) and (D–F) 14.0 months of age (TLG C031). Skulls shown in (A, D) rostral, (B, E) left lateral, and (C, F) dorsal views with elements that contribute to casque false colored (maroon = nasals; green = median casque element; blue = mesethmoid; orange = lacrimals; purple = frontals; see Appendix A for additional specimen information).

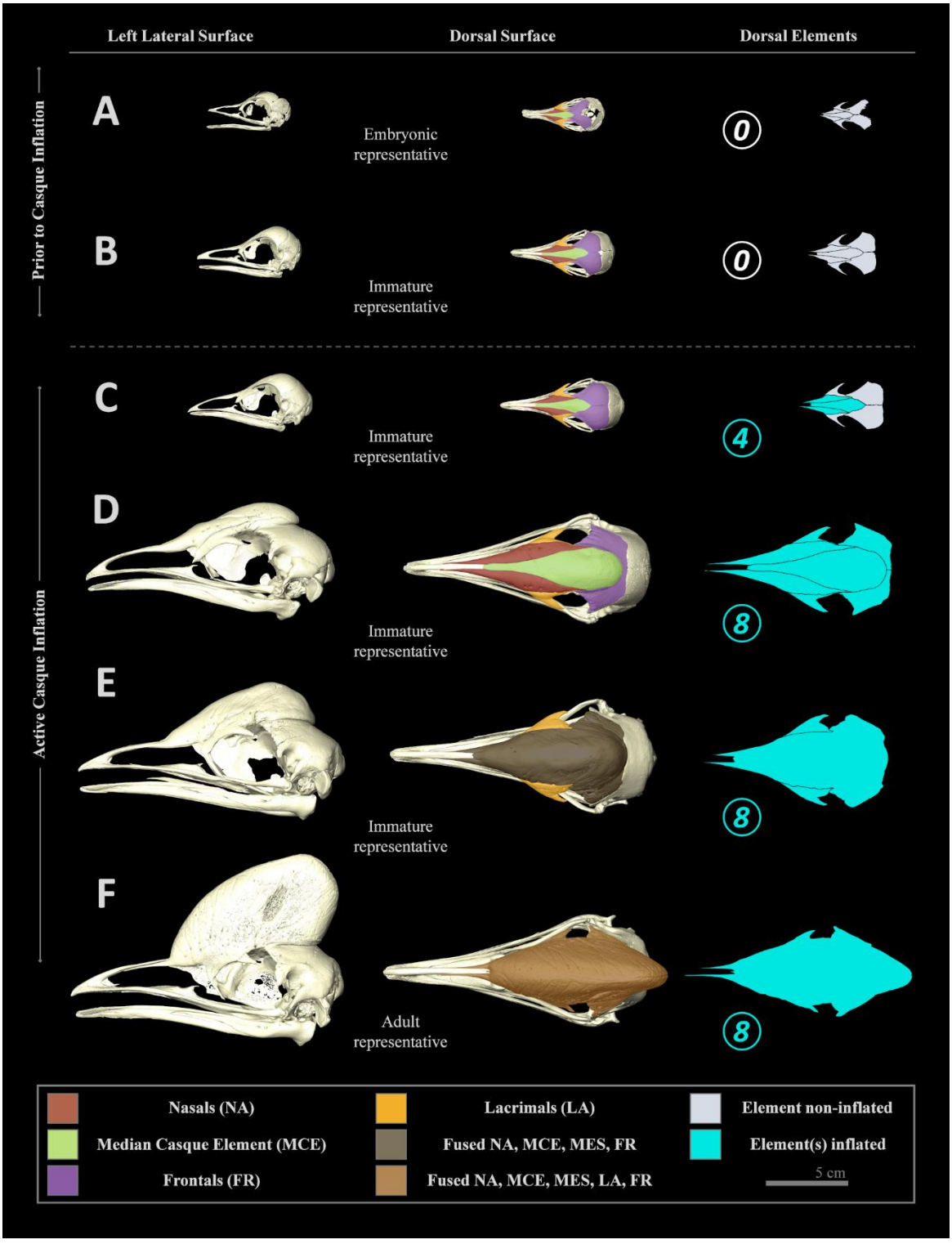
Left Lateral Surface
Dorsal Surface
Dorsal Elements
Prior to Casque Inflation
Active Casque Inflation
A
Embryonic representative
0
B
Immature representative
0
C
Immature representative
4
D
Immature representative
8
E
Immature representative
8
F
Adult representative
8
Nasals (NA)
Lacrimals (LA)
Element non-inflated
Median Casque Element (MCE)
Fused NA, MCE, MES, FR
Element(s) inflated
Frontals (FR)
Fused NA, MCE, MES, LA, FR
5 cm

Figure 10. Sequence of casque development of *Casuarius casuarius* individuals from embryo to adult (A = embryo, ~HH40, TLG C032; B = immature, one day old, TLG C010; C = immature, 1.5 months old, TLG C037; D = immature, 14.0 months old, TLG C031; E = immature, ~24.0 months old, AMNH SKEL 963; F = adult, ~4.0–5.0 years, AMNH SKEL 962) in left lateral view (left column). Colors indicate casque bones and completed bony fusions (middle column), and pneumatic inflations (right column). (1) Casque bones: maroon = nasals, green = median casque element, orange = lacrimals, purple = frontals; (2) completed bony fusions: dark brown = NA (nasals) + MCE (median casque element) + MES (mesethmoid) + FR (frontals); light brown = NA + MCE + MES + FR + LA (lacrimals); and (3) pneumatic inflations: grey = non-inflated, light blue = inflated; circled. Encircled Arabic numbers indicate the number of inflated casque elements from zero–eight (this count includes the mesethmoid, which is not visible from the dorsal view). For additional specimen details see Appendix A.

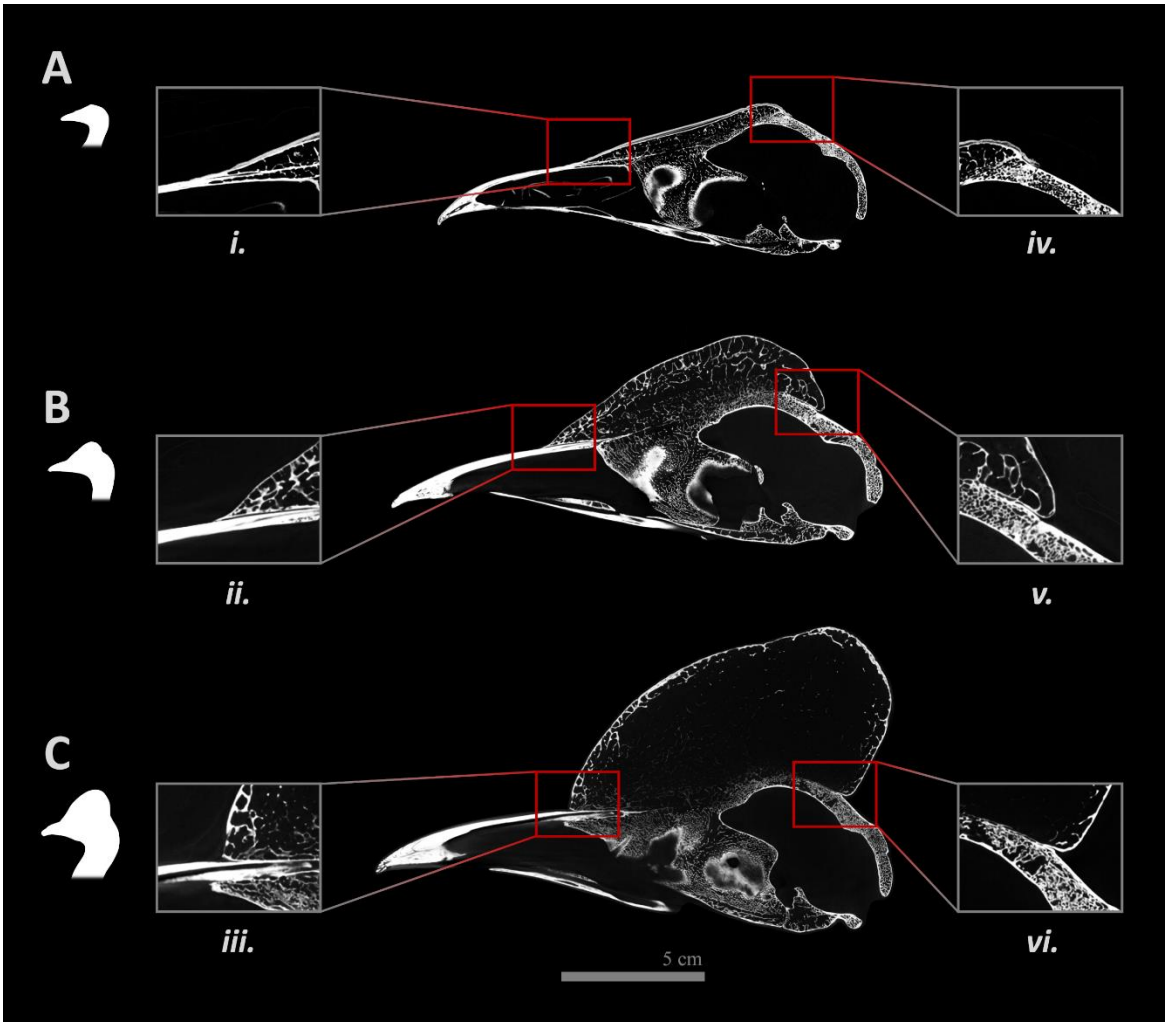

Figure 11. Osteological progression of *Casuarius casuarius* casques with parasagittal sections taken adjacent to the midline (A = immature, ~5.5 months , TLG C002; B = immature, ~24.0 months, AMNH SKEL 963; C = adult, ~4.0–5.0 years, AMNH SKEL 962). Smaller red rectangles contain areas of developmental casque folding, which are highlighted in larger grey rectangles for (i–iii) rostral folding over the caudodorsal process of the premaxilla and (iv–vi) caudal folding over the frontals. White silhouettes indicate progress in overall casque maturity for each individual; for additional specimen details see Appendix A.

CHAPTER III

ONTOGENETIC ALLOMETRY AND FUNCTIONAL IMPLICATIONS OF THE SOUTHERN CASSOWARY CASQUE

Abstract

Cranial ornaments are common among extant and extinct archosaurs, having evolved independently numerous times. Ontogenetic analysis of these structures is fairly uncommon; however, such studies on living taxa are particularly important for the clarification of growth, functional correlations, and evolutionary processes that shape ornaments. In the current study, I examined how the bony cranial casques and keratinous coverings of extant southern cassowaries (*Casuarius casuarius*) grow throughout ontogeny. I used ontogenetic allometry to test the hypotheses that (1) keratinous casque scaling is sexually dimorphic and (2) the bony and keratin components of the casque both scale with positive allometry compared to non-casque linear measurements of the skull. Casque variation appears moderate compared to other birds; however, I did not detect differences in male and female keratinous casque growth trajectories. My data suggest that height and basal length (of bony and keratinous casques) scale with strong positive allometry from the point of casque initiation through adulthood compared to skull length and width. Much of the osseous and keratinous casque growth occurs prior to sexual maturity, which leads me to consider how ornament scaling relates to issues of cassowary ecology and life history. I find that

casque ontogeny and its resulting phenotype are plausibly aligned with proposed biological roles as a visual signal of reproductive capability and status as well as for temperature and osmotic regulation.

1. Introduction

Modern cassowaries (*Casuarius* spp.) are unique among paleognathous birds (e.g., ostriches, rheas, emus, kiwis, tinamous) in possessing cranial ornamentation in the form of elaborate casques. The southern cassowary (*C. casuarius*) casque is a soft-tissue covered, dorsal expansion of the skull. Osteologically, it consists of eight cranial bones, including the midline median casque element and mesethmoid bones as well as right and left nasal, frontal, and lacrimal bones (Green & Gignac, 2020; Chapter II). Once skeletally mature, these elements compose a casing of thin-walled cortical bone with a highly pneumatized internal network of trabeculae (Pycraft, 1900; Naish & Perron, 2016; Green & Gignac, 2020; Chapter II), surrounded fully by a keratinous sheath. As a unit, therefore, the casques of cassowaries are composed of a visible keratinous outer component and deeper bony core (see Figs. 1, 2). Previous studies of neognathous birds (Angst et al., 2019) and bovid mammals (Calamari & Fossum, 2017) have established exemplar, baseline anatomical comparisons of the keratinous and osseous portions of cranial ornaments. These have helped shape our understanding outer keratinous ornaments in behavioral, developmental, and evolutionary contexts, as well as frame homologies of ornament bony cores across modern fossilized taxa (Calamari & Fossum, 2017; Angst et al., 2019). Currently, we lack this quantitative understanding for how the casque grows in cassowaries. As a result, the relationship between ornament features, cassowary behaviors, and life-history milestones, such as sexual maturity (see Naish & Perron, 2016), is also poorly understood. Filling this gap is necessary to place the headgear of cassowaries into a comparative framework with other ornamented birds,

which will enable researchers to implicate casque function(s) in ecological and evolutionary contexts. In this study I address ontogenetic scaling of the casque by examining its bony core and keratinous sheath separately to provide such a foundation.

Southern cassowary casque ontogeny can be broadly separated into three periods—neonate, immature, and mature—with specific osteological traits characterizing each (Green & Gignac, 2020; Chapter II). Phase 1 is the period prior to casque initiation, which does not occur until approximately 1.5 months of age (Green & Gignac, 2020; Chapter II; see Fig. 1A). Post-hatching cassowaries superficially resemble other immature ratites (e.g., emus) in profile during this period. Casque initiation (beginning of phase 2) occurs first as the bony dorsal expansion of the midline casque elements superior to the orbit Green & Gignac (2020). This developmental milestone is difficult to discern superficially due to overlying keratin. However, it is specifically evident in micro-computed tomography (μCT) transverse slices as the dorsalmost surface of the median casque element progresses from convex to sinusoidal in shape (Green & Gignac, 2020; Chapter II). Following this is a relatively rapid period of skull growth during immaturity, characterized by osteological fusions and casque expansions (Green & Gignac, 2020; Chapter II). Inflation (i.e., extreme pneumatic expansion that leads to element enlargement) of individual casque bones will eventually leads to a series of weak sutural fusions of individual casque elements to one another: first the median casque element and mesethmoid fuse, followed sequentially by the nasals, frontals, and lacrimals (Green & Gignac, 2020; Chapter II). Sutures become largely obliterated between all casque elements prior to sexual maturity, producing a smooth and uniform bony surface. During phase 3 the casque inflates as a unit, continuing to expand the now-joined pneumatic sinuses simultaneously into adulthood (Green & Gignac, 2020; Chapter II). Externally, keratinous sheathing appears to conform tightly to the bony core in especially neonate and immature individuals. At maturity, both female and male southern cassowaries possess the iconically tall, laterally compressed, and rostrocaudally expanded headgear commonly associated with these birds (Green & Gignac, 2020; Chapter II; see Fig. 2). It appears that either the keratin

only, or both the bony and keratin components of the casque, continue to enlarge in adulthood (albeit at a much-reduced rate; Dodson, 1975); however, this life stage has not been well studied.

Transitions between osteological growth periods and the resulting expansion of the casque may correlate or contribute to major life-history shifts by differentiating sexes, signaling maturity, and/or enabling new behaviors, such as thermoregulation (Bubenik & Bubenik 1990; Buchholz, 1991; Jones & Hunter, 1999; Jared et al., 2005; Gamble, 2007; Stankowich, 2012; Naish & Perron, 2016; Mayr, 2018; Eastick et al., 2019). However, evaluating the potential functional morphologies of the casque remains difficult because we do not have a quantitative understanding of its developmental morphologies. Gaining this understanding would enable us to better interpret the ecological and evolutionary significance of the structure as well as potentially inform the origins of such ornaments in cassowaries, other birds, and more distantly related archosaurs (e.g., Padian & Horner, 2011; Knell & Sampson, 2011; Hone et al., 2012). I address this gap by quantifying bony and keratinous casque size as well as evaluated potential sexual dimorphism of the keratinous casque across ontogeny in *C. casuarius*. To achieve these aims, I (1) tested whether sexual dimorphism in keratinous cassowary casque growth trajectories can be detected, and (2) evaluated the hypothesis that the hypertrophy of the casque is due to positive allometry of both the bony and keratinous casque components. I investigated this through inspection of intraspecific linear measurements for osseous and keratinous casque height and basal length across ontogeny, including sampling of known-sex *C. casuarius* specimens. I compared bony growth to that of the overlying keratin sheath to discuss how southern cassowary ornaments relate to their life history and ecology, propose how casque growth is compatible with previously proposed display and thermoregulatory functions, and provide a framework for cassowaries as a modern analog to interpret bony and keratinous cranial headgear in the archosaur fossil record.

2. Material and Methods

2.1. Data Collection

In total, 74 *C. casuarius* specimens (20 immature, 54 adults) were sampled for this study (see Table 1, 2). Because some samples were µCT scanned, nine individuals were used in both the bony and keratinous casque samples (5 immature, 4 adults). The sample ranged from individuals at the earliest casque initiation stage (1.5 months) to older, mature adults (at least 35.7 years). Because the casque does not initiate until after phase 1, I focused on phase 2 and phase 3 individuals, which were combined in my analyses because there were not enough individuals from each category to be tested separately with sufficient statistical power. *Casuarius casuarius* data were collected from specimens from the American Museum of Natural History (AMNH; New York, NY, USA), Cassowary Conservation Project (CCP; Fort Pierce, FL, USA), Denver Museum of Nature and Science (DMNS; Denver, CO, USA), Melbourne Museum (Museums Victoria, MV; Melbourne, VIC, AU), Museum of Osteology (MOO; Oklahoma City, OK, USA), Natural History Museum (NHMUK; Tring, UK), Queensland Museum (QM; Brisbane, QLD, AU), Sedgwick County Zoo (SCZ; Wichita, KS, USA), and T. L. Green Research Collection (TLG; Tulsa, OK, USA). Status as immature individuals was confirmed based on size, the presence of brown feathers, and osteological correlates indicated by Green & Gignac (2020), such as unfused elements of the interorbital septum. Because many species-specific colorations develop fully only in adults, detailed histories that included taxonomic description and collection location data were required for positive identification of immature individuals as *C. casuarius*, specifically (Rothschild, 1900; Perron, 2016). Adult specimens were identified based on presence of exclusively black plumage, breeding success, or museum voucher specifying maturity. Taxonomic status of adults as *C. casuarius* was determined based on previously established criteria relating to casque appearance, wattle number, and coloration (Marshall, 1872; Rothschild, 1900; Perron, 2016) as well as

osteological correlates identified by Green & Gignac (2020), such as fused elements of the interorbital septum. Sexes were determined for 49 individuals (bony and keratinous specimens) via institutional records, dissections, or genetic testing (Animal Genetics, Avian Biotech, Tallahassee, FL, USA). No institutional animal care and use protocol was required for this study as all data were obtained from museum collections or cadaveric specimens collected opportunistically after death.

The bony casques of 28 *C. casuarius* specimens (nine immature, 19 adults) were examined. Nine of these individuals were of known sex (five females, four males). Nineteen specimens were osteologically prepared via dermestid beetle cleaning or maceration, enabling physical removal of keratinous sheathing for bony measurements. The remaining nine specimens were scanned via µCT, allowing for digital removal of overlying keratin for osteological measurements. Osteological specimen information is available in Table 1.

The keratinous casques of 55 *C. casuarius* specimens (16 immature, 39 adults) were also examined. Forty-seven of these individuals were of known sex (18 females, 29 males). The keratin sheathings of the casque and bill were preserved intact on all of these cranial specimens. The same nine µCT scanned specimens used in the osteological sample were included here although they were remeasured for related morphologies. Keratinous specimen information is available in Table 2.

Micro-computed tomography image data were collected on two scanning systems: (1) a 2010 GE phoenix v|tome|x s240 high-resolution microfocus computed tomography system (General Electric, Fairfield, CT, USA) housed in the Microscopy and Imaging Facility of the AMNH, and (2) a 2018 Nikon XT H 225 ST µCT system housed at the MicroCT Imaging Consortium for Research and Outreach (MICRO; Fayetteville, AR, USA). Based on system optimizations, scanning parameters of specimens varied from 60–196 kilovolts (kV), 60–207 microamps (µA), and 200–500 millisecond (ms) exposures with isometric voxel size at resolutions between 52.67–117.97 micrometers (µm). Computed tomography TIFF stacks were exported and cropped of peripheral background pixels to minimize file volumes using ImageJ (v. 1, US National

Institutes of Health, Bethesda, MD). Digital skull models were rendered three-dimensionally (3D) in the programs Avizo (versions 9–9.7; Visualization Science Group, Burlington, MA, USA; Thermo-Fisher Scientific; Waltham, MA, USA) and AvizoLite (version 2019; Thermo-Fisher Scientific), using a combination of automatic and manual segmentation.

Linear measurements were taken for physical and digital specimens. For samples in hand a 300-Millimeter (mm) Stainless Steel Absolute Digital Caliper (Taylor Toolworks, Columbia, MO, USA; accuracy of ±0.03 mm per 300 mm) was used. Bony specimens were measured (in mm) to determine bony casque basal length (distance between rostral and caudalmost extents of the bony casque at the base), bony casque height (distance between the most dorsal extent of the bony casque and most dorsal extent of bone contributing to the orbit), skull length (from the rostral tip of the premaxilla to the caudalmost extent of the supraoccipital bone), and skull width (span across lateral surfaces of right and left jugal-quadratojugal junctions) (Fig. 3). Linear measurements (in mm) were taken from physical, keratinous specimens in order to determine keratinous casque basal length (distance between rostral and caudalmost extents of the keratinous casque at the base), keratinous casque height (distance between the most dorsal extent of the keratinous casque and most dorsal extent of skin contributing to the orbit), head length (from the rostral tip of the premaxillary keratin to the caudalmost extent of the supraoccipital region; palpated for bony landmarks), and head width (span across lateral surfaces of right and left jugal-quadratojugal regions; palpated for bony landmarks) (Fig. 4). The same linear distances were collected from digital samples (in mm) in Avizo and Avizo Lite by drawing straight lines using the "Measurement" module, which allowed keratinous and bony casque measurements to be collected from the nine µCT-scanned individuals. Casque height measurements were specifically taken as the highest dorsal extent of the casque perpendicular to the measurement of casque basal length (Fig. 3). By evaluating perpendicular casque dimensions, I attempt to maximize signals of size along the largest two dimensions of the ornament. Seventeen single measurements from three of the immature and

thirteen of the adult specimens could not be assessed due to in-life injury or post-mortem damage, and thus those specific measurements were not included in the analyses.

2.2. Data Inspection

I used log-transformation (base-10) to render exponential variables linear for analyses. Data were analyzed and statistical tests were completed using the program R (version 3.4.3; R Core Team, 2018). I first visualized and inspected the data using D'Agostino's K^2 tests (quantifies data skewness and Kurtosis), quantile-quantile plots (visualizes data normality), Shapiro-Wilk tests (tests for data normality), Breusch-Pagan tests (test for data heteroskedasticity), box plots (visualizes data distribution and outliers), and chi-squared tests (identifies for data outliers). Analyses were performed using base R and the *moments*, *outliers*, *smatr*, *lmtest* packages (Komsta & Novomestky, 2013; Komsta, 2015; Warton et al., 2018; Hothorn et al., 2019) to evaluate heteroscedasticity, normality, and outliers (see Appendix B for code). Inspection showed each morphometric to be heteroscedastic and non-normal with left-tailed, negative skew indices raging from −1.538 to −3.993. Outliers consisted of measurements from the smallest four immature birds in my ontogenetic series. Outlier measurements (TLG C037, all measurements; TLG C021, all measurements; TLG C004, keratin casque height; TLG C031, keratin casque height) were removed from my sexual dimorphism tests (see Analysis of Covariance). However, I retained them for my allometry analyses, which is discussed below.

2.3. Analysis of Covariance

In order to test for potential differences in growth trajectory between male and female keratinous casques and between immature and adult keratinous casques I performed additive analyses of covariance (ANCOVAs) in R for my keratinous casque dataset (see Appendix B for

code). If sexual dimorphism characterizes southern cassowary casque height and basal length, then it would be detectable visually by conspecifics. Because the bony casque is not visible to cassowaries, I focused my efforts on the externally visible keratinous component of the casque for sex comparisons. If maturity characterizes southern cassowary keratinous casque height, then it would be detectable in immature and adult categories. Analyses of covariance assumes normality, and outliers may bias the outcome. Therefore, immature individuals that were previously identified as outliers were not included in the ANCOVAs. Notably, this step did not eliminate all immature individuals from the analysis. Evaluations, therefore, included non-outlier immature specimens and mature individuals. I conducted ANCOVAs for log keratin casque height vs. log head length (n = 37; 15 females, 22 males) and log keratin casque basal length vs. log head length (n = 41; 16 females, 25 males), using sex as a cofactor, and I conducted an ANCOVA for log keratin casque height vs. log head length (n = 55; 16 immatures, 39 adults), using maturity as a cofactor. I performed ANCOVAs prior to linear regressions in order to assess whether it would be appropriate to analyze sexes as a combined dataset or separately.

2.4. Linear Regressions

My ANCOVAs did not detect significant differences between sexes (see Results), so female, male, and unknown-sex individuals were included in the same regression analyses. Bivariate plots were constructed in R for (1) bony log casque height vs. log skull length, (2) log bony casque height vs. log skull width, (3) log bony casque basal length vs. log skull length, (4) log bony casque basal length vs. log skull width, (5) keratin log casque height vs. log head length, (6) log keratin casque height vs. log head width, (7) log keratin casque basal length vs. log head length, and (8) log casque basal length vs. log head width. Regressions were completed using the R package *lmodel2* (Legendre & Oksanen, 2018). Scaling relationships were determined using ordinary least squares (OLS) regressions, and 95% confidence slopes (CSs) were constructed.

Scaling relationships that derived from isometry were identified as those regressions and CSs deviating from 1.0 (as would otherwise be expected for geometric increases in linear measures; Kilmer & Rodríguez, 2017). Osseous and keratinous samples were evaluated separately; however, all individuals (including outliers) were included in the OLS regressions. I regressed the complete dataset because I specifically wished to evaluate casque growth in an allometric framework common to biological studies of scaling (Macleod & MacLeod, 2009; Macleod, 2010). My outliers consisted of the smallest individuals, which provide important biological signal of early casque growth. Removing these would otherwise bias the regressions by narrowing the scope of ontogeny samples, greatly reducing the covariance between dependent and independent variables, and eliminating my ability to quantitively evaluate casque initiation. While I recognize that including outliers will impact OLS regressions, I discuss these effects below, alongside whether or not they alter my interpretations of allometry.

3. Results

3.1. Analysis of Sex Covariance

All ANCOVAs with sex as a cofactor yielded $p > 0.05$ ($p = 0.708$ and 0.548; Table 3). Therefore, I identified no significant relationships between morphometric comparisons (log keratin casque height vs. head length; log keratin casque basal length vs. log head length) with sex as the covariate. I reject the hypothesis that southern cassowary casque ontogenies are sexual dimorphic. Non-significance provided justification for combining sexes as well as unknown-sex individuals for specific regression analyses. The ANCOVA with maturity as a cofactor yielded a $p < 0.05$ ($p = 0.003$; Table 3). Therefore, I identified a significant relationship between morphometrics comparisons (log keratin casque height vs. log head length) with maturity as the covariate.

3.2. Linear Regressions of Osseous Casques

Measurement data for individual osteological specimens can be found in Table 1 (eight unmeasurable features identified by dashes; see Materials and Methods). The OLS regression analyses (Table 4; Fig. 5) revealed that *C. casuarius* bony and keratinous casque measurements scaled with substantially higher regression and CS values than 1.0. These findings support the hypothesis that the basal bony casque basal length and casque height both increase with positive allometry during ontogeny as compared to non-casque skull measurements. Although I did not run ANCOVAs on the known-sex bony casque data (due to insufficient sample sizes when outliers were removed), male (n = 4) and female individuals (n = 5) both plotted above and below best-fit regressions (Figs. 3, 4)., indicating no obvious qualitative bias in morphologies based on sex. The osteological pattern in consistent with the failure to detect sexual dimorphism in keratinous casque ontogenies. Best-fit OLS regression slopes (with CSs) ranged from 1.652 ± 0.197 to 5.770 ± 1.586, and R^2 values also ranged from 0.73 to 0.93.

3.3. Linear Regressions of Keratinous Casques

Measurement data for individual osteological specimens can be found in Table 2 (ten unmeasurable features identified by dashes; see Materials and Methods). The OLS regression analyses (Table 4, Fig. 6) revealed that *C. casuarius* keratin casque measurements also scaled with substantially higher regression and CS values than 1.0, indicating positive allometry. Slopes (with CSs) for best fit regressions on OLS plots ranged from 1.551 ± 0.137 to 5.063 ± 0.705, and R^2 values ranged from 0.71 to 0.92.

4. Discussion

I identified no significant dimorphism in relative keratinous casque size in my dataset. Regression analyses showed that all casque features, especially casque height, scale with strong positive allometry. Osseous and keratinous casque measurements show broadly overlapping OLS slopes, indicating comparable scaling relationships. Below I discuss my choice of analyses, compare patterns of casque ontogeny, and evaluate display and thermoregulatory functions of the casque from the perspective of ornament growth.

4.1. Data Assumptions

Studies of allometry are typically undertaken using either OLS or reduced major axis (RMA) regressions (Legendre & Legendre, 1998; MacLeod & MacLeod, 2009; Kilmer & Rodríguez, 2017). Critiques of both methods abound in the literature (e.g., Smith, 2009; Friedman et al., 2013; Kilmer & Rodríguez, 2017), but what warrants commentary regarding my sample is the inclusion of outliers in the allometric regression analyses. Outliers in this study were the smallest individuals, and this was likely due to the lower number of immature cassowaries sampled—a common reality when studying rare and endangered species, like *C. casuarius* (Latch, 2007; IUCN, 2020). I retained these individuals in my regressions because they accurately characterize an important period of initial casque growth, following the non-casque condition. Excluding them truncates our understanding of casque ontogeny. These individuals tended to fall below best fit regressions. As a result, these outliers caused the regression slopes to be steeper. Reduced major axis also has this effect due to incorporation of error from the independent variable (Kilmer & Rodríguez, 2017). I chose not to use RMA in this case because it would have exaggerated the effect of outliers, rendering my slopes unrealistically steep and obfuscating the biological signal. Still, I interpret my OLS results conservatively because, for example, the negative

residuals of my most immature individuals indicate that the regressions over-estimate casque morphometrics at smaller body sizes. This renders the regressions insufficient to predict immature casque sizes from immature skull dimensions. I recommend that future studies focus their sampling on cassowaries with incipient casques to clarify this issue. Other approaches, such as generalized additive models, could also be used with expanded datasets (MacLeod and MacLeod, 2009; MacLeod, 2010) to assist in accurately predicting casque size across a wider range of skull ontogeny.

4.2. Casque Scaling

In life, the bones of cassowary casques are encased in a thin, outer keratinous covering. Although the bony core comprises the vast majority of the casque's overall size (Pycraft, 1900; Crome & Moore, 1988; Richardson, 1991; Naish & Perron, 2016), the development of the osseous and keratinous portions of the casque are intimately related. This is demonstrated, for example, by the overlapping ontogenetic trajectories (regressions and CSs) between these two components in my linear regression analyses (Table 4; Figs. 5, 6). The slopes and confidence slopes for keratinous casque height plotted against head length include the slope for bony casque height plotted against skull length. This indicates that the two scaling relationships cannot be differentiated using OLS regressions. I treat them as not non-different for the purposes of this discussion. Overall, I found that osseous and keratinous casques both scale with high positive allometry compared to non-casque skull dimensions (Table 4; Figs. 5, 6). Once casque growth initiates at approximately 1.5 months of age (Green & Gignac, 2020; Chapter II), its osseous and keratinous basal length increase at a rate approximately 1.6- to 1.8-fold greater than the rest of the skull. More extreme, is osseous and keratinous casque height, which increase at a rate of approximately 5- to 6-fold greater. Measurements from μCT scans of individuals in my sample with both osseous and keratinous components of their casques intact (n = 9) indicate that the keratin sheath is relatively thin and

keratinous casque height ranged from only 1.04% to 1.32% greater than that of bony casque height (see Table 1, 2; Figs. 1, 2).

My findings align well with Dodson (1975), which was the first study to measure cassowary cranial growth. Although Dodson (1975) did not take casque-exclusive measurements (e.g., rather taking measurements of overall skull height), data from the study indicate a 4-fold greater difference in the rate of change in skull height compared to skull length. By focusing on casque-specific measurements explicitly, my data indicate that the disproportionate increase in skull height that Dodson (1975) identified over ontogeny is dominated by extreme positive allometry in casque height. The primary interest of cassowary cranial osteology in Dodson (1975) was as a model archosaur system for understanding ornament growth. The tight relationship I identify between the osseous and keratinous casque may be particularly useful in this context. For example, since soft tissue like keratin does not fossilize, paleontologists could potentially gain important insight on external ornament appearance based solely on the anatomy and scaling of the bony scaffold (Calamari & Fossum, 2017). My analysis of the bony and keratin casque portions of *C. casuarius* specifically suggests that the keratin sheath, although similar in allometric scaling to the underlying bony core, does have slightly different growth dynamics. Therefore, in paleontological studies I recommend that bony ornament cores of fossilized taxa could be compared to the bony ornament cores of modern analogs.

4.3. Developmental Timing

Prior to reaching adulthood, the osseous casques of immature southern cassowaries undergo osteological shifts that are characterized by pneumatized inflations and obliterations of sutures between casque elements (Green & Gignac, 2020; Chapter II). The extremely rapid period of osseous casque enlargement that Dodson (1975) and I detect begins in late immature individuals (i.e., 2–4 years of age). During this period casque sutures obliterate, internal trabeculae become

more widely spaced, and the internal, common pneumatic compartment of the inflating casque (a.k.a. "endocasque") expands dramatically. Keratin growth tracks underlying bone, covering the entirety of the bony casque surface during these osteological changes. Cassowaries reach maturity at approximately 4–7 years of age, indicating that maturation of the casque can take at least four years (Rothschild, 1900; Dodson, 1975; CCP, R.G. Hood, *pers. comm.*). This illustrates that even with extreme positive allometry in both osseous and keratinous casque heights, a considerable period of growth is necessary to enlarge the ornament in both males and females. Additionally, my ANCOVA results illustrate that casque growth trajectories between immature and mature *C. casuarius* are significantly different (Table. 3). Unsurprisingly, the tallest and most laterally compressed casques in my bony and keratin samples are indicative of adult southern cassowaries. Overall, the casque phenotype at the onset of maturity appears to be synchronized with soft-tissue characters such as black plumage, well-defined apteria, and brightly colored craniocervical skin of blue, red, and purple that indicate adulthood (Rothchild, 1900; Green & Gignac, 2020; Chapter II). This finding suggests that casque which are at least twice as high as they are wide should also be considered as a component of the adult character suite that differentiates immature and mature *C. casuarius* individuals.

I note that the oldest known-age individuals in my dataset (see ages ~20–35.7 years in Table 1) do not necessarily have the largest casque dimensions in order of increasing age. Differences in casque size between mature individuals may be in part related to the onset of or rate at which pneumatization proliferates during ontogeny. Earlier or more rapid inflation, for example, may result in an adult with a larger ornament than its conspecifics, given the same head size or age. Notably, casque pneumatization is thought to be somewhat convoluted, occurring from the tympanic sinuses via caudal and caudolateral bones of the cranium (i.e., quadrates, squamosals, laterosphenoids, parietals; Starck, 1995; Green & Gignac, 2020; Chapter II) before converging dorsally as the endocasque. Sequential proliferation of each sinus should be further evaluated to

address how whole-skull integration and how the onset of pneumatic expansions may facilitate rate differences in ornament growth between individuals.

4.4. Female Size

There are a number of extant avian taxa that exhibit sexual dimorphism in cranial ornament size, including curassows (*Crax*; Buchholz, 1991; Mayr, 2018), guinea fowl (*Numida*; Angst et al., 2019), and hornbills (e.g., *Bycanistes*, *Ceratogymna*; Kemp et al., 2001; Gamble, 2007). These dimorphisms appear to stem from sex-specific ornament ontogenies resulting in size-standardized individuals that sport differently sized headgear. Given my ANCOVA results, it appears that there are no detectable differences in female and male casque growth trajectories for southern cassowaries, suggesting ontogeny is shared between the sexes. Nonetheless, the casques with the largest absolute dimensions in my sample tend to belong to females (see Fig. 6). Adult female *C. casuarius* are approximately 30% larger in body mass than their male counterparts (see Olson & Turvey, 2013), which suggests that one source of casque variation may be due to female-biased body size dimorphism. As a result of sharing casque ontogeny with males but also obtaining larger absolute body sizes, female cassowaries are capable of growing absolutely larger casques as well. Overall body-size gains and associated dominance behaviors (e.g., aggressive posturing or charging) become apparent during mid-immaturity in females, specifically, after casque initiation but prior to adulthood (CCP, R.G. Hood, *pers. comm.*). This suggests that body-size trajectories (either due to growth rates or periods of growth) may differ between males and females even though relative casque sizes do not. Additional studies on sexually active adults may elucidate the potential for statistically significant adult female bias in absolute casque height and how that may impact cassowary behavior.

4.5. The Role of Ontogeny in Casque Function

The substantial rates of osseous and keratinous casque development that I identified present an opportunity to consider proposed functions of the overall casque in the context of ontogeny. Two of the primary functional hypotheses for cassowary casques (see Naish & Perron, 2016 for review) align with my scaling results: (1) visual display (e.g., Dodson, 1975) and (2) thermoregulation (e.g., Phillips & Sanborn, 1994; Eastick et al., 2019). I evaluate whether or not these biological roles are consistent with lifetime function or function only in adults.

Previously, sexual maturity and honest competitive signals have been proposed as visual display functions for the casque (see Naish & Perron, 2016). These functions are not unique to cassowaries as they have also been proposed for the cranial ornaments of artiodactyls (Bubenik & Bubenik, 1990), galliform birds (Buchholz, 1991), and casque-headed frogs (Jared et al., 2005) among others. Visual display functions have particularly been suggested in birds based on their neurosensory commitment to broad spectrum vision (Gill, 2007; McCoy & Prum, 2019), which necessarily includes the brightly colored skin of cassowaries. Although black-brown and grey-green in color, the obviousness of the cassowary casque as a prominent feature of the head, located directly above the eyes, is generally consistent with hypotheses of display (Dodson, 1975; Naish & Perron, 2016). The rapid growth of the casque that I identified seems to enable the timing of casque maturity to be achieved near the end of immaturity, approximately coincident with soft-tissue indicators of adulthood such as black plumage, well-defined apteria, and brightly colored craniocervical skin (Rothchild, 1900; Green & Gignac, 2020; Chapter II). This provides correlated support that the casque could act as an additional visual signal for sexual maturity, resulting in a whole-body commitment to signaling sexual status (Rosen & Tarvin, 2006; Kekäläinen et al., 2010; Dakin, 2011). Among these traits, casque growth begins early, followed years later by integumentary color shifts. Because changes in these features are gradual and appear to occur at different rates in *C. casuarius* (Rothschild, 1900), their combination as a suite of reinforcing

maturity signals may be crucial to indicate sexual status (Kekäläinen et al., 2010). In this case, function would be limited to adults (male and female), with the earliest onset of casque initiation as a necessary means to synchronize casque size at the onset of maturity with secondary sexual characteristics.

Establishing status may also provide for an important display role of the casque. Adult southern cassowaries are generally solitary in the wild, and they often behave aggressively when interacting with conspecifics (Crome, 1976). Although rare, intraspecific conflicts can escalate to blows with each cassowary using its large feet and elongated digit II claws to kick their opponent (Crome, 1976). Initially when birds approach one another, each exhibit a ritualized stretch display in which the legs, body, and neck are extended vertically, with the casque pointed skyward (Crome, 1976). Following the display, one of the birds usually withdraws, avoiding physical altercation (Crome, 1976). During this "sizing up" behavior, taller casques appear to give their bearers a perceived height advantage, allowing the shorter individual to escape without direct confrontation (CCP, R.G. Hood, *pers. comm.*). Extreme casque scaling, therefore, seems to enable the tall, adult casque morphology that signals competitor status. Indeed, stretch displays are commonly associated agonistic behavior in other large-bodied ratites as well (e.g., ostriches, emus; Bolwig, 1973; Menon et al., 2014), indicating that evolution of a casque may have augmented a behavior that had already existed ancestrally. In this case casque positive allometry serves to exaggerate overall tallness, which was historically a means to achieve an honest signal of body-size comparison between individuals. Runaway selection (Fisher, 1930; Pomiankowski & Iwasa, 1998), herein with fitness benefits accrued (e.g., Chandler et al., 2012) to relatively taller individuals regardless of sex, might therefore underly the evolution of casque ontogeny in cassowaries. Female cassowaries appear to take this to an extreme by achieving the largest body sizes and tallest casques, providing them opportunity to present as most competitive, which is in line with their polyandrous mating behaviors (Crome, 1976; Moore, 2007).

I also propose that casque ontogeny is consistent with its use for thermoregulation. In general, birds have high core body temperatures (Prinzinger et al., 1991), and larger birds tend to have relatively lower amounts of surface area across which to dissipate body heat (Crawford & Schmidt-Nielsen, 1967; Phillips & Sanborn, 1994). Cassowaries are the largest rainforest birds alive today and, therefore, it is reasonable to assume that may have physical and physiological accommodations to cope with warm and humid conditions (Phillips & Sanborn, 1994; Eastick et al., 2019). Aside from the surface of the bill, craniocervical apteria, and distal hindlimbs, the casque has been proposed as feature involved in temperature regulation (Phillips & Sanborn, 1994; Eastick et al., 2019). A recent study proposed vascular control of vessels along the surface of the casque in *C. casuarius* as a means for the ornament to act as a thermal window (*sensu* Eastick et al., 2019). The broad lateral surfaces of adult *C. casuarius* casques would provide large areas for heat exchange, and positively allometric ornament height and basal length (Figs. 5, 6) necessarily results in positively allometric casque surface area as well. Southern cassowaries in general, therefore, may be more effective at cranial heat exchange (and potentially, related osmoregulation; Maloney, 2008; Strauss et al., 2017) than their non-casques relatives. In addition, the disproportionately large casque surface of adults would render their casques into even more effective heat transfer structures as compared to juveniles. In this case function would be expected in male and female birds during mid- to-late immaturity, and maturity individuals but with the greatest capacities for thermoregulation in mature birds with the largest casques.

4.6. Summary

Here I provided the first formal analysis of intraspecific casque scaling in southern cassowaries. There were no significant differences in keratinous casque growth trajectories between female and male *C. casuarius* (though female casques tended to be absolutely larger in size), and I found moderate to extreme positive allometry in casque dimensions. Casque scaling

appears consistent with both display and thermoregulatory functions although further examination of potential reinforcement between these factors is warranted (Fisher, 1930; Chandler et al., 2012). Renewed interest in the ornaments of these charismatic megafauna (Naish & Perron, 2016; Brassey & O'Mahoney, 2018; Mayr, 2018; Eastick et al., 2019; Green & Gignac, 2020; Chapter II) since their initial descriptions (Parker, 1866; Flower, 1871; Marshall, 1872; Pycraft, 1900; Rothschild, 1900) points to a nascent, modern community engaged in addressing the questions that are essential to augment our understanding of cassowaries. I hope this study helps to fuel additional interest in the biology and life histories of these unique animals.

Table 1. Osteological *Casuarius casuarius* specimen list, indicating preparation history, sex, age, and linear measurements (in millimeters)

Specimen ID	Type	Sex	Age	B CSQ HT	B CSQ LH	SK LH	SK WD
TLG (CCP) C037	Frozen	M	IM (1.5 mo.)	1.4	29.7	80.3	34.6
TLG (CCP) C021	Fluid	F	IM (5.2 mo.)	3.2	53.0	126.8	53.4
TLG C002	Skeleton	U	IM (~5.5 mo.)	7.4	78.5	149.3	57.4
TLG (CCP) C004	Fluid	F	IM (10.5 mo.)	14.2	90.3	171.0	69.6
TLG (CCP) C031	Frozen	M	IM (14.0 mo.)	15.6	89.9	159.0	70.5
NHMUK S/2010.1.21	Skeleton	U	IM (~14.0–24.0 mo.)	17.0	85.5	178.5	68.0
AMNH SKEL 963	Skeleton	U	IM (~24.0 mo.)	28.9	99.5	170.9	73.4
AMNH SKEL 1106	Skeleton	U	IM (~24.0–36.0 mo.)	40.1	115.2	177.9	78.3
AMNH SKEL 3200	Skeleton	U	IM (~24.0–36.0 mo.)	47.2	108.8	176.4	69.0
AMNH SKEL 14823	Skeleton	U	AD (≥4.0 yr.)	58.1	108.0	170.9	69.4
AMNH SKEL 1517	Skeleton	U	AD (≥4.0 yr.)	65.0	100.8	176.1	72.8
AMNH SKEL 3870	Skeleton	U	AD (≥4.0 yr.)	63.4	112.9	177.3	73.8
NHMUK 1972.1.12	Skeleton	U	AD (≥4.0 yr.)	90.3	113.0	180.1	71.6
AMNH SKEL 1519	Skeleton	U	AD (≥4.0 yr.)	99.4	110.0	180.9	70.0
QM O.30105	Skeleton	U	AD (≥4.0 yr.)	99.5	116.5	184.2	75.6
NHMUK S/2010.1.20	Skeleton	U	AD (≥4.0 yr.)	96.6	117.4	—	74.1
AMNH SKEL 1717	Skeleton	U	AD (≥4.0 yr.)	74.4	120.2	185.2	73.7
QM O.31352	Skeleton	F	AD (≥4.0 yr.)	—	125.9	186.1	75.9
QM O.31137	Skeleton	U	AD (≥4.0 yr.)	—	111.6	190.4	66.2
AMNH SKEL 1695	Skeleton	U	AD (≥4.0 yr.)	—	115.0	190.4	—
MV B12907	Skeleton	F	AD (≥4.0 yr.)	98.5	127.2	194.1	76.2
NHMUK 1939.12.9.1052	Skeleton	U	AD (≥4.0 yr.)	87.0	113.9	194.5	—
QM O.30604	Skeleton	U	AD (≥4.0 yr.)	—	128.4	197.8	75.8
AMNH SKEL 962	Skeleton	U	AD (~4.0–5.0 yr.)	63.8	100.2	179.6	71.0
TLG C001	Skeleton	U	AD (~5.0–20.0 yr.)	95.4	117.3	195.9	70.6
TLG (SCZ) C022 (12126)	Skeleton	M	AD (21.4 yr.)	82.7	124.0	191.3	77.4
DMNS ZB.50012	Dried	M	AD (22.1 yr.)	60.0	119.5	168.6	73.4
MOO 8031	Skeleton	F	AD (35.7 yr.)	90.0	137.0	—	78.9

M = male; F = female; IM = immature; U = unknown; AD = adult; B CSQ HT = bony casque height; B CSQ LH = bony casque basal length; SK LH = skull length; SK WD = skull width

Table 2. Keratinous *Casuarius casuarius* specimen list, indicating preparation history, sex, age, and linear measurements (in millimeters)

Specimen ID	Type	Sex	Age	K CSQ HT	K CSQ LH	HD LH	HD WD
TLG (CCP) C037	Frozen	M	IM (1.5 mo.)	1.7	30.0	80.6	34.6
TLG (CCP) C021	Fluid	F	IM (5.2 mo.)	3.5	53.4	128.6	53.4
TLG C002	Skeleton	U	IM (~5.5 mo.)	9.2	79.2	149.8	57.4
TLG (CCP) C004	Fluid	F	IM (10.4 mo.)	14.9	94.5	172.5	69.6
TLG (CCP) C031	Frozen	M	IM (14.0 mo.)	16.5	91.8	159.7	70.5
NHMUK 1939.12.9.893	Dried	U	IM (~24.0–36.0 mo.)	41.7	104.5	174.0	74.5
QM O.30102	Fluid	F	IM (~24.0–36.0 mo.)	44.4	109.7	188.3	75.1
MV R11280	Dried	U	IM (~30.0–42.0 mo.)	50.0	106.1	169.3	73.3
NHMUK 1916.5.30.1480	Dried	M	IM (~30.0–42.0 mo.)	47.2	113.0	178.0	86.4
NHMUK 1939.12.9.879	Dried	U	IM (~30.0–42.0 mo.)	48.6	112.0	189.0	—
NHMUK 1939.12.9.902	Dried	M	IM (~30.0–47.0 mo.)	52.3	116.5	168.2	83.1
DMNS ZB.47879	Dried	U	IM (~30.0–47.0 mo.)	55.8	125.0	—	76.0
MV 61245	Dried	U	IM (~30.0–47.0 mo.)	61.4	122.0	195.4	85.5
MV R12278	Dried	M	IM (~30.0–47.0 mo.)	75.4	119.7	—	77.0
MV R2861	Dried	F	IM (~30.0–47.0 mo.)	70.9	122.0	191.5	83.5
MV R12281	Dried	U	IM (~30.0–47.0 mo.)	67.2	136.1	209.7	79.3
NHMUK 1939.12.9.946	Dried	F	AD (≥ 4.0 yr.)	81.7	108.5	183.4	71.2
NHMUK 1939.12.9.947	Dried	M	AD (≥ 4.0 yr.)	74.7	109.8	188.0	74.2
NHMUK 1939.12.9.957	Dried	M	AD (≥ 4.0 yr.)	—	109.9	199.8	77.5
QM O.5400	Dried	M	AD (≥ 4.0 yr.)	103.6	110.8	191.6	75.7
NHMUK 1996.41.889	Dried	M	AD (≥ 4.0 yr.)	80.7	111.3	181.1	77.1
AMNH SKIN 424915	Dried	M	AD (≥ 4.0 yr.)	72.5	112.6	178.9	73.8
NHMUK 1939.12.9.969	Dried	M	AD (≥ 4.0 yr.)	65.5	112.7	190.5	77.1
MOO 6994	Skeleton	M	AD (≥ 4.0 yr.)	69.5	114.3	—	71.5
NHMUK 1996.41.895	Dried	M	AD (≥ 4.0 yr.)	53.3	115.2	—	70.0
MV R11696	Dried	F	AD (≥ 4.0 yr.)	83.6	116.9	176.6	72.2
NHMUK 1939.12.9.950	Dried	M	AD (≥ 4.0 yr.)	103.3	117.5	202.7	77.5
AMNH SKIN 11574	Dried	M	AD (≥ 4.0 yr.)	70.0	117.7	182.4	80.3
NHMUK 1939.12.9.944	Dried	M	AD (≥ 4.0 yr.)	83.4	118.7	188.6	—
QM O.20563	Dried	M	AD (≥ 4.0 yr.)	90.2	120.0	197.3	72.4
NHMUK 1939.12.9.894	Dried	M	AD (≥ 4.0 yr.)	100.7	120.5	198.6	—
AMNH FLUID 12483	Fluid	M	AD (≥ 4.0 yr.)	72.6	121.2	192.6	78.0
NHMUK 1996.41.892	Dried	M	AD (≥ 4.0 yr.)	92.2	121.6	192.3	79.9
AMNH FLUID 15261	Fluid	M	AD (≥ 4.0 yr.)	87.9	122.4	195.8	77.5
MV R12279	Dried	M	AD (≥ 4.0 yr.)	69.8	123.2	185.4	76.6
NHMUK 1939.12.9.907	Dried	M	AD (≥ 4.0 yr.)	83.3	123.9	201.2	83.2
NHMUK 1996.41.905	Dried	F	AD (≥ 4.0 yr.)	95.7	124.2	189.1	83.0
NHMUK 1939.12.9.967	Dried	M	AD (≥ 4.0 yr.)	64.4	126.7	195.4	77.4
NHMUK 1996.41.888	Dried	M	AD (≥ 4.0 yr.)	72.9	127.9	187.4	74.7
NHMUK 1965.30.1484	Dried	F	AD (≥ 4.0 yr.)	89.6	130.1	211.1	76.7
NHMUK 1939.12.9.953	Dried	M	AD (≥ 4.0 yr.)	131.3	130.1	202.1	81.0
AMNH SKIN 421657	Dried	F	AD (≥ 4.0 yr.)	104.5	130.7	192.8	78.1
NHMUK 1939.12.9.34	Dried	F	AD (≥ 4.0 yr.)	90.0	131.1	198.9	80.0
NHMUK 1942.5.29.1	Dried	F	AD (≥ 4.0 yr.)	95.7	131.1	200.9	76.8
AMNH FLUID 15259	Fluid	F	AD (≥ 4.0 yr.)	97.0	132.1	204.4	83.4
NHMUK 1939.12.9.948	Dried	F	AD (≥ 4.0 yr.)	135.9	132.1	204.4	76.8
NHMUK 1942.4.14.1	Dried	F	AD (≥ 4.0 yr.)	122.6	133.2	205.3	79.0
AMNH FLUID 15262	Fluid	F	AD (≥ 4.0 yr.)	88.6	133.9	202.0	85.7

Table 2. cont…

Specimen ID	Type	Sex	Age	K CSQ HT	K CSQ LH	HD LH	HD WD
NHMUK 1916.5.30.1483	Dried	F	AD (≥ 4.0 yr.)	114.8	136.0	212.0	75.6
NHMUK 1939.12.9.945	Dried	M	AD (≥ 4.0 yr.)	—	137.8	213.7	80.9
NHMUK 1939.12.9.4	Dried	F	AD (≥ 4.0 yr.)	132.2	137.6	222.3	85.8
TLG C001	Skeleton	U	AD (~5.0–20.0 yr.)	100.2	122.1	197.0	70.6
TLG (SCZ) C022 (12126)	Frozen	M	AD (21.4 yr.)	86.0	126.2	194.3	77.4
DMNS ZB.50012	Dried	M	AD (22.1 yr.)	67.9	124.9	170.1	73.4
MOO 8031	Skeleton	F	AD (35.7 yr.)	91.2	138.2	—	78.9

M = male; F = female; IM = immature; U = unknown; AD = adult; K CSQ HT = keratin casque height; K CSQ LH = keratin casque basal length; HD LH = head length; HD WD = head width

Table 3. ANCOVAs for *Casuarius casuarius* linear cranial measurements.

	Number of Females	Number of Males	F Value (Sex)	P Value (Sex)
Log K CSQ HT vs. Log HD LH	15	22	0.143	0.708 (not significant)
Log K CSQ LH vs. Log HD LH	16	25	0.367	0.548 (not significant)
	Number of Immature	**Number of Mature**	**F Value (Maturity)**	**P Value (Maturity)**
Log K CSQ HT vs. Log HD LH	16	39	16.580	0.003* (significant)

B CSQ HT = bony casque height; K CSQ HT = keratinous casque height; K CSQ LH = casque basal length; HD LH = head length

Table 4. Ordinary least squares (OLS) regression parameters for *Casuarius casuarius* osseous & keratinous casques.

		Slope ± Confidence Slopes	Y-Intercept	R^2	Scaling
Osseous	Log B CSQ HT vs. Log SK LH	5.450 ± 1.364	−10.573	0.78	Positive
	Log B CSQ HT vs. Log SK WD	5.770 ± 1.586	−9.019	0.73	Positive
	Log B CSQ LH vs. Log SK LH	1.652 ± 0.197	−1.691	0.93	Positive
	Log B CSQ LH vs. Log SK WD	1.828 ± 0.236	−1.358	0.91	Positive
Keratinous	Log K CSQ HT vs. Log HD LH	5.063 ± 0.705	−9.687	0.82	Positive
	Log K CSQ HT vs. Log HD WD	5.033 ± 0.932	−7.647	0.71	Positive
	Log K CSQ LH vs. Log HD LH	1.551 ± 0.137	−1.463	0.92	Positive
	Log K CSQ LH vs. Log HD WD	1.629 ± 0.190	−0.996	0.86	Positive

B CSQ HT = bony casque height; B CSQ LH = bony casque basal length; K CSQ HT = keratin casque height; K CSQ LH = keratin casque length; HD LH = head length; HD WD = head width; SK LH = skull length; SK WD = skull width

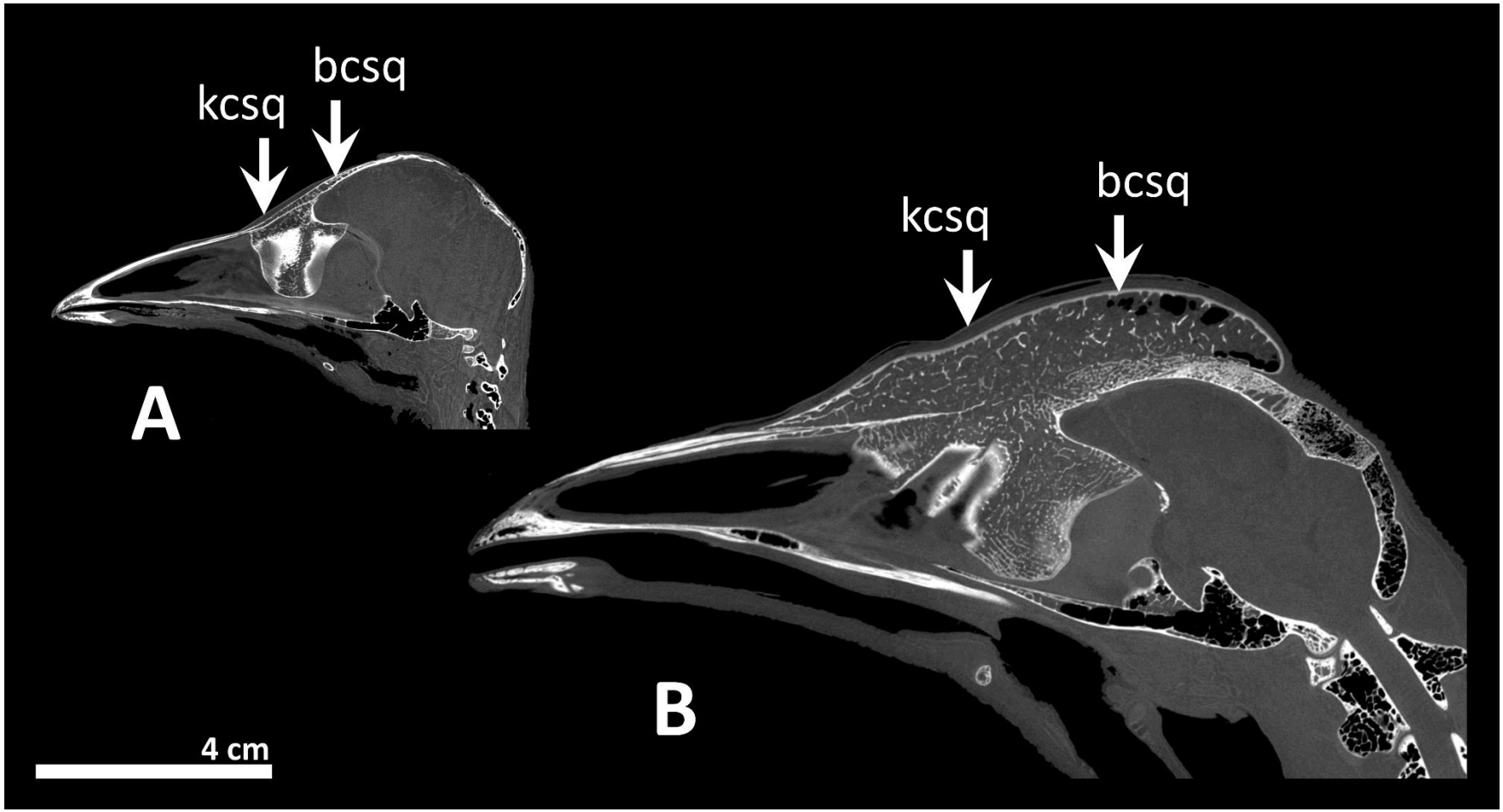

Figure 1. Parasagittal µCT digital sections taken at the approximate midline through the heads of immature *Casuarius casuarius* specimens (A = 1.5 months old, TLG C037; B = 14.0 months old, TLG C031). White arrows indicate the keratinous casque (kcsq) and the bony casque (bcsq), which can be differentiated by lower and higher densities, respectively.

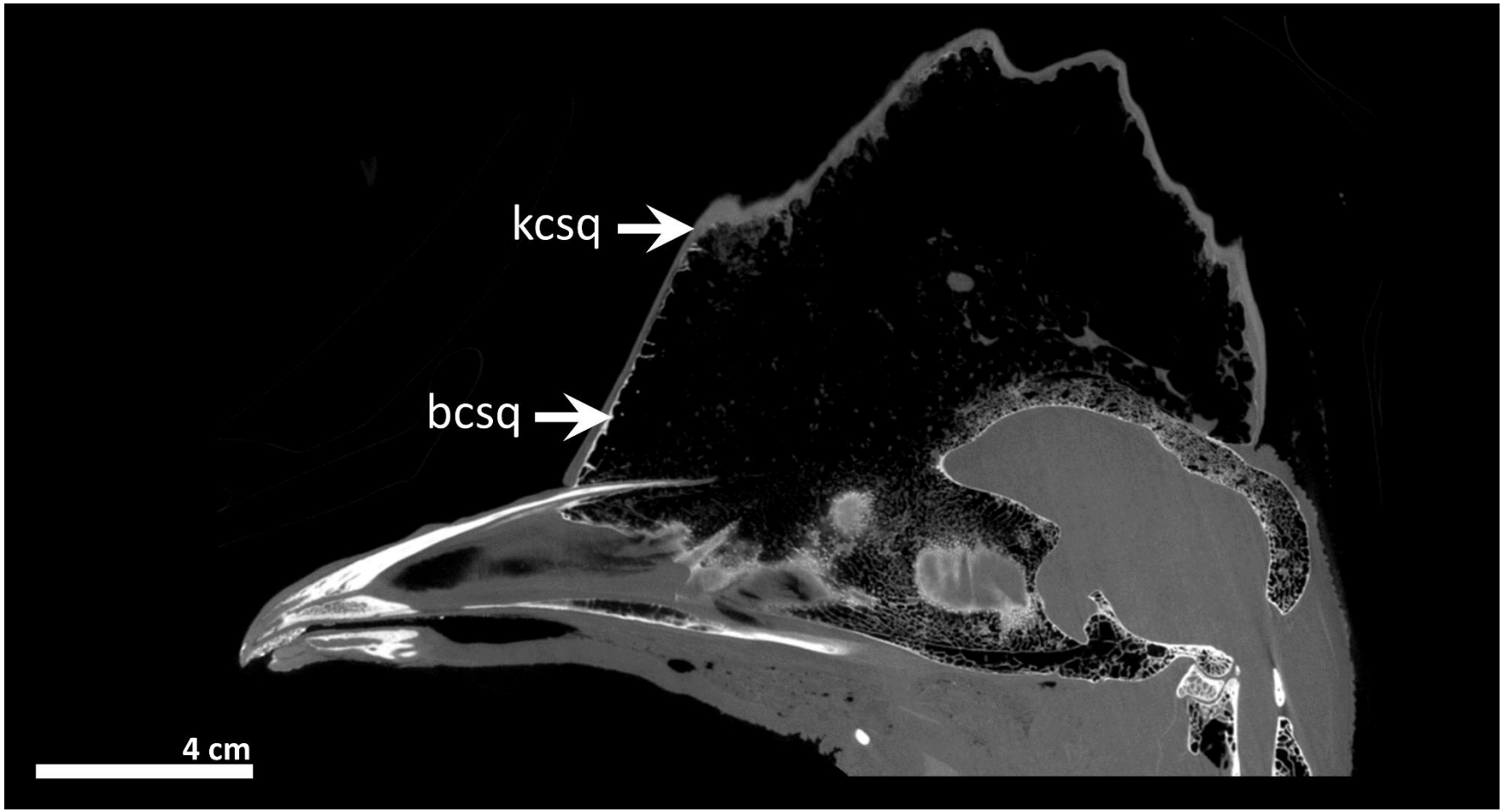

Figure 2. Parasagittal µCT digital section taken at the approximate midline through the head of an adult *Casuarius casuarius* specimen (21.4 years old, TLG C022). White arrows indicate the keratinous casque (kcsq) and the bony casque (bcsq), which can be differentiated by lower and higher densities, respectively. The dorsalmost cortical bone of the bcsq may become exceptionally thin in adult individuals, as illustrated here.

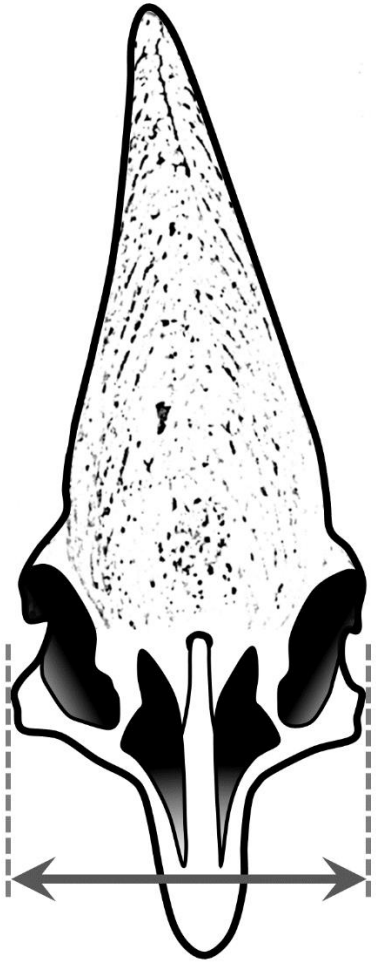

Skull width

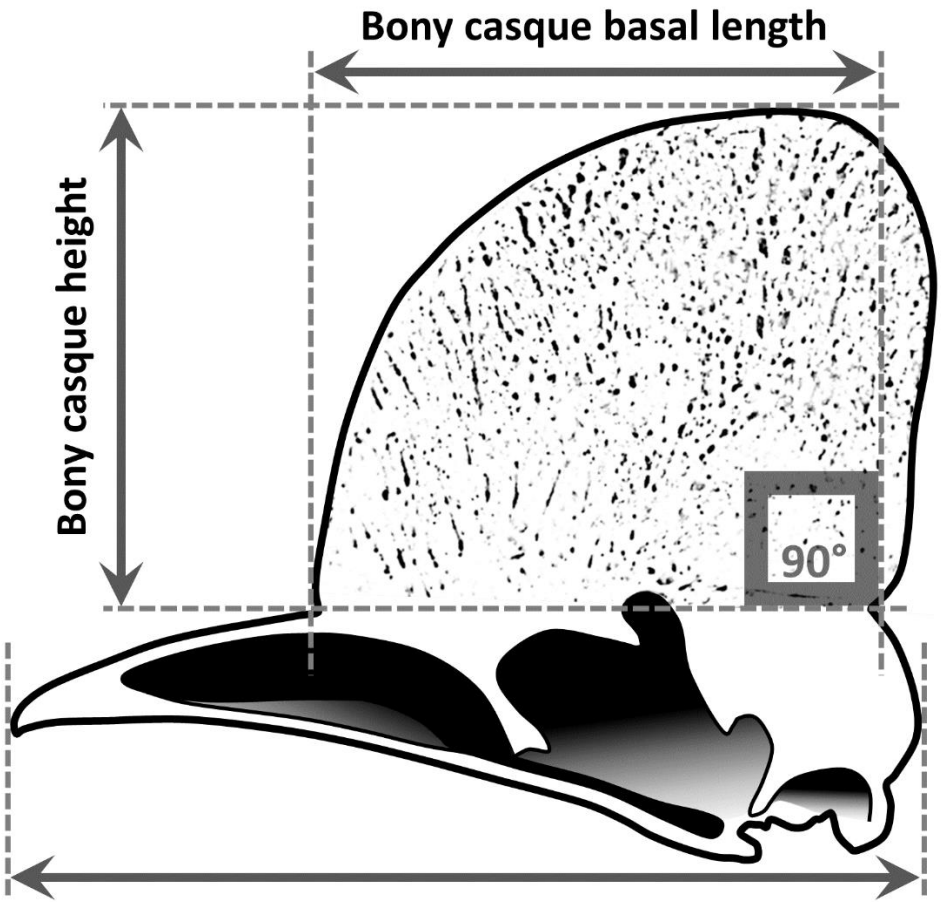
Bony casque basal length
Bony casque height
90°
Skull length

Figure 3. Diagram of linear measurements (bony casque height, bony casque basal length, skull length skull width) collected from bony *Casuarius casuarius* skulls in anterior (left) and left lateral (right) views. Solid lines with arrows represent the actual measurements taken, and dashed lines are guidelines for terminating edges of bony surfaces.

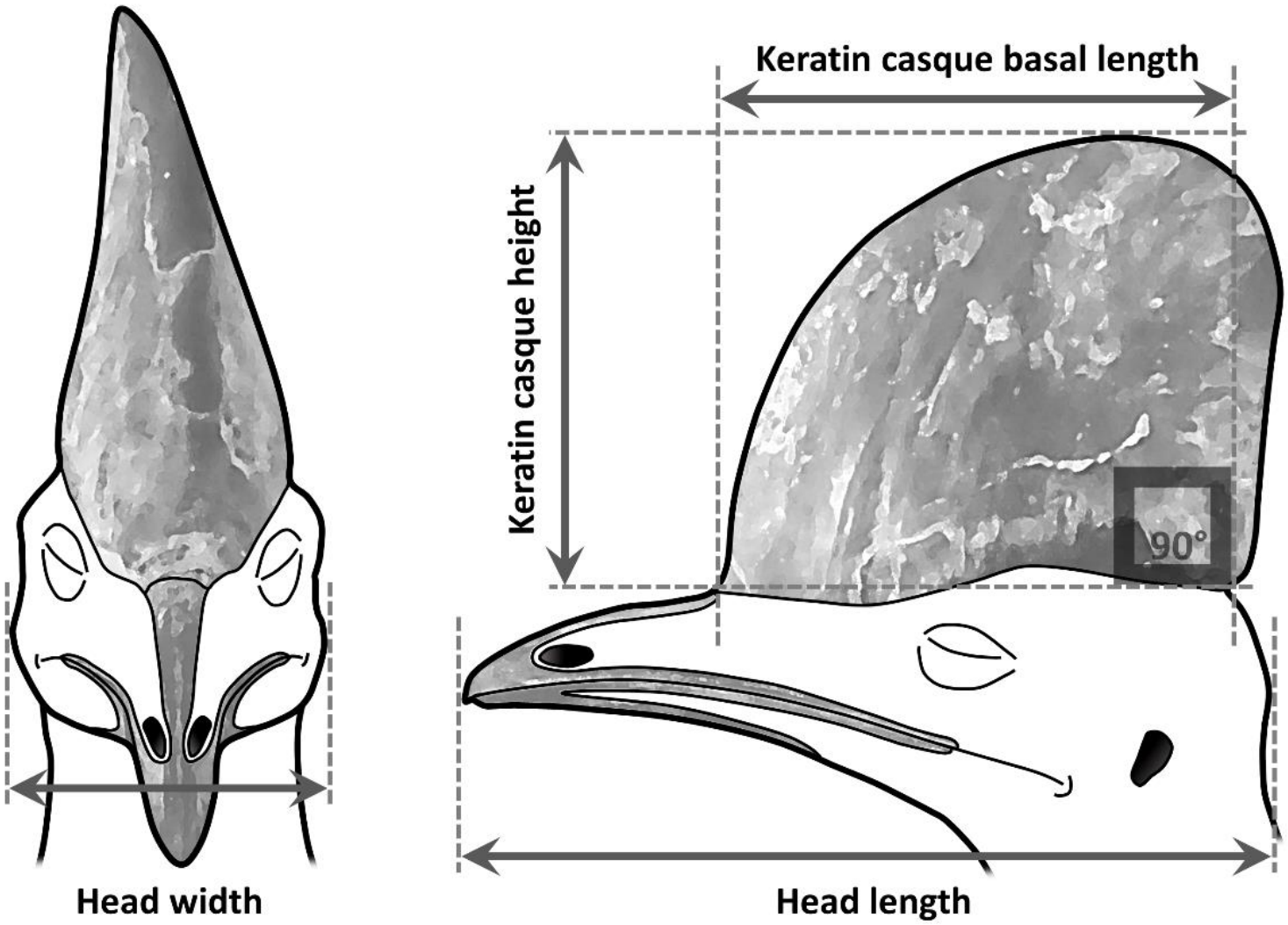
Keratin casque basal length
Keratin casque height
90°
Head width
Head length

Figure 4. Diagram of linear measurements (keratin casque height, keratin casque basal length, head width, head length,) collected from *Casuarius casuarius* heads with keratin sheathing on the casque and bill in anterior (left) and left lateral (right) views. Solid lines with arrows represent the actual measurements taken, and dashed lines are guidelines for terminating edges of bony surfaces.

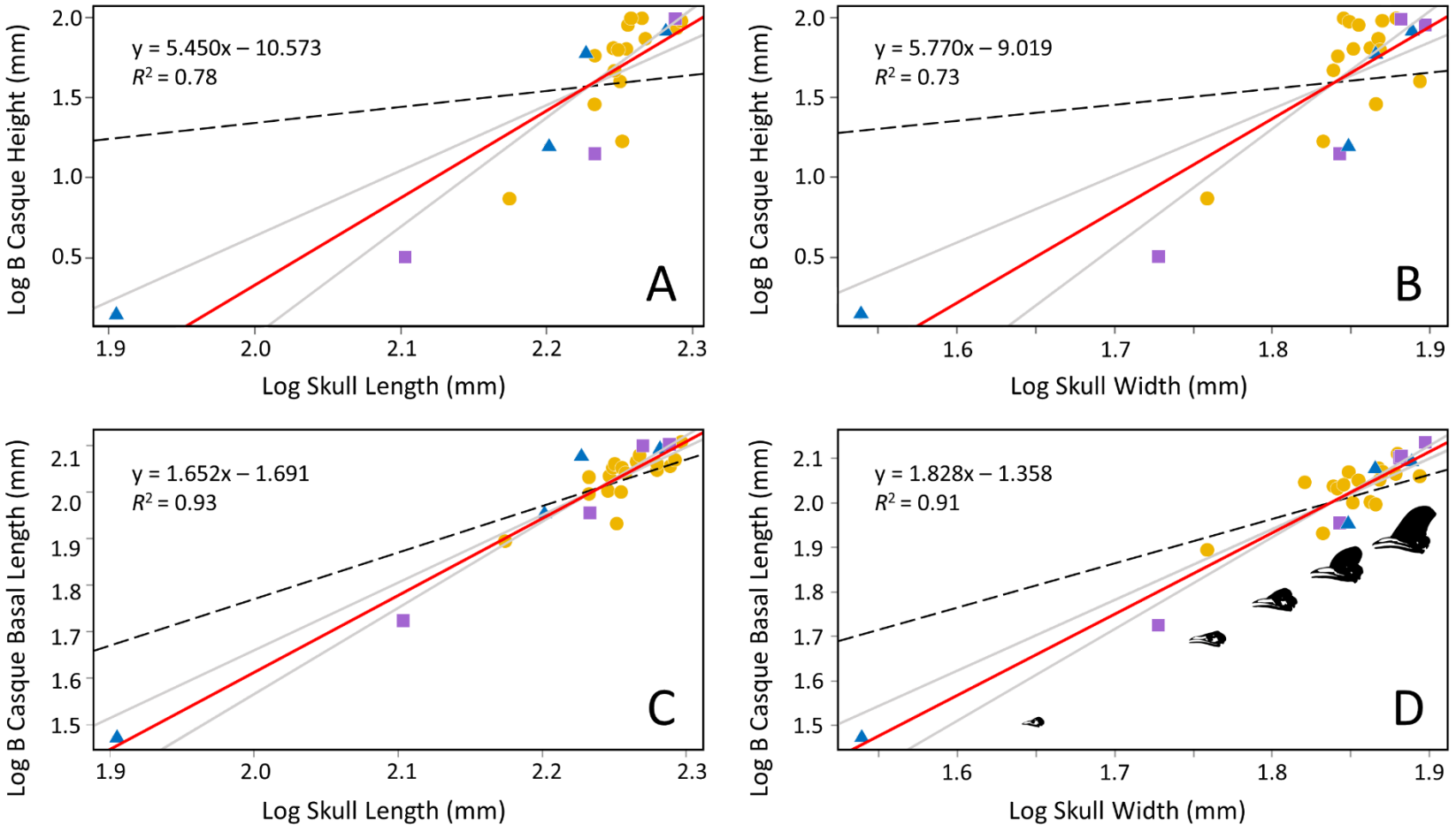
y = 5.450x – 10.573
R^2 = 0.78
A
Log B Casque Height (mm)
Log Skull Length (mm)
y = 5.770x – 9.019
R^2 = 0.73
B
Log B Casque Height (mm)
Log Skull Width (mm)
y = 1.652x – 1.691
R^2 = 0.93
C
Log B Casque Basal Length (mm)
Log Skull Length (mm)
y = 1.828x – 1.358
R^2 = 0.91
D
Log B Casque Basal Length (mm)
Log Skull Width (mm)

Figure 5. Ordinary least squares (OLS) plots for linear measurements of *Casuarius casuarius* osseous casques and skulls over ontogeny. Log-transformed data is plotted for (A) bony casque height versus skull length (n = 22), (B) bony casque height versus skull width (n = 23), (C) bony casque basal length versus skull length (n = 26), and (D) bony casque basal length versus skull width (n = 26). Best fit regression lines (solid red lines), regression equations, R^2 values, 95% confidence slopes (solid light grey lines) and indication of isometry slope (dashed black lines) are shown for each corresponding plot. Datapoints indicate female (purple squares), male (blue triangles), and unknown-sex (yellow circles) individuals. Black silhouettes of cassowary skulls (in left lateral view) illustrate the progression of osseous casque growth (plot D).

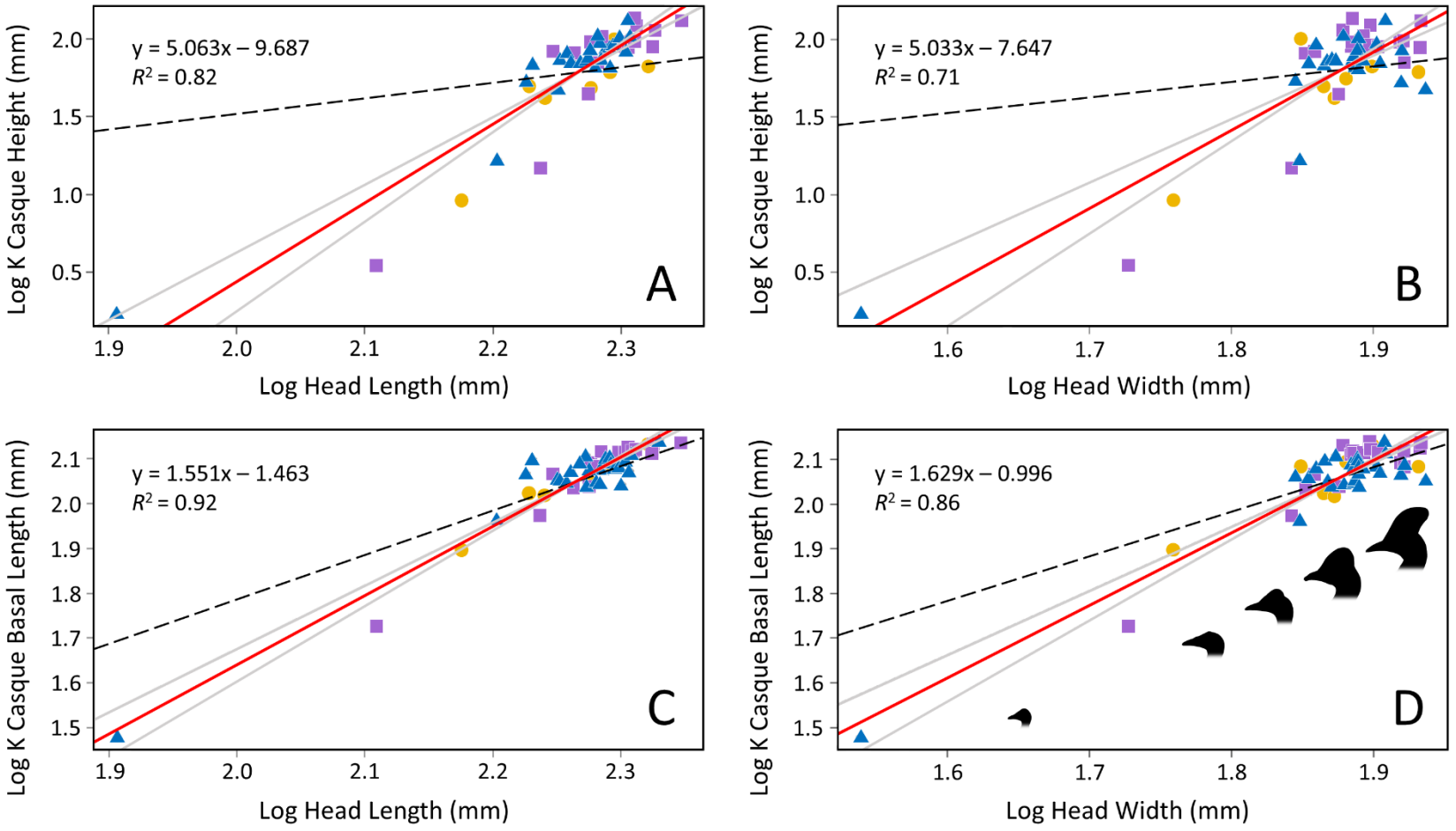
y = 5.063x – 9.687
R^2 = 0.82
Log K Casque Height (mm)
Log Head Length (mm)
A
y = 5.033x – 7.647
R^2 = 0.71
Log K Casque Height (mm)
Log Head Width (mm)
B
y = 1.551x – 1.463
R^2 = 0.92
Log K Casque Basal Length (mm)
Log Head Length (mm)
C
y = 1.629x – 0.996
R^2 = 0.86
Log K Casque Basal Length (mm)
Log Head Width (mm)
D

Figure 6. Ordinary least squares (OLS) plots for linear measurements of *Casuarius casuarius* keratinous casques and heads over ontogeny. Log-transformed data is plotted for (A) keratin casque height versus head length (n = 48), (B) keratin casque height versus head width (n = 50), (C) keratin casque basal length versus head length (n = 50), and (D) keratin casque basal length versus head width (n = 52). Best fit regression lines (solid red lines), regression equations, R^2 values, 95% confidence slopes (solid light grey lines) and indication of isometry slope (dashed black lines) are shown for each corresponding plot. Datapoints indicate female (purple squares), male (blue triangles), and unknown-sex (yellow circles) individuals. Black silhouettes of cassowary heads (in left lateral view) illustrate the progression of keratinous casque growth (plot D).

CHAPTER IV

ADULT CASQUE DISPARITY IN THE GENUS *CASUARIUS* AND IMPLICATIONS FOR VISUAL DISPLAY

Abstract

The cranial casques of modern cassowaries (*Casuarius*) have long intrigued researchers; however, in-depth studies regarding their morphological variation are scarce. Through visual inspection it has been recognized that ornament variability exists between species (i.e., *C. bennetti*, *C. casuarius*, *C. unappendiculatus*) as well as between conspecifics. Although hypothesized to be targeted by natural selection, inter- and intraspecific casque variation has not been quantified previously. Through a large sample *C. casuarius* (n = 103) I compared casque shape (lateral and rostral views) between sexes and geographical regions via a two-dimensional (2D) geometric morphometrics approach. I also compared casque shape across the genus *Casuarius* (n = 166). In *C. casuarius* I found no statistically significant differences between the casque shape of females and males and few substantial shape differences between geographic areas. Much of the intraspecific variation within *C. casuarius* is due to casque asymmetries (77.5% rightward deviating, 20.7% leftward deviating, and 1.8% non-deviating from the midline). This asymmetry explains the high variability of southern cassowary casque shape, particularly from the rostral aspect. Although my casque morphospace across the genus had some areas of overlap, casques of

the species were significantly different from one another. Casque shapes of *C. bennetti* and *C. casuarius* were particularly unique. The casques of *C. unappendiculatus* were predicted to share shape characteristics with the other two species most frequently. As the most comprehensive casque variation study on cassowaries to date, these findings provide important context for better interpretations of cassowary biology, casque function, and cranial ornament evolution in this unique group of birds as well as for archosaurs more broadly.

1. Introduction

Birds are visually-based organisms that use the colors, shapes, and body distributions of feathers, fleshy appendices, and hard-tissue ornaments for interspecific and intraspecific display (Gill, 2007). Ornaments represent important ways that birds communicate their age, sex, social status, reproductive capability, and species identity (Raikow, 1969; Bolwig, 1973; Frith, 1978, Diamond, 1986; Buchholz, 1991; Gill, 2007; Jones & Hunter, 1999; Kemp, 2001; Hagelin, 2002, Kinnaird et al., 2003; Mayr, 2018), and deciphering ornament meanings helps us as address how their functions impact avian life-histories and evolution. Here I focus on the uniquely ornamented cassowaries (*Casuarius*), a flightless ratite and relative of ostriches, rheas, kiwis, and emus. Unlike their immediate living relatives, cassowaries are exceptionally conspicuous, possessing vividly colored apteria (e.g., blue, red, yellow, orange, purple, pink, white; Fig. 1) carunculated skin, pendulous wattles, glossy feathers, and an unmistakably prominent cranial casque. The casque, in particular, has long been a source of inquiry (e.g., Parker, 1866; Flower, 1871; Marshall, 1872; Pycraft 1900; Rothschild, 1900) although few studies have formally addressed if and how the ornamental casque may be used as a visual display feature.

Compositionally, the casques of cassowaries contain an osteologically convoluted bony core (see Green & Gignac, 2020; Chapter II), as well as a thin, external sheathing of keratin. The

bony core makes up the majority of the ornament size, but the keratinous sheath impacts the outer shape and color (e.g., black, grey, brown, green) of the ornament. Cassowaries hatch without casques but proceed to incorporate several cranial bones into the ornament during ontogeny. More is known about southern cassowaries (*C. casuarius*) than their congeners, with the former having casques that consist of the mesethmoid bone and median casque element as well as the left and right nasals, lacrimals, and frontals (Green & Gignac, 2020; Chapter II). Ornament growth in these birds begins at approximately 1.5. months of age and proceeds through adulthood (Green & Gignac, 2020; Chapter II). The majority of the casque size is attained via strong positive allometric growth by the point at which sexual maturity is reached (see Chapter III). Following this, casque enlargement appears to continue, albeit more slowly, throughout adulthood (Dodson, 1975; Green & Gignac, 2020; Chapter II; Chapter III). As a result of its bony complexity and relatively rapid growth (as compared to the rest of the head), there may be opportunities for variation in one or more of its bony components or outer keratin to contribute to overall variation in casque size or shape. Such patterns could explain, for example, how the casques of *C. bennetti* develop into relatively short trigonal pyramids (Fig. 1A–B), whereas those of *C. casuarius* become vertically tall, and laterally compressed keels (Fig. 1C–D), and yet the casques of *C. unappendiculatus* grow into vertically tall, but trigonally-shaped, headgear (Fig. 1E–F; Marshall, 1872; Rothschild, 1900; Perron, 2016). In addition, casques are frequently asymmetrical in all three species (Rothschild, 1900; Perron, 2016). This can be particularly extreme in *C. casuarius* (Rothschild, 1900), which tend to have casques that deviate laterally rightward or leftward of the midline (Fig. 2). Regardless, casque phenotypes have been used for species diagnosis for almost 150 years (Marshall, 1872; Rothschild, 1900). Whether cassowaries themselves utilize the casque for species recognition; however, has recently been debated (Hone & Naish 2013; Naish & Perron, 2016).

In addition to the high variability of the casque within species (Rothschild, 1900), cassowaries are endangered in some regions and considered to be dangerous birds (Rothschild, 1900; Kofron, 1999; IUCN, 2020)—all of which makes them difficult to study. Potential, rare

hybrids between pairs of recognized species (e.g., *C. casuarius* with *C. unappendiculatus*; Naish & Perron, 2016; Perron, 2016) that have intermediate phenotypes have similarly muddled the perceived distinctiveness of casque sizes, and especially shapes. Moreover, ornamental structures can function in multiple social contexts depending on behavior and audience, which could lead to differing display functions for the casque in different environments. Here, I formally examine casque shape variation across three scales of cassowary population organization in order to detect signals for ornament display in life-history and evolutionary contexts: (1) sexual dimorphism, (2) intraspecific geographic isolation, and (3) species recognition. I focused on *C. casuarius* as a central taxon of interest because the most is known about its behaviors, biology, and casque phenotypes among cassowaries. This enabled the opportunity to address the potential for sexual dimorphism and intraspecific, population-level differences within *C. casuarius*. I also examined how *C. casuarius* casques compare to those of their *C. bennetti* and *C. unappendiculatus* counterparts to quantify the extent of interspecific variation to differentiate each species. My overall aim, therefore, is to determine if casque shape is consistent with between-sexes, between-region, and between-species recognition hypotheses. I outline these hypotheses below.

Sexual dimorphism is common among birds, including cassowaries wherein females are approximately 30% larger than males (Olson & Turvey, 2013). In some avian species sexual dimorphism has been detected specifically in cranial ornaments, such as the casques of guinea fowl (*Numida*; Angst et al., 2019) and hornbills (e.g., *Bycanistes*, *Ceratogymna*; Kemp, 2001; Gamble, 2007), the fleshy knobs of curassows (i.e., *Crax*; Buchholz, 1991; Mayr, 2018), and the feather crests of peafowl (i.e., *Pavo*; Dakin, 2011). It has been previously hypothesized that the casques of *C. casuarius* may be sexually dimorphic (Rothschild, 1900; Crome & Moore, 1988; Hone et al., 2012; Naish & Perron, 2016), enabling females to be distinguished from males based on casque shape (e.g., relative tallness). If true, I hypothesize that sexes differ in casque shape, predictably. Support for this hypothesis would indicate that sexual dimorphism characterizes the *C. casuarius* casque, and sex may be an important source of variation for the casque phenotype.

Geographic segregation of conspecific populations can lead to opportunities for morphological divergences that increase variation. In extreme cases, major population-level differences in phenotype or resultant behavior can lead to reproductively isolating members of the same species, so much so that the populations can become reproductively incompatible (see Grant & Grant, 2009). Today, *C. casuarius* are widely distributed across several islands and mainland Australia. This is primarily the result of ancestral cassowary immigration across periodic land bridges between Australia, New Guinea, and smaller islands starting approximately 800,000 years ago (Naish & Perron, 2016). Glacially influenced sea level changes may have contributed to the geographic segregation of several populations of *C. casuarius* during this period (Naish & Perron, 2016). This history suggests that morphological variation in the casque may derive in part from the wide geographic distribution and regional isolation that *C. casuarius* experienced. If casque shape has evolved independently in these populations, then I hypothesize that shape differences within regional populations will be less than shape differences between regional populations, allowing for accurate categorization of *C. casuarius* subgroups based on casque shape. Support for this hypothesis would indicate that independent evolution due to geographic isolation may be an important source of *C. casuarius* casque variation.

Species recognition models propose that visually distinct ornaments and plumage can assist in distinguishing members of closely related species (Andersson, 1994). This appears to be the case for feather color patterns in birds like trogons (i.e., *Trogon*; Bitton & Doucet, 2016) and the headgear of artiodactyl mammals (Bubenik & Bubenik, 1990). The clear visual cues they provide are thought to indicate whether a potential mate is likely to be a compatible partner (Darwin, 1871; Andersson, 1994) when closely related species share geographic distributions. Cassowary species co-occur geographically. This is especially the case in New Guinea. There, *C. casuarius* and *C. bennetti* share territorial overlap across nearly their entire, shared southernly range edge as well as much of eastern Papua New Guinea, whereas *C. casuarius* and *C. unappendiculatus* overlap in only a relatively small region of western Indonesian Papua (Fig. 3; BirdLife International, 2019). If the

casque is capable of distinguishing *C. casuarius* from *C. bennetti* and *C. unappendiculatus*, then species recognition may contribute to genus-level variation in cassowary casques. To address this, I hypothesize that (1) species comparisons of casque shapes reliability distinguish *C. casuarius* from its congeners, and (2) casque shape differences will be greater between *C. casuarius* and *C. bennetti* because they interact more due to shared ranges, requiring more effective reproductive isolation mechanisms. Support for these hypotheses would indicate that species recognition characterizes the *C. casuarius* casque, that it is more important for sympatric *C. casuarius* and *C. bennetti* to tell each other apart, and that the nature of this variation may be necessary for the maintenance of casque variation between species.

I address each of these hypotheses by examining casque shape variation in a large, multi-species *Casuarius* dataset. To accomplish this, I utilized photographic data collection, 2D geometric morphometrics, and elliptical Fourier analyses. My findings support an incipient pattern of independent casque evolution due to geographic isolation for Australian *C. casuarius* as well as the opportunity for species recognition between southern and non-southern cassowaries. I interpret my findings in the context of behavior, biogeography, and speciation, specifically, and discuss how the results position cassowaries as a useful extant model to address ornament variation and evolution across Archosauria.

2. Material and Methods

2.1. Specimen Sample

In total, 163 adult cassowaries encompassing all currently recognized extant species ($N_{C.\ bennetti}$ = 34 $N_{C.\ casuarius}$ = 111; $N_{C.\ unappendiculatus}$ = 18) were sampled for this study (Table 1). Photographic data were collected from 155 cassowaries ($N_{C.\ bennetti}$ = 34; $N_{C.\ casuarius}$ = 103; $N_{C.}$

unappendiculatus = 18). All specimens possess intact keratinous casque sheaths. Photographs were taken for living animals as well as from fluid preserved, dry skins, and skeletally prepared (with keratin preserved) individuals (Table 1). Specimen data were collected from the American Museum of Natural History (AMNH; New York, NY, USA), Brevard Zoo (BVZ; Melbourne, FL, USA), Cassowary Conservation Project (CCP; Fort Pierce, FL, USA), Denver Museum of Nature and Science (DMNS; Denver, CO, USA), Melbourne Museum (Museums Victoria, MV; Melbourne, VIC, AU), Museum of Osteology (MOO; Oklahoma City, OK, USA), Natural History Museum (NHMUK; Tring, UK), Queensland Museum (QM; Brisbane, QLD, AU), Sedgwick County Zoo (SCZ; Wichita, KS, USA), T. L. Green Research Collection (TLG; Tulsa, OK, USA), University of New England Natural History Museum, (UNE; Armidale, NSW, AU), and the Wet Tropics of Queensland (WTQLD; Cape Tribulation, QLD, AU and Etty Bay, QLD, AU). Adult status was ascertained via prior documentation of successful breeding activity, exclusively black plumage, and/or museum-voucher indication of maturity. Taxonomic determination of each *Casuarius* species was based on a combination of previously established, species-specific anatomical characteristics, including wattle number, apteria coloration, and casque appearance (Marshall, 1872; Rothschild, 1900; Perron, 2016). No institutional animal care and use protocol was required for this study. Vouchered specimens were obtained from museum collections or as opportunistically-collected cadaveric specimens after death. For living specimens, only non-intrusive, photographic data were obtained with organization permission from captive specimens (BVZ, CCP) and wild birds (WTQLD), which required no direct interaction with the animals.

2.2. Photographic Data Collection

Photographs for morphometric analyses were collected by T. L. G. using a Panasonic DMC-ZS60, Lecia DC Vario-Elmar 1:3.3-6.4/4.3-129 ASPH Lens (Panasonic Corporation, Kadoma, JP; Lecia Microsystems, Wetzlar, GER) and a Canon EOS D60, Tamron SP 200-500mm

F/5.0-6.3 Lens (Canon Inc., Tokyo, JP; Tamron Corp., Saitama, JP). Photographs were taken at ≥ 1.0 m distance from each sample with solid-contrasting backgrounds (when possible) to ensure visibility of casque outlines. All vouchered and living specimens were photographed with the Panasonic DMC-ZS60 (n = 159) except for those taken of living cassowaries at WTQLD (n = 4). Photos of living cassowaries were collected behind chain-link fencing at BVZ and CCP and with a telephoto lens (but no barrier) at WTQLD, both of which served to ensure safely for the observer. To avoid potential image distortion due to the use of two lenses, I standardized the photography protocol following steps for common specimen framing, alignment, and position recommended by Marugán-Lobón and Buscaliono (2004). Specimens were photographed individually with each head centered, occupying < 50% of the frame, and with all anatomical structures of interest in focus and absent from the image edges. Specifically for lateral photographs, crosshairs were centered upon the middle of the eye (or orbit if the eye was not present). For rostral photographs crosshairs were centered upon on the rostralmost midpoint of the casque, aligned with the midpoint of the eyes (Fig. 4).

2.3. Casuarius casuarius *Sex Data Collection*

In order to test for morphological differences between sexes in *C. casuarius*, I sampled mature individuals of both sexes (n = 24 females, n = 35 males; Table 1). Depending on the condition of the casques and access to all casque view of specific individuals, there were instances in which know-sex specimens were used for one analysis and not others (see sex breakdown for each respective section). Sex was determined based on museum voucher data, known breeding status, or sex-specific behavioral observations (e.g., males incubating eggs or rearing chicks, which are standard behaviors for male cassowaries; Crome, 1976).

2.4. Geographic Data Collection

I sampled cassowaries broadly from across their known, present-day and historical ranges. Geographic specimen data were not historically recorded for all specimens in my sample, and those that included collection regions often did not describe precise localities (Table 1). Nonetheless, *C. casuarius* specimens provided the highest resolution spatial data. Each individual (n = 45) was categorized into broad geographic regions: Australia (AUS), INDP = Indonesian Papua; southern Papua New Guinea (SPNG); western islands near New Guinea (WIS); Fig. 5; Table 1). These regions represent populations from across a > 650 km range that have experienced periodic geographic isolation (Naish & Perron, 2016). I note that *C. casuarius* from islands west of New Guinea (i.e., Seram and Aru Islands) likely comprise native and introduced (BirdLife International, 2019) individuals. I combined the two islands into a single region for my analyses (Fig. 5) because they potentially represent an admixture from other populations that cannot be accounted for. I also discounted specimens that were geographically too broad (e.g., "New Guinea"), or were described as captive for all or part of their life (indicated by dashes in geography column of Table 1). Finally, *C. casuarius* is found in a relatively small region of northern Papua New Guinea (Fig. 5); however, I did not sample any individuals known to have come from this region. Modern cassowary range distribution data for all three species (*C. bennetti*, *C. casuarius*, *C. unappendiculatus*) were used with permission from BirdLife International (2019).

2.5. Casuarius *2D Geometric Morphometric Analyses*

Only cassowary individuals with undamaged and non-pathologic casques (e.g., sections of casque broken off in life) were included in the 2D geometric morphometric analyses, 155 in all ($N_{C.\ bennetti}$ = 34; $N_{C.\ casuarius}$ = 103; $N_{C.\ unappendiculatus}$ = 18). One hundred fifty-three lateral and 139 rostral photographs were taken to assess 2D shape differences across 155 individuals (Table 1). In some

instances, casques were suitable for one view (lateral or rostral) and not the other due to slight damage (i.e., keratin flaking) or physical access to all sides of a specimen. Photos were imported into Microsoft PowerPoint 365 (Microsoft Corp., Redmond, WA, USA) and closed outlines were traced using the Bézier curve tool. The resulting shapes were filled (which created a standardized, straight-lined casque base from rostralmost to caudalmost edges in lateral view, or from right to left lateral edges in anterior view, to account for the ventral casque margin), saved as Portable Network Graphics files (PNGs), converted to a binary mask in ImageJ (v. 1, US National Institutes of Health, Bethesda, MD), and exported as Joint Photographic Experts Group files (JPGs). Most (n = 140) of the lateral shapes were drawn from photos taken of the left side of the animal; however, 13 individuals ($N_{C.\ bennetti}$ = 1; $N_{C.\ casuarius}$ = 11; $N_{C.\ unappendiculatus}$ = 1) were photographed from the right side only. The right-lateral casque shapes were mirrored before combining with those from the left side. In order to confirm that left and right-mirrored casques could be accurately pooled together for analysis, I compared a random subset of shapes from 20 *C. casuarius* that were photographed from both left and right sides. I removed the effects of orientation, location, and scale from the outline data with a generalized Procrustes alignment, quantified outline shape using an elliptical Fourier analysis, ordinated the resultant harmonic data (e.g., Fig. 6) using a principal coordinate analysis (PCOa), conducted a multivariate analysis of variance (MANOVA) to test for significant differences between left and right-mirrored casque shapes, and evaluated the classifiability of left and right-mirrored shape data with a linear discriminant analysis (LDA) on the principal coordinates (for specifics see more detailed workflow below; see Appendix C for R code). The PCOa for *C. casuarius* left and right-mirrored lateral casque shapes resulted in 26 principal coordinates with the first two capturing 83.2% of the total shape variation (PCO1 = 70.0%; PCO2 = 13.2%). Six axes were retained for the MANOVA as they explained 99.0% of data variance. The MANOVA failed to detect a significant difference ($\alpha = 0.05$) between left and right-mirrored casques ($p = 0.282$). Linear discriminant analysis results for lateral casque shapes indicate an overall cross-validation rate of 62.5% with 65.0% accuracy for left casque shapes and 60.0%

accuracy for right mirrored casque shapes. The LDA on PCOa results indicate that shape predicts left versus right-mirrored shapes about as well as random chance. These results provide a justification for combining the thirteen mirrored right lateral shapes with the left lateral shapes in my formal analyses. I also tested for outliers in the entire casque shape outline set, using the *Momocs* package (Bonhomme et al., 2014) in R (v 3.6.3; R Core Team, 2020), to identify lateral and rostral outliers within each species (see Appendix C for R code). Four potential shape outliers were flagged for *C. bennetti* (one lateral, three rostral), 12 for *C. casuarius* (eight lateral, four rostral), and two for *C. unappendiculatus* (one lateral, one rostral). These individuals were re-evaluated for labelling issues, tracing errors, photographic artifacts, and pathologies. None were identified; therefore, it was determined that these specimens were likely flagged because they have casque shapes that are relatively rare for their respective species in the overall shape space (e.g., particularly tall, as was a case for *C. casuarius* outliers). Two of these flagged individuals were right-mirrored lateral-casque tracings; however, I also found these individuals to have rarer shapes for *C. casuarius*. Therefore, I recognize these individuals as statistical—not biological—outliers, and did not remove them from the analyses. Below I account for incorporation of statistical outliers in my MANOVAs.

I ran six shape analyses in total. In my lateral-view casque shape analyses, I tested three primary factors: (1) sex in *C. casuarius* (n = 23 females, n = 30 males), (2) geographic region in *C. casuarius* (n = 20 AUS, n = 8 INDP, n = 9 SPNG, n = 8 WIS), and (3) species identity (n = 34 *C. bennetti*, n = 101 *C. casuarius*, n =18 *C. unappendiculatus*). In my rostral-view casque shape analyses, I tested the same three primary factors: (1) sex in *C. casuarius* (n = 18 females, n= 24 males), (2) geographic region in *C. casuarius* (n = 15 AUS, n = 8 INDP, n = 9 SPNG, n = 6 WIS), and (3) species identity (n = 34 *C. bennetti*, n = 87 *C. casuarius*, n = 18 *C. unappendiculatus*). All shape quantification and statistical analyses were completed in R (v 3.6.3; R Core Team, 2020; see Appendix C for R code) using the *Vegan*, *MASS*, and *Momocs* packages (Oksanen, et al., 2007; Ripley, 2013; Bonhomme et al., 2014). I imported, assigned and converted into coordinate outlines,

and aligned (i.e., oriented, scaled, and centered) my binary casque shape files using generalized Procrustes analyses. Next, casque outlines were quantified using elliptical Fourier analyses (EFAs; see Felice & O'Connor, 2014). Elliptical Fourier analyses were selected for this study because the casques of adult cassowaries do not have easily-placed homologous landmarks, particularly on the distal areas of interest. Instead, EFA uses x-y coordinates as semi-landmarks and quantifies shape with harmonic variables. The number of harmonics were chosen to capture 99.9% of casque shape (14–16 harmonics for each analysis; 16 for lateral sex in *C. casuarius*, 14 for rostral sex in *C. casuarius*; 16 for lateral geographic region in *C. casuarius*, 14 for rostral geographic region in *C. casuarius*, 15 for lateral species identity in *Casuarius*, and 15 for rostral species identity in *Casuarius*) while maintaining statistical power by assigning fewer harmonics than samples tested. Harmonic data were ordinated by conducting principal components analyses (PCAs). The principal component (PC) scores were plotted to visualize and inspect the resultant morphospace as well as and convex hulls of grouping factors for each analysis (i.e., sex, geographical region, or species identity) Using PC-score data representing 99.0% of variance (6–14 axes), MANOVAs were run to test for significant differences ($\alpha = 0.01$) between casques, and pairwise MANOVAs were used to test the comparisons between grouping factors. Alpha values of 0.01 were chosen for all MANOVAs to reduce the potential for Type 1 error, which could be inflated by including statistical outliers in my analyses. Linear discriminate analyses were run to evaluate the ability of the different groups within each factor to be classified given their shape data.

In order to better interpret my *C. casuarius* rostral shape output results for sex and geography, I additionally analyzed and categorized casque asymmetry. I analyzed asymmetries from 111 *C. casuarius* and compared specific deviation degree categories from 88 specimens. Asymmetries from 43 known-sex *C. casuarius* individuals were also compared (n = 19 females, n = 24 males). *Casuarius casuarius* casques grow from unpaired bones located along the midline (mesethmoid and median casque element) as well as paired bones located immediately parasagittal to the midline (frontals, lacrimals, and nasals), covered in tightly adhering keratin (Gignac and

Green, 2020). Casque initiation and early inflation tends to align with the mid-sagittal axis. However, adult casques commonly deviate away from midline (Rothschild, 1900; Perron, 2016; Fig. 2), taking on a left or right-sided convexities as they mature with the dorsal most aspect of the casque sometimes deviating dramatically to the left or right. This phenomenon is most dramatic in *C. casuarius* as compared to the other two species and can result from asymmetries in both the underlying bone and keratinous sheath (T. L. G. personal observation). To capture casque variations as they relate to deviation, I assessed asymmetries in all *C. casuarius* specimens from rostral-view photographs (Fig. 4D–F). I defined a deviation as the direction of the casque offset from the midline within the transverse plane. Deviation phenotypes (non-deviated, leftward, rightward, sinusoidal leftward, sinusoidal rightward; Fig. 2B–F) were described visually and the amount of deviation was defined quantitatively, using angles based on the absolute value of degrees (rounded to the nearest 1°). Sinusoidal casques are those that deviate in one direction at the anteroproximal base only to recurve on themselves to deviate in the other direction at the distal tip. The measurement for casque deviation angle was characterized by a line passing along the midsagittal plane from above the orbits to the rostralmost casque base to the lateralmost point of the deviated dorsal casque, ignoring the previously mentioned sinuous topology: (1) none–minimal leftward or rightward (0–5°), (2) slight–moderate leftward (6–30°), (3) slight–moderate rightward (6–30°), (4) severe–radical leftward (31–60°), and (5) severe–radical rightward (31–60°) (Fig. 7; Table 1). Although I documented several examples of sinusoidal casques there were no phenotypes in the sample which casque morphology was both sinusoidal and the overall angular measurement of asymmetry was non-deviated.

3. Results

3.1. Casuarius casuarius *Casque Shape – Sex*

The PCA for *C. casuarius* known-sex lateral casque shapes resulted in 53 principal components with the first two capturing 80.2% of the total shape variation (PC1 = 66.0%; PC2 = 14.2%; Fig. 8). The PCA for *C. casuarius* known-sex, rostral casque shapes resulted in 42 principal components with the first two capturing 78.7% of the total shape variation (PC1 = 51.8%; PC2 = 26.9%; Fig. 9). Convex hulls around female and male PC scores overlap substantially in the morphospace plots for both lateral and rostral PCAs (Figs. 8, 9), suggesting the females and male casques share similar shapes and shape variances. Multivariate analysis of variances for *C. casuarius* known-sex, lateral and rostral casques yielded non-significant p-values ($p > 0.01$; Table 2), indicating that neither lateral nor rostral casque shape differences are apparent between *C. casuarius* females and males. Linear discriminant analysis results for *C. casuarius* known-sex, lateral casques indicates an overall cross-validation rate of 60.4% with 47.8% accuracy for females and 70.0% accuracy for males (Fig. 10). Linear discriminant analysis results for rostral casque shapes indicate an overall cross-validation rate of 61.9% with accuracy for females and 50.0% and 70.8% accuracy for males (Fig. 10). Given that the MANOVAs are not significantly different, the LDA results indicate that shape predicts sex about as well as random chance. The finding fails to support my hypothesis that sex can be predicted from casque shape in *C. casuarius*.

3.2. Casuarius casuarius *Casque Shape – Geography*

The PCA for *C. casuarius* known-geography, lateral casque shapes resulted in 45 principal components with the first two capturing 78.1% of the total shape variation (PC1 = 60.7%; PC2 = 17.4%; Fig. 11). The PCA for *C. casuarius* known-geography, rostral casque shapes resulted in 37

principal components with the first two capturing 77.8% of the total shape variation (PC1 = 48.5%; PC2 = 29.3%; Fig. 12). Convex hulls around AUS, INDP, SPNG, and WIS PC scores overlap substantially in the morphospace plots for both lateral and rostral PCAs (Figs. 11, 12), suggesting regional groups share similar shapes and shape variances. Multivariate analysis of variances and pairwise comparisons for *C. casuarius* known-geography, lateral and rostral casque shapes generally yielded non-significant p-values ($p > 0.01$; Table 2). Exceptions were significant p-values in pairwise comparisons between lateral AUS–WIS and rostral AUS–INDP. This result indicates that AUS cassowaries in my sample differ from INDP and WIS groups, each in just a single view, whereas the rest of the sampled *C. casuarius* populations share similar overall shapes. Linear discriminant analysis results for *C. casuarius* known-geography, lateral casque shapes indicate an overall cross-validation rate of 51.1% with 55.0% accuracy for AUS, 25.0% for INDP, 44.4% for SPNG, and 75.0% for WIS (Fig. 13). Linear discriminant analysis results for rostral casque shapes indicate an overall cross-validation rate of 43.2% with 60.0% accuracy for AUS, 16.7% for INDP, 33.3% for SPNG, and 42.8% for WIS (Fig. 13). The LDA results indicate that shape consistently predicts geography poorly. The finding fails to support my hypothesis that geographic locality can be reliably predicted from casque shape in non-Australian *C. casuarius*.

3.3. Casuarius casuarius *Casque Asymmetry*

In *C. casuarius*, casques were non-deviated in 1.8% of the sample, followed by leftward and leftward sinusoidal deviations (i.e., 20.7%), and most commonly deviated to the rightward and rightward sinusoidal (i.e., 77.5%; Table 1). Quantitatively, casques of 60.2% of my *C. casuarius* sample had slight–moderate rightward deviations from midline (6–30°), whereas 22.7% showed none–minimal deviations (left or right 0–5°), 9.1% showed severe–radical rightward deviations (31–60°), 6.8% showed slight–moderate leftward deviations (6–30°), and only 1.1% showed severe–radical leftward deviations (31–60°; Fig. 14). Among female and male *C. casuarius*, an

approximately equal number of each sex had slight–moderate deviations (68.4% and 75.0%, respectively) regardless of side. Among severe–radical deviations, females were more commonly represented than males (26.3% and 4.2%, respectively), whereas among non–minimal deviations, males were more commonly represented than females (20.8% and 5.3%, respectively; Fig. 15).

3.4. Casuarius *Casque Shape – Species Identity*

The PCA for known-species, lateral casque shapes resulted in 153 principal components with the first two capturing 79.3% of the total shape variation (PC1 = 61.6%; PC2 = 17.7%; Fig. 16). The PCA for known-species rostral casques resulted in 139 principal components with the first two capturing 80.3% of the total shape variation (PC1 = 57.1%; PC2 = 23.2%; Fig. 17). Convex hulls around *C. bennetti*, *C. casuarius*, and *C. unappendiculatus* PC scores overlap partially for both lateral and rostral shape spaces (Figs. 16, 17), suggesting that species-specific casque shapes and shape variances may be distinguished. Multivariate analysis of variances and pairwise tests for species-identity dyads yielded significant p-values ($p < 0.01$; Table 2) for both lateral and rostral casque shape comparisons. This indicates that the casque shapes of *C. casuarius* are significantly different in lateral and rostral views from those of *C. bennetti* and *C. unappendiculatus*. Moreover, this result also documents that the casque shapes of *C. bennetti* and *C. unappendiculatus* can also be distinguished from each other in these views. Linear discriminate analysis results for known-species, lateral casque shapes indicate an overall cross-validation rate of 88.9% with 94.1% accuracy for *C. casuarius*, 97.1% accuracy for *C. bennetti*, and 44.4% for *C. unappendiculatus* (Fig. 18). Linear discriminate analysis results for rostral casque shapes indicate an overall cross-validation rate of 88.5% with 94.3% accuracy for *C. casuarius*, 88.2% for *C. bennetti*, and 61.1% for *C. unappendiculatus* (Fig. 18). Significant MANOVAs alongside the LDA results indicate that shape predicts species identity especially well for *C. casuarius* and *C. bennetti*. The findings support my hypotheses that, (1) species identity can be predicted from casque shape, and (2) casque

shapes are more distinct between *C. casuarius* and *C. bennetti*, which share the greatest geographic overlap.

4. Discussion

4.1. Intraspecific Casque Shape Variation in Casuarius casuarius

I examined casque variation in *C. casuarius* from three perspectives: between male and female casque shapes, between geographic region casque shapes, and among casque asymmetries. Despite variability between the casques of *C. casuarius* individuals, I did not find significant differences in lateral or rostral casque shapes ($p = 0.082$ and 0.239, respectively) between females and males (Table 2; Figs. 8, 9, 10). *Casuarius casuarius* females are approximately 30% larger in body mass than males (see Olson & Turvey, 2013). This has likely led to speculation as to whether *C. casuarius* casques are also dimorphic (Rothschild, 1900; Crome & Moore, 1988; Hone et al., 2012; Naish & Perron, 2016). Despite this size differential between sexes, female and male cassowaries appear to possess relatively similar external features, and my study suggests that casque shape is indistinguishable between sexes. A female with a large casque, for example, is also a large-bodied female, suggesting that overall size, to which the casque contributes but is not separate from, provides a signal of sex for some *C. casuarius*. Adult females of moderate size compared to those of adult male cassowaries; however, do not appear to have casques with female-specific shapes, precluding the opportunity for distinguishing sex based on casque shape in those females that have not achieved maximum size. Overall, this finding supports previous results that casque developmental trajectories between male and female *C. casuarius* are also non-dimorphic (see Chapter III).

My results identified significant differences in lateral and rostral casque shape between just a small number of *C. casuarius* regional populations, namely Australian populations appear to stand out from those in Indonesian Papua and western islands near New Guinea (p = 0.010 and 0.003, respectively; Table 2; Figs. 11, 12, 13). These findings suggest that casque variation can harbor a regional signature, albeit a relatively weak one in my overall sample. Notably, subspecies interpretations among *C. casuarius* involve distinguishing traits like region-specific apteria coloration, whereas the inclusion of casque morphologies have been contentious (Rothschild, 1900; Naish & Perron, 2016; Perron, 2016). My data are ambiguous as to whether casque shape is reliable for subspecies designations, but genetic comparisons alongside additional morphological and behavioral studies will assist my understanding of how these characters are distributed among *C. casuarius*. I recommend that focusing on Australian cassowaries may be the most fruitful, considering that casques from AUS individuals involved two instances of shape significance in my MANOVA pairwise tests.

Cranial asymmetries are relatively common in some vertebrate groups, such as crossbills (i.e., *Loxia*, Benkman, 1996), ‘akepa (*Loxops*; Hatch, 1985), owls (e.g., *Aegolius*, *Bubo*; Norberg, 1977), and cetaceans (e.g., *Monodon*, *Phocoena*; Ness, 1967; Yurick & Gaskin, 1988). Often, cranial asymmetry is proposed to offer a functional advantage (e.g., feeding efficiency; acoustic triangulation; Norberg, 1977; Benkman, 1996). To my knowledge, this is the first study in which symmetrical casque deviations have been classified among cassowaries. Deviated casques provide an important piece of information about *C. casuarius* casque phenotypes. For example, one aspect of the wide morphological variance they demonstrate is due to their asymmetry, which is captured along PC1 of rostral casque shapes for both male-female (Fig. 9) and geographic region comparisons (Fig. 12). This indicates that asymmetry strongly influences the shape space that *C. casuarius* casques occupy. It may be tempting to assume that directly vertical growth of the tall, narrow casques of *C. casuarius* are difficult to maintain against the force of gravity, mechanical damage from walking through dense forests, or fighting among conspecifics (agonistic behaviors

such as charging, chasing, kicking are common for cassowaries; Rothschild, 1900; Crome, 1976; Kofron, 1999). However, the tallest casques in my sample are non-deviated, indicating that symmetry is not necessarily a corollary of tallness. Additionally, the uneven (rightward biased) directional asymmetry suggests a developmental bias, which could be due to nutritional availability, environmental influences, genetic predisposition, or a combination of the three. For example, *C. casuarius* casques are thought to function in thermoregulation (Phillips & Sanborn, 1994; Eastick et al., 2019), and casque deviations may play a role in optimizing the casque as a thermal window, and this function may differ geographically or with altitude. On the other hand, proclivity for rightward asymmetry may be due to historic sampling biases for extravagant casques, unidentified factors from regional collection sites, or random chance in my specific sample. Ultimately, a better understanding of late ontogeny casque development, wherein asymmetries appear to be more common, may help elucidate this issue.

4.2. Interspecific Casque Shape Variation in Casuarius

My results detected significant differences in lateral (p = 2.8e−52, 1.8e−14, and 6.4e−11) and rostral casque shape (p = 2.0e−30, 3.0e−08, and 4.0e−13) between all three cassowary species (Figs. 16, 17, 18). I proposed that such a pattern would be consistent with species recognition if it were strongest for the species pair that shared the greatest interactions due to geographic overlap, which my data also support. Previous observational studies of apteria color patterns, wattle number, (i.e., two wattles, *C. casuarius*; one wattle, *C. unappendiculatus*; no wattles, *C. bennetti*), and casque morphology aided in taxonomic arrangement of species within *Casuarius* (see Rothschild, 1900; Perron, 2016). My study is the first to quantitatively test casque shape differences between the three cassowary species, and it supports the current taxonomic designation (Table 2; Figs. 16, 17, 18). The casques of *C. bennetti* and *C. casuarius* are the most classifiable based on lateral (accuracy of 97.1% for *C. bennetti*, 94.1% for *C. casuarius*) and rostral shapes (accuracy of 88.2%

for *C. bennetti*, 94.3% for *C. casuarius*; Fig. 18). *Casuarius casuarius* casque shapes had the largest convex hulls (lateral and rostral) compared to the other two species. Convex hulls for *C. unappendiculatus* casque shapes (lateral and rostral; Figs. 16, 17) illustrate that its casques share shape characteristics with *C. casuarius*, and to a lesser degree *C. bennetti*, even though *C. unappendiculatus* is considered significantly different from the other two species based on my MANOVA pairwise tests (p = 1.8e−14 and 6.4e−11 in lateral shape; p = 3.0e−08 and 4.0e−13 in rostral shape; Table 2). Notably, there is speculation that *C. casuarius* and *C. unappendiculatus* may hybridize due to specimens with cosmopolitan phenotypic characters of the two species (Naish & Perron, 2016; Perron, 2016). To my knowledge, however, there is are published genetic or pedigree data to confirm hybridization is a phenomenon between any *Casuarius* species.

It has been proposed that current cassowary distribution may be explained by a combination of factors, including elevational suitability, periodic redistribution via land bridges, and human transport (see Naish & Perron, 2016; Perron, 2016). *Casuarius casuarius* inhabits regions below 1,400 meters (m) of northeastern Australia, southeastern Papua New Guinea, and southwestern and northwestern Indonesia. *Casuarius unappendiculatus* inhabits regions below 700 m of northern Papua New Guinea and northern and northwestern Indonesia. *Casuarius bennetti* inhabits regions below 3,600 m of northwestern, southeastern, and central Papua New Guinea and northwestern, northeastern, and central Indonesia (Fig. 3; BirdLife International, 2019; IUCN, 2020). For the most part, each species has an exclusive home range; however, all three cassowary species overlap near the edges of their natural distributions (see Fig. 3; BirdLife International, 2019). Reports of *C. bennetti* inhabiting the higher elevations than the other two species, as well as reports of it living at sea level (Fig. 3; BirdLife International, 2019) suggests it has the widest elevational distribution. For example, not only is there is range overlap along much of the boundary between *C. casuarius* and *C. bennetti*, but the elevational range of *C. bennetti* contributes to especially substantial overlaps for *C. casuarius* and *C. bennetti* in eastern Papua New Guinea along coastal regions facing the Gulf of Papua, the Huon Gulf, and the Coral Sea. Range overlap also

occurs in northwestern Indonesia between all three species (Fig. 3; BirdLife International, 2019). This is the only region where *C. casuarius* and *C. unappendiculatus* overlap, which I argue contributes to limited opportunities for reproductive isolation to develop between this species pairing as compared to *C. casuarius* and *C. bennetti*.

Within my sample for *C. unappendiculatus*, I also noticed that casque morphology varied substantially across "yellow-necked" and "red-necked" birds (see Fig. 1E–F). Although *C. unappendiculatus* had the lowest sample size of all three species, individuals with predominantly yellow necks in my sample also tended to have flatter dorsal casque surfaces while the predominately red-necked individuals appear to possess taller casques with less of a dorsal platform. Subspecies delineations for *C. unappendiculatus* are tentative due to these yellow and red color variations of the apteria. Perron (2016) offers the suggestion that individuals with primarily yellow necks occur in northwestern New Guinea and individuals with primarily red necks occur in northeastern New Guinea, producing gradational color morphologies to exist in between. If this is the case, it may also elucidate potentially clinal *C. unappendiculatus* casque morphologies. I recommend future anatomical studies with more precise location data to test these patterns in *C. unappendiculatus*.

4.3. Conceptual Model for Casque Evolution and Implications for its Current Display Functions

I propose that the casque serves as a visual display function in modern cassowaries. In *C. casuarius* it appears to contribute to whole-body signals of maturity, alongside feather and apteria coloration (see Chapter III). In addition, I further propose that the casque is potentially a species recognition feature, capable of assisting cassowaries in distinguishing conspecifics from non-conspecifics. Across my study of variation, the results suggest a general scenario for the evolutionary history and maintenance of the cassowary casque. My conceptual model requires five steps: (1) one or more ancestral behaviors that provided a suitable selective regime prior to the

origin of the casque, (2) co-option of previously generalized anatomy or evolution of a neomorphic feature capable of exploiting ancestral behavioral preferences, (3) the opportunity for variation in this focal anatomy, (4) the opportunity for speciation to occur within the proposed timeline of trait evolution, and (5) the reinforcement of novel trait variants that maintain species distinctness. Specifically, for cassowaries, these five steps conform to the following:

1. Selective Regime: Stretch displays are ancestral for paleognathous birds as demonstrated by their common use in *Struthio*, *Dromaius*, and *Casuarius* (Bolwig, 1973; Crome, 1976; Menon et al., 2014), which are thought to share a common ancestor 72.8 million years ago (Mitchell et al., 2014). The stretch display is a full body exhibition, in which neck and torso are extended vertically (Bolwig, 1973; Crome, 1976; Menon et al., 2014). This behavior is based on visually evaluating competitor height, which is consistent with the means by which dominant animals establish their tallness (Bolwig, 1973; Menon et al., 2014). Long legs and long necks were already favored in this context (e.g. *Struthio*), so evolution of prominent headgear was able to be selected for. In cassowaries, the casque is the pinnacle of the stretch display, which adds to overall height. Due to their solitary nature and mostly frugivorous diet (Rothschild, 1900; Crome, 1976; Stocker & Irvine, 1983), it has been hypothesized that aggressive displays in cassowaries may associated with the guarding of spatial areas with accessible rainforest fruits (Rothschild, 1900; Kofron, 1999). Stretch displays may also enable this perceived height advantage to minimize physical confrontation with competitors (Crome, 1976). In *C. casuarius* females are dominant in association with their absolutely larger size (Olson & Turvey, 2013). Because casque ontogeny appears to be shared between male and female cassowaries (Chapter III) and because casque shapes do not differ meaningfully between male and female adult *C. casuarius*, the larger body size of females enables them to also have absolutely taller

casques, which provides a reinforcing mechanism for prevailing during stretch displays.

2. Morphological Evolution: All modern cassowaries have casques, whereas all other tall-bodied paleognaths lack a casque. This suggests a single origin for the casque at the base of the clade *Casuarius*. The casque of *C. casuarius* is composed of seven plesiomorphic bones present in the skulls of most archosaurs: right and left nasals, lacrimals, and frontals as well as the mesethmoid (Green & Gignac, 2020; Chapter II). In addition, a probable, neomorphic median casque element appeared prior to or during the evolution of the casque (at least in *C. casuarius*; Green & Gignac, 2020; Chapter II). Together, these bones expand during cassowary ontogeny with positive allometry, enabling the casque to contribute meaningfully to stretch displays of adult individuals in particular.
3. Morphological Variation: Although tallness appears to be a priority in *C. casuarius* casque ontogeny, it is possible for casque shapes to deviate due to population isolation as I demonstrate for Australian *C. casuarius*. This finding establishes that independent evolution of casque shape, leading to morphological divergence, is possible for *C. casuarius*. While composed of eight bony elements and tightly covered in a keratinous sheathing (Green & Gignac, 2020; Chapter II), the complexity of the casque does not preclude the opportunity for significant variation.
4. Speciation: *Casuarius* underwent a series of geographic isolations due to sea level changes starting in the middle Pleistocene (Naish & Perron, 2016). Isolation paired with population level independent evolution in casque morphologies between isolated groups is demonstrated by Australian *C. casuarius*, providing evidence that within-species casque morphologies can become different enough that allopatric speciation may have been possible for cassowaries.

5. Reinforcement of Species Boundaries: As would be expected by mechanisms that minimize opportunities for interbreeding, cassowaries that share the greatest geographic overlap (i.e., *C. casuarius* and *C. bennetti*), have the most distinct casques. This suggests that reinforcement of species boundaries has been stronger between *C. casuarius* and *C. bennetti* than between *C. casuarius* and *C. unappendiculatus*.

If valid, I am proposing the casque functioned historically for status assessment via intraspecific display before being co-opted for use in interspecific recognition. Today, extant cassowaries appear capable of using their casques for both biological roles.

Whether the unique median casque element evolved prior to the evolutionary appearance of the casque could be addresses by documenting casque composition in *C. bennetti* and *C. casuarius*, and previous anatomical figures of similarly aged specimens suggest this is likely the case (Parker, 1866; Pycraft, 1900). If all three species incorporate a dorsalmost midline bone into their casques that is unique for the avian skull and shares developmental origins with the median casque element in *C. casuarius*, then this would suggest a single origin for the median casque element that likely occurred early in the evolution of the cassowary casque as we know it today.

I further anticipate that future molecular evolution research into *Casuarius* biodiversity will correspond to the morphological differences I have uncovered here, providing genetic evidence for divergence periods associated with Pleistocene glacial maxima and geographic isolation of *C. casuarius* from *C. bennetti*. To that end, a focus on the location and duration of transitory land bridges in Oceana during the last 800,000 years represent additional key pieces of information to piece together cassowary evolutionary history.

4.4. Casuarius *Casques as a Modern Analog for the Evolution of Bony Cranial Ornaments*

Casuarius has long been considered a focal taxon for addressing the development, function, and evolution of bony cranial ornaments (Parker, 1866; Flower, 1871; Marshall, 1872; Pycraft, 1900; Rothschild, 1900; Dodson, 1975; Crome & Moore, 1988; Richardson, 1991; Phillips & Sanborn, 1994; Starck, 1995; Mack & Jones, 2003; Hone at al., 2012; Farke et al., 2013; Naish & Perron, 2016; Perron, 2016; Lü et al., 2017; Mayr, 2018; Eastick et al., 2019; Green & Gignac, 2020; Chapter II). This perspective gained prominence in association with hypotheses that explain the disparity of bony cranial ornaments in the non-avian dinosaur fossil record, including for hadrosaur, ceratopsian, pachycephalosaur, and theropod dinosaurs (e.g., Dodson, 1975; Molnar, 2005; Evans, 2006; Horner & Goodwin, 2006; Evans, 2010; Knell & Sampson, 2011; Padian & Horner, 2011; Schott et al., 2011; Hone at al., 2012; Peterson & Vittore, 2012; Farke et al., 2013; Hone & Naish, 2013; Farke, 2014; Gates et al., 2016; Lü et al., 2017). Prior work evaluating cassowary casques for this purpose has concluded that the casque is unlikely to function primarily for display or species recognition (Hone & Naish, 2013; Naish & Perron, 2016). My results suggest that these conclusions may have been premature. Previous efforts to quantify the variation of bony cranial ornaments has not focused on cassowaries, which has caused a gap between our hypotheses about the role of osseous headgear in species recognition and our appreciation of how extant archosaurs might clarify evidence of this function.

I propose that cassowaries are an appropriate model for exploring the development, function, and evolution of the casque as an archosaurian bony display structure with biological roles for the recognition of maturity and status within species and mating compatibility between species. Importantly, I recommend that behavior and biogeography are critical for outlining the origin and evolution of the cassowary casque, and that these are likely essential corollaries to further unravel in the dinosaur fossil record as well. Additional examination of cassowary ontogeny, life-history, population biology, biogeography, and evolution all hold the potential to further define this

natural experiment in cranial variation and more deeply inform our understanding of non-avian dinosaur cranial disparity and ornament evolution. Cassowaries are rare, at risk (IUCN, 2020), and potentially dangerous birds to work with (Kofron, 1999; Rothschild, 1900). However, they represent an uncommon window into exploring the processes and patterns that contribute to the extreme morphologies which commonly capture the popular and technical interests of amateur and professional paleontologists alike. Future cassowary research presents the opportunity to bear fruit not just for our appreciation of modern avian biodiversity, but also for formally examining long-held hypotheses about the nature of such biodiversity in the distant past.

Table 1. Adult *Casuarius* specimen list, indicating sex, preparation history, and data collected.

Species	Specimen ID	Sex	Type	LAT	ROS	DEV	DEG	GEO
C. bennetti	AMNH FLUID 12482	U	Fluid	x	x	—	—	—
C. bennetti	AMNH SKIN 268350	F	Dried	x	x	—	—	—
C. bennetti	AMNH SKIN 333637	F	Dried	x	x	—	—	—
C. bennetti	AMNH SKIN 333638	F	Dried	x	x	—	—	—
C. bennetti	AMNH SKIN 419269	U	Dried	x	x	—	—	—
C. bennetti	AMNH SKIN 422441	M	Dried	x	x	—	—	—
C. bennetti	NHMUK 1876.4.24.1	U	Dried	x	x	—	—	—
C. bennetti	NHMUK 1916.4.26.1	U	Dried	x	x	—	—	—
C. bennetti	NHMUK 1916.5.30.1479	U	Dried	x	x	—	—	—
C. bennetti	NHMUK 1939.12.20.1	U	Dried	x	x	—	—	—
C. bennetti	NHMUK 1939.12.20.11	F	Dried	x	x	—	—	—
C. bennetti	NHMUK 1939.12.20.8	U	Dried	x	x	—	—	—
C. bennetti	NHMUK 1939.12.9.1014	U	Dried	x	x	—	—	—
C. bennetti	NHMUK 1939.12.9.1015	U	Dried	x	x	—	—	—
C. bennetti	NHMUK 1939.12.9.1016	U	Dried	x	x	—	—	—
C. bennetti	NHMUK 1939.12.9.887	U	Dried	x	x	—	—	—
C. bennetti	NHMUK 1939.12.9.897	U	Dried	x	x	—	—	—
C. bennetti	NHMUK 1939.12.9.911	U	Dried	x	x	—	—	—
C. bennetti	NHMUK 1939.12.9.914	U	Dried	x	x	—	—	—
C. bennetti	NHMUK 1939.12.9.916	U	Dried	x	x	—	—	—
C. bennetti	NHMUK 1939.12.9.918	U	Dried	x	x	—	—	—
C. bennetti	NHMUK 1939.12.9.921	U	Dried	x	x	—	—	—
C. bennetti	NHMUK 1939.12.9.924	U	Dried	x	x	—	—	—
C. bennetti	NHMUK 1939.12.9.932	U	Dried	x	x	—	—	—
C. bennetti	NHMUK 1939.12.9.937	U	Dried	x	x	—	—	—
C. bennetti	NHMUK 1939.12.9.939	U	Dried	x	x	—	—	—
C. bennetti	NHMUK 1939.12.9.940	U	Dried	x	x	—	—	—
C. bennetti	NHMUK 1939.12.9.991	U	Dried	x	x	—	—	—
C. bennetti	NHMUK 1939.12.9.992	F	Dried	x	x	—	—	—
C. bennetti	NHMUK 1939.12.9.996	F	Dried	x	x	—	—	—
C. bennetti	NHMUK 1939.12.9.998	U	Skel.	x	x	—	—	—
C. bennetti	NHMUK 1953.17.266	F	Dried	x	x	—	—	—
C. bennetti	NHMUK 1996.41.906	F	Dried	x	x	—	—	—
C. bennetti	QM O.26829	U	Dried	x	x	—	—	—
C. casuarius	AMNH FLUID 12483	M	Fluid	x	x	R	SM	SPNG
C. casuarius	AMNH FLUID 15259	F	Fluid	x	x	R	SR	SPNG
C. casuarius	AMNH FLUID 15261	M	Fluid	x	x	R	SM	SPNG
C. casuarius	AMNH FLUID 15262	F	Fluid	x	x	R	SR	SPNG
C. casuarius	AMNH FLUID 6401	U	Fluid	x	x	R	NM	—
C. casuarius	AMNH SKIN 10804	U	Dried	x	x	R	SM	WIS
C. casuarius	AMNH SKIN 11574	M	Dried	x	x	R	SM	WIS
C. casuarius	AMNH SKIN 155232	U	Dried	x	x	R	SM	—
C. casuarius	AMNH SKIN 155401	U	Dried	x	x	R	NM	—
C. casuarius	AMNH SKIN 300522	U	Dried	x	x	L	NM	—
C. casuarius	AMNH SKIN 421657	F	Dried	x	x	R	SR	SPNG
C. casuarius	AMNH SKIN 424915	M	Dried	x	x	R	SM	SPNG
C. casuarius	BVZ Juliet 2020	F	Live	x	x	R	SM	—
C. casuarius	BVZ Romeo 2020	M	Live	x	x	L	SM	—
C. casuarius	CCP Dino 2019	M	Live	x	x	R	SM	—

Table 1. cont…

Species	Specimen ID	Sex	Type	LAT	ROS	DEV	DEG	GEO
C. casuarius	CCP Eyegore 2020	M	Live	x	x	L	SM	—
C. casuarius	CCP Fred 2020	M	Live	x	x	R	SM	—
C. casuarius	CCP Ginger 2019	F	Live	x	x	L	SM	—
C. casuarius	CCP Godiva 2020	F	Live	x	x	L	SM	—
C. casuarius	CCP Lucky 2019	F	Live	x	x	R	SM	—
C. casuarius	CCP Nemesis 2019	F	Live	x	x	R	SM	—
C. casuarius	CCP Pugsley 2019	M	Live	x	x	L	SM	—
C. casuarius	CCP Quattles 2020	M	Live	x	x	R	SM	—
C. casuarius	CCP Wednesday 2019	F	Live	x	x	R	SM	—
C. casuarius	DMNS ZB. 33689	M	Dried	x	—	L	—	—
C. casuarius	DMNS ZB. 33690	F	Dried	x	—	R	—	—
C. casuarius	DMNS ZB. 50012	M	Dried	—	—	R	—	—
C. casuarius	MOO 3914	U	Skel.	x	x	L	NM	—
C. casuarius	MOO 6994	M	Skel.	x	x	R	SM	—
C. casuarius	MOO 8031	F	Skel.	x	x	L	SR	—
C. casuarius	MV 51886	U	Dried	x	—	R	—	—
C. casuarius	MV B17741	U	Dried	x	x	R	NM	—
C. casuarius	MV R11696	F	Dried	x	x	R	SM	AUS
C. casuarius	MV R12279	M	Dried	x	—	N	—	AUS
C. casuarius	MV R12282	U	Dried	x	x	R	SM	AUS
C. casuarius	MV R3089	U	Dried	x	x	R	SM	AUS
C. casuarius	MV R5243	U	Dried	x	x	R	SM	AUS
C. casuarius	MV R8046	U	Dried	x	x	R	SM	AUS
C. casuarius	NHMUK 1852.12.5.20	U	Skel.	x	x	R	SM	—
C. casuarius	NHMUK 1878.3.29.1	U	Dried	x	—	L	—	INDP
C. casuarius	NHMUK 1916.5.30.1481	U	Dried	x	x	R	SM	INDP
C. casuarius	NHMUK 1916.5.30.1482	U	Dried	x	x	R	SR	—
C. casuarius	NHMUK 1916.5.30.1483	F	Dried	x	x	R	SM	INDP
C. casuarius	NHMUK 1939.12.20.10	U	Dried	x	x	R	SM	—
C. casuarius	NHMUK 1939.12.20.2	U	Dried	x	x	N	NM	WIS
C. casuarius	NHMUK 1939.12.20.3	U	Dried	x	x	R	SM	AUS
C. casuarius	NHMUK 1939.12.9	U	Dried	x	x	R	SR	SPNG
C. casuarius	NHMUK 1939.12.9.34	F	Dried	x	—	R	—	—
C. casuarius	NHMUK 1939.12.9.4	F	Dried	x	x	R	SM	AUS
C. casuarius	NHMUK 1939.12.9.877	U	Dried	x	x	R	SM	—
C. casuarius	NHMUK 1939.12.9.880	U	Dried	x	x	R	SM	INDP
C. casuarius	NHMUK 1939.12.9.882	U	Dried	x	x	R	SM	—
C. casuarius	NHMUK 1939.12.9.884	U	Dried	x	x	R	SM	—
C. casuarius	NHMUK 1939.12.9.890	U	Dried	x	x	L	NM	—
C. casuarius	NHMUK 1939.12.9.894	M	Dried	x	—	R	—	—
C. casuarius	NHMUK 1939.12.9.895	U	Dried	x	x	R	SM	WIS
C. casuarius	NHMUK 1939.12.9.896	U	Dried	x	x	R	SM	SPNG
C. casuarius	NHMUK 1939.12.9.899	U	Dried	—	x	R	SM	—
C. casuarius	NHMUK 1939.12.9.907	M	Dried	x	—	R	—	WIS
C. casuarius	NHMUK 1939.12.9.910	U	Dried	x	x	R	SM	WIS
C. casuarius	NHMUK 1939.12.9.919	U	Dried	x	x	L	SM	INDP
C. casuarius	NHMUK 1939.12.9.930	U	Dried	x	x	R	SM	—
C. casuarius	NHMUK 1939.12.9.944	M	Dried	x	x	R	SR	AUS

Table 1. cont…

Species	Specimen ID	Sex	Type	LAT	ROS	DEV	DEG	GEO
C. casuarius	NHMUK 1939.12.9.945	M	Dried	—	—	R	—	—
C. casuarius	NHMUK 1939.12.9.946	F	Dried	x	x	R	SM	AUS
C. casuarius	NHMUK 1939.12.9.947	M	Dried	x	x	R	NM	AUS
C. casuarius	NHMUK 1939.12.9.948	F	Dried	x	x	R	SM	AUS
C. casuarius	NHMUK 1939.12.9.950	M	Dried	x	x	R	SM	AUS
C. casuarius	NHMUK 1939.12.9.953	M	Dried	x	x	R	SM	AUS
C. casuarius	NHMUK 1939.12.9.957	M	Dried	—	—	R	—	—
C. casuarius	NHMUK 1939.12.9.964	U	Dried	x	x	R	SM	INDP
C. casuarius	NHMUK 1939.12.9.967	M	Dried	x	x	R	SM	—
C. casuarius	NHMUK 1939.12.9.968	U	Dried	x	—	R	—	—
C. casuarius	NHMUK 1939.12.9.969	M	Dried	x	x	LS	NM	WIS
C. casuarius	NHMUK 1939.12.9.975	M	Dried	—	—	L	—	—
C. casuarius	NHMUK 1942.4.14.1	F	Dried	x	x	R	NM	—
C. casuarius	NHMUK 1942.5.29.1	F	Dried	x	x	R	SM	—
C. casuarius	NHMUK 1965.30.1484	F	Dried	x	x	R	SR	INDP
C. casuarius	NHMUK 1996.41.888	M	Dried	x	x	R	NM	—
C. casuarius	NHMUK 1996.41.889	M	Dried	x	x	R	SM	—
C. casuarius	NHMUK 1996.41.890	U	Dried	x	x	R	SM	—
C. casuarius	NHMUK 1996.41.892	M	Dried	x	x	L	NM	—
C. casuarius	NHMUK 1996.41.895	M	Dried	x	x	L	NM	—
C. casuarius	NHMUK 1996.41.905	F	Dried	x	x	R	SM	WIS
C. casuarius	NHMUK 2002.10.1	U	Fluid	x	x	R	NM	—
C. casuarius	NHMUK S/1979.37.5	U	Skel.	x	—	R	—	—
C. casuarius	NHMUK S/2010.1.20	U	Skel.	x	x	R	SM	—
C. casuarius	QM Exhibition Mount A	U	Dried	x	x	R	SM	—
C. casuarius	QM Exhibition Mount C	U	Dried	x	x	R	SM	—
C. casuarius	QM O.20563	M	Dried	x	x	R	SM	SPNG
C. casuarius	QM O.26746	U	Dried	x	x	R	SM	—
C. casuarius	QM O.26825	U	Dried	x	x	R	SR	—
C. casuarius	QM O.26826	U	Dried	x	x	R	SM	—
C. casuarius	QM O.26827	U	Dried	—	x	R	NM	—
C. casuarius	QM O.30059	F	Dried	—	—	R	—	—
C. casuarius	QM O.30105	U	Dried	—	—	LS	—	—
C. casuarius	QM O.3435	U	Dried	x	—	R	NM	INDP
C. casuarius	QM O.3510	U	Dried	x	x	L	NM	—
C. casuarius	QM O.3775	U	Dried	x	x	L	NM	—
C. casuarius	QM O.5400	M	Dried	x	x	RS	SM	AUS
C. casuarius	QM QEB1687	U	Dried	x	—	L	—	—
C. casuarius	QM QEB1688	U	Dried	—	—	R	—	—
C. casuarius	QM QEB26828	U	Dried	x	x	R	NM	—
C. casuarius	QM WSERZ214	M	Skel.	x	x	R	SM	—
C. casuarius	TLG 001	U	Skel.	x	x	R	SM	—
C. casuarius	TLG (SCZ) C022 (12126)	M	Froz.	—	—	L	—	—
C. casuarius	UNE 01138	U	Froz.	x	x	LS	NM	AUS
C. casuarius	WTQLD Bob 2019	M	Live	x	—	R	—	AUS
C. casuarius	WTQLD Bumbella 2019	F	Live	x	—	R	—	AUS
C. casuarius	WTQLD Krakatoa 2019	F	Live	x	—	R	—	AUS
C. casuarius	WTQLD Relaxowary 2019	M	Live	x	—	L	—	AUS

Table 1. cont…

Species	Specimen ID	Sex	Type	LAT	ROS	DEV	DEG	GEO
C. unappendiculatus	AMNH FLUID 15258	F	Fluid	x	x	—	—	—
C. unappendiculatus	AMNH SKIN 291990	U	Dried	x	x	—	—	—
C. unappendiculatus	AMNH SKIN 338114	M	Dried	x	x	—	—	—
C. unappendiculatus	AMNH SKIN 338115	M	Dried	x	x	—	—	—
C. unappendiculatus	AMNH SKIN 836371	U	Dried	x	x	—	—	—
C. unappendiculatus	CCP Artemis 2020	F	Live	x	x	—	—	—
C. unappendiculatus	CCP Liberace 2019	M	Live	x	x	—	—	—
C. unappendiculatus	CCP Piggy 2020	M	Live	x	x	—	—	—
C. unappendiculatus	NHMUK 1939.12.9.883	U	Dried	x	x	—	—	—
C. unappendiculatus	NHMUK 1939.12.9.889	U	Dried	x	x	—	—	—
C. unappendiculatus	NHMUK 1939.12.9.891	U	Dried	x	x	—	—	—
C. unappendiculatus	NHMUK 1939.12.9.920	U	Dried	x	x	—	—	—
C. unappendiculatus	NHMUK 1939.12.9.931	U	Dried	x	x	—	—	—
C. unappendiculatus	NHMUK 1939.12.9.938	U	Dried	x	x	—	—	—
C. unappendiculatus	NHMUK 1939.12.9.942	U	Dried	x	x	—	—	—
C. unappendiculatus	NHMUK 1939.12.9.979	U	Dried	x	x	—	—	—
C. unappendiculatus	NHMUK 1939.12.9.986	U	Dried	x	x	—	—	—
C. unappendiculatus	NHMUK 1996.41.34.3498	U	Dried	x	x	—	—	—

F = female; M = male; U = unknown; Froz. = Frozen; Skel. = Skeleton; LAT = lateral; ROS = rostral; DEV = deviation type; DEG = degree of deviation; L = left; LS = left sinusoidal; N = none; R = right; RS = right sinusoidal; NM = none–minimal; SM = slight–moderate; SR = severe–radical; AUS = Australia; SPNG = southern Papua New Guinea; INDP = Indonesian Papua; WIS = islands west of New Guinea

Table 2. MANOVA outputs for *Casuarius* shape data

MANOVA	Pairwise Test	Degrees of Freedom	F-value	P-value
Sex (*C. casuarius*) – Lateral	—	52	1.796	0.082
Sex (*C. casuarius*) – Rostral	—	41	1.364	0.239
Geography (*C. casuarius*) – Lateral				
	AUS–INDP	27	1.771	0.146
	AUS–SPNG	28	2.401	0.054
	AUS–WIS	27	4.550	0.003*
	INDP–SPNG	16	2.265	0.134
	INDP–WIS	15	5.261	0.021
	SPNG–WIS	16	5.708	0.012
Geography (*C. casuarius*) – Rostral				
	AUS–INDP	20	4.510	0.010*
	AUS–SPNG	23	2.279	0.085
	AUS–WIS	21	2.810	0.049
	INDP–SPNG	14	0.771	0.614
	INDP–WIS	12	5.714	0.026
	SPNG–WIS	15	5.070	0.015
Casuarius species – Lateral				
	CB–CC	134	81.51	2.8e−52*
	CB–CU	51	24.50	1.8e−14*
	CC–CU	118	8.362	6.4e−11*
Casuarius species – Rostral				
	CB–CC	120	29.83	2.0e−30*
	CB–CU	51	9.270	3.0e−08*
	CC–CU	104	10.06	4.0e−13*

AUS = Australia; INDP = Indonesian Papua; SPNG = southern Papua New Guinea; WIS = islands west of New Guinea; CB = *Casuarius bennetti*; CC = *Casuarius casuarius*; CU = *Casuarius unappendiculatus*; * = significant difference ($\alpha = 0.01$). Values are rounded to the nearest thousandth.

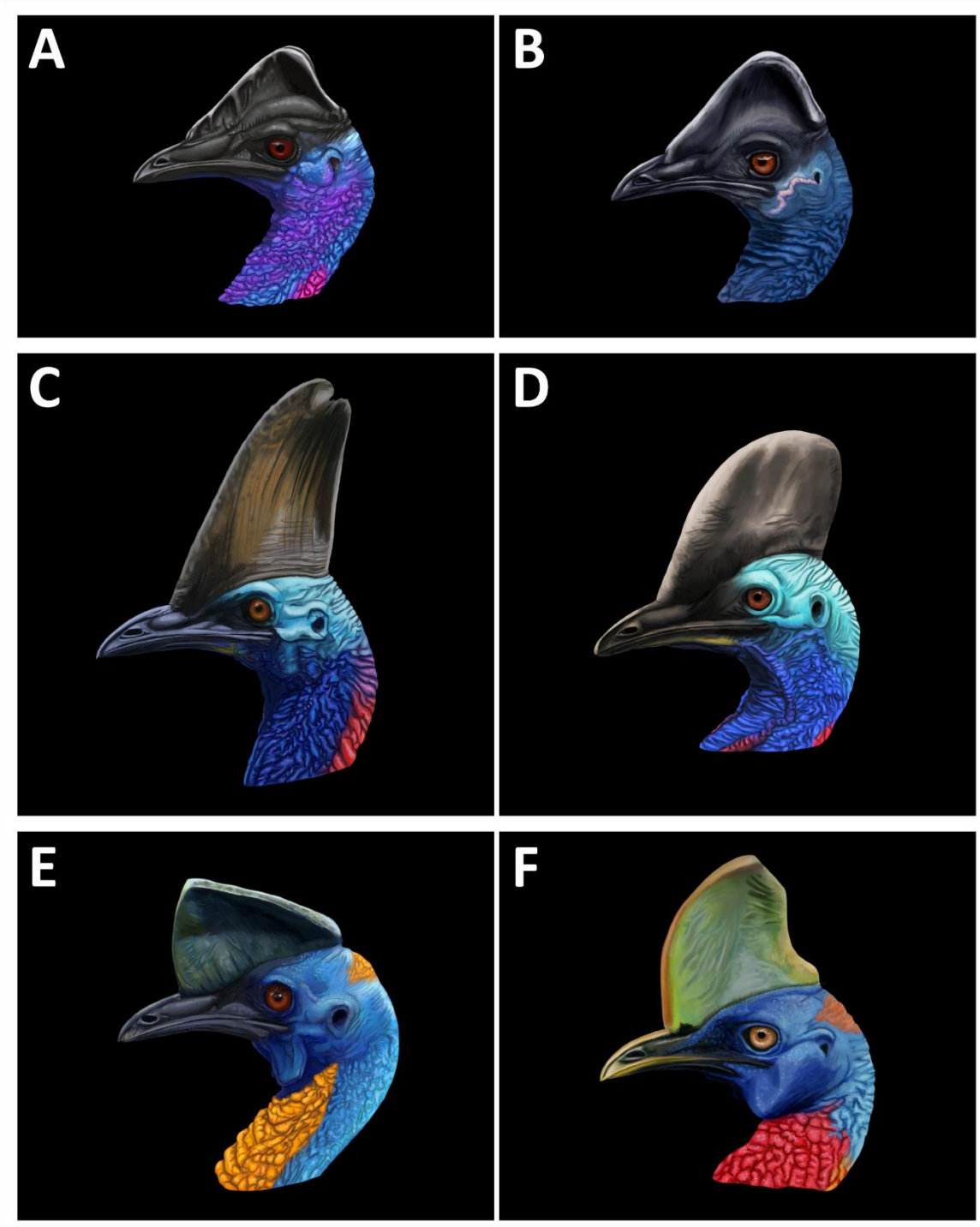

Figure 1. Illustrations depicting the phenotypic range variation for adult casque and apteria coloration across the *Casuarius* genus (A−F) and within species: (A−B) *Casuarius bennetti*, (C−D) = *Casuarius casuarius*, (E−F) = *Casuarius unappendiculatus*. All species are based on female representatives. Artwork by J. A. Campbell-Smith.

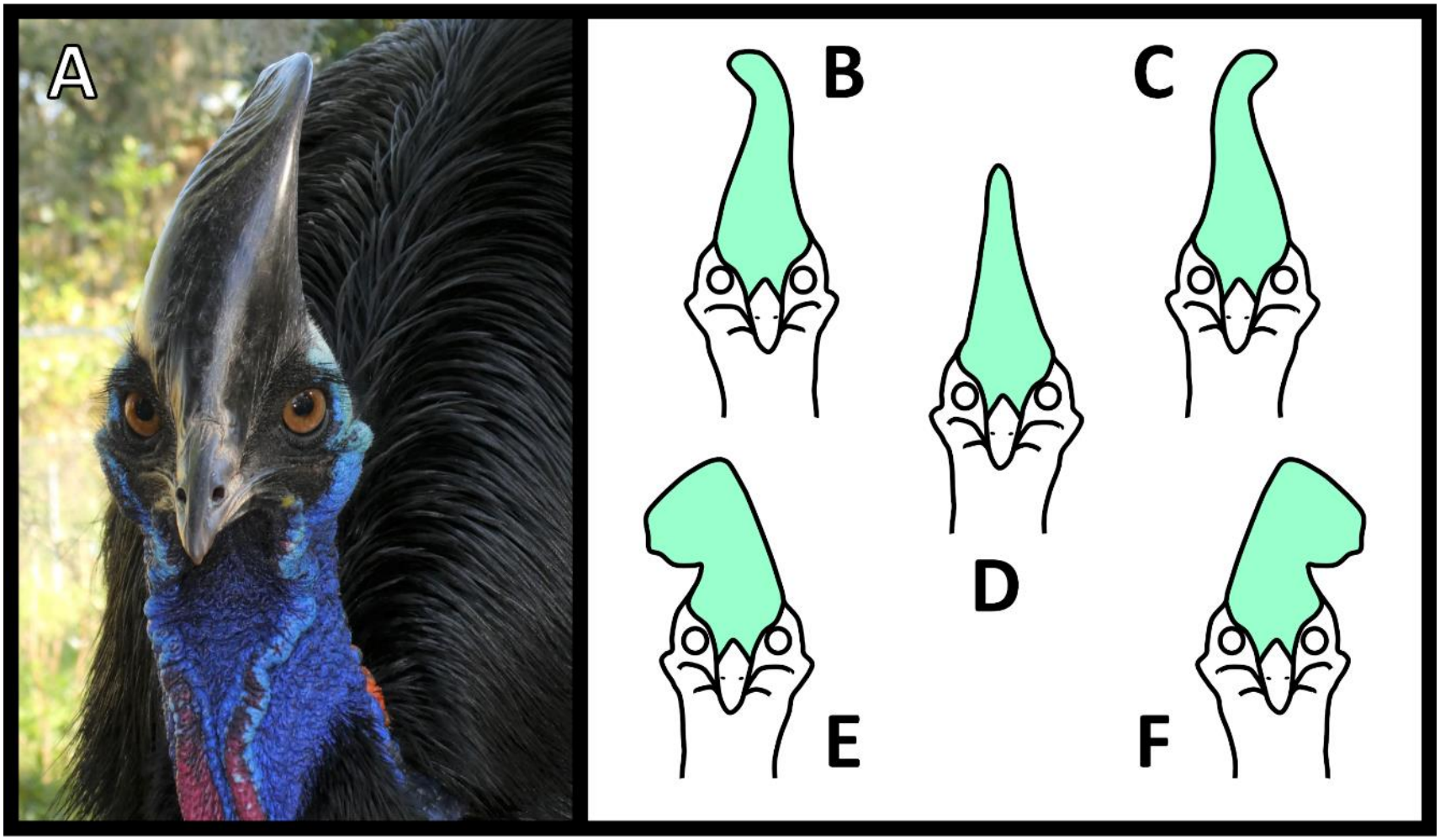
A
B
C
D
E
F

Figure 2. Photograph illustrating casque asymmetry in (A) *Casuarius casuarius*, a common anatomical feature in cassowaries. Casque asymmetries in *C. casuarius* manifest as either (B) rightward sinusoidal, (C) leftward sinusoidal, (D) non-deviated, (E) rightward, and (F) leftward deviations from the midline. Photo by T. L. G.

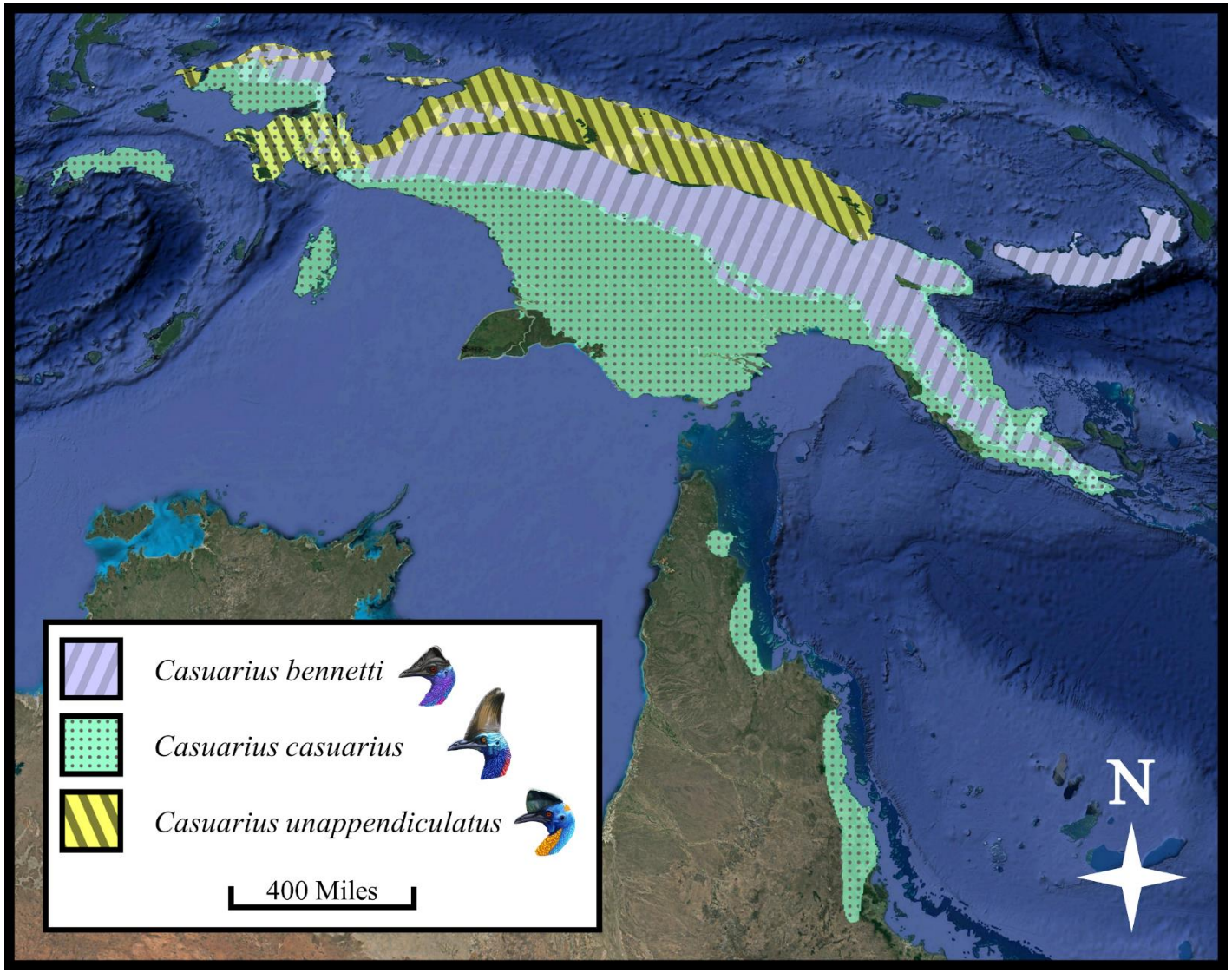
Casuarius bennetti
Casuarius casuarius
Casuarius unappendiculatus
400 Miles
N

Figure 3. Map of Australasian region in which cassowaries are native. Species ranges delineated by specific color shading (*Casuarius bennetti* = pastel purple; *Casuarius casuarius* = pastel green; *Casuarius unappendiculatus* = pastel yellow). Primary areas where multiple species coincide are indicated by semi-transparent, colored species boundary overlap. Geographical range data used with permission from BirdLife International (2019) via Google Earth Pro 7.3.3.7721.

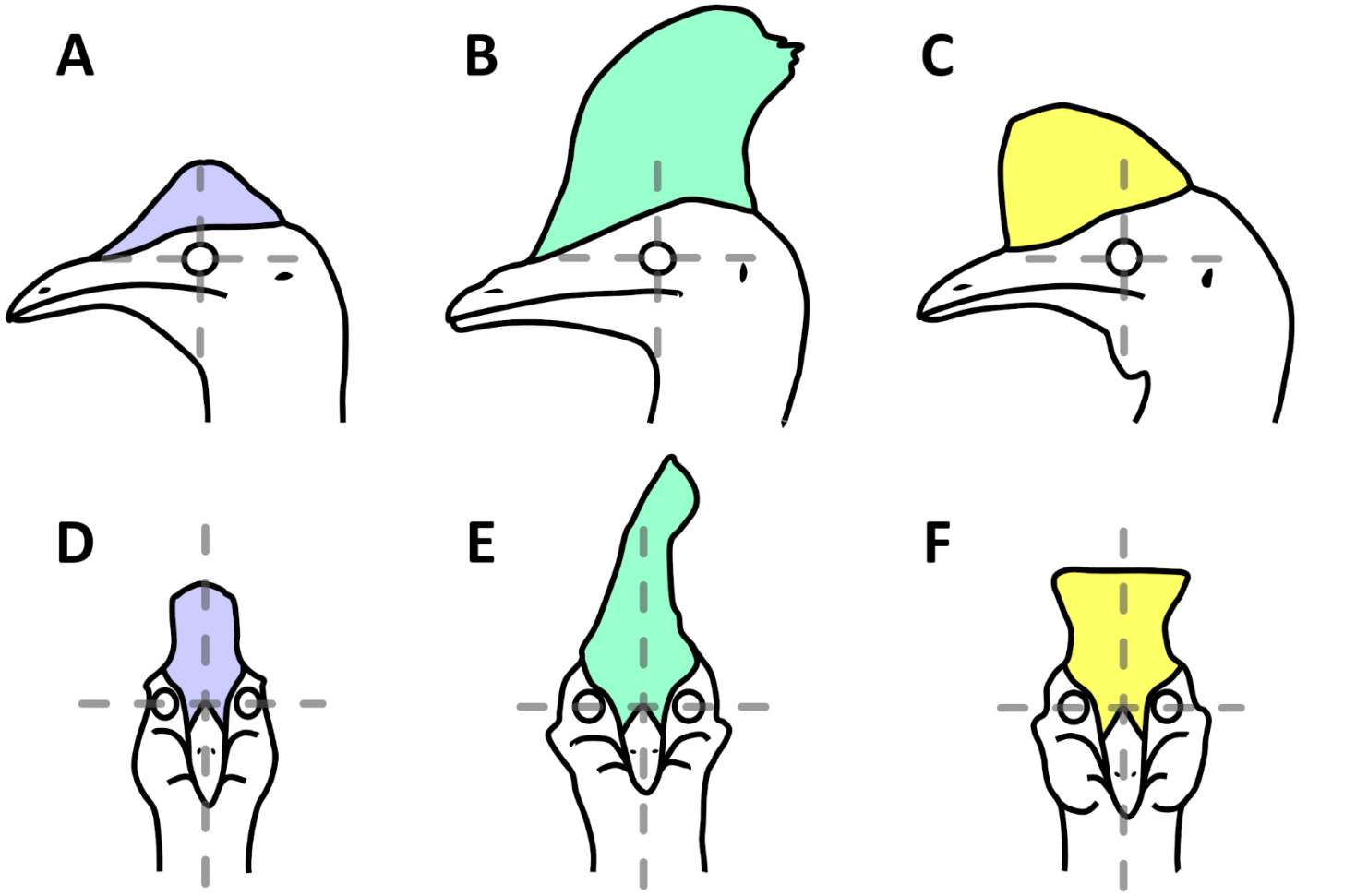
A
B
C
D
E
F
Casuarius bennetti
Casuarius casuarius
Casuarius unappendiculatus

Figure 4. Cranial line illustrations of the three species of cassowaries **(***Casuarius bennetti* = pastel purple; *Casuarius casuarius* = pastel green; *Casuarius unappendiculatus* = pastel yellow) in lateral (A−C) and rostral views (D−F), which were the two anatomical aspects morphometric photographs were collected from. Crosshairs were centered vertically and horizontally on the eye/orbit for lateral samples, and the alignment of the horizontal center of the eye/orbit and rostralmost boundary of the casque with the cranial midline for rostral samples (indicated by transparent grey dashed lines).

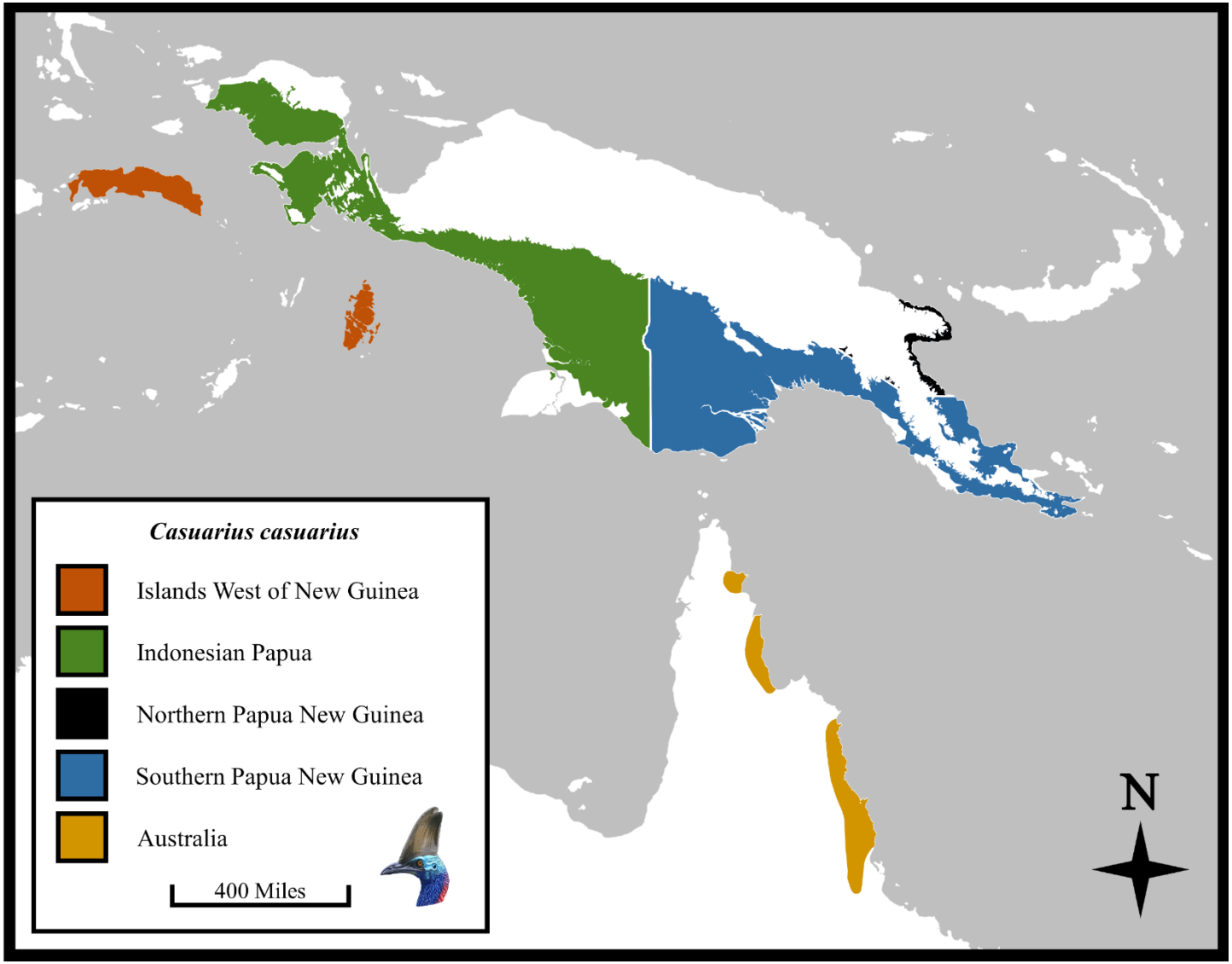
Casuarius casuarius
Islands West of New Guinea
Indonesian Papua
Northern Papua New Guinea
Southern Papua New Guinea
Australia
400 Miles
N

Figure 5. Map of Australasian *Casuarius casuarius* range with regional subdivisions based on historical and physical boundaries indicated on museum voucher tags (western islands near New Guinea = dark orange; Indonesian Papua = green; Northern Papua New Guinea = black; Southern Papua New Guinea = blue; Australia = dark yellow). Redrawn from BirdLife International (2019) geographical range data.

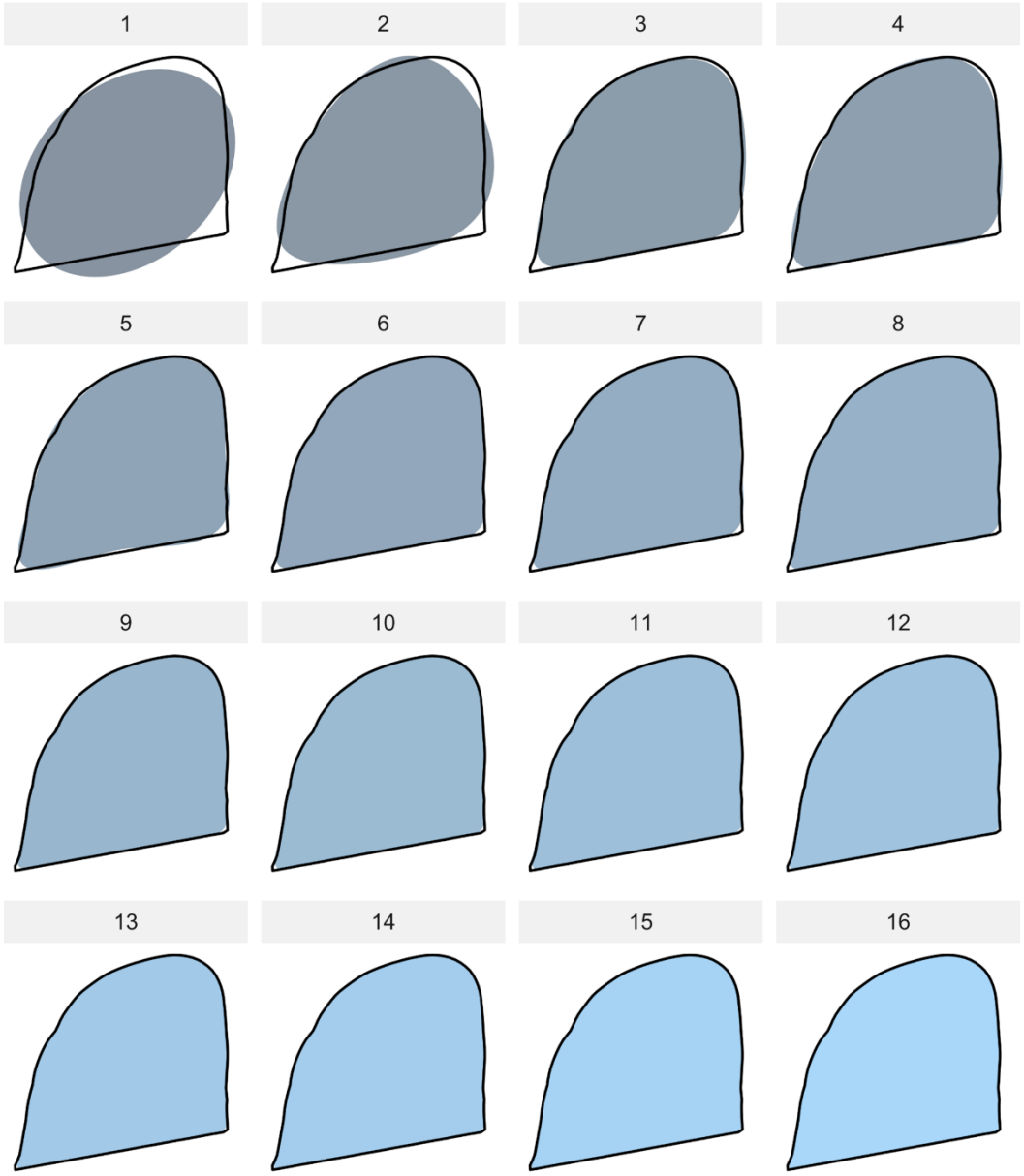

Figure 6. Exemplar harmonics (1–16; black outlines filled grey to blue) of casque outlines from an elliptical Fourier analysis. This type of analysis uses these harmonic coefficients to approximate shape of the casques across my sample. Considering that it is difficult to place homologous landmarks on cassowary casques, this non-landmark-based approach is a practical means to accurately capture shape data.

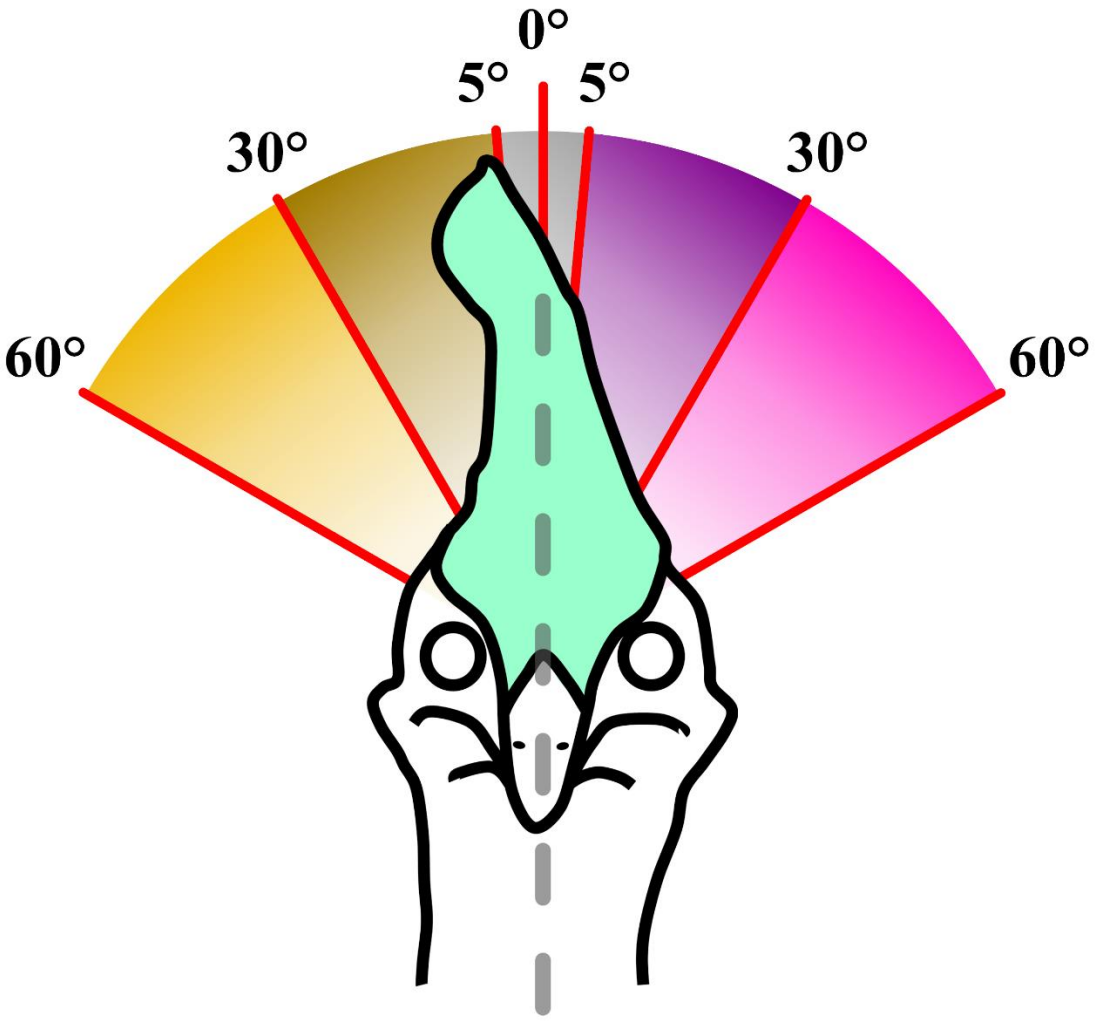

Figure 7. Methods for determining degrees of deviation categories (none–minimal, 0° to 5° leftward/rightward = grey; slight–moderate rightward, 6° to 30° = dark gold); slight–moderate leftward, 6° to 30° = light gold; severe–radical rightward, 31° to 60° = dark purple), and (5) severe–radical leftward, 31° to 60°; = light purple) for *Casuarius casuarius* casques from rostral view (pastel green).

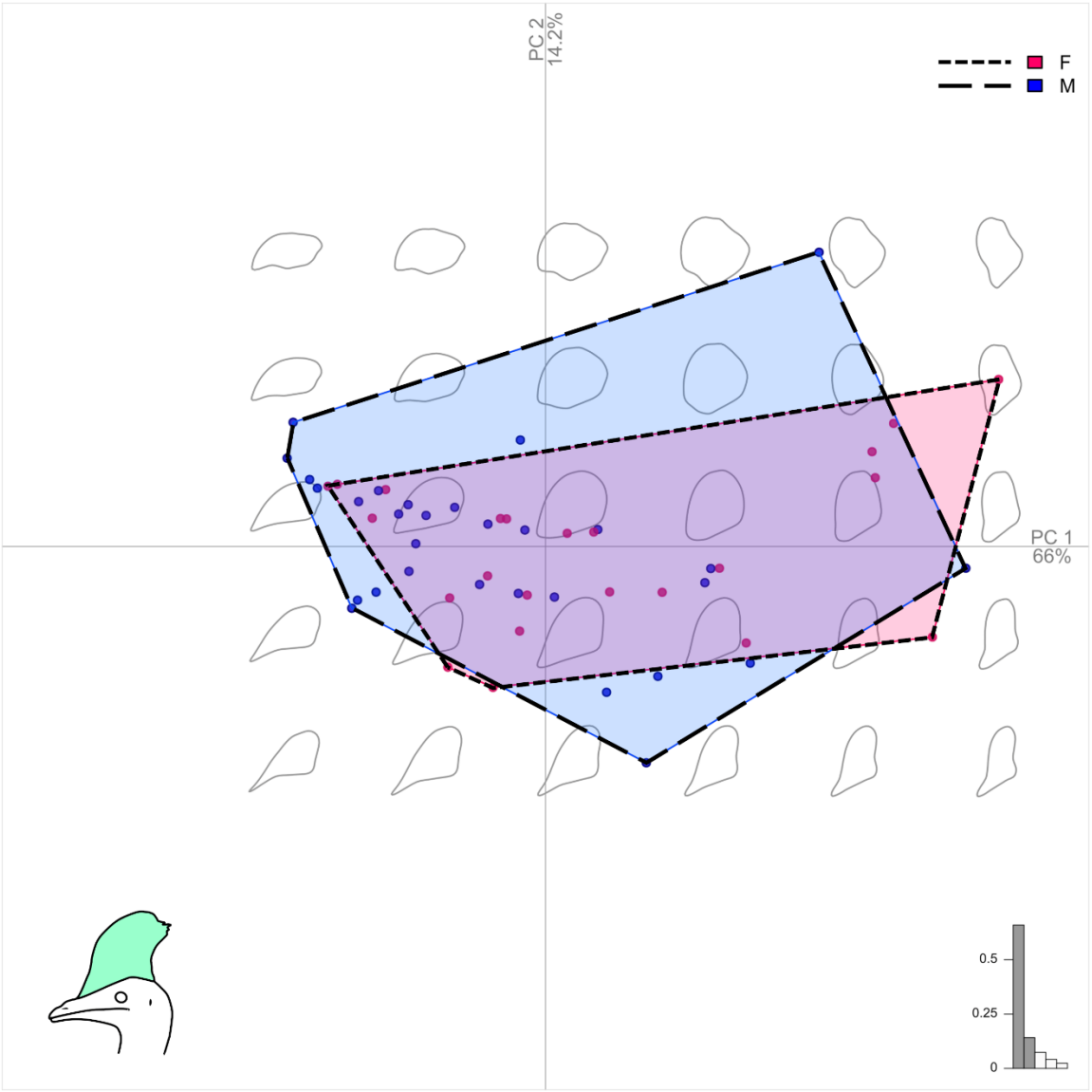

Figure 8. Output of the PCA comparing lateral casque outlines between sexes (female = pink datapoints and polygon; male = blue datapoints and polygon) of *Casuarius casuarius* (pastel green casque icon at lower left). Female and male convex hulls illustrate substantial overlap in lateral casque morphospace between the sexes. Theoretical casque shape based on the principal component axes shown as grey outlines, scree plot in lower right shows principal components used in analysis.

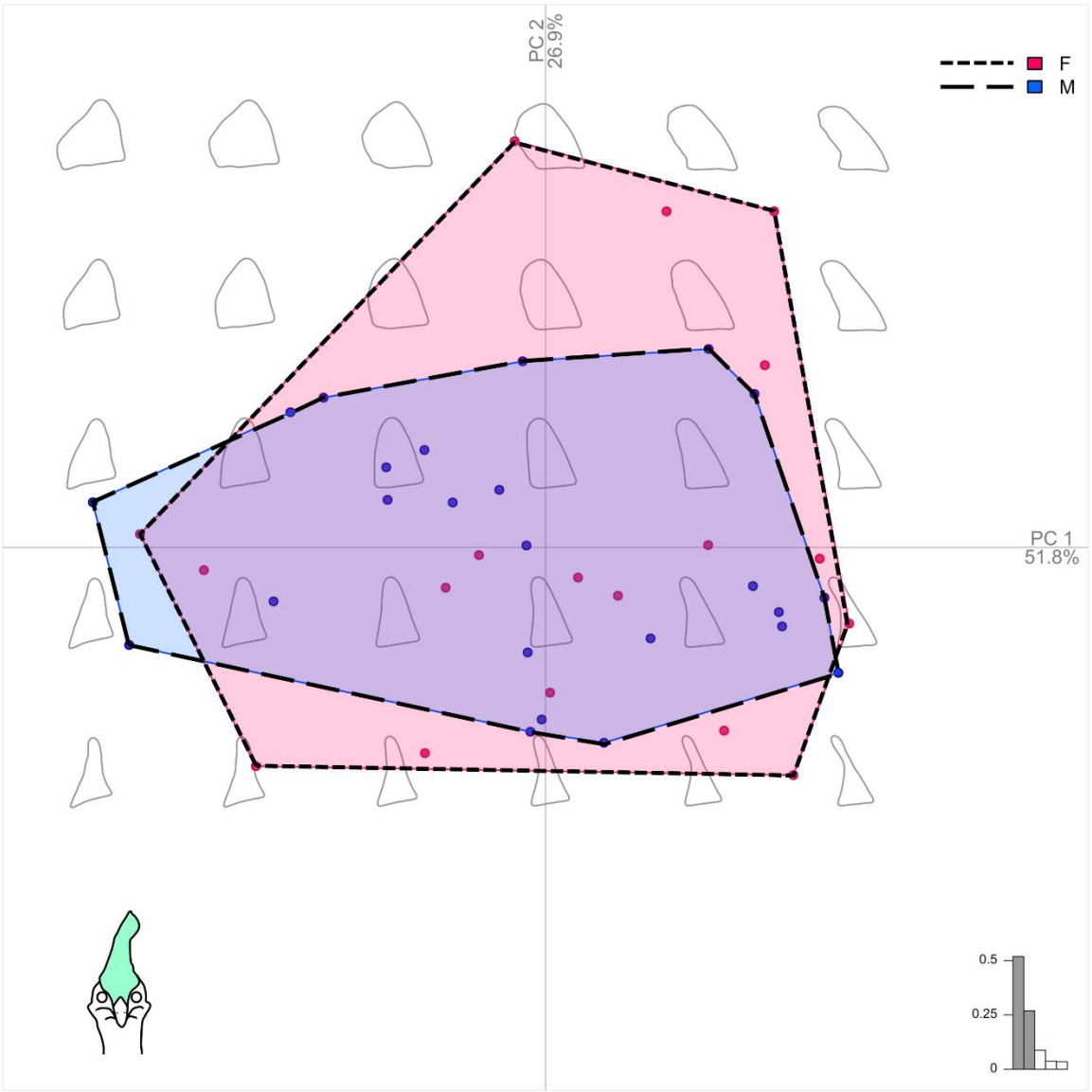

Figure 9. Output of the PCA comparing rostral casque outlines between sexes (female = pink datapoints and polygon; male = blue datapoints and polygon) of *Casuarius casuarius* (pastel green casque icon at lower left). Female and male convex hulls illustrate substantial overlap in rostral casque morphospace between the sexes. Theoretical casque shape based on the principal component axes shown as grey outlines, scree plot in lower right shows principal components used in analysis.

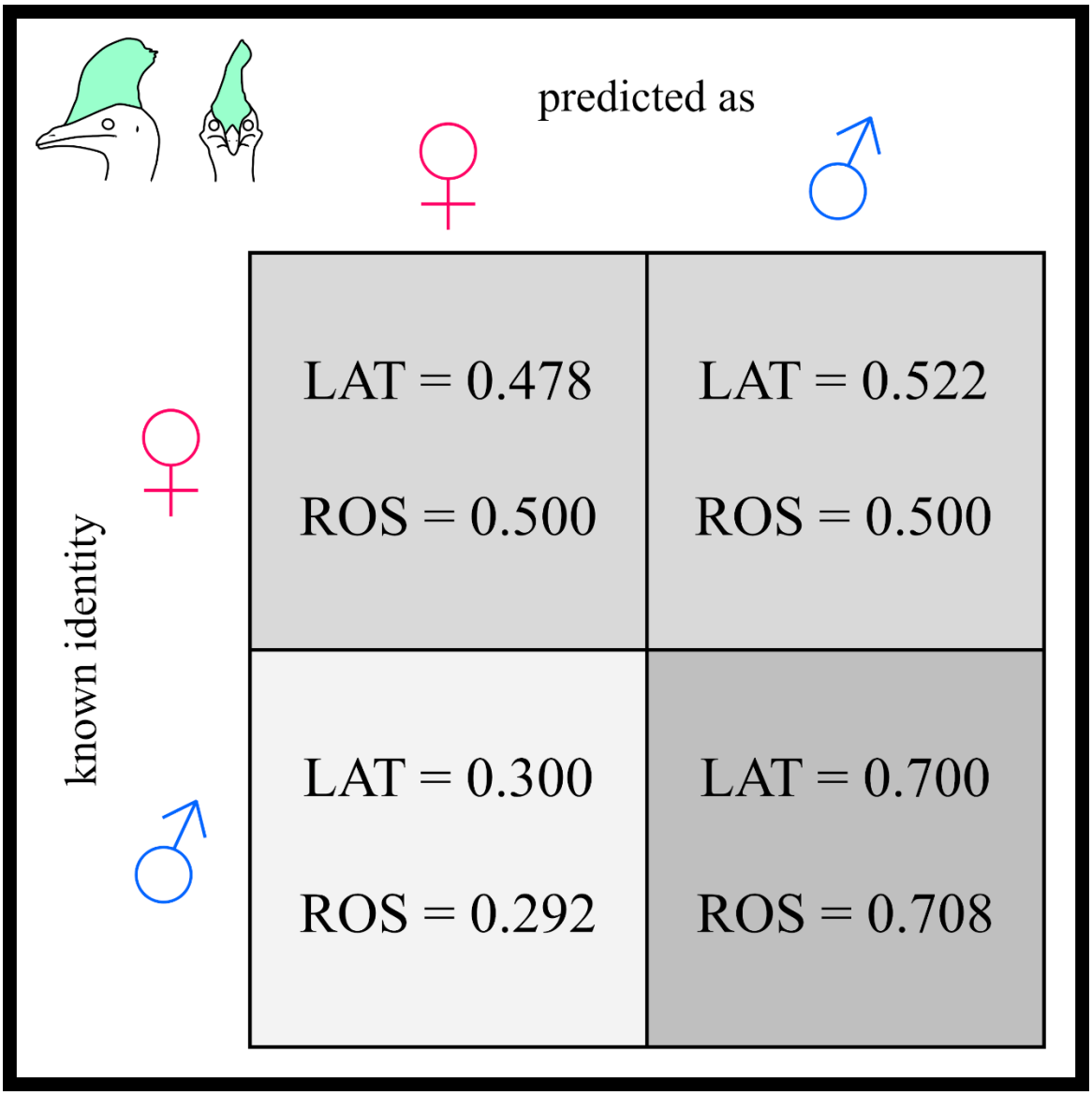

Figure 10. Results of linear discriminant analysis (LDA) comparing principal components of female and male *Casuarius casuarius* casque outlines (lateral = LAT; rostral = ROS). The LDA was unable to consistently classify (represented by pastel green icon at upper left) casque shape between sexes. Box greyness increases with more frequent classifiability. Values are rounded to the nearest thousandth.

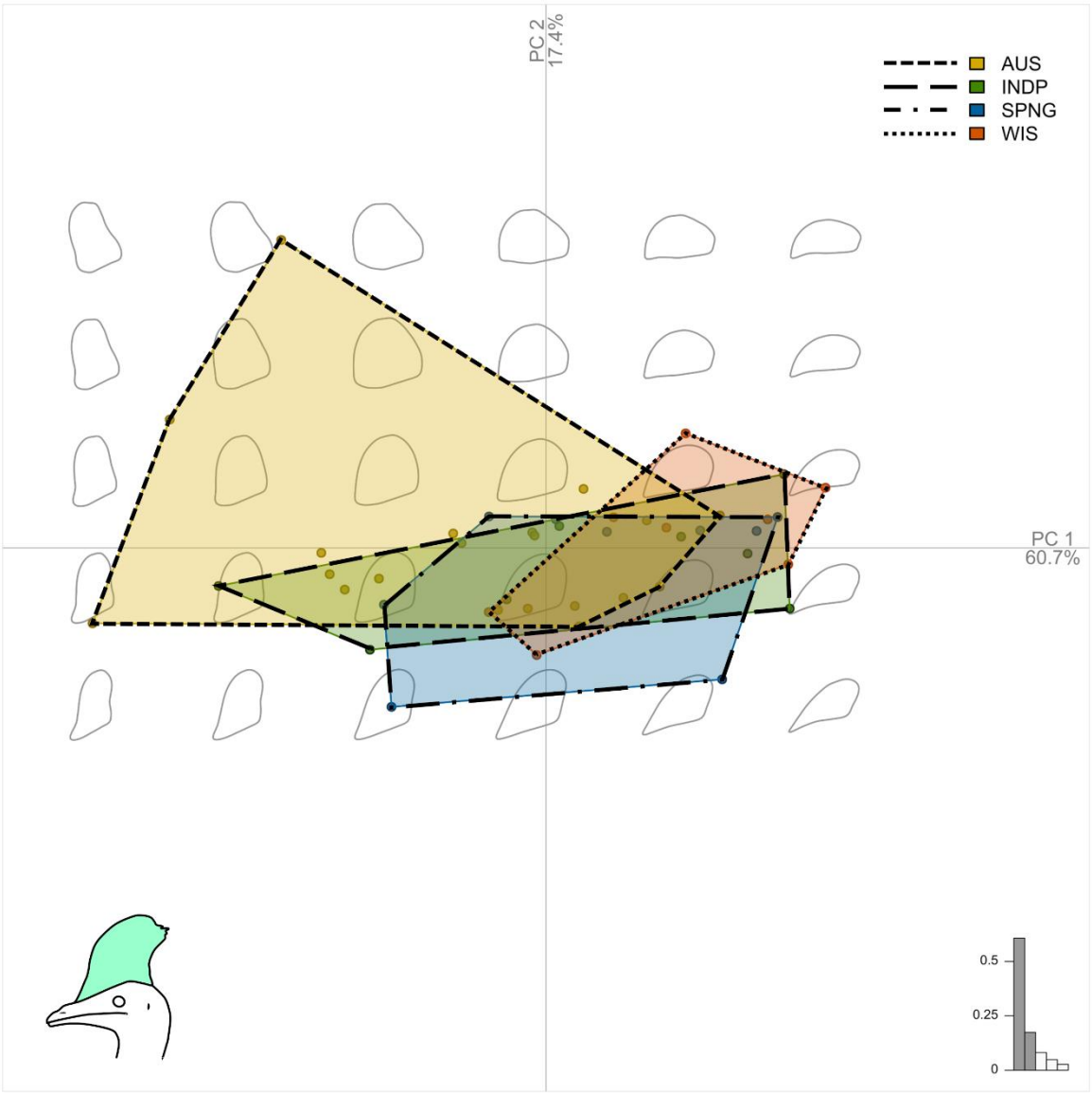

Figure 11. Output of the PCA comparing lateral *Casuarius casuarius* (pastel green casque icon at lower left) casque outlines between geographical regions: Australia (AUS = dark yellow), Indonesian Papua (INDP = green), Southern Papua New Guinea (SPNG = blue), and Western Islands Near New Guinea (WIS = dark orange). Geographic convex hulls illustrate substantial overlap in lateral casque morphospace between the regions. Theoretical casque shape based on the principal component axes shown as grey outlines, scree plot in lower right shows principal components used in analysis.

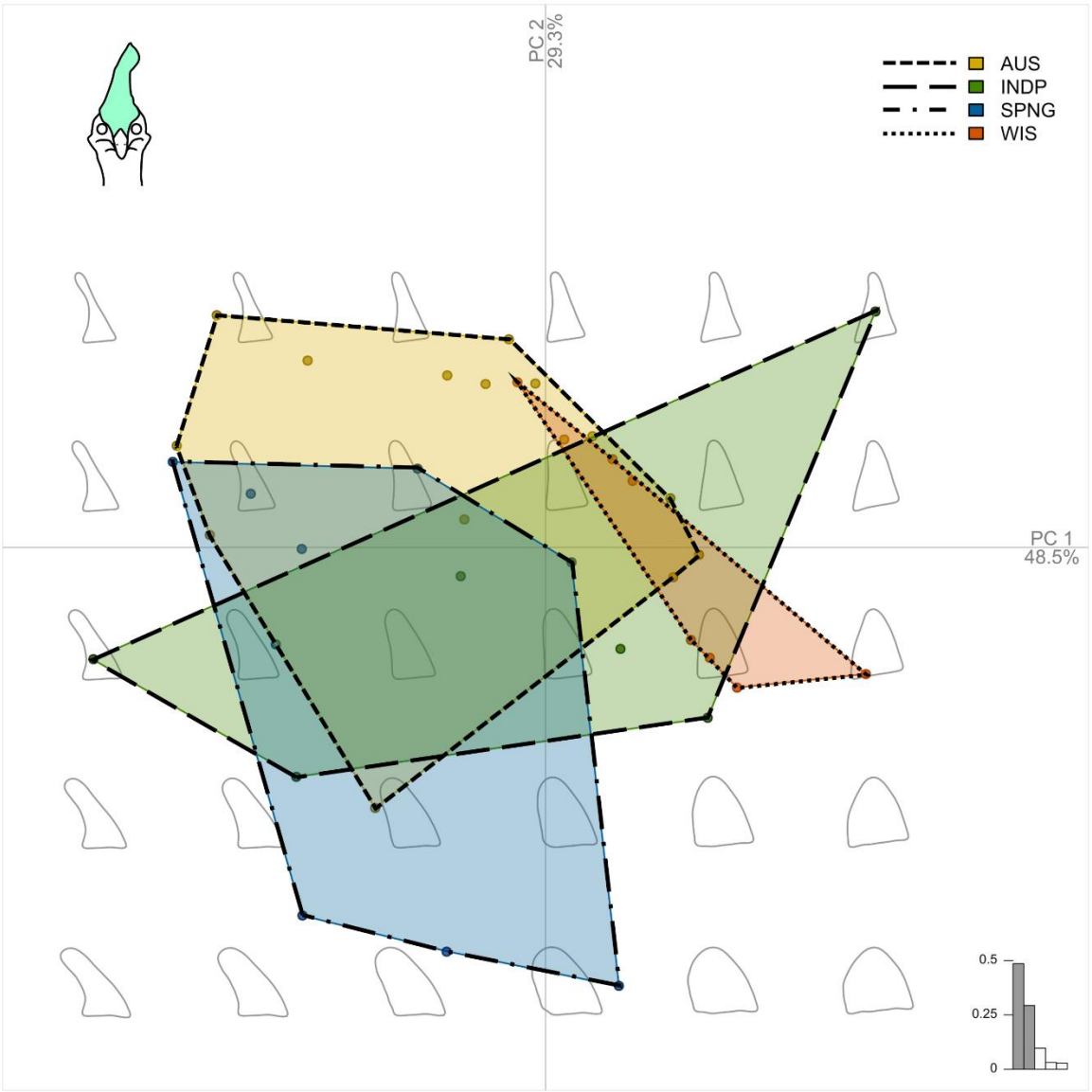

Figure 12. Output of the PCA comparing rostral *Casuarius casuarius* (pastel green casque icon at upper left) casque outlines between geographical regions: Australia (AUS = dark yellow), Indonesian Papua (INDP = green), Southern Papua New Guinea (SPNG = blue), and Western Islands Near New Guinea (WIS = dark orange). Geographic convex hulls illustrate substantial overlap in rostral casque morphospace between the regions. Theoretical casque shape based on the principal component axes shown as grey outlines, scree plot in lower right shows principal components used in analysis.

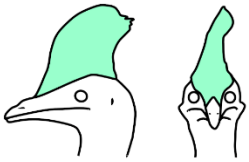

predicted as

known identity	AUS	INDP	SPNG	WIS
AUS	LAT = 0.550 ROS = 0.600	LAT = 0.250 ROS = 0.067	LAT = 0.100 ROS = 0.133	LAT = 0.100 ROS = 0.200
INDP	LAT = 0.250 ROS = 0.167	LAT = 0.250 ROS = 0.167	LAT = 0.375 ROS = 0.333	LAT = 0.125 ROS = 0.333
SPNG	LAT = 0.111 ROS = 0.444	LAT = 0.333 ROS = 0.000	LAT = 0.444 ROS = 0.333	LAT = 0.111 ROS = 0.222
WIS	LAT = 0.250 ROS = 0.571	LAT = 0.000 ROS = 0.000	LAT = 0.000 ROS = 0.000	LAT = 0.750 ROS = 0.429

Figure 13. Results of linear discriminant analysis (LDA) comparing principal components of casque outlines (lateral = LAT; rostral = ROS) of *Casuarius casuarius* from different geographical regions: Australia (AUS = dark yellow), Indonesian Papua (INDP = green), Southern Papua New Guinea (SPNG = blue), and Western Islands Near New Guinea (WIS = dark orange). The LDA was unable to consistently classify (represented by pastel green icon at upper left) casque shape based on sex. Box greyness increases with more frequent classifiability. Values are rounded to the nearest thousandth.

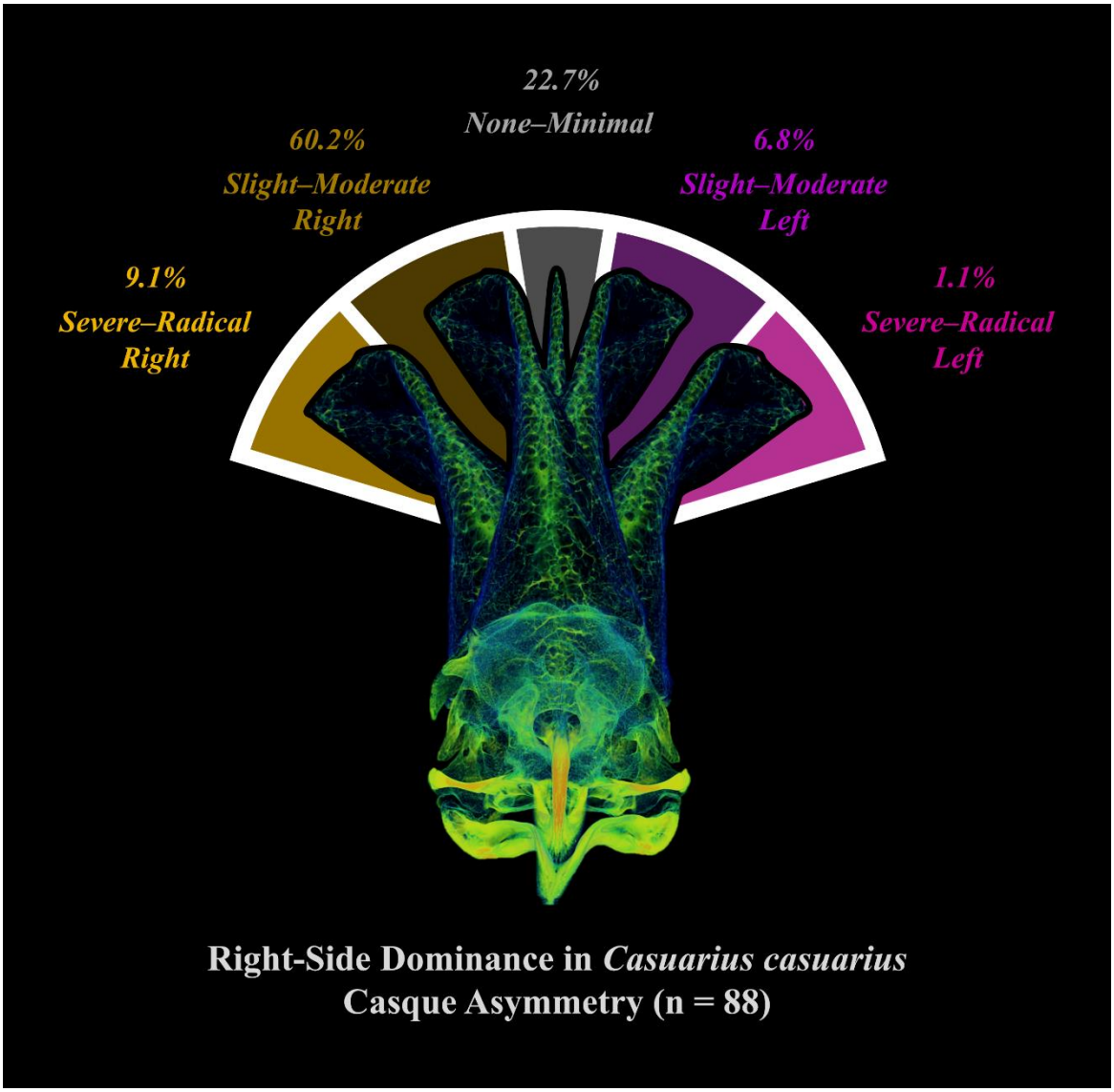

Figure 14. Figure summarizing the degree of deviation results (by percentage; rounded to the nearest tenth) for the *Casuarius casuarius* casque sample, which exhibited a right directional asymmetry. Rendering of cassowary skull (green) pictured from rostral view, and various casque asymmetry positions superimposed. Deviation categories included: (1) none–minimal (0° to 5° leftward/rightward; grey), (2) slight–moderate rightward (6° to 30°; dark gold), (3) slight–moderate leftward (6° to 30°; light gold), (4) severe–radical rightward (31° to 60°; dark purple), and (5) severe–radical leftward (31° to 60°; light purple).

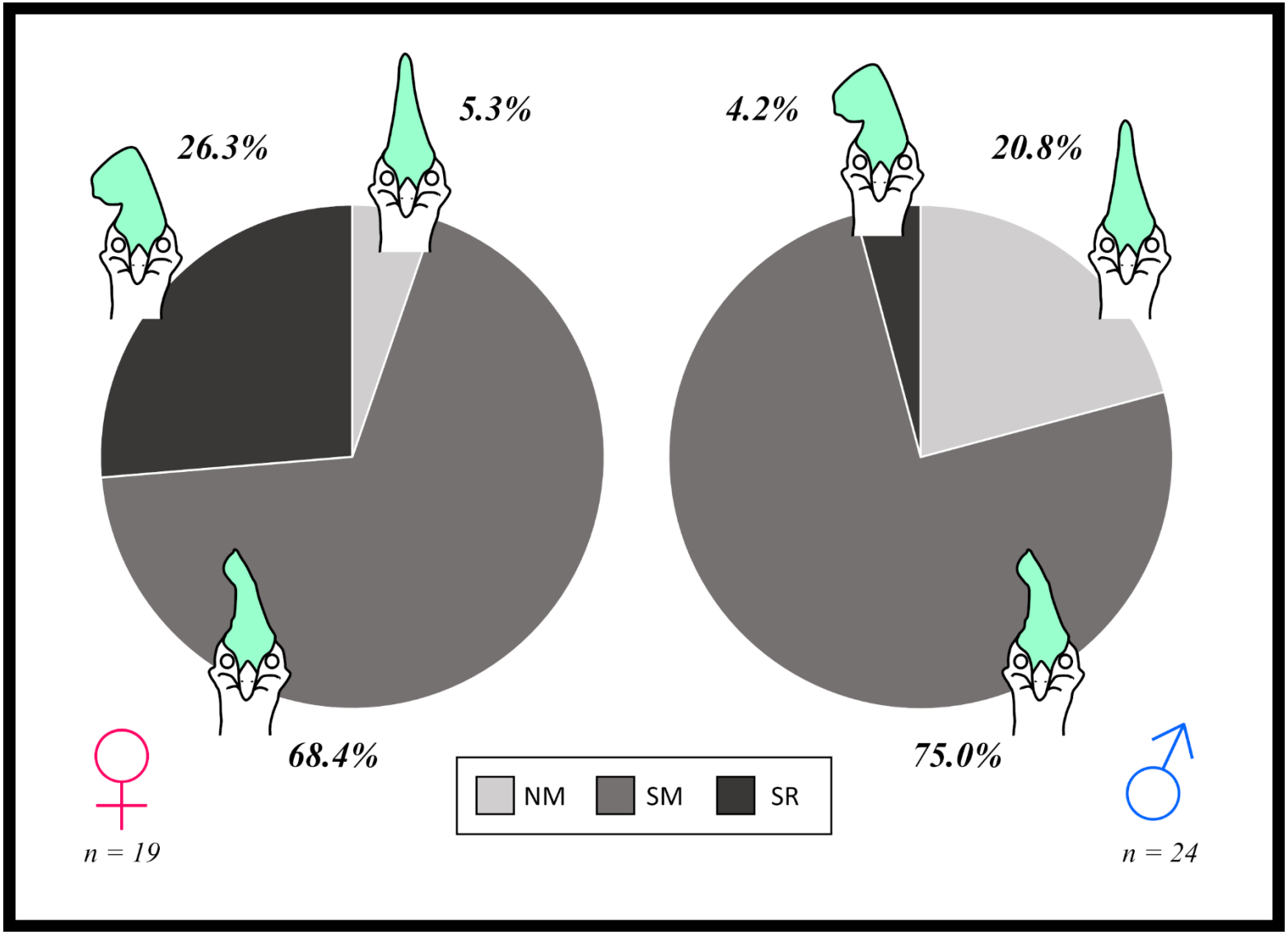
26.3%
5.3%
68.4%
4.2%
20.8%
75.0%
NM
SM
SR
n = 19
n = 24

Figure 15. Pie charts summarizing degree of casque deviation results of know-sex *Casuarius casuarius* samples (female = pink symbol; male = blue symbol). Leftward and rightward deviation categories were combined into the following categories: (NM) none–minimal (0° to 5° leftward/rightward; lightest grey), (SM) slight–moderate leftward/rightward (6° to 30°; middle grey), (SR) severe–radical leftward/rightward (31° to 60°; darkest grey). Superimposed cassowary icons (rostral views) represent degrees of casque asymmetry deviations (pastel green). Percentages are rounded to the nearest tenth and sample sizes are indicated (n) under each sex symbol.

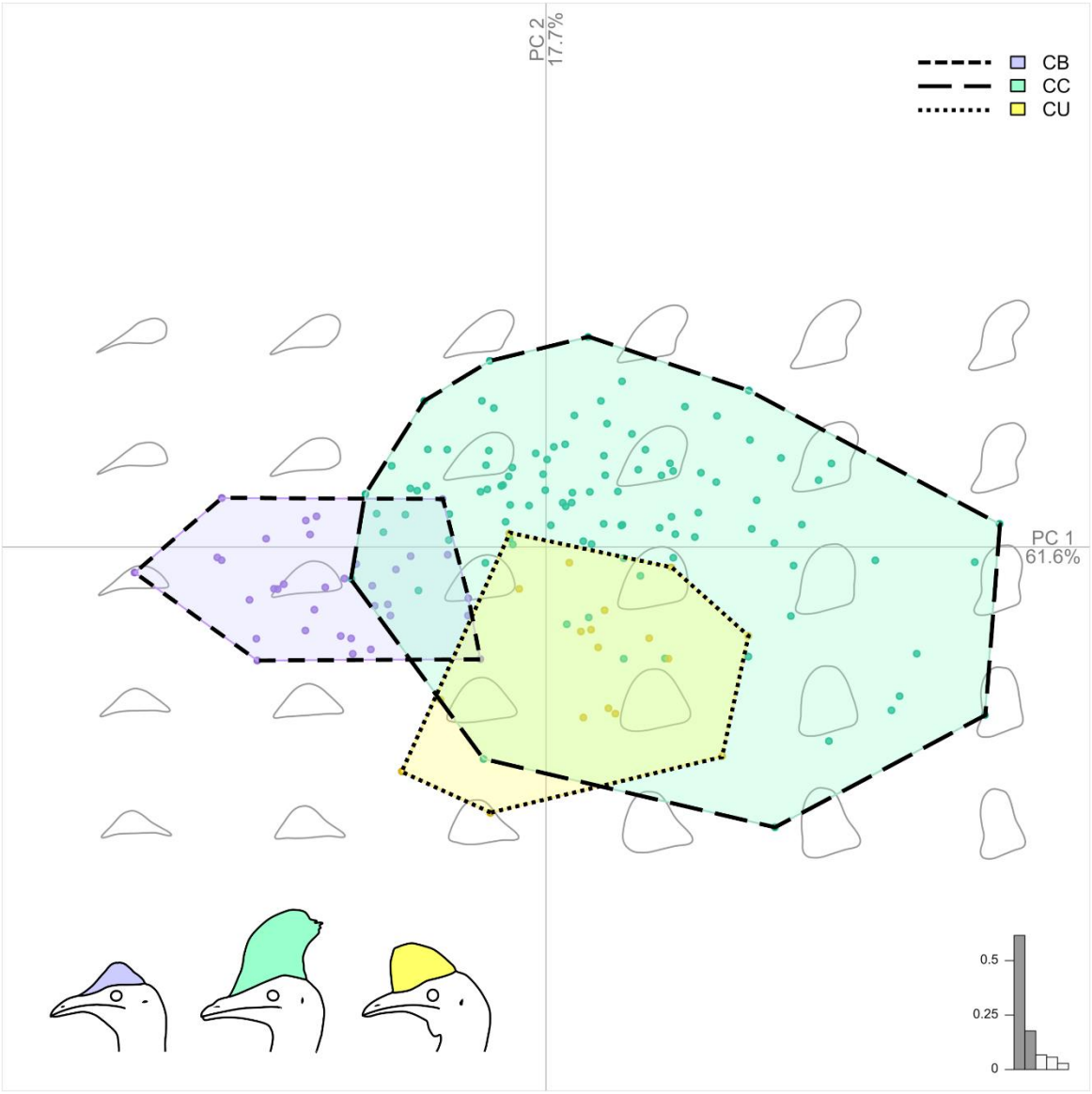

Figure 16. Output of the PCA comparing lateral casque outlines between cassowary species (*Casuarius bennetti*, CB = pastel purple; *Casuarius casuarius*, CC = pastel green; *Casuarius unappendiculatus*, CU = pastel yellow), indicated by colored casque icons at lower left. Convex hulls of species illustrate only partial overlap in lateral casque morphospace. Theoretical casque shape based on the principal component axes shown as grey outlines, scree plot in lower right shows principal components used in analysis.

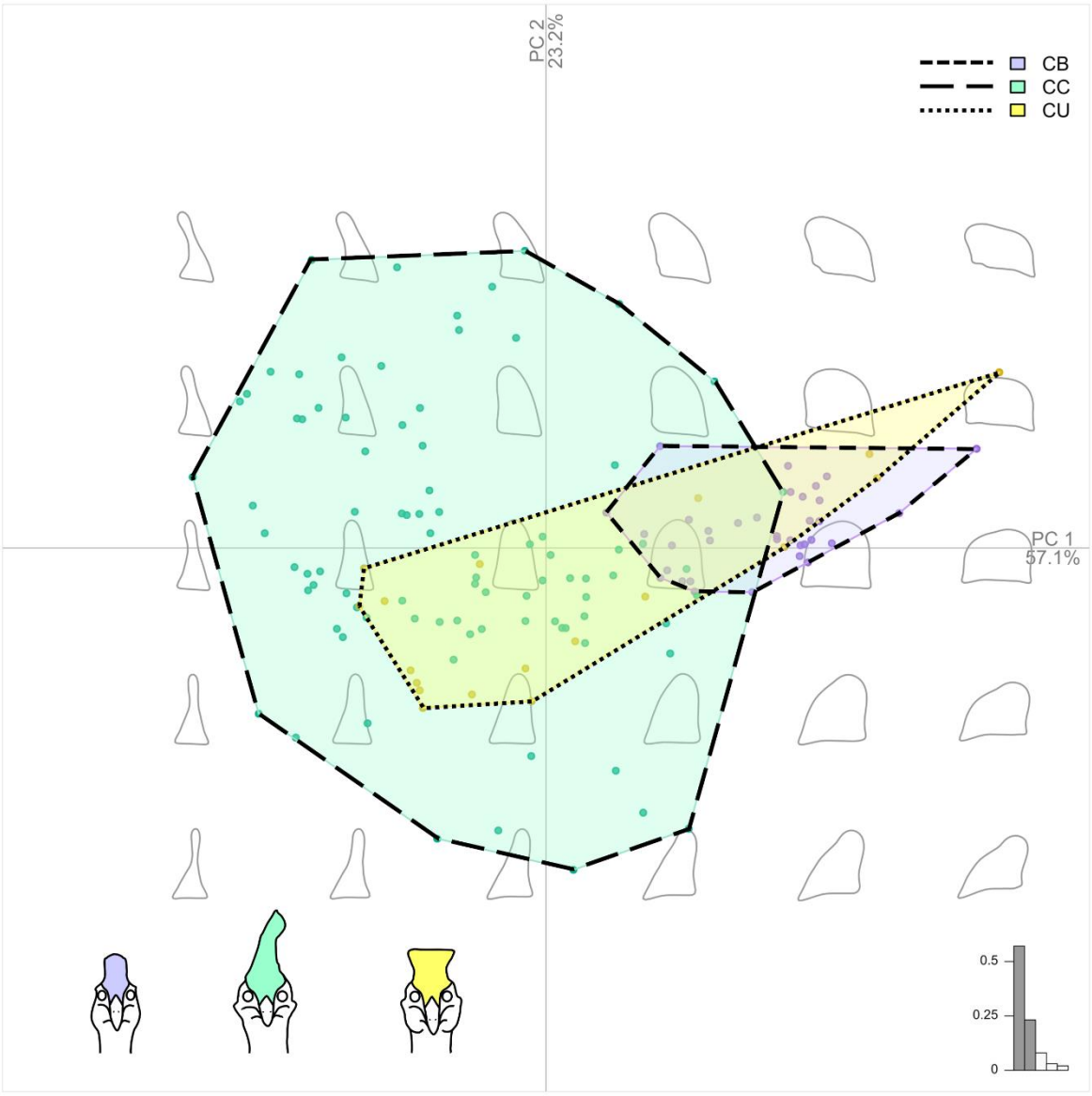

Figure 17. Output of the PCA comparing rostral casque outlines between cassowary species (*Casuarius bennetti*, CB = pastel purple; *Casuarius casuarius*, CC = pastel green; *Casuarius unappendiculatus*, CU = pastel yellow), indicated by casque icons at lower left. Convex hulls of species illustrate only partial overlap in rostral casque morphospace. Theoretical casque shape based on the principal component axes shown as grey outlines, scree plot in lower right shows principal components used in analysis.

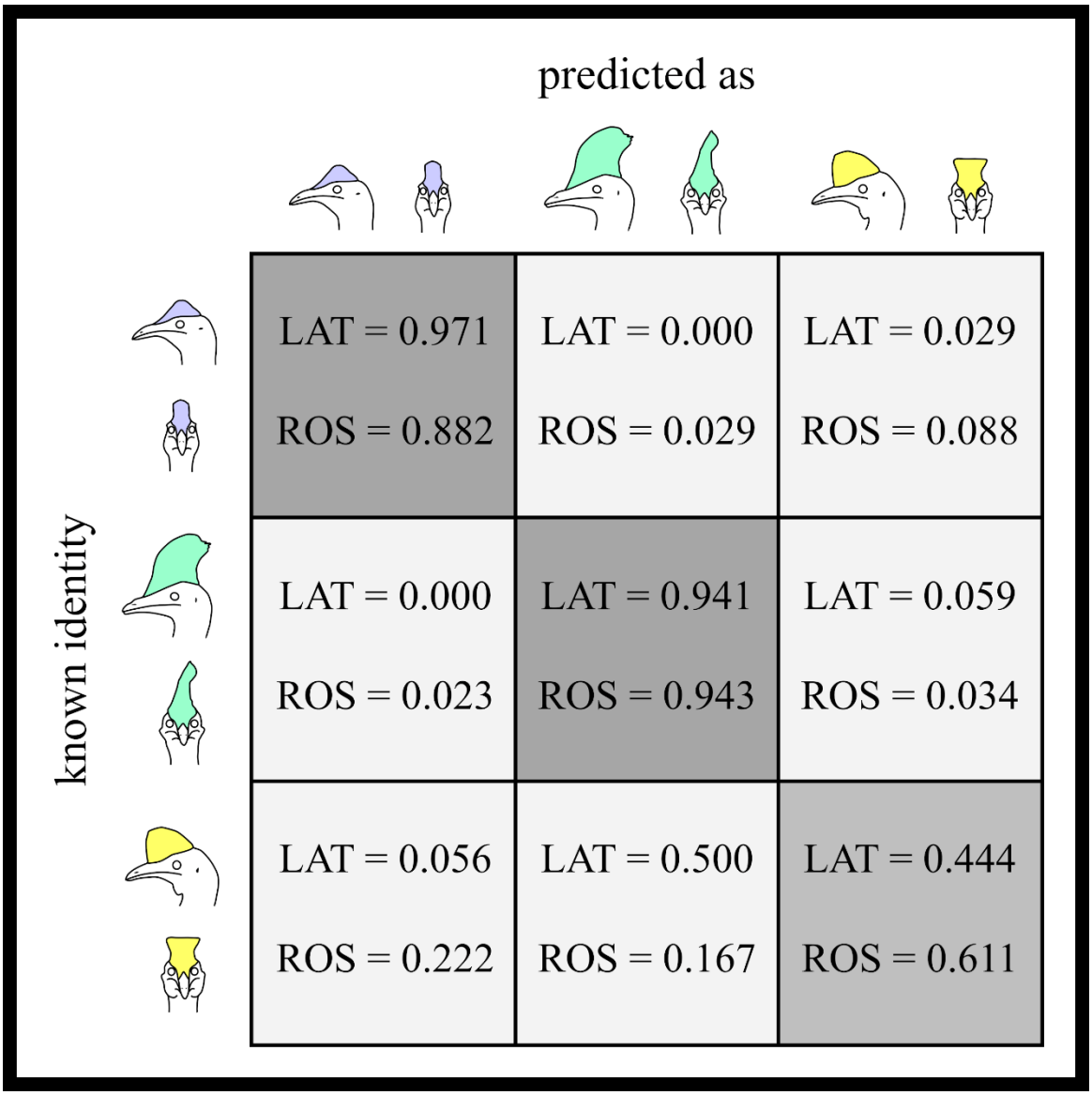

Figure 18. Results of linear discriminant analysis (LDA) comparing principal components of casque outlines (lateral = LAT; rostral = ROS) of *Casuarius* species: (*Casuarius bennetti*, CB = pastel purple; *Casuarius casuarius*, CC = pastel green; *Casuarius unappendiculatus*, CU = pastel yellow). The LDA was able to consistently classify casque shape within species in *C. bennetti* and *C. casuarius*. Although *C. unappendiculatus* was less consistently classifiable, the LDA predicted casques of its own species more consistently than comparing *C. unappendiculatus* to other species. Box greyness increases with more frequent classifiability. Values are rounded to the nearest thousandth.

CHAPTER V

OSTEOLOGICAL COMPARISON OF CASQUE ONTOGENY IN PALEOGNATHOUS AND NEOGNATHOUS BIRDS: IMPLICATIONS FOR SELECTING MODERN ANALOGS IN THE STUDY OF CRANIAL ORNAMENTS FROM EXTINCT, NON-AVIAN DINOSAURS

Abstract

Extant members from both neognathous and paleognathous avian lineages possess cranial bony ornamentation. The evolutionary significance and function of these structures has gone largely unaddressed. However, a deep understanding of the phenotypic complexity of ornamental headgear would be useful for comparative studies among Aves, as well as between other extinct, ornamented archosaurs (e.g., suchians, pterosaurs, and non-avian dinosaurs). To bridge this knowledge gap and broaden our understanding of osseous ornament variation in modern birds, I used micro-computed tomography imaging to examine the cranial casque components, structural composition, and developmental changes of two neognathous (*Numida meleagris*, *Macrocephalon maleo*) and one paleognathous species (*Casuarius casuarius*). I also surveyed the avian osteology literature to better understand the cranial morphologies of the 11 orders of Aves that contain members with osseous cranial ornamentation. Tracing casque development showed that two of my focal taxa acquired the majority of their casque size prior to sexual maturity (*M. maleo, C. casuarius*), while the other acquired most of its casque size afterwards (*N. meleagris*). My

anatomical analyses suggest two broad configuration categories: (1) geminal, in which ornaments consisted of paired elements only (i.e., within Neognathae), and (2) disunited, in which ornaments consisted of unpaired, midline elements along with paired bones (i.e., within Paleognathae). Ornament bones were considered to contribute to either casque elevation (proximal ornament support), elaboration (distal ornament shape), or both. Geminal casques tend to incorporate fewer bones than disunited ones, which necessarily translates to a higher percentage of elements simultaneously involved in both elevation and elaboration in geminal casques. My results have implications for unraveling the selection processes that shaped modern avian casques as well as for use of extant avians as comparative analogs of non-avian dinosaurs with ornamental headgear. For example, I found that neognathous casques tended to be more suitable analogs for the osteological patterns of non-avian dinosaur ornaments generally due to broadly similar geminal constitutions. However, both neognathous and paleognathous casques analogize elevatory and elaborative elements as well as patterns of developmental timing and period. Paleognathous birds are particularly well suited for studying patterns of bone elongation and the incorporation of new bones into casque phenotypes.

1. Introduction

There is a propensity for some groups of tetrapods to derive seemingly bizarre cranial structures, such as enlarged dentitions (e.g., Monodontidae, Nimravidae, Proboscidea), exaggerated sensory organs (e.g., Cetacea, *Condylura*, Dipodomyinae), and prominent bony ornaments (e.g., Artiodactyla, Ceratopsia, Chamaeleonidae). Studies addressing the phenotypic complexity of these anatomies are essential for determining the putative relationships between form and function (Bock, 1980), particularly for those with ambiguous biological roles. Exemplar taxa from all major groups of modern tetrapods have ornamented heads, for example, including amphibians (e.g., casqued

frogs; Jared et al., 2005), non-avian reptiles (e.g., chameleons; Bickel & Losos, 2002), mammals (e.g., artiodactyls; Bubenik & Bubenik, 1990), and birds (e.g., hornbills; Mayr, 2018). Among birds, the range of cranial ornament composition is diverse. For example, soft tissues (i.e., feathers, keratin, skin), hard tissues (bone), or a combination of each may contribute structurally to avian headgear. Soft-tissue ornaments have flexibility utility. They can be highly mobile (e.g., feather crests of *Upupa epops*; Ruiz-Rodríguez et al., 2017), enabling startling and impressive display behaviors, or seasonally present (keratinous breeding crests of *Pelecanus erythrorhynchos*; see Hieronymus, 2009), signaling narrow periods for breeding receptivity. Hard-tissue ornaments, on the other hand, are relatively permanent, appearing and changing in size and shape across the lifetime of an individual (e.g., osseous and keratinous casques of *C. casuarius*; Green & Gignac, 2020; Chapter II).

Avian cranial ornaments constructed with bone are typically composed of multiple osseous elements (Mayr, 2018), which neither move nor articulate like soft-tissue headgear. The cranial casques of the southern cassowaries, for example, represents the most osteologically complex ornament among extant Aves known to date, with eight different cranial bones that fuse during ontogeny (Green & Gignac, 2020; Chapter II). Cassowaries (*C. bennetti*, *C. casuarius*, *C. unappendiculatus*) are flightless birds from Australasia and the only paleognathous group to possess bony cranial ornamentation (Paleognathous birds are differentiated from all other living birds, Neognathae, based on a synapomorphic palatal configuration that primarily involves the vomer, palatine, and pterygoid bones [Huxley, 1867; Pycraft, 1900]—none of which have been unambiguously demonstrated to be directly involved in ornament contribution in any archosaurs to my knowledge.) Numerous species of neognathous birds also have cranial ornaments (see Mayr, 2018), and the headgear of both groups is dominated by external skull elements (homologous and non-homologous bones) that expand dorsally as the casque grows. Whether or not developmental or evolutionary "rules" govern the organization of these ornaments within Aves remains an

unresolved question, particularly in light of the recently clarified, complex casque osteology of cassowaries (Green & Gignac, 2020; Chapter II).

Display structures reflect important aspects of animal behaviors and life histories because they are used in social interactions and, therefore, should develop on a timeline apropos to those interactions. Documenting ontogenetic progression of cranial ornaments aids in the understanding of changes in osteological form (i.e., inflations and fusions) that enable ornament function(s). For example, in Chapter II, we identified the sequence of fusions that brings about the adult *C. casuarius* casque. In Chapter III, I explained how the fused casque underlies signaling of reproductive capability due to positive allometry that enables the majority of casque growth to occur by the time sexual maturity is reached. Together, these findings illustrate that it can take several bones to elevate and elaborate the casque before it appears able to provide an adult signal. As a result, it appears that casques must necessarily begin their rapid growth during early ontogeny.

By comparing developmental series of multiple casqued birds, it is possible to detect whether or not casques mature at different rates relative to life-history parameters, such as the onset of sexual maturity. Because the elements that make up casques can become incorporated into the ornament at different developmental stages (see Green & Gignac, 2020; Chapter II), the sequence and timing by which this takes place may further elucidate shared or divergent evolutionary pathways between taxa (Gignac & O'Brien, 2016; O'Brien et al., 2019; Prieto-Márquez et al., 2020). Capturing developmental shifts in ornament osteology is particularly important because, as adults, the bones that comprise the casque typically fuse together, obscuring suture boundaries needed to confidently identify individual elements. Distinguishing each element exemplifies whether it serves to either (1) elevate the casque, wherein proximal support internal or external to the ornament (e.g., midline sphenoidal, ethmoidal, and septal bones) enables it to rise prominently from the rest of the skull; (2) elaborate the casque, wherein distal elements tend to expand the size and appearance of the ornament (e.g., paired nasals); or (3) both, wherein an element extends along the proximo-distal axis of the ornament enabling support and expansion simultaneously.

Development sequences of elaboration and elevation make it possible to infer whether homologous bones that make up the casques of closely related birds may have evolved by following comparable developmental-evolutionary pathways (i.e., shared elevatory and elaborative components) or independent ones (i.e., differing elevatory and elaborative components).

In this study, I selected one paleognathous (*C. casuarius*; Fig. 1C) and two neognathous species (maleo, *Macrocephalon maleo* Fig. 1B; helmeted guineafowl, *Numida meleagris*; Fig. 1A), all with derived bony ornaments, for direct ontogenetic comparison. These three species were chosen because, (1) they have prominent casques composed of bony cores with epidermal coverings (Pycraft, 1900; Naish & Perron, 2016; Mayr, 2018; Angst et al., 2019), (2) vary in their rates of skeletal development and sexual maturity (Starck & Sutter, 2000; Biggs, 2013; Angst et al., 2019), and (3) have established breeding programs in the United States (enabling opportunistic collection of primarily known-age individuals). In order to visualize internal and external ornament boundaries, identify sutures between developing bones, and describe casque morphologies, I imaged ontogenetic series of each taxon via micro-computed tomography (μCT). My three aims (below) address which bones make up each ornament, how they are incorporated structurally, and when during ontogeny their incorporation takes place. I used this information to formally compare casque growth both between my three focal taxa as well as to ornament descriptions of other birds available in the literature. To achieve this, I:

1) Identified and tracked casque elements across ontogeny, including the extent of casque development at the point of sexual maturity;
2) Determined which elements are elevatory and which are elaborative in each of my developmental stages for all species; and
3) Documented homologous and non-homologous casque elements to infer generalized patterns of casque construction.

Additionally, by analyzing the hard-tissue ornaments of extant birds, I anticipate that my results can be used to compare and interpret the bony ornaments of extinct taxa that are preserved through fossilization. Modern, ornamented analogs—living animals with comparable structures, lifestyles, and biology—have been proposed in order to aid inferences about extinct, ornamented taxa, particularly those among non-avian dinosaurs. These include artiodactyl mammals, squamate lizards, neognathous birds, and paleognathous birds (Dodson, 1975; Farlow & Dodson, 1975; Bubenik & Bubenik, 1990; Hieronymus et al., 2009; Snively & Theodor, 2011; Lü et al., 2017; Angst et al., 2019; Eastick et al., 2019). However, bony cranial ornament function is little explored in extant tetrapods outside of mammals, including for birds, despite that birds are living dinosaurs. Because they are flightless, large-bodied, and generally resemble non-avian theropods, modern *Casuarius* is one of the most commonly referenced avian analogs for the ornaments of extinct non-avian dinosaurs (e.g., Dodson, 1975; Hone at al., 2012; Farke et al., 2013; Lü et al., 2017). Nonetheless, volant, smaller-bodied birds with osseous cranial ornaments may also represent valuable comparative systems (Angst et al., 2019). Indeed, sampling broadly across avifauna holds the potential to capture novel phenotypes and ecologies that may enable more robust comparisons with the archosaur fossil record. In light of new information discussed in the first three chapters (see Chapter II–IV) regarding cassowary casque configuration, ontogeny, and disparity, as well as osteological patterns and ornament developmental of paleognaths and neognaths discussed in this chapter, I conclude by framing the findings of my three aims to specifically address how ornaments of modern birds may be useful as paleontological analogs.

2. Material and Methods

2.1. Specimen Acquisition/Access

Ontogenetic series of *C. casuarius* (n = 17), *N. meleagris* (n = 7) and *M. maleo* (n = 7) were collected from individuals representing early immature stages through sexual maturity (Table 1). Cranial specimens prior to ornament growth, through incipient growth, and including adult casque morphologies were examined across the three species. This allowed me to track the development of bony elements to better categorize patterns of osteological variation. Data were collected from specimens from the American Museum of Natural History (AMNH; New York, NY, USA), Boucher Family Farms (BFF; Longmont, CO, USA), Cassowary Conservation Project (CCP; Fort Pierce, FL, USA), Denver Museum of Nature and Science (DMNS; Denver, CO, USA), Museum of Osteology (MOO; Oklahoma City, OK, USA), Pueblo Zoo (PBZ; Pueblo, CO, USA), Sedgwick County Zoo (SCZ; Wichita, KS, USA), T. L. Green Research Collection (TLG; Tulsa, OK, USA), Tulsa Zoo (TLZ; Tulsa, OK, USA), and Wildlife Conservation Society at Bronx Zoo (WCS; Bronx, NY, USA). All specimens were analyzed from museum collections or opportunistically obtained from zoological or breeding organizations. All individuals died of natural causes, except for two birds with respiratory disease states that prompted the decision for euthanasia by veterinarians. Samples were obtained independently after euthanasia, and no birds were killed or harmed for the purpose of this study.

2.2. Micro-CT Data Collection/Digital Reconstruction

Micro-computed tomography image data were collected from all specimens (n = 31) via one of three μCT systems: (1) a 2010 GE phoenix v|tome|x s240 high-resolution microfocus computed tomography system (General Electric, Fairfield, CT, USA) located in the Microscopy

and Imaging Facility of the AMNH, (2) a 2012 Nikon XT H 225 ST µCT system (Nikon Metrology, Brighton, MI, USA) located at the Dentsply Research and Development Office (Dentsply; Tulsa, OK, USA), and (3) a 2018 Nikon XT H 225 ST µCT system located at the MicroCT Imaging Consortium for Research and Outreach (MICRO; Fayetteville, AR, USA). Scanning parameters varied from 60–202 kilovolts (kV), 48–300 microamps (µA), and 200–1000 millisecond (ms) exposures with isometric voxel size at resolutions ranging from 29.86–117.97 micrometers (µm). See Table 1 for specimen-specific parameters. ImageJ (v. 1, US National Institutes of Health, Bethesda, MD) was used to crop peripheral background pixels in order to reduce CT TIFF stack sizes. I used the programs Avizo (versions 9–version 9.7; Visualization Science Group, Burlington, MA, USA; Thermo-Fisher Scientific; Waltham, MA, USA) and AvizoLite (version 2019; Thermo-Fisher Scientific), to render three-dimensional (3D) digital skull models via a combination of automatic and manual segmentation.

2.3. Definition of Osteological Traits for Bones Contributing to Casque

Avian casques appear to enlarge through pneumatization of cranial bones (e.g., Starck, 1995). Osseous cranial casques are considered to be expansions of the skull roof that exceeds the dorsal skull height compared to non-ornamented, related taxa (Mayr, 2018; Green & Gignac, 2020; Chapter II). Specifically, developmental series of cranial specimens of emus (*Dromaius novaehollandiae*; see Figure 4 and 5 from Green & Gignac, 2020; Chapter II) were used for comparisons with *C. casuarius* and domesticated chickens (*Gallus gallus*; see Figure 1 from Watanabe et al., 2019) for comparisons with *Numida meleagris* and *Macrocephalon maleo* (Fig. 2). For consistency with previous studies (Mayr, 2018; Green & Gignac, 2020; Chapter II), bones that contribute partially or fully to overall casque expansions at each sampled developmental stage are considered casque elements. Ornament-contributing bones were subdivided into elevating

elements (those primarily involved with basal internal support), elaborative elements (those primarily involved in the dorsal expansion or elongation), or elements that fit both categories.

2.4. Definition of Osteological Traits for Bones Not Contributing to Casque:

Those cranial bones that do not interact partially or fully with the structural composition of the casque were considered non-contributing elements. Importantly, cranial bones are often pneumatized (Witmer, 1990) although these elements may not specifically be involved with casque expansions. Micro-computed tomography allowed me to analyze external and internal suture boundaries in order to distinguish pneumatized bones that do not interact with the casque from those that do.

2.5. Consistent Osteological Descriptions

I structured my osteological descriptions consistently by determining which bones that comprise the casque become involved in the structural support or inflation of the ornament at each developmental stage. The entire bone does not have be fully involved, but part of that element must exhibit contribution to structure, inflation, or both. This was determined by elevating position, relative size, and internal expansions of homologous bones between focal casqued taxa and those of their non-casqued, outgroup counterparts, using µCT data. Developmental stages were organized based on the osteological correlates such as progression of the interorbital septum ossification and skull length (measured from the rostral tip of the premaxillae to the caudalmost margin of the supraoccipital bone).

2.6. Definition of Immature Specimens

I define immature specimens as individuals that were not reproductively capable as recorded by an observer or listed by museum voucher. Soft tissues (e.g., brown juvenile plumage coloration) were used to assist *C. casuarius* immature age status, and osteological correlates (i.e., incomplete ossification of the interorbital septum, skull length) for were used to verify immaturity status for *C. casuarius* and *N. meleagris*. In all other cases, the exact age of an individual was required below average breeding age for the species (Rothschild, 1900; Dodson, 1975; Dahouda et al., 2008; Wildlife Conservation Society, 2016; CCP, R.G. Hood, *pers. comm.*). This was essential for *M. maleo*, because I observed that the interorbital septum ossification appears to occur prior to sexual maturity.

2.7. Definition of Mature Specimens

I define mature specimens as individuals that were reproductively capable as recorded by an observer or listed by museum voucher. Soft tissues (e.g., fully black adult plumage coloration) were used to assist *C. casuarius* mature age status and osteological correlates (i.e., complete ossification of the interorbital septum, skull length) for were used to verify adult status for *C. casuarius* and *N. meleagris*. In all other cases, the exact age of an individual was required to be at or above the average breeding age for the species (Rothschild, 1900; Dodson, 1975; Dahouda et al., 2008; Wildlife Conservation Society, 2016; CCP, R.G. Hood, *pers. comm.*).

3. Results

3.1. Casque Developmental Timing

Immature individuals with incipient casques were the most useful in determining bones that comprise the casques in adult skulls with obliterated sutures (see Fig. 3). This allowed for the detection of bony changes throughout development.

I found the youngest *N. meleagris* individual in my sample possesses no ornamental structure (Fig. 4A). By approximately 5.0 months of age the incipient casque, comprising paired frontals, is present (Figs. 3, 4B). The incipient casque appears as midline projection from the most dorsomedial regions of both frontals, which at this point are not fused together (Fig. 4B). It should be noted that this immature *N. meleagris* specimen TLG NM002 (Fig. 4B) is the same individual that was figured in the Mayr (2018) study. As casque expansion proceeds dorsally, rostrally, and caudally, the frontals fuse at the sagittal midline, and the casque becomes more dorsally rounded and laterally compressed, particularly in adult specimens (Figs. 3, 4C–E). In the largest adult specimen in my sample, the rostralmost extent of the casque is approximately at the boundary between the frontals, premaxillae, and nasals while the caudalmost extent occurs within the boundary of the frontals (i.e., does not extend to the transverse suture between frontals and parietals; Figs. 3, 4E). In my sample, only a minority of casque growth occurred prior to sexual maturity (~8 months; Dahouda et al., 2008; Fig. 4). Even though casques are generally symmetrical, those of mature individuals tend to show a wider range of phenotypes.

I found the youngest *M. maleo* individual in my sample possesses no ornamental structure (Fig. 5A). The inflation originates from four elements: the paired frontal and parietal bones. The caudalmost halves of the frontals are inflated into a low-profile and domed, incipient casque by 11.0 months of age (Figs. 3, 5B). The frontals are not yet fused to one another at this point although the transverse sutures between frontals and parietals are partially closed (Figs. 3, 5B). By 2.6 years

of age the paired frontals and parietals are fully fused into a more prominent dome-shaped ornament, which is now more caudally elongated (Fig. 5C). From late immaturity to the oldest, adult specimen in my sample, the casque is fairly similar in size and shape, only becoming slightly more robust in the region of the mushroom-like distal casque (Fig. 5C–E). In my sample, the vast majority of ornament expansion has already occurred in immature individuals (Fig. 5C–D) prior to sexual maturity (3.0–5.0 years; Wildlife Conservation Society, 2016; Fig. 5E). Moreover, *M. maleo* casques are generally symmetrical, meaning that the casques of mature individuals show a narrow range of phenotypes.

Here I summarize the findings of Green & Gignac (2020), which described casque ontogeny in *C. casuarius*. I found the youngest *C. casuarius* individual in my sample to possess no ornamental structure (Fig. 6A). An incipient casque expands at 1.5 months of age, with the median casque element, mesethmoid, and nasals being incorporated first (Figs. 3, 6B). By 5.2 months of age, the frontals additionally participate in the casque structure, followed by all eight elements by 10.4 months. Although the casque is only slightly dorsally expanded at the point at which all elements participate, the casque continues to grow (and becomes laterally compressed) rapidly in height until maturity (Fig. 6C–E), with additional, albeit limited, growth thereafter. Most of casque growth in *C. casuarius* appears to occur prior to sexual maturity (4.0–7.0 years; Rothschild, 1900; Dodson, 1975; CCP, R.G. Hood, *pers. comm.*; Fig. 6); however, casque asymmetries in mature individuals result in a wide range of adult casque phenotypes (see Chapter IV).

3.2. Ornament Contributions – Elevatory & Elaborative Elements

My ontogenetic analysis for bone identities determined that the casque of the adult *N. meleagris* was comprised of two elements (left and right frontals; Figs. 3A, 4) that are both elevating and elaborative. To achieve this, the lateralmost and caudalmost portions of the frontal retain their plesiomorphic contribution to the orbits and neurocranium (as compared to *G. gallus*;

Fig. 2). It is the rostromedial portions of the frontals that expand upwards at the midline. Thus, middling dorsal curvature of the body of the frontal bones elevates the medial boundaries of the contacting frontals, which become the primary elaborative component of the casque. This phenotype is in place by early ontogeny (~5 months; Fig. 4B) with additional (elaborative) growth of the medial portions of the frontal bones thereafter. This is the only species in my sample that has a single paired element comprising the casque. However, casques of *Oreophasis derbianus* and *Anseranas semipalmata* (belonging to avian orders Galliformes and Anseriformes; Mayr, 2018) are similarly constructed from a single right-left pair of cranial bones, which necessarily requires both to elevate and elaborate the ornament, albeit in taxon-specific ways.

I determined that the casque of the adult *M. maleo* was comprised of two primarily elevating elements (left and right parietals) and two primarily elaborative elements (left and right frontals; Figs. 3B, 5). Although frontals anchor the rostral casque base, they contribute to the majority of dorsal casque expansion, so they are primarily elaborative. To achieve this, the rostralmost portions of the frontals and the caudalmost portions of the parietals retain their plesiomorphic contribution to the orbits and neurocranium (as compared to *G. gallus*; Fig. 2). The caudal and lateral portions of the frontals and, to a greater degree, the rostral and lateral positions of the parietals elevate dorsally and caudally. The parietals are, therefore, primarily elevatory with a minor elaborative contribution. The rounded expansion of the caudalmost portions of the frontals as well as lesser contributions from the rostralmost parietals become the elaborative aspect of the casque. There are other birds that incorporate the frontals and parietals, albeit with different ornament morphologies, such as the dual cranial protuberances of *Balearica* (Mayr, 2018).

I determined the casque of the adult *C. casuarius* was comprised of five elevating elements (mesethmoid, left and right lacrimals, left and right frontals) and three elaborative elements (median casque element, left and right nasals; Figs. 3C, 6). To achieve this, the rostralmost nasals, lateralmost lacrimals, and lateralmost frontals, and interorbital portion of the mesethmoid retain their plesiomorphic contributions to the rostrum, orbits, and neurocranium (as compared to *D.*

novaehollandiae; Fig. 2). The mesethmoid proximally supports the internal casque base and the lacrimals and frontals support the external casque base (Green & Gignac, 2020; Chapter II). All elevate the casque during growth. It is important to note that, although the rostralmost portions of the nasals provide some support to the rostral casque base, adult nasals are expansive and are primarily involved in the elaborative, distal casque. These along with the median casque element elongate caudally and dorsally to become the majority of the enlarged visible casque in the skulls of adults.

3.3. Ornament Contributions – Homologous & Non-homologous Construction

The casques of *N. meleagris* arise from of one pair of cranial elements, the frontals (Figs. 3A, 4). The casques of *M. maleo* form from of two pairs of cranial elements, the frontals and parietals (Figs. 3B, 5). Casques of *C. casuarius* arise from eight elements: two unpaired, midline bones (median casque element, mesethmoid) and three paired bones (nasals, lacrimals, frontals; Figs. 3C, 6). Based on my detailed developmental examination, I identified two, broad, and mutually exclusive osteological patterns to cranial ornaments of these birds that also corresponds to my literature survey. *Numida meleagris* and *M. maleo* along with all other casqued neognathous birds surveyed (e.g., Mayr, 2018) show a "geminal" pattern of casque construction. Namely, the headgear of these birds consists exclusively of bilaterally paired bones, such as the right and left frontals along with the right and left parietals (e.g., *M. maleo*). *Casuarius casuarius* characterizes the second pattern that is "disunited", in which right-left pairs of cranial bones are displaced parasagittally by one or more midline elements. In the case of *C. casuarius* displacement is caused by the mesethmoid bone and the median casque element. Geminal casques appear to incorporate fewer bones because they consist of paired bones only. Bird orders with members that appear to have geminal ornaments include Galliformes, Anseriformes, Charadriiformes, Columbiformes, Pelecaniformes, Gruiformes, Cuculiformes, Musophagiformes, Bucerotiformes, Passeriformes

(see Mayr, 2018). The osteological descriptions that correspond to my categorization of ornaments with paired elements only (e.g., left and right nasals, left and right frontals, left and right parietals) were identified by Mayr (2019) through direct and photographic observation of avian cranial osteology. Disunited ornaments, on the other hand, are currently exemplified exclusively by *Casuarius* (Parker, 1866; Pycraft, 1900; Mayr, 2018; Green & Gignac, 2020; Chapter II), as far as is known.

4. Discussion

4.1. Modern Avian Casque Disparity

Elemental components between the ornaments of modern birds vary. My results alongside those of other comparative studies (e.g., Mayr, 2018) illustrate two overarching patterns of ornament construction, disunited and geminal, that are associated with the two major lineages of living birds, paleognaths and neognaths, respectively. Notably, casqued neognaths are not thought to all share a casqued common ancestor, implying that each order independently evolved members with geminal headgear. The adult casques of all species contained at least one pair of bones that participate both to elevate and elaborate the ornament. Augmenting the number of distinct bones that participate in the casque appears to enable the proportion of bones serving exclusively in either elevatory or elaborative roles to also increase. The casque of *C. casuarius* was the only case in which a bone (i.e., the median casque element) serves completely in casque elaboration.

No casques from my focal taxa were present prior to hatching, instead I observed that elements begin to inflate over immaturity. In all three species, incipient ornaments incorporate some part of all adult-participating casque bones prior to sexual maturity. However, the majority of casque size is attained prior to reproductive capability in only *C. casuarius* and *M. maleo*. In the

case of *N. meleagris*, the majority of casque variation appears to occur in sexually mature individuals (Angst et al., 2019). These patterns suggest full-sized casques may function differently in display for *C. casuarius* and *M. maleo* compared to *N. meleagris*. For example, neither *C. casuarius* nor *M. maleo* casques are sexually dimorphic (see Chapters III and IV; Widnyana et al., 2019), whereas this is the case for *N. meleagris* (Angst et al., 2019). Dimorphic bony casques that mature after reproductive capability is attained may differentiate reproductively active males and females (as in *N. meleagris*; Angst et al., 2019), whereas monomorphic casques that mature prior to reproductive capability imply status, species recognition, or both (as is proposed for *C. casuarius*; Chapter IV). These putative relationships should be further elucidated by contrasting the timing of ornament ontogeny and sexual maturity in other members of Galliformes, Anseriformes, Charadriiformes, Columbiformes, Pelecaniformes, Gruiformes, Cuculiformes, Musophagiformes, Bucerotiformes, Passeriformes, and Casuariiformes with osseous headgear.

4.2. Extinct Dinosaur Ornament Disparity

Complexly constructed cranial ornaments consisting of multiple bony partitions (e.g., horns, domes, rugosities, crests, casques) were common among extinct archosaurs (e.g., suchians, pterosaurs, dinosaurs; Hone et al., 2012; Carvalho et al., 2005; Molnar, 2005) and particularly iconic among non-avian dinosaurs (Molnar, 2005). However, due to preservation biases and low sample sizes of paleontological datasets, we have limited information about the ontogeny and natural morphological variation of these structures. As a result, the developmental processes and selective regimes that bring about these seemingly bizarre features remains a mystery. The evolution of dinosaur headgear is not well understood despite several hypotheses addressing the origin and selection processes that may have shaped these structures (i.e., species recognition, see Padian & Horner, 2011; mate competition, see Knell & Sampson, 2011; sexual selection, see Hone et al., 2012; mechanical functionality, see Farke, 2014). Anatomical, biomechanical, and

pathological studies of numerous fossilized specimens notwithstanding, direct behavioral observations of extinct, ornamented taxa cannot be made.

Among non-avian dinosaurs, ornaments (e.g., crests, frills, horns, domes, rugosities) appear to have independently evolved numerous times with various anatomical configurations (Fig. 7) and bony compositions (e.g., Molnar, 2005; Padian & Horner, 2011; Gates et al., 2016). For example, the crest of *Saurolophus osborni* is comprised of the paired nasals, prefrontals, and frontals (Bell, 2011); the frill of *Protoceratops andrewsi* is comprised of the paired parietals and squamosals (Dodson, 1976); the dome of *Stegoceras validum* is comprised of the paired frontals and parietals (Schott et al., 2011); the crest of *Citipati osmolskae* is comprised of the paired premaxillae, nasals, and frontals (Clark et al., 2002; Fig. 7); the horns of *Carnotaurus sastrei* are comprised of the paired frontals only (Paulina Carabajal, 2011; Fig. 7); and the crest of *Monolophosaurus jiangi* is comprised of the paired premaxillae, nasals, lacrimals, prefrontals and frontals (Brusatte et al., 2010; Fig. 7). Despite the variable elements that constitute these ornaments, all are composed of paired dermatocranial bones that meet at the midline (Clark et al., 2002; Goodwin & Horner, 2004; Molnar, 2005; Brusatte et al., 2010; Bell, 2011; Paulina Carabajal, 2011; Hone at al., 2016), epiossification, or other metaplastic tissue (Horner et al., 2016). These appear to be common skull arrangements by which dinosaurs evolved their bony headgear—and even highly convergent with those of distantly related taxa (e.g., mammals, O'Brien et al., 2016). Such broadly similar patterns suggest that there are a limited number of developmental-evolutionary pathways by which hard-tissue ornaments can arise in this group, and potentially others. Moreover, the osteology is consistent with my findings in birds that geminal bony ornaments (i.e., those consisting of paired skull bones without unpaired, midline elements) are evolutionarily more common than disunited ones (i.e., those featuring one or more unpaired, midline bones). *Casuarius casuarius* with its disunited casque appears to be an outlier, not just among Aves, but perhaps among all of Dinosauria, and this calls into question its utility for comparisons with the non-avian

dinosaur fossil record. Below, I re-assess these comparisons and propose a framework for comparative ornament studies in dinosaurs.

4.3. Bridging the Gap Between the Ornaments of Extant & Extinct Dinosaurs

There are numerous, valuable ways in which the headgear of modern tetrapods can inform those of extinct organisms in comparative contexts. For example, the anatomical makeup of a structure (e.g., organic material, bone homologies, overall shapes) can be directly garnered from fossils if complete and undistorted. Osteology (see Chapter II) provides the substrate for determining underlying developmental patterns, and ontogenetic changes and timing of ornament growth (see Chapter III) can assist in informing functional hypotheses. Additionally, the morphological variance of structures can be useful for detection of evolutionary signals that shape ornaments (see Chapter IV). Approaches such as these that seek to address the nature of morphological variation are likely to garner the clearest inferences for those extinct species that have large, age-specific sample sizes. However, they can also serve as natural experiments that inform potential pathways for headgear evolution in less well represented, but anatomically or behaviorally similar species. Thus, using analogies for paleontological systems can provide meaningful inferences about ornament paleobiology.

One aim in the current chapter is to assess the ability of living, ornamented archosaurs to act as natural experiments for addressing headgear evolution in the deep past. In addition to ornamented paleognathous birds (for which cassowaries are the only extant group), numerous other birds across Neognathae also possess osseous casques, crests, and other ornamental structures (Marshall, 1872; Möller, 1969; Zusi, 1993; Mayr, 2018). Birds are living theropod dinosaurs, which means that they tend to share similar bauplans, osteology, and behaviors (Smith-Paredes et al., 2018; Wiemann et al., 2018) with may non-avian dinosaur groups. In addition, birds are remarkably diverse (~10,000 recognized species; Gill, 2007), providing a rich source of morphological

disparity for identifying comparable ornament-development-evolution triads between modern avians and extinct dinosaurs.

I propose three interrelated criteria, mirrored by the results in this chapter, by which modern birds with osseous cranial ornaments may serve as useful models for extinct archosaur headgear: (1) by strict homology, (2) by analogous or homologous structural composition (i.e., elevatory or elaboratory elements), and (3) by developmental timing. Through systematic identification of like morphologies as a comparative baseline, modern birds as evolutionary experiments in cranial ornamentation provide the opportunity to biologically ground-truth behaviors, ecologies, and evolutionary sequences, which then provide a bridge to fossil datasets and paleo-environmental factors that can identify convergence (e.g., O'Brien et al., 2016), homoplasy (e.g., ornaments with frontals; Clark et al., 2002; Brusatte et al., 2010; Bell, 2011; Paulina Carabajal, 2011; Schott et al., 2011), heterochrony (e.g., Prieto-Márquez et al., 2020), or potentially differentiate adaptation from exaptation (e.g., Hieronymus et al., 2009). Much of this research has focused on mammals as model systems because they are well studied ecologically, developmentally, and evolutionarily (see Calamari & Fossum, 2017 and references therein). The well understood biology of mammals has helped to make opportunities for analogy clearer. I propose a similar framework for birds:

1. The timing and period of ornament development can elucidate whether the ornament as a whole is capable of playing a role in identifying maturity, social status, or species identity. In terms of timing and period of ornament development, my analyses suggest that the casques of extant neognaths and paleognaths are both suitable analogs for non-avian dinosaurs. Some studies have examined modern ornamented bird ontogenies alongside those of non-avian dinosaurs (Dodson, 1975; Farke et al., 2013; Angst et al., 2019). Building on these efforts, I suggest that the sequence of element incorporation into ornaments, scaling of ornament features during ontogeny, and timing of ornament

maturity all further elucidate this developmental picture. For example, the nasals, median casque element, and mesethmoid bones of *C. casuarius* become involved in the casque at a relatively small body size (<50% skull length; see Green & Gignac, 2020; Chapter II), which is similar to the incorporation of premaxillae and nasals into the crest of *Parasaurolophus* at similar, relatively small body sizes (<50% skull length; Dodson, 1975; Farke et al., 2013). In fact, the earlier onset of casque initiation for *C. casuarius* than was previously realized (see Chapter II; Dodson, 1975; Farke, et al., 2013), better positions the paleognath as a developmental analog for lambeosaurine hadrosaur ornament growth because both show incipient casques in early ontogeny (Fig. 8) that will subsequently elongate substantially (also see no. 2 below). Although sexual maturity may not be precisely known for many non-avian dinosaurs, those that can be estimated based off histological analyses of growth series (e.g., Erickson et al., 2007) or by inferred behaviors (e.g., Norell et al. 2018) offer additional ground-truthing. Addressing how headgear maturity relates to sexual maturity facilitates comparisons of fossil taxa with modern analogs that either (1) specifically attain the majority of ornament size by the point that sexual maturity is reached (e.g., *C. casuarius*, *M. maleo*), or (2) which attain the majority of ornament size after sexual maturity (*N. meleagris*). In the former, monomorphic casques (with regard to sex) are thought to relate to adult display biology by indicating social status and species recognition (e.g., Chapters III, IV), whereas dimorphic casques of the later may serve in male-female differentiation (Angst et al., 2019).

Considering *C. casuarius* explicitly, Chapter IV proposed that the genus *Casuarius* (composed of *C. bennetti*, *C. casuarius*, and *C. unappendiculatus*) may provide a living, natural experiment in cranial ornament variation. Namely, that ornaments are evolutionarily maintained in various forms within a clade for the purpose of species recognition. This is a long-proposed hypothesis for the function of cranial ornaments

in hadrosaur and ceratopsian dinosaurs (see Padian & Horner, 2011), but one that has rarely been tested in extant systems. Determining if developmental factors that contribute to adult cassowary ornamentation also correlate with biogeography and cladogenesis in a similar way for extinct groups enables formal testing of species-recognition hypotheses against a *Casuarius* model through use of comparative methods. I, therefore, propose that it would be particularly meaningful to contrast ornament ontogenies in extinct taxa broadly against those of modern birds in order to develop conceptual models for potential ornament display function(s) relative to life-history ecologies and diversification patterns.

2. Structural composition should also be considered. Homologous or non-homologous bones located in similar regions of the skull may take on comparable functions to support (i.e., elevate) the ornament or augment (i.e., elaborate) the visual signal or other function(s) it may provide. For example, casques and crests can be elevated internally by unexposed bones (i.e., mesethmoid of *C. casuarius*), whereas visible protuberances are due to elaborations of superficial elements that lie immediately deep to keratin or rhamphotheca (i.e., culmen of some Corvidae and Vangidae [Passeriformes]; Mayr, 2018). How the structural components of grossly similar ornaments differ provides for valuable macroevolutionary information regarding if and how headgear diversification may be constrained to a limited number of selective regimes. In terms of structural composition, my analysis suggests the casques of extant neognaths and paleognaths are both suitable analogs for non-avian dinosaurs. For example, paleognathous, *C. casuarius* casques consist of numerous elevating and elaborating elements that elongate caudally during development. Although not all ornament bones are homologous, the pattern of osseous elongation is reminiscent of the crests of many of the lambeosaurine hadrosaurs and oviraptorosaurs (i.e., *Saurolophus osborni*, Bell, 2011; *Citipati osmolskae*, Clark et al., 2002, respectively;

Fig. 8). Neognathous, *N. meleagris* casques are simpler, however, comprised only of right-left homologs that are both elevatory and elaborative, which is comparable to the ornaments of some non-avian theropods (i.e., *Carnotaurus sastrei*; Paulina Carabajal, 2011; Fig. 8). I, therefore, also propose that it would be particularly meaningful to examine bones that are not necessarily homologous but that share similar functions within the casque in order to develop conceptual models for how cranial elements evolve into either elevatory or elaborative roles or are able to serve both functions.

3. Finally, evolutionary comparison of homologous structures enables the tracking of like traits across evolutionary events in order to quantify the rate, sequence, and magnitude of character changes that result from altering bony phenotypes. To study headgear through the lens of homology, it is necessary for extinct groups and their modern analogs to incorporate homologous bones onto their ornaments. Capturing the disparity of extant archosaur headgear improves opportunities to match analogous taxa with their fossilized precursors. For example, avian frontal bones are involved in the ornaments of many modern birds (see Mayr, 2018; Green & Gignac, 2020; Chapter II), just like with their fossilized precursors. However, some birds evolved ornaments with alternative osteology, like *C. casuarius* with casques that contain a potentially neomorphic bone (Pycraft, 1900; Green & Gignac, 2020; Chapter II). Sampling more broadly across modern Aves instead of focusing on cassowaries may provide for extant species that hold greater utility relative to extinct counterparts by sharing independently derived but homologous ornament osteology. I find that geminal osteology characterizes the vast majority of dinosaur ornaments. Therefore, homologous comparison should focus on geminal analogs, namely neognathous birds (Fig. 8). In certain instances, the specific ornament elements are identical, as is the case of *M. maleo* and the dome of the pachycephalosaur, *S. validum* (i.e., frontals and parietals; Schott et al., 2011). I, therefore, propose that it would be particularly

meaningful to examine *M. maleo* in order to develop a conceptual model for how frontal and parietal bone pairings evolve into an enlarged bony ornament.

4.4. Concluding Summary

To address how modern birds may inform our understanding of the distant past, I utilized μCT imaging to document the osteological make up of paleognathous and neognathous casques. I characterized adult anatomical element contributions that are elevatory from those that are elaborative in order to define broad patterns that characterize common ornament configurations, and I examined ornament ontogeny and timing of sexual maturity to clarify how life-history patterns may correspond to presumed ornament function. Using my above proposed framework, I recommend a schema for comparing ornaments in modern casqued birds to those of extinct archosaurs, particularly hadrosaur, theropod, and pachycephalosaur dinosaurs: (1) Homology examination explicitly ensures that similar evolutionary units are compared; (2) examination of structural composition enables study of casque expansions, regardless of constituent homologies; and (3) examination of ontogeny facilitates ecological inferences to inform evolutionary conclusions. Taken together, my findings demonstrate that paleognathous and neognathous birds both hold utility for analogizing the headgear of non-avian dinosaurs, depending upon the contexts in which they are compared. I hope that a more systematic selection method for modern analogs will enable more rigorous hypothesis testing and more robust resolutions for palaeobiological questions.

Table 1. Specimen list indicating preparation history, sex, age, and µCT parameters and facilities.

Species	Specimen ID	Type	Sex	Age	kV	µA	µm	ms	Filter (mm)	Facility
C. casuarius	TLG (CCP) C007	skeleton	U	IM (1 d.)	90	110	74.93	200	Cu (0.100)	AMNH
C. casuarius	TLG (CCP) C010	fluid	U	IM (1 d.)	110	110	105.58	200	Cu (0.100)	AMNH
C. casuarius	TLG (CCP) C025	frozen	U	IM (7 d.)	160	57	53.77	508	—	Dentsply
C. casuarius	TLG (CCP) C024	frozen	U	IM (9 d.)	160	57	41.97	508	—	Dentsply
C. casuarius	TLG (CCP) C011	fluid	U	IM (24 d.)	140	120	99.96	200	Cu (0.100)	AMNH
C. casuarius	TLG (CCP) C043	frozen	M	IM (42 d.)	198	200	39.89	267	Cu (0.125)	MICRO
C. casuarius	TLG (CCP) C037	frozen	M	IM (1.5 mo.)	150	90	52.67	500	—	MICRO
C. casuarius	TLG (CCP) C021	fluid	F	IM (5.2 mo.)	150	200	75.75	333	Cu (0.100)	AMNH
C. casuarius	TLG C002	skeleton	U	IM (~5.5 mo.)	80	60	81.23	200	Cu (0.100)	AMNH
C. casuarius	TLG (CCP) C004	fluid	F	IM (10.4 mo.)	130	180	105.89	400	Cu (0.100)	AMNH
C. casuarius	TLG (CCP) C031	frozen	M	IM (14.0 mo.)	175	200	114.36	267	—	MICRO
C. casuarius	AMNH SKEL 963	skeleton	U	IM (~24.0 mo.)	140	130	93.42	200	—	AMNH
C. casuarius	AMNH SKEL 962	skeleton	U	AD (~4.0–5.0 yr.)	140	130	93.42	200	—	AMNH
C. casuarius	TLG C001	skeleton	U	AD (~5.0–20.0 yr.)	60	80	96.90	200	Cu (0.100)	AMNH
C. casuarius	TLG (SCZ) C022 (12126)	frozen	M	AD (21.4 yr.)	196	70	117.67	500	—	MICRO
C. casuarius	DMNS ZB.50012	dried	M	AD (22.1 yr.)	190	207	117.97	267	—	MICRO
C. casuarius	MOO 8031	skeleton	F	AD (35.7 yr.)	120	100	87.85	200	—	AMNH
M. maleo	OSUCHS (WCS) MM005 (B19124)	fluid	F	IM (2.5 mo.)	175	200	35.07	267	—	MICRO
M. maleo	OSUCHS (WCS) MM003 (B16291)	fluid	U	IM (11.0 mo.)	120	110	90.15	200	—	AMNH
M. maleo	OSUCHS (TLZ) MM001 (17648)	frozen	M	IM (2.3 yr.)	150	61	110.87	708	—	Dentsply
M. maleo	OSUCHS (WCS) MM004 (B16361)	fluid	M	IM (2.6 yr.)	165	250	70.80	267	Cu (0.125)	MICRO
M. maleo	OSUCHS (WCS) MM002 (B13138)	fluid	M	IM (4.0 yr.)	202	300	60.58	267	Cu (0.125)	MICRO
M. maleo	OSUCHS (WCS) MM006 (B14197)	fluid	M	AD (5.1 yr.)	200	270	56.55	267	—	MICRO
M. maleo	AMNH SKEL 27152	skeleton	F	AD (~5.0–8.0 yr.)	100	100	89.59	200	—	AMNH
N. meleagris	TLG (BFF) NM005	frozen	U	IM (14 d.)	150	164	29.86	267	—	MICRO
N. meleagris	TLG (BFF) NM006	frozen	U	IM (35 d.)	150	200	31.91	267	—	MICRO
N. meleagris	TLG NM002	skeleton	U	IM (~5.0 mo.)	120	250	40.05	267	Cu (0.125)	MICRO
N. meleagris	TLG (BFF) NM004	frozen	M	AD (9.0 mo.)	150	300	59.95	267	Cu (0.125)	MICRO
N. meleagris	TLG NM003	skeleton	U	AD (~2.0–3.0 yr.)	120	250	46.29	267	Cu (0.125)	MICRO
N. meleagris	TLG (PBZ) NM001	frozen	M	AD (5.5 yr.)	197	48	92.53	1000	—	Dentsply
N. meleagris	TLG NM007	skeleton	U	AD (~3.0–6.0 yr.)	150	300	59.95	267	Cu (0.125)	MICRO

C. casuarius = *Casuarius* casuarius; *M. maleo* = *Macrocephalon maleo*; *N. meleagris* = *Numida meleagris*; F = female; M = male; U = unknown sex; IM = immature; AD = adult; kV = kilovolts; µA = microamps; µm = voxel micrometers; ms = millisecond exposures; mm = millimeters; Cu = copper

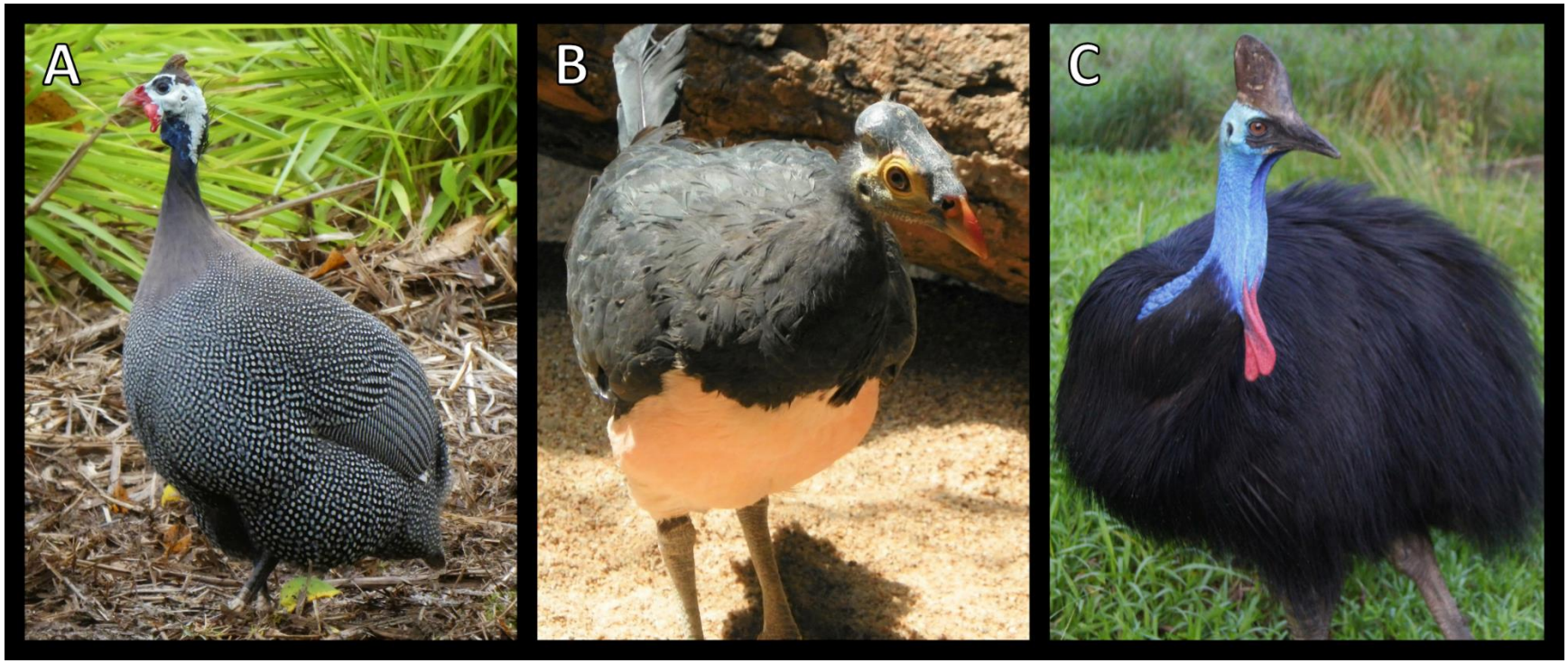

Figure 1. Photographs of adult (A) helmeted guinea fowl (*Numida meleagris*), (B) maleo (*Macrocephalon maleo*), and (C) southern cassowary (*Casuarius casuarius*). All three species possess osseous casques dorsal to their orbits and neurocranium. Photos by T. L. G.

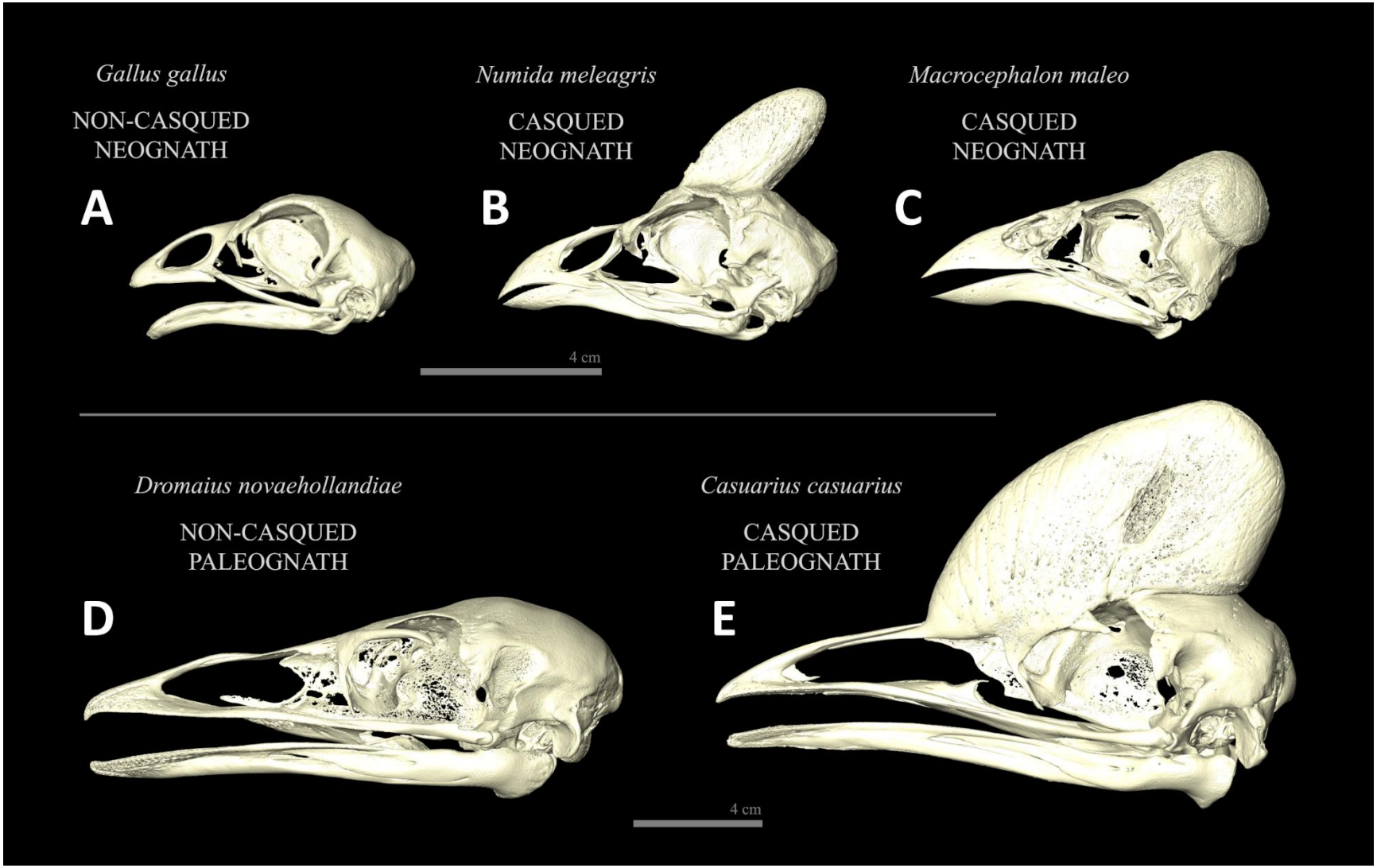
Gallus gallus
NON-CASQUED
NEOGNATH
A
Numida meleagris
CASQUED
NEOGNATH
B
Macrocephalon maleo
CASQUED
NEOGNATH
C
4 cm
Dromaius novaehollandiae
NON-CASQUED
PALEOGNATH
D
Casuarius casuarius
CASQUED
PALEOGNATH
E
4 cm

Figure 2. Three-dimensional renderings from micro-computed tomography data of adult neognaths, (A) *Gallus gallus* (PMG GG001), (B) *Numida meleagris* (TLG NM007), (C) *Macrocephalon maleo* (OSUCHS MM006) along with paleognaths, (D) *Dromaius novaehollandiae* (TLG E054) and (E) *Casuarius casuarius* (AMNH SKEL 962). In order to determine the cranial bones contributing to casques of ornamented taxa, the cranial osteology of non-casqued neognathous and paleognathous relatives were used for comparison; (A) *G. gallus* and (D) *D. novaehollandiae*, respectively. Micro-computed tomography image data of the two non-casqued taxa were collected via a 2010 GE phoenix v|tome|x s240 high-resolution microfocus computed tomography system housed in the Microscopy and Imaging Facility of the AMNH. Scanning parameters were 110–120 kilovolts (kV), 130–170 microamps (µA), ranging from 84.52–103.82 micrometers (µm),200 millisecond (ms) exposures with isometric voxel size at resolutions, W target, and no filter.

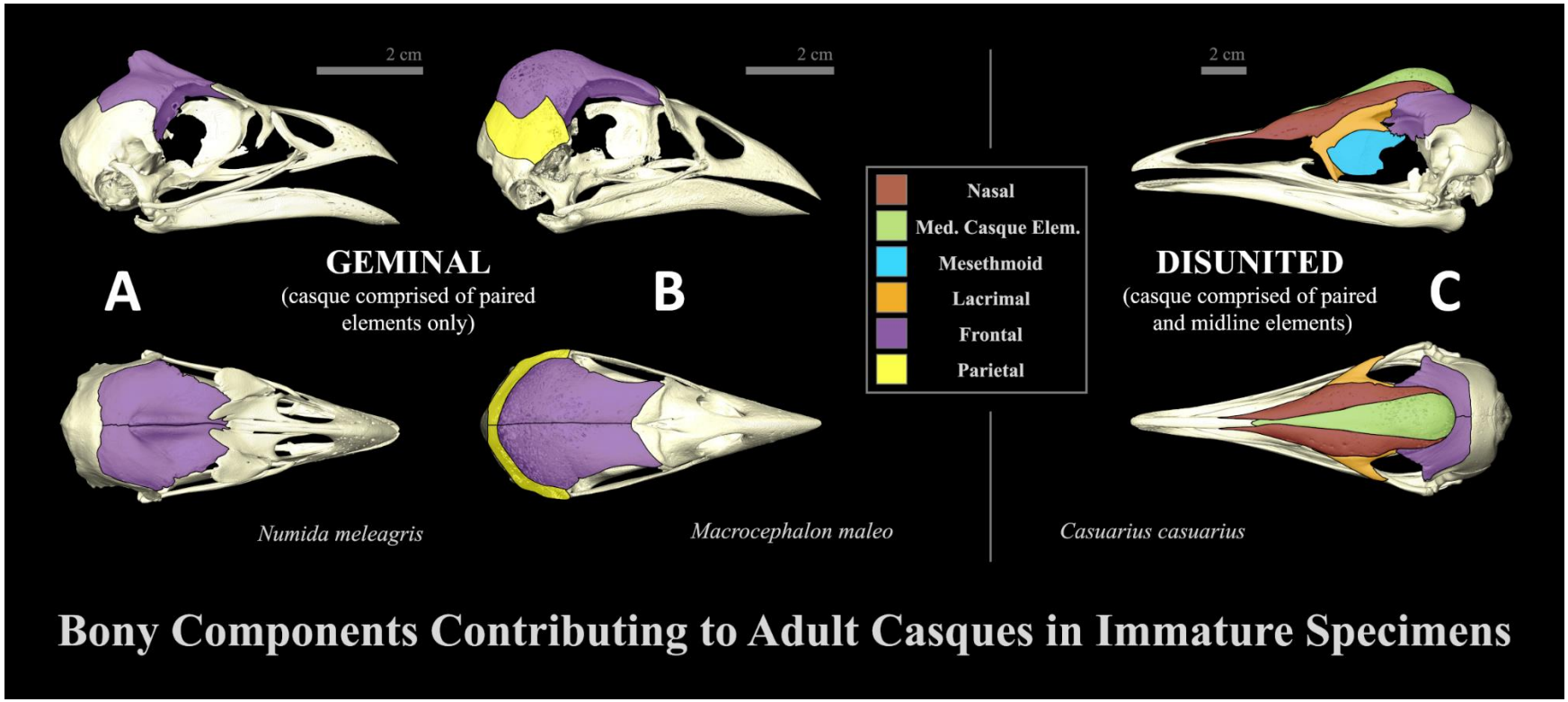

Figure 3. Three-dimensional renderings from micro-computed tomography data of immature (A) *Numida meleagris* (TLG NM002), (B) *Macrocephalon maleo* (OSUCHS MM003), and (C) *Casuarius casuarius* (TLG C004). Broad cranial casque patterns divided into geminal (sampled neognaths; *N. meleagris* and *M. maleo*) and disunited (sampled paleognath; *C. casuarius*). Skulls are shown in (top) lateral and (bottom) dorsal views with elements that will contribute to the fully matured adult casque false colored (maroon = nasals; green = median casque element; blue = mesethmoid; orange = lacrimals; purple = frontals; yellow = parietals).

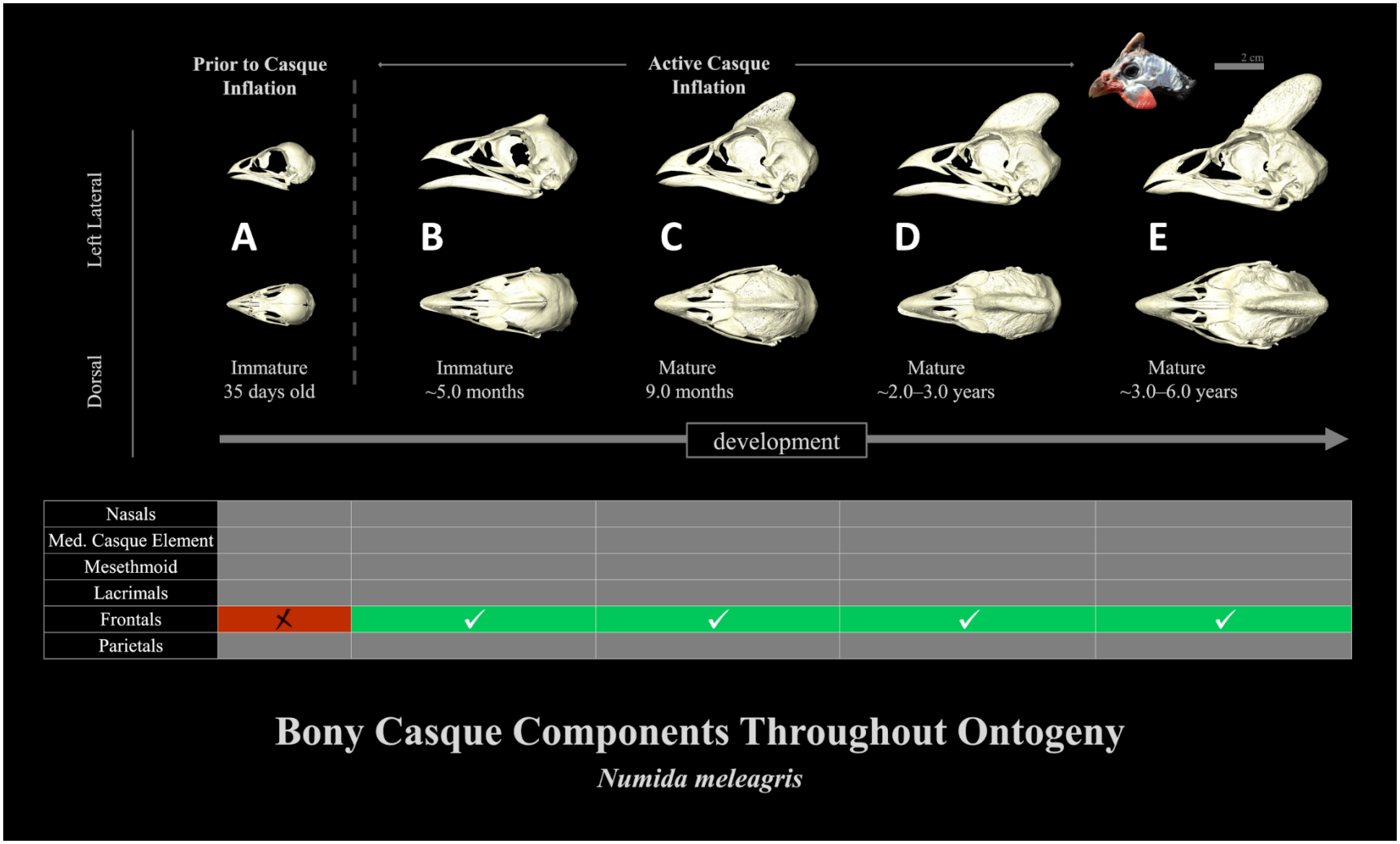
Prior to Casque Inflation
Active Casque Inflation
2 cm
Left Lateral
Dorsal
A
B
C
D
E
Immature
35 days old
Immature
~5.0 months
Mature
9.0 months
Mature
~2.0–3.0 years
Mature
~3.0–6.0 years
development
Nasals
Med. Casque Element
Mesethmoid
Lacrimals
Frontals
Parietals
✗
✓
✓
✓
✓
Bony Casque Components Throughout Ontogeny
Numida meleagris

Figure 4. Three-dimensional renderings from micro-computed tomography data of a developmental series of *Numida meleagris*: (A) TLG NM006, (B) TLG NM002, (C) TLG NM004, (D) TLG NM003, (E) TLG NM007 (see Table 1). Skulls are shown in (top) left lateral and (bottom) dorsal views. Casque elements specific to *N. meleagris* are indicated by colored cells (dark red [X] = element not participating at specific age; dark green [✓] = element participating at specific age) in the table, and grey cells indicate bones that do not contribute to bones in the species represented in this figure, but do contribute to others in the study. Dashed line indicates the diving line between specimens without (left) and with (right) casques developmentally present.

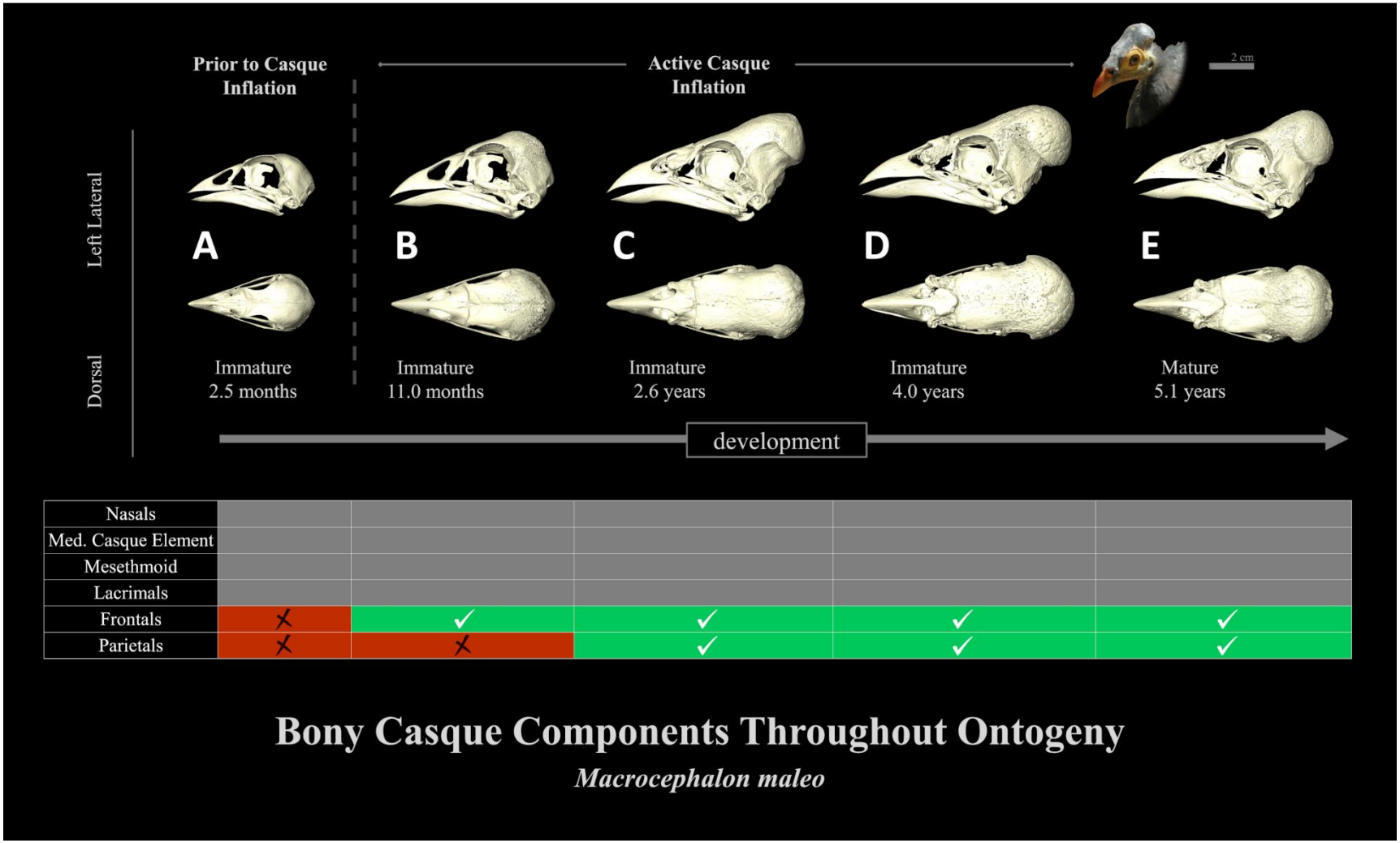
Prior to Casque Inflation
Active Casque Inflation
2 cm
Left Lateral
Dorsal
A
B
C
D
E
Immature 2.5 months
Immature 11.0 months
Immature 2.6 years
Immature 4.0 years
Mature 5.1 years
development
Nasals
Med. Casque Element
Mesethmoid
Lacrimals
Frontals
Parietals
Bony Casque Components Throughout Ontogeny
Macrocephalon maleo

Figure 5. Three-dimensional renderings from micro-computed tomography data of a developmental series of *Macrocephalon maleo*: (A) OSUCHS MM005, (B) OSUCHS MM003, (C) OSUCHS MM004, (D) OSUCHS MM002, (E) OSUCHS MM006 (see Table 1). Skulls are shown in (top) left lateral and (bottom) dorsal views. Casque elements specific to *M. maleo* are indicated by colored cells (dark red [X] = element not participating at specific age; dark green [✓] = element participating at specific age) in the table, and grey cells indicate bones that do not contribute to bones in the species represented in this figure, but do contribute to others in the study. Dashed line indicates the diving line between specimens without (left) and with (right) casques developmentally present.

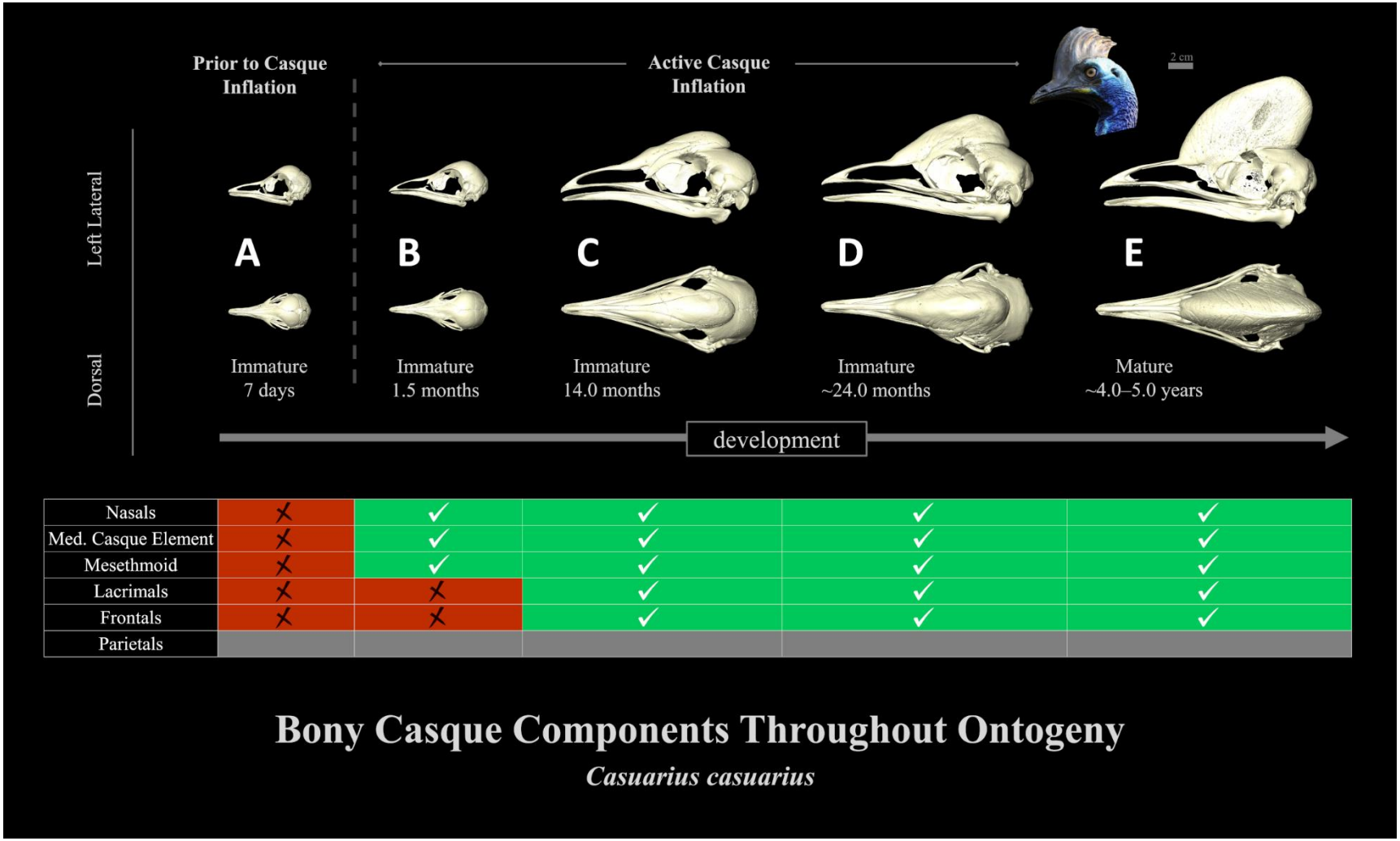
Prior to Casque Inflation
Active Casque Inflation
2 cm
Left Lateral
Dorsal
A
B
C
D
E
Immature 7 days
Immature 1.5 months
Immature 14.0 months
Immature ~24.0 months
Mature ~4.0–5.0 years
development
Nasals
Med. Casque Element
Mesethmoid
Lacrimals
Frontals
Parietals
Bony Casque Components Throughout Ontogeny
Casuarius casuarius

Figure 6. Three-dimensional renderings from micro-computed tomography data of a developmental series of *Casuarius casuarius*: (A) TLG C025, (B) TLG C037, (C) TLG C031, (D) AMNH SKEL 963, (E) AMNH SKEL 962 (see Table 1). Skulls are shown in (top) left lateral and (bottom) dorsal views. Casque elements specific to *C. casuarius* are indicated by colored cells (dark red [X] = element not participating at specific age; dark green [✓] = element participating at specific age) in the table, and grey cells indicate bones that do not contribute to bones in the species represented in this figure, but do contribute to others in the study. Dashed line indicates the diving line between specimens without (left) and with (right) casques developmentally present.

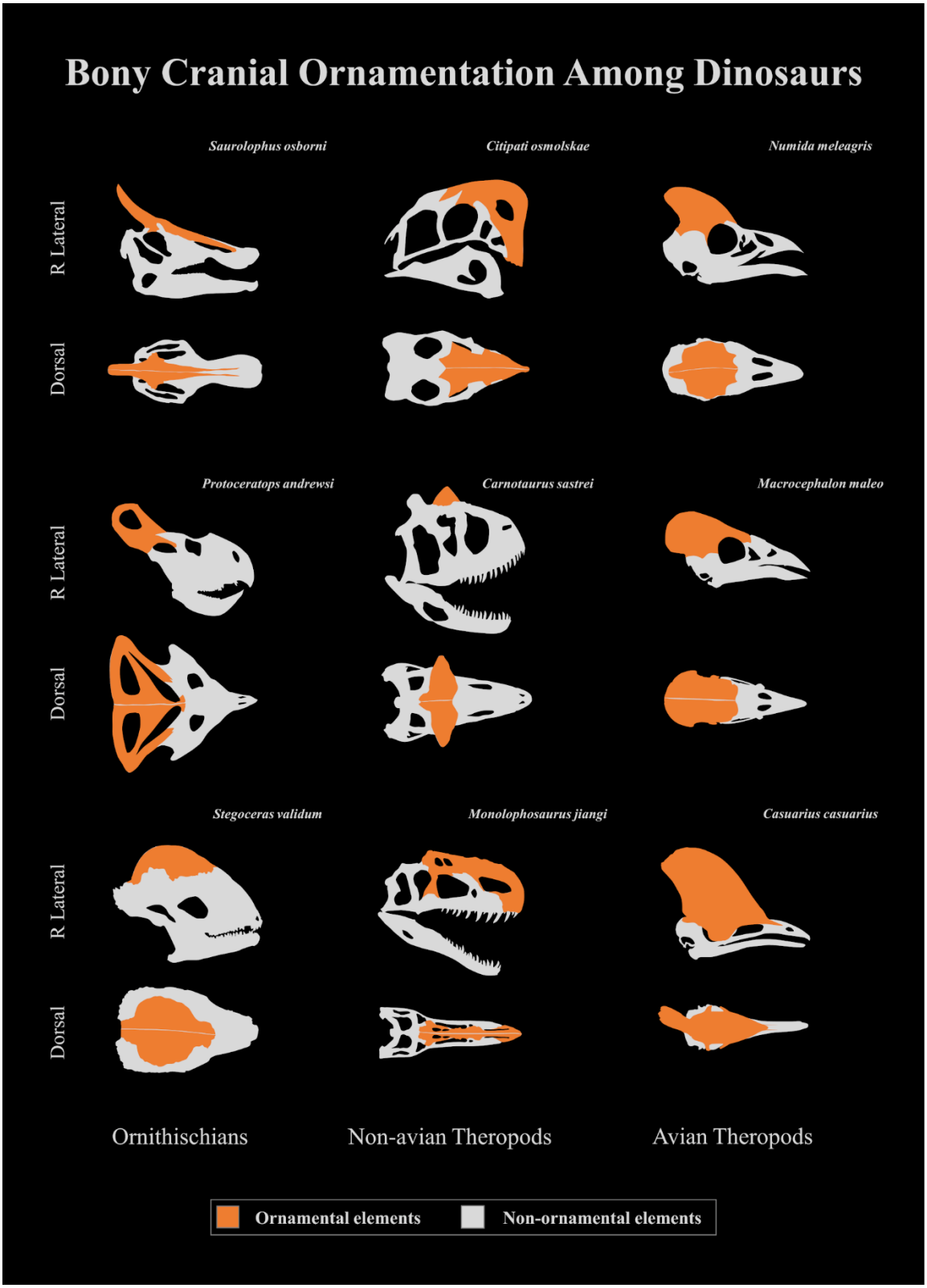
Bony Cranial Ornamentation Among Dinosaurs
Saurolophus osborni
Citipati osmolskae
Numida meleagris
R Lateral
Dorsal
Protoceratops andrewsi
Carnotaurus sastrei
Macrocephalon maleo
R Lateral
Dorsal
Stegoceras validum
Monolophosaurus jiangi
Casuarius casuarius
R Lateral
Dorsal
Ornithischians
Non-avian Theropods
Avian Theropods
Ornamental elements
Non-ornamental elements

Figure 7. Illustrations of bony cranial anatomy among exemplar dinosaurs with skull ornamentation (i.e., *Saurolophus osborni* (paired nasals, prefrontals, and frontals; Bell, 2011), *Protoceratops andrewsi* (paired parietals and squamosals; Dodson, 1976), *Stegoceras validum* (paired frontals and parietals; Schott et al., 2011), *Citipati osmolskae* (paired premaxillae, nasals, and frontals; Clark et al., 2002), *Carnotaurus sastrei* (paired frontals; Paulina Carabajal, 2011), *Monolophosaurus jiangi* (paired premaxillae, nasals, lacrimals, prefrontals and frontals; Brusatte et al., 2010), *Numida meleagris* (paired frontals), *Macrocephalon maleo* (paired frontals and parietals); *Casuarius casuarius* (mesethmoid, median casque element, paired nasals, paired lacrimals, and paired frontals; Green & Gignac, 2020; Chapter II). Each skull shown in right lateral (top) and dorsal (bottom) views. Grey regions depict non-ornamental elements and orange-highlighted regions depict ornamental elements for each represented species.

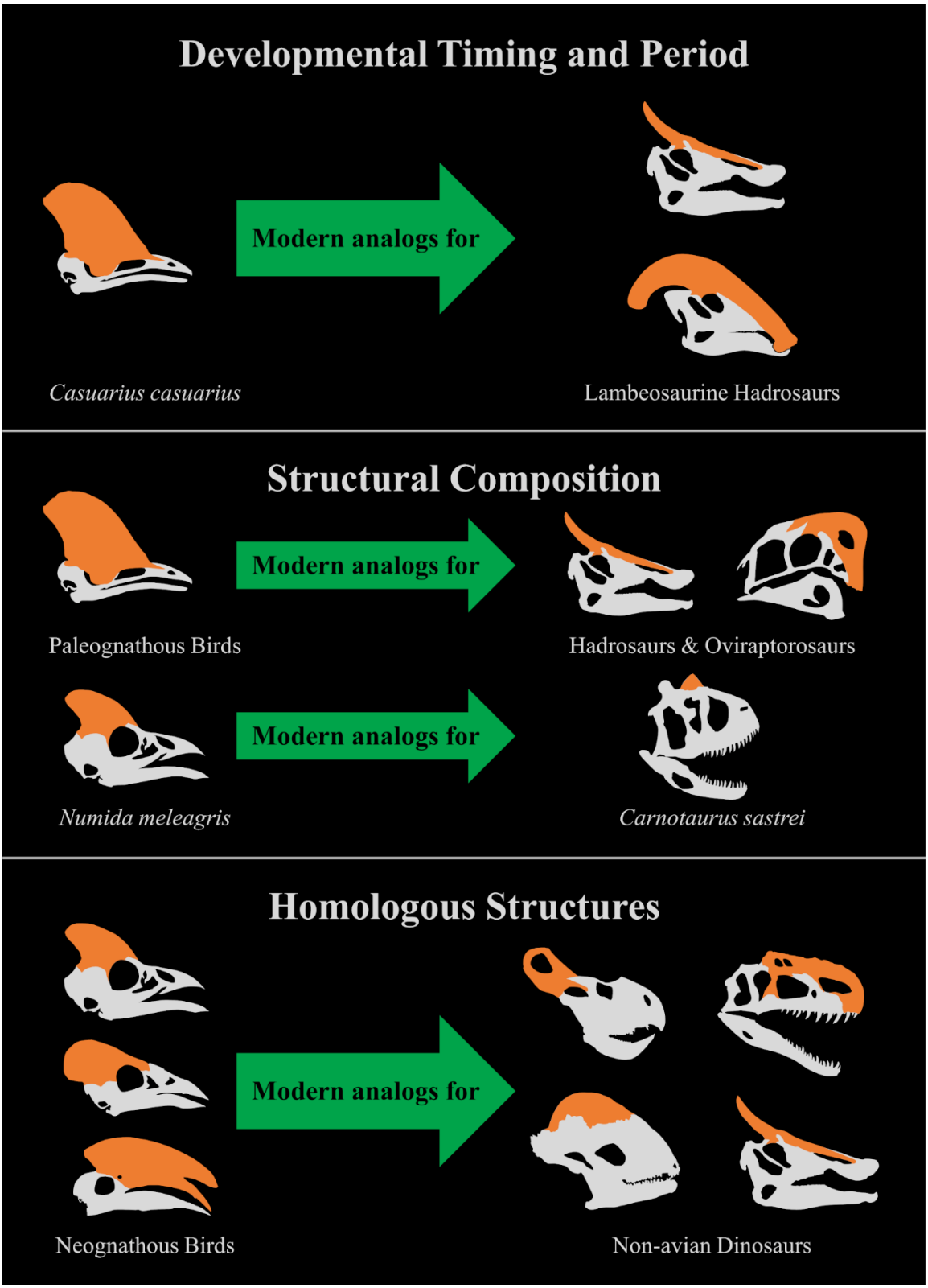
Developmental Timing and Period
Modern analogs for
Casuarius casuarius
Lambeosaurine Hadrosaurs
Structural Composition
Modern analogs for
Paleognathous Birds
Hadrosaurs & Oviraptorosaurs
Modern analogs for
Numida meleagris
Carnotaurus sastrei
Homologous Structures
Modern analogs for
Neognathous Birds
Non-avian Dinosaurs

Figure 8. Examples of modern casque analogs suitable for specific non-avian dinosaur ornamentation comparisons in the context of (top row) development, (middle row) structural composition, and (bottom row) homologous structures. Each skull shown in right lateral view. Grey regions depict non-ornamental elements, and orange-highlighted regions depict ornamental elements for each represented species (see main text for relevant osteology); neognathous birds surveyed from the literature collectively represented by hornbill illustration (lowest left).

CHAPTER VI

CONCLUSION: THE LONGVIEW OF CASSOWARY RESEARCH

Despite their unusual and charismatic appearance, surprisingly few studies on cassowaries have been undertaken. Their rarity (Campbell et al., 2012; IUCN, 2020), solitary lifestyle (Crome, 1976; Stocker & Irvine, 1983), and lethal tendencies (Rothschild, 1900; Kofron, 1999) may have made cassowaries unfavorable for the formal, structured evaluation associated with the scientific process. However, their bright colors, unusual headgear, and departure from traditional avian traits (e.g., inability to fly) have attracted the attention of a handful of devoted researchers. A monograph of the genus *Casuarius* was published in 1900 by Lord Walter Rothschild and was the first work to showcase its vast range of soft tissue characteristics, particularly the color patterns adorning the craniocervical skin. Accompanying this Rothschild (1900) publication in the same issue of *Transactions of the Zoological Society of London* was another lengthy monograph that included descriptive cassowary internal anatomy, alongside the breakdown of anatomical features among other living birds (Pycraft, 1900). These two documents may have also attributed to the dearth of subsequent (particularly, post-cranial) anatomical cassowary studies, as they were written in extreme detail from one of the largest private collections of cassowaries ever complied (> 150 individuals; T.L. Green, *pers. obs.*). As a result, they have stood for more than a century as the go-to resources for information on these mercurial birds. Other than these monographs, the primary focus of most published cassowary studies has been speculation on anatomical composition

(Parker, 1866; Flower, 1871; Marshall, 1872; Richardson, 1991; Naish & Perron, 2016; Mayr, 2018) and assessment of the functionality (Crome & Moore, 1988; Phillips & Sanborn, 1994; Mack & Jones, 2003; Hone et al., 2012; Naish & Perron, 2016; Eastick et al., 2019) of their exaggerated cranial casques. In fact, there appears to have been a recently revived interest in cassowary studies. It was recognized that cassowaries are a vital, but declining, aspect of rainforest ecology as primary seed dispersers for large number of tropical plants (e.g., Stocker & Irvine, 1983; Mack, 1995; Webber & Woodrow, 2004; Bradford & Westcott, 2010; Bradford & Westcott, 2011). This instigated numerous additional studies clarifying cassowary ecology and behavior, followed by government programs protecting cassowaries from threats, such as habitat loss, forest fragmentation, car strikes, and dog attacks (e.g., Crome, 1976; Crome & Moore, 1990; Bentrupperbaumer, 1997; Kofron, 1999; Moore, 2007; Goosem et al., 2011; Campbell et al., 2012; IUCN, 2020).

Even after these efforts, cassowary casques are not well understood developmentally or functionally. Nonetheless, paleontological studies have continued to propose and used cassowaries as modern analogs for contextualizing the cranial ornaments of non-avian dinosaurs (Dodson, 1975; Padian & Horner 2011, Hone at al., 2012; Farke et al., 2013; Naish & Perron, 2016; Lü et al., 2017; Eastick et al., 2019). In this dissertation, I sought to determine if such an analogy was appropriate through a series of integrative studies aimed at addressing cassowary casque biology. I used information from these previous studies, large sample sizes of cassowaries preserved in museums, as well as modern imaging, geometric morphometric, and statistical methods to cross disciplines for a more wholistic understanding of cassowary biology at the interfaces between their behavior, ecology, development, and diversity. I focused my efforts on the casque and forged new understanding in four areas of cassowary biology:

1. The osseous casques of southern cassowaries are more complex than previously thought, composed of eight separate cranial elements (nasals, median casque element, mesethmoid,

lacrimals, and frontals). One of these bones, the median casque element, appears to be a derived feature in cassowaries (Chapter II), a novelty that certainly demands additional focus;

2. Both the osseous and keratinous portions of the casque scale with strong positive allometry over ontogeny, and there are no significant differences between casque growth trajectories between males and females. Most casque growth occurs prior to sexual maturity, suggesting a possible display role in signaling sexual maturity or status, regardless of individual sex (Chapter III);
3. Casque shape does not differ between *C. casuarius* sexes, may differ between *C. casuarius* regional populations, and significantly differs between all three extant *Casuarius* species. This supports the potential of the casque in serving multiple display roles, including in the recognition of species (Chapter IV);
4. The casques of paleognathous cassowaries are not the most suitable analogs for the ornaments of non-avian dinosaurs based on homology alone, instead neognaths birds are. Cassowary casques are more useful as modern analogs for structural composition as well as developmental timing and period for these extinct taxa (Chapter V).

This study adds to the recent revival of cassowary-related research (Mack & Jones, 2003; Perron, 2011; Campbell et al., 2012; Hone at al., 2012; Farke et al., 2013; Naish & Perron, 2016; Lü et al., 2017; Mayr, 2018; Angst et al., 2019; Eastick et al., 2019; McInerney et al., 2019; Eliason & Clarke, 2020). By studying cassowaries in a multidisciplinary fashion, a more wide-ranging perspective can be gained about their life history and diversification—and this will in turn place cassowaries into morphological, behavioral, ecological contexts for comparative studies with other avian taxa and well as non-avian dinosaurs. Additionally, results from this dissertation point to new efforts that we as a cassowary research community can now establish for studying these animals. Global efforts to coordinate large-scale studies that link anatomical (e.g., McInerney et al., 2019; Green &

Gignac, 2020; Chapter II), genetic (e.g., Perron, 2011; Mitchell et al., 2014), and conceptual studies (e.g., Hone at al., 2012; Naish & Perron, 2016) with direct observations of cassowaries across their native habitat (e.g., Bradford & Westcott, 2011; Campbell et al., 2012) should be a future aim. I predict the next big topics to be undertaken in cassowary research are likely cranial tissue development, genetic taxonomic resolution, and casque ecomorphology. I propose that a common agenda built on a firm foundation of continued ontogeny, disparity, and functional research will allow for increasingly more comprehensive conclusions to be drawn about cassowary conservation, ratite evolution, avian development, and phenotypic complexity among archosaurs. It is exceptional that cassowaries—a rare and unique group of birds—offer so much potential for understanding the nuanced processes that shape our natural world.

REFERENCES

Andersson, M. (1994). *Sexual Selection*. Princeton: Princeton University Press.

Angst, D., Barnoud, J., Cornette, R. & Chinsamy, A. (2019). Sex and ontogenetic variation in the crest of *Numida meleagris*: Implications for crested vertebrates. *Anat. Rec.* **303**, 1018–1034.

Arnold, S.J. (1983). Morphology, performance and fitness. *Am. Zool.* **23**, 347–361.

Baker, A.J., Haddrath, O., McPherson, J.D. & Cloutier, A. (2014). Genomic support for a moa–tinamou clade and adaptive morphological convergence in flightless ratites. *Mol. Biol. Evol*. **31**, 1686–1696.

Baumel, J.J. & Witmer, L.M. (1993). Osteologia. In *Handbook of avian anatomy: nomina anatomica avium*. Second Edition: 45–132. Baumel, J.J., King, A.S., Breazile, J.E., Evans, H.E., & Vanden Berge, J.C. (Eds.). Cambridge: Nuttall Ornithological Club.

Bell, P.R. (2011). Cranial osteology and ontogeny of *Saurolophus angustirostris* from the Late Cretaceous of Mongolia with comments on *Saurolophus osborni* from Canada. *Acta Palaeontol. Pol.* **56**, 703–722.

Benkman, C.W. (1996). Are the ratios of bill crossing morphs in crossbills the result of frequency-dependent selection? *Evol. Ecol.* **10**, 119–126.

Bentrupperbaumer J. (1997). *Reciprocal ecosystem impact and behavioural interactions between cassowaries,* Casuarius casuarius*, and humans,* Homo sapiens*: exploring the natural-human environment interface and its implications for endangered species recovery in North Queensland, Australia*. PhD dissertation, James Cook University.

Bickel, R. & Losos, J.B. (2002). Patterns of morphological variation and correlates of habitat use in chameleons. *Biol. J. Linn. Soc.* **76**, 91–103.

Biggs, J. (2013). Captive Management Guidelines for the Southern Cassowary. Cairns Tropical Zoo.

BirdLife International and Handbook of the Birds of the World (2019). Bird species distribution maps of the world. Version 2019.1. Available at http://datazone.birdlife.org/species/requestdis.

Bitton, P.P. & Doucet, S.M. (2016). Sympatric black-headed and elegant trogons focus on different plumage characteristics for species recognition. *Anim. Behav.* **116**, 213–221.

Bock, W.J. (1980). The definition and recognition of biological adaptation. *Am. Zool.* **20**, 217–227.

Bock, W.J. & Von Wahlert, G. (1965). Adaptation and the form-function complex. *Evolution* 269-299.

Bolwig, N. (1973). Agonistic and sexual behavior of the African Ostrich (*Struthio camelus*). *Condor* **75**, 100–105.

Bradford, M.G. & Westcott, D.A. (2010). Consequences of southern cassowary (*Casuarius casuarius,* L.) gut passage and deposition pattern on the germination of rainforest seeds. *Austral. Ecol.* **35**, 325–333.

Bradford, M.G. & Westcott, D.A. (2011). Predation of cassowary dispersed seeds: is the cassowary an effective disperser? *Integr. Zool.* **6**, 168–177.

Brassey, C.A. & O'Mahoney, T. (2018). Pneumatisation and internal architecture of the Southern Cassowary *Casuarius casuarius* casque: a microCT study. Report from a BOU Funded Project.

Brusatte, S.L., Benson, R.B., Currie, P.J. & Xijin, Z. (2010). The skull of *Monolophosaurus jiangi* (Dinosauria: Theropoda) and its implications for early theropod phylogeny and evolution. Zool. J. Linn. Soc. **158**, 573–607.

Bubenik, G.A. & Bubenik, A.B. (1990). *Horns, pronghorns, and antlers: evolution, morphology, physiology, and social significance*. New York: Springer-Verlag.

Buchholz, R. (1991). Older males have bigger knobs: correlates of ornamentation in two species of curassow. *Auk* **108**, 153–160.

Calamari, Z.T. & Fossum, R. (2018). Shape disparity of bovid (Mammalia, Artiodactyla) horn sheaths and horn cores allows discrimination by species in 3D geometric morphometric analyses. *J. Morphol.* **279**, 361–374.

Campbell, H.A., Dwyer, R.G., Fitzgibbons, S., Klein, C.J., Lauridsen, G., McKeown, A., Olsson, A., Sullivan, S., Watts, M.E. & Westcott, D. A. (2012). Prioritising the protection of habitat utilised by southern cassowaries *Casuarius casuarius johnsonii*. *Endanger. Species Res.* **17**, 53–61.

Carvalho, I.S., Campos, A.D.C.A. & Nobre, P.H. (2005). *Baurusuchus salgadoensis*, a new crocodylomorpha from the Bauru Basin (Cretaceous), Brazil. *Gondwana Res.* **8**, 11–30.

Chandler, C.H., Ofria, C. & Dworkin, I. (2012). Runaway sexual selection leads to good genes. *Evolution* **67**, 110–119.

Clark, J.M., Norell, M.A. & Rowe, T. (2002). Cranial anatomy of *Citipati osmolskae* (Theropoda, Oviraptorosauria), and a reinterpretation of the holotype of *Oviraptor philoceratops*. *Am. Mus. Novit.* 1–24.

Crawford, E.C., & Schmidt-Nielsen, K. (1967). Temperature regulation and evaporative cooling in the ostrich. *Am. J. Physol.* **212**, 347–353.

Crome, F.H.J. (1976). Some observations on the biology of the cassowary in northern Queensland. *Emu* **76**, 8–14.

Crome, F.H.J. & Moore, L.A. (1988). The cassowary's casque. *Emu* **88**, 123–124.

Crome, F. H. & Moore, L.A. (1990). Cassowaries in North-Eastern Queensland-Report of a survey and a review and assessment of their status and conservation and management needs. *Wildl. Res.* **17**, 369–385.

Dakin, R. (2011). The crest of the peafowl: a sexually dimorphic plumage ornament signals condition in both males and females. *J. Avian Biol.* **42**, 405–414.

Dahouda, M., Sènou, M., Toléba, S.S., Boko, C.K., Adandédjan, J.C. & Hornick, J.L. (2008). Comparison of local Guinea fowl (*Meleagris numida*) production characteristics in experimental station and rural area in soudano-guinean zone of Bénin. *Livest. Res. Rural* **20** [http://www.lrrd.org/lrrd20/12/daho20211.htm].

Darwin, C. (1871). *The descent of man, and selection in relation to sex*. Princeton: Princeton UP.

Diamond, J. (1986). Biology of birds of paradise and bowerbirds. *Annu. Rev. Ecol. Evol. Syst.* **17**, 17–37.

Dodson, P. (1975). Taxonomic implications of relative growth in lambeosaurine hadrosaurs. *Syst. Biol.* **24**, 37–54.

Dodson, P. (1976). Quantitative aspects of relative growth and sexual dimorphism in *Protoceratops*. *J. Paleontol.* 929–940.

Eastick, D.L., Tattersall, G.J., Watson, S.J., Lesku, J.A. & Robert, K.A. (2019). Cassowary casques act as thermal windows. *Sci. Rep.* **9**, 1–7.

Eliason, C.M. & Clarke, J.A. (2020). Cassowary gloss and a novel form of structural color in birds. *Sci. Adv.* **6**, eaba0187.

Erickson, G.M., Curry Rogers, K., Varricchio, D.J., Norell, M.A. & Xu, X. (2007). Growth patterns in brooding dinosaurs reveals the timing of sexual maturity in non-avian dinosaurs and genesis of the avian condition. *Biol. Lett.* **3**, 558–561.

Evans, D.C. (2006). Nasal cavity homologies and cranial crest function in lambeosaurine dinosaurs. *Paleobiology*, **32**, 109–125.

Evans, D.C. (2010). Cranial anatomy and systematics of *Hypacrosaurus altispinus*, and a comparative analysis of skull growth in lambeosaurine hadrosaurids (Dinosauria: Ornithischia). *Zool. J. Linn. Soc.* **159**, 398–434.

Farke, A.A. (2014). Evaluating combat in ornithischian dinosaurs. *J. Zool.* **292**, 242–249.

Farke, A.A., Chok, D.J., Herrero, A., Scolieri, B. & Werning, S. (2013). Ontogeny in the tube crested dinosaur *Parasaurolophus* (Hadrosauridae) and heterochrony in hadrosaurids. *PeerJ* **1**, e182.

Farlow, J.O. & Dodson, P. (1975). The behavioral significance of frill and horn morphology in ceratopsian dinosaurs. *Evolution* 353–361.

Felice, R.N. & O'Connor, P.M. (2014). Ecology and caudal skeletal morphology in birds: the convergent evolution of pygostyle shape in underwater foraging taxa. *PLoS One* **9**, e89737.

Fisher, R.A. (1930). *The genetical theory of natural selection*. Oxford: Clarendon Press.

Flower, W.H. (1871). On the skeleton of the Australian cassowary (*Casuarius australis*). *Proc. Zool. Soc. Lond.* **3**, 32–35.

Friedman, J., Bohonak, A.J. & Levine, R.A. (2013). When are two pieces better than one: fitting and testing OLS and RMA regressions. *Environmetrics* **24**, 306–316.

Frith, C.B. (1978). The function of display and coloration in the sunbittern. *Avic. Mag.* **84**, 150–157.

Gamble, K.C. (2007). Internal anatomy of the hornbill casque described by radiography, contrast radiography, and computed tomography. *J. Avian Med. Surg.* **21**, 38–49.

Gates, T.A., Organ, C. & Zanno, L.E. (2016). Bony cranial ornamentation linked to rapid evolution of gigantic theropod dinosaurs. *Nat. Commun.* **7**, 1–10.

Gignac, P. & O'Brien, H. (2016). Suchian feeding success at the interface of ontogeny and macroevolution. *Integr. Comp. Biol.* **56**, 449–458.

Gill, F.B. (2007). *Ornithology*. 3rd edn. New York: W. H. Freeman and Company.

Goosem, M., Moore, L.A., Byrnes, P. & Gibson, M. (2011) Mission Beach Road Research: Impacts on Cassowaries and other Fauna and Strategies for Mitigation. School of Earth and Environmental Science, James Cook University, Cairns.

Grant, P.R. & Grant, B.R. (2009). The secondary contact phase of allopatric speciation in Darwin's finches. *PNAS* **106**, 20141–20148.

Green, T.L. & Gignac, P.M. (2020). Osteological description of casque ontogeny in the southern cassowary (*Casuarius casuarius*) using micro-CT imaging. *Anat. Rec.* [https://doi.org/10.1002/ar.24477].

Hagelin, J.C. (2002). The kinds of traits involved in male-male competition: a comparison of plumage, behavior, and body size in quail. *Behav. Ecol*. **13**, 32–41.

Hamburger, V. & Hamilton, H.L. (1951). A series of normal stages in the development of the chick embryo. *J. Morphol.* **88**, 49–92.

Harshman, J., Braun, E.L., Braun, M.J., Huddleston, C.J., Bowie, R.C., Chojnowski, J.L., Hackett, S.J., Han, K., Kimball R.T., Marks, B.D., Miglia, K.J., Moore, W.S., Reddy, S., Sheldon, F.H., Steadman, D.W., Steppan, S.J., Witt, C.C. & Yuri. T. (2008). Phylogenomic evidence for multiple losses of flight in ratite birds. *PNAS* **105**, 13462–13467.

Hatch, J.J. (1985). Lateral asymmetry of the bill of *Loxops coccineus* (Drepanidinae). *Condor* **87**, 546–547.

Heather, B. & Robertson, A. (1997). *The field guide to the birds of New Zealand*. Oxford: Oxford University Press.

Hieronymus, T.L. (2009). *Osteological correlates of cephalic skin structures in Amniota: documenting the evolution of display and feeding structures with fossil data*. PhD dissertation, Ohio University.

Hieronymus, T.L., Witmer, L.M., Tanke, D.H. & Currie, P.J. (2009). The facial integument of centrosaurine ceratopsids: morphological and histological correlates of novel skin structures. *Anat. Rec.* **292**, 1370–1396.

Hone, D.W.E. & Naish, D. (2013). The 'species recognition hypothesis' does not explain the presence and evolution of exaggerated structures in non-avialan dinosaurs. *J. Zool.* **290**, 172–180.

Hone, D.W., Naish, D. & Cuthill, I.C. (2012). Does mutual sexual selection explain the evolution of head crests in pterosaurs and dinosaurs? *Lethaia* **45**, 139–156.

Hone, D.W., Wood, D. & Knell, R.J. (2016). Positive allometry for exaggerated structures in the ceratopsian dinosaur *Protoceratops andrewsi* supports socio-sexual signaling. *Palaeontol. Electron.* **19**, 1–13.

Horner, J.R. & Goodwin, M.B. (2006). Major cranial changes during *Triceratops* ontogeny. *Proc. Royal Soc. B* **273**, 2757–2761.

Hothorn, T., Zeileis, A., Farebrother, R.W., Cummins, C., Millo, G., Mitchell, D. & Zeileis, M.A. (2019). Package 'lmtest'. Online at https://cran.r-project.org/web/packages/lmtest/lmtest.pdf.

Huxley, T.H. (1867). On the classification of birds: and on the taxonomic value of the modifications of certain of the cranial bones observable in that class. *P. Zool. Soc. Lond.* **1967**, 415–471.

IUCN (2020). The IUCN Red List of Threatened Species. Version 2020-1. https://www.iucnredlist.org. Downloaded on 24 March 2020.

Jared, C., Antoniazzi, M.M., Navas, C.A., Katchburian, E., Freymüller, E., Tambourgi, D.V. & Rodrigues, M.T. (2005). Head co-ossification, phragmosis and defence in the casque-headed tree frog *Corythomantis greeningi*. *J. Zool.* **265**, 1–8.

Jones, I.L. & Hunter, F.M. (1999). Experimental evidence for mutual inter- and intra-sexual selection favouring a crested auklet ornament. *Anim. Behav.* **57**, 521–528.

Kekäläinen, J., Valkama, H., Huuskonen, H. & Taskinen, J. (2010). Multiple sexual ornamentation signals male quality and predicts female preference in minnows. *Ethology* **116**, 895–903.

Kemp, A.C. (2001). Family Bucerotidae (hornbills). In *Handbook of the birds of the world. Vol. 6. (mousebirds to hornbills)*: 436–523. del Hoyo, J., Elliott, A. & Sargatal J., (Eds.). Barcelona: Lynx Edicons.

Kesteven, H.L. (1942). The ossification of the avian chondrocranium, with special reference to that of the emu. *Proc. Linn. Soc. NSW* **67**, 213–237.

Kilmer, J.T. & Rodríguez, R.L. (2017). Ordinary least squares regression is indicated for studies of allometry. *J. Evol. Biol.* **30**, 4–12.

Kinnaird, M.F., Hadiprakarsa, Y.Y. & Thiensongrusamee, P. (2003). Aerial jousting by helmeted hornbills *Rhinoplax vigil*: Observations from Indonesia and Thailand. *Ibis* **145**, 506–508.

Knell, R.J. & Sampson, S. (2011). Bizarre structures in dinosaurs: species recognition or sexual selection? A response to Padian and Horner. *J. Zool.* **283**, 18–22.

Kofron, C.P. (1999). Attacks to humans and domestic animals by the southern cassowary (*Casuarius casuarius johnsonii*) in Queensland, Australia. *J. Zool.* **249**, 375–381.

Komsta, L. & Novomestky, F. (2013). Package 'moments'. Online at https://cran.r-project.org/web/packages/moments/moments.pdf.

Komsta, L. (2015). Package 'outliers'. Online at https://cran.r-project.org/web/packages/outliers/outliers.pdf.

Latch, P. (2007). National recovery plan for the southern cassowary *Casuarius casuarius johnsonii*. Report to Department of the Environment, Water, Heritage and the Arts, Canberra. Environmental Protection Agency.

Legendre, P. & Legendre, L. (1998). *Numerical ecology: developments in environmental modelling, 20*. 2nd edn. Amsterdam: Elsevier Science.

Legendre, P. & Oksanen, M.J. (2018). Package 'lmodel2'. Online at https://cran.r-project.org/web/packages/lmodel2/lmodel2.pdf.

Lü, J., Li, G., Kundrát, M., Lee, Y.N., Sun, Z., Kobayashi, Y., Shen, C., Teng, F. & Liu, H. (2017). High diversity of the Ganzhou Oviraptorid Fauna increased by a new "cassowary-like" crested species. *Sci. Rep.* **7**, 6393.

Mack, A.L. (1995). Distance and non-randomness of seed dispersal by the dwarf cassowary *Casuarius bennetti*. *Ecography* **18**, 286–295.

Mack, A.L. & Jones, J. (2003). Low-frequency vocalizations by cassowaries (*Casuarius* spp.). *Auk* **120**, 1062–1068.

MacLeod, C.D. (2010). Assessing the shape and topology of allometric relationships with body mass: a case study using testes mass allometry. *Methods Ecol. Evol.* **1**, 359–370.

MacLeod, C.D. & MacLeod, R.C. (2009). The relationship between body mass and relative investment in testes mass in amniotes and other vertebrates. *Oikos* **118**, 903–916.

Maderspacher, F. (2017). Evolution: flight of the ratites. *Curr. Biol.* **27**, R110–R113.

Maloney, S.K. (2008). Thermoregulation in ratites: a review. *Aust. J. Exp. Agric.* **48**, 1293–1301.

Marchant, S. & Higgins, P.J. (1990). *Handbook of Australian, New Zealand and Antarctic birds. Vol 1. Ratites to ducks*. Melbourne: Oxford University Press.

Marshall, W. (1872). Über die knöchernen Schädelhöcker der Vögel. *Niederl. Arch. Zool.* **1**, 133–179.

Marugán-Lobón, J. & Buscalioni, Á.D. (2004). Geometric morphometrics in macroevolution: morphological diversity of the skull in modern avian forms in contrast to some theropod dinosaurs. In *Morphometrics*: 157–173. Berlin: Springer.

Maxwell, E.E. (2008). Ossification sequence of the avian order Anseriformes, with comparison to other precocial birds. *J. Morphol.* **269**, 1095–1113.

Maxwell, E.E. (2009). Comparative ossification and development of the skull in palaeognathous birds (Aves: Palaeognathae). *Zool. J. Linn. Soc.* **156**, 184–200.

Mayr, G. (2018). A survey of casques, frontal humps, and other extravagant bony cranial protuberances in birds. *Zoomorphology* **137**, 457–472.

McCoy, D.E. & Prum, R.O. (2019). Convergent evolution of super black plumage near bright color in 15 bird families. *J. Exp. Biol.* **222**, jeb208140.

McInerney, P.L., Lee, M.S., Clement, A.M. & Worthy, T.H. (2019). The phylogenetic significance of the morphology of the syrinx, hyoid and larynx, of the southern cassowary, *Casuarius casuarius* (Aves, Palaeognathae). *BMC Evol. Biol.* **19**, 1–18.

Menon, D.G., Bennett, D.C. & Cheng, K.M. (2014). Understanding the behavior of domestic emus: a means to improve their management and welfare—major behaviors and activity time budgets of adult emus. *J. Anim.* **2014**, [https://doi.org/10.1155/2014/938327].

Minnaar, P. & Minnaar, M. (1992). *The emu farmer's handbook. Vol. 1*. Texas: Induna Publishing Co.

Minnaar, P. & Minnaar, M. (1998). *The emu farmer's handbook. Vol. 2.* Texas: Nyoni Publishing Co.

Mitchell, K.J., Llamas, B., Soubrier, J., Rawlence, N.J., Worthy, T.H., Wood, J., Lee, M.S.Y. & Cooper, A. (2014). Ancient DNA reveals elephant birds and kiwi are sister taxa and clarifies ratite bird evolution. *Science* **344**, 898–900.

Möller W. (1969). Vergleichend-morphologische Untersuchungenan Schädeln höckertragender Anatiden, mit einem Beitrag zur Mechanik des Anatidenschädels. *Gegenbaurs. Morphol. Jb.* **113**, 160–200; 321–345.

Molnar, R.E. (2005). Sexual selection and sexual dimorphism in theropods. In *The carnivorous dinosaurs*: 484–312. Carpenter, K. (Ed.). Bloomington & Indianapolis: Indiana University Press.

Moore, L.A. (2007). Population ecology of the southern cassowary *Casuarius casuarius johnsonii*, Mission Beach north Queensland. *J. Ornithol.* **148**, 357–366.

Nagai, H., Mak, S.S., Weng, W., Nakaya, Y., Ladher, R. & Sheng, G. (2011). Embryonic development of the emu, *Dromaius novaehollandiae*. *Dev. Dynam.* **240**, 162–175.

Naish, D. & Perron, R. (2016). Structure and function of the cassowary's casque and its implications for cassowary history, biology and evolution. *Hist. Biol.* **28**, 507–518.

Ness, A.R. (1967). A measure of asymmetry of the skulls of odontocete whales. *J. Zool.* **153**, 209–221.

Norberg, R.Å. (1977). Occurrence and independent evolution of bilateral ear asymmetry in owls and implications on owl taxonomy. *Philos. T. R. Soc. B* **280**, 375–408.

Norell, M.A., Balanoff, A.M., Barta, D.E. & Erickson, G.M. (2018). A second specimen of *Citipati osmolskae* associated with a nest of eggs from Ukhaa Tolgod, Omnogov Aimag, Mongolia. *Am. Mus. Novit.* **2018**, 1–44.

O'Brien, H.D., Faith, J.T., Jenkins, K.E., Peppe, D.J., Plummer, T.W., Jacobs, Z.L., Li, B., Joannes-Boyau, R., Price, G., Feng, Y.X. & Tryon, C.A. (2016). Unexpected convergent evolution of nasal domes between Pleistocene bovids and Cretaceous hadrosaur dinosaurs. *Curr. Biol.* **26**, 503–508.

O'Brien, H.D., Lynch, L.M., Vliet, K.A., Brueggen, J., Erickson, G.M. & Gignac, P.M. (2019). Crocodylian head width allometry and phylogenetic prediction of body size in extinct crocodyliforms. *Integr. Comp. Biol.* **1**, obz006.

Oksanen, J., Kindt, R., Legendre, P. & O'Hara, B. (2007). Vegan: community ecology package. R package version 1.8-5. Available at: http://cran.r-project.org/.

Olson, V.A. & Turvey, S.T. (2013). The evolution of sexual dimorphism in New Zealand giant moa (*Dinornis*) and other ratites. *Proc. R. Soc. B* **280**, 20130401.

Padian, K. & Horner, J.R. (2011). The evolution of 'bizarre structures' in dinosaurs: biomechanics, sexual selection, social selection or species recognition? *J. Zool.* **283**, 3–17.

Parker, W.K. (1866). VIII. On the structure and development of the skull of the ostrich tribe. *Proc. Zool. Soc. Lond.* **14**, 112–114.

Paulina Carabajal, A. (2011). The braincase anatomy of *Carnotaurus sastrei* (Theropoda: Abelisauridae) from the Upper Cretaceous of Patagonia. *J. Vertebr. Paleontol.* **31**, 378–386.

Perron, R.M. (2011). The taxonomic status of *Casuarius bennetti papuanus* and *C. b. westermanni*. *Bull. Brit. Ornithol. Club* **131**, 54–58.

Perron, R.M. (2016). *Taxonomy of the genus* Casuarius*: the defined and known living cassowary species and subspecies*. United Kingdom: Quantum Conservation.

Peterson, J.E. & Vittore, C.P. (2012). Cranial pathologies in a specimen of *Pachycephalosaurus*. *PLoS One* **7**, e36227.

Phillips, P.K. & Sanborn, A.F. (1994). An infrared, thermographic study of surface temperature in three ratites: ostrich, emu and double-wattled cassowary. *J. Therm. Biol.* **19**, 423–430.

Phillips, M.J., Gibb, G.C., Crimp, E.A. & Penny, D. (2010). Tinamous and moa flock together: mitochondrial genome sequence analysis reveals independent losses of flight among ratites. *Syst. Biol.* **59**, 90–107.

Pomiankowski, A. & Iwasa, Y. (1998). Runaway ornament diversity caused by Fisherian sexual selection. *PNAS* **95**, 5106–5111.

Prieto-Márquez, A., Garcia-Porta, J., Joshi, S.H., Norell, M.A. & Makovicky, P.J. (2020). Modularity and heterochrony in the evolution of the ceratopsian dinosaur frill. *Ecol. Evol.* [doi: 10.1002/ece3.6361].

Prinzinger, R., Preßmar, A. & Schleucher, E. (1991). Body temperature in birds. *Comp. Biochem. Phys. A* **99**, 499–506.

Pycraft, W.P. (1900). On the morphology and phylogeny of the palæognathæ (ratitæ and crypturi) and neognathæ (carinatæ). *Trans. Zool. Soc. London* **15**, 149–290.

R Core Team (2020). R: A language and environment for statistical computing. Vienna: R Foundation for Statistical Computing.

Raikow, R.J. (1969). Sexual and agonistic behavior of the Common Rhea. *Wilson Bull.* 196–206.

Richardson, K.C. (1991). The bony casque of the Southern Cassowary *Casuarius*. *Emu* **91**, 56–58.

Ripley, B. (2013): R package MASS. http://www.cran.r-project.org/package=MASS

Romagnano, A., Hood, R.G., Snedeker, S. & Martin, S.G. (2012). Cassowary pediatrics. *Vet. Clin. Exot. Anim.* **15**, 215–231.

Rosen, R.F. & Tarvin, K.A. (2006). Sexual signals of the male American goldfinch. *Ethology* **112**, 1008–1019.

Rothschild, W. (1900). A monograph of the genus *Casuarius*. *Trans. Zool. Soc. London* **15**, 109–148.

Ruiz-Rodríguez, M., Martín-Vivaldi, M. & Avilés, J.M. (2017). Multi-functional crest display in hoopoes *Upupa epops*. *J. Avian Biol.* **48**, 1425–1431.

Russell, E.S. (1916). *Form and function*. John Murray, London.

Schott, R K., Evans, D.C., Goodwin, M.B., Horner, J.R., Brown, C.M. & Longrich, N.R. (2011). Cranial ontogeny in *Stegoceras validum* (Dinosauria: Pachycephalosauria): a quantitative model of pachycephalosaur dome growth and variation. *PLoS One* **6**, e21092.

Smith, R.J. (2009). Use and misuse of reduced major axis for line-fitting. *Am. J. Phys. Anthropol.* **140**, 476–486.

Smith-Paredes, D., Núñez-León, D., Soto-Acuña, S., O'Connor, J., Botelho, J.F. & Vargas, A.O. (2018). Dinosaur ossification centres in embryonic birds uncover developmental evolution of the skull. *Nat. Ecol. Evol.* **2**, 1966–1973.

Snively, E. & Theodor, J.M. (2011). Common functional correlates of head-strike behavior in the pachycephalosaur *Stegoceras validum* (Ornithischia, Dinosauria) and combative artiodactyls. *PLoS One* **6**, e21422.

Stankowich, T. (2012). Armed and dangerous: predicting the presence and function of defensive weaponry in mammals. *Adapt. Behav.* **20**, 32–43.

Starck, J.M. (1995). Comparative anatomy of the external and middle ear of palaeognathous birds. *Adv. Anat. Embryol. Cell Biol.* **131**, 1–137.

Starck, J.M. & Sutter, E. (2000). Patterns of growth and heterochrony in moundbuilders (Megapodiidae) and fowl (Phasianidae). *J. Avian Biol.* **31**, 527–547.

Stocker, G.C. & Irvine, A.K. (1983). Seed dispersal by cassowaries (*Casuarius casuarius*) in North Queensland's rainforests. *Biotropica* 170–176.

Strauss, W.M., Hetem, R.S., Mitchell, D., Maloney, S.K., O'Brien, H.D., Meyer, L.C. & Fuller, A. (2017). Body water conservation through selective brain cooling by the

carotid rete: a physiological feature for surviving climate change? *Conserv. Physiol.* **5**, [https://doi.org/10.1093/conphys/cow078].

Warton, D., Duursma, R., Falster, D., Taskinen, S. & Duursma, M.R. (2018). Package 'smatr'. Online at https://cran. r-project.org/web/packages/smatr/smatr.pdf.

Watanabe, A., Gignac, P.M., Balanoff, A.M., Green, T.L., Kley, N.J. & Norell, M.A. (2019). Are endocasts good proxies for brain size and shape in archosaurs throughout ontogeny? *J. Anat*. **234**, 291–305.

Webber, B.L. & Woodrow, I.E. (2004). Cassowary frugivory, seed defleshing and fruit fly infestation influence the transition from seed to seedling in the rare Australian rainforest tree, *Ryparosa* sp. nov. 1 (Achariaceae). *Funct. Plant Biol.* **31**, 505–516.

Weishampel, D. B. (1981). Acoustic analyses of potential vocalization in lambeosaurine dinosaurs (Reptilia: Ornithischia). *Paleobiology* 252–261.

Widnyana, I.G.N.P., Sundu, B. & Tanari, M. (2019). Sex detection in maleo bird (*Macrocephalon maleo* Sal Muller 1846) nurtured in ex-situ conservation through body morphological and hormonal studies. *Int. J. Vet. Sci. Agric. Res.* **1**, 17–22.

Wiemann, J., Yang, T.R. & Norell, M.A. (2018). Dinosaur egg colour had a single evolutionary origin. *Nature* **563**, 555–558.

Wildlife Conservation Society (2016). Maleo, *Macrocephalon maleo*, Husbandry and Conservation at the Wildlife Conservation Society.

Witmer, L.M. (1990). The craniofacial air sac system of Mesozoic birds (Aves). *Zool. J. Linn. Soc.* **100**, 327–378.

Yurick, D.B. & Gaskin, D.E. (1988). Asymmetry in the skull of the harbour porpoise *Phocoena phocoena* (L.) and its relationship to sound production and echolocation. *Can. J. Zool.* **66**, 399–402.

Zusi, R.L. (1993). Patterns of diversity in the avian skull. In *The skull. Vol 2: patterns of structural and systematic diversity*: 391–437. Hanken, J. & Hall, B.K., (Eds.). Illinois: University of Chicago Press.

APPENDICES

Appendix A. The following Microsoft Excel tables include specimen and μCT parameter data for Chapter II.

Species	Institution Code	Specimen #	Sex	Relative Age	Pre-Hatching Age (years)	Post-Hatching Age (years)	# of Casque Compenents (0-8)
Casuarius casuarius	TLG (CCP)	C047	U	embryonic (~HH32)	~0.055	—	0
Casuarius casuarius	TLG (CCP)	C032	U	embryonic (~HH40)	~0.104	—	0
Casuarius casuarius	TLG (CCP)	C030	F	embryonic (~HH41)	~0.110	—	0
Casuarius casuarius	OUVC	11592	U	embryonic (~HH43)	~0.118	—	0
Casuarius casuarius	TLG (CCP)	C018	U	embryonic (~HH43)	~0.121	—	0
Casuarius casuarius	OUVC	10520	U	embryonic (~HH45)	~0.126	—	0
Casuarius casuarius	TLG (CCP)	C007	U	immature (1 day)	—	0.003	0
Casuarius casuarius	TLG (CCP)	C010	U	immature (1 day)	—	0.003	0
Casuarius casuarius	TLG (CCP)	C025	U	immature (7 days)	—	0.019	0
Casuarius casuarius	TLG (CCP)	C024	U	immature (9 days)	—	0.025	0
Casuarius casuarius	TLG (CCP)	C011	U	immature (24 days)	—	0.066	0
Casuarius casuarius	TLG (CCP)	C043	M	immature (42 days)	—	0.115	0
Casuarius casuarius	TLG (CCP)	C037	M	immature (1.5 months)	—	0.129	4
Casuarius casuarius	TLG (CCP)	C021	F	immature (5.2 months)	—	0.432	6
Casuarius casuarius	TLG	C002	U	immature (~5.5 months)	—	~0.460	6
Casuarius casuarius	TLG (CCP)	C004	F	immature (10.4 months)	—	0.868	8
Casuarius casuarius	TLG (CCP)	C031	M	immature (14.0 months)	—	1.164	8
Casuarius casuarius	AMNH	SKEL 963	U	immature (~24.0 months)	—	~2.000	8
Casuarius casuarius	AMNH	SKEL 962	U	adult (~4.0–5.0 years)	—	~4.000–5.000	8
Casuarius casuarius	TLG	C001	U	adult (~5.0–20.0 years)	—	~5.000–20.000	8
Casuarius casuarius	TLG (SCZ)	C022 (12126)	M	adult (21.4 years)	—	21.353	8
Casuarius casuarius	DMNS	ZB.50012	M	adult (22.1 years)	—	22.088	8
Casuarius casuarius	MOO	8031	F	adult (35.7 years)	—	35.666	8

Appendix A. cont… *CT Specimen Sample*

Species	Institution Code	Specimen #	Specimen Type	Sex	Relative Age	kV	µA	Voxel Size (µm)	Exposure Timing (ms)	Target Material	Filter Type	Filter Thickness (mm)	Scanner Facility
Casuarius casuarius	TLG (CCP)	C047	fixed in formalin	U	embryonic (~HH32)	182	55	13.29	267	W	None	N/A	Dentsply
Casuarius casuarius	TLG (CCP)	C032	fixed in formalin	U	embryonic (~HH40)	120	333	35.67	267	W	Cu	0.125	Dentsply
Casuarius casuarius	TLG (CCP)	C030	fixed in formalin	F	embryonic (~HH41)	120	333	36.63	267	W	Cu	0.125	Dentsply
Casuarius casuarius	OUVC	11592	skeleton	U	embryonic (~HH43)	120	32000	24.70	63	W	Al	4.000	OUµCT
Casuarius casuarius	TLG (CCP)	C018	frozen	U	embryonic (~HH43)	179	101	64.45	708	W	None	N/A	MICRO
Casuarius casuarius	OUVC	10520	skeleton	U	embryonic (~HH45)	120	32000	24.70	63	W	Al	4.000	OUµCT
Casuarius casuarius	TLG (CCP)	C007	skeleton	U	immature (1 day)	90	110	74.93	200	W	Cu	0.100	AMNH
Casuarius casuarius	TLG (CCP)	C010	fixed in formalin	U	immature (1 day)	110	110	105.58	200	W	Cu	0.100	AMNH
Casuarius casuarius	TLG (CCP)	C025	frozen	U	immature (7 days)	160	57	53.77	508	W	None	N/A	Dentsply
Casuarius casuarius	TLG (CCP)	C024	frozen	U	immature (9 days)	160	57	41.97	508	W	None	N/A	Dentsply
Casuarius casuarius	TLG (CCP)	C011	fixed in formalin	U	immature (24 days)	140	120	99.96	200	W	Cu	0.100	AMNH
Casuarius casuarius	TLG (CCP)	C043	frozen	M	immature (42 days)	198	200	39.89	267	W	Cu	0.125	MICRO
Casuarius casuarius	TLG (CCP)	C037	frozen	M	immature (1.5 months)	150	90	52.67	500	W	None	N/A	MICRO
Casuarius casuarius	TLG (CCP)	C021	fixed in formalin	F	immature (5.2 months)	150	200	75.75	333	W	Cu	0.100	AMNH
Casuarius casuarius	TLG	C002	skeleton	U	immature (~5.5 months)	80	60	81.23	200	W	Cu	0.100	AMNH
Casuarius casuarius	TLG (CCP)	C004	fixed in formalin	F	immature (10.4 months)	130	180	105.89	400	W	Cu	0.100	AMNH
Casuarius casuarius	TLG (CCP)	C031	frozen	M	immature (14.0 months)	175	200	114.36	267	W	None	N/A	MICRO
Casuarius casuarius	AMNH	SKEL 963	skeleton	U	immature (~24.0 months)	140	130	93.42	200	W	None	N/A	AMNH
Casuarius casuarius	AMNH	SKEL 962	skeleton	U	adult (~4.0–5.0 years)	140	130	93.42	200	W	None	N/A	AMNH
Casuarius casuarius	TLG	C001	skeleton	U	adult (~5.0–20.0 years)	60	80	96.90	200	W	Cu	0.100	AMNH
Casuarius casuarius	TLG (SCZ)	C022 (12126)	frozen	M	adult (21.4 years)	196	70	117.67	500	W	None	N/A	MICRO
Casuarius casuarius	DMNS	ZB.50012	dried with skin	M	adult (22.1 years)	190	207	117.97	267	W	None	N/A	MICRO
Casuarius casuarius	MOO	8031	skeleton	F	adult (35.7 years)	120	100	87.85	200	W	None	N/A	AMNH
Dromaius novaehollandiae	TLG (VVE)	E139	fixed in ethanol	U	embryonic (~HH40)	185	53	36.09	354	W	None	N/A	Dentsply
Dromaius novaehollandiae	TLG (VVE)	E137	fixed in ethanol	U	embryonic (~HH43)	185	53	44.25	354	W	None	N/A	Dentsply
Dromaius novaehollandiae	TLG (DAER)	E086	fixed in ethanol	U	embryonic (~HH45)	185	53	44.25	354	W	None	N/A	Dentsply
Dromaius novaehollandiae	TLG (RCER)	E006	skeleton	U	immature (4 days)	110	170	72.16	200	W	None	N/A	AMNH
Dromaius novaehollandiae	TLG (DAER)	E093	frozen	U	immature (5 days)	125	290	36.53	267	W	None	N/A	MICRO
Dromaius novaehollandiae	TLG (SME)	E074	frozen	U	immature (~14 days)	190	73	74.73	267	W	None	N/A	MICRO
Dromaius novaehollandiae	TLG (DAER)	E098	frozen	U	immature (30 days)	124	333	59.39	267	W	None	N/A	MICRO
Dromaius novaehollandiae	TLG (RCER)	E056	skeleton	U	immature (~3.0 months)	100	120	60.92	200	W	Cu	0.100	AMNH
Dromaius novaehollandiae	TLG (DAER)	E115	frozen	U	immature (12.0 months)	176	333	97.16	267	W	None	N/A	MICRO
Dromaius novaehollandiae	TLG (SME)	E077	frozen	U	adult (≥ 3.0 years)	160	57	120.37	508	W	None	N/A	MICRO
Dromaius novaehollandiae	TLG (SME)	E078	frozen	U	adult (≥ 3.0 years)	160	57	103.21	508	W	None	N/A	Dentsply
Dromaius novaehollandiae	TLG (HLB)	E114	frozen	M	adult (≥ 3.0 years)	170	80	112.83	708	W	None	N/A	MICRO
Dromaius novaehollandiae	TLG (DAER)	E054	skeleton	M	adult (~8.0–10.0 years)	110	170	103.82	200	W	None	N/A	AMNH
Struthio camelus	TLG (LNR)	SC032	frozen	U	immature (1 day)	196	70	112.15	500	W	Cu	0.500	MICRO
Struthio camelus	TLG (LNR)	SC027	frozen	U	immature (2.5 months)	139	101	70.81	354	W	None	N/A	MICRO
Struthio camelus	TLG (LNR)	SC008	frozen	F	immature (14.0 months)	200	69	117.64	708	W	Cu	0.100	MICRO
Struthio camelus	TLG (LNR)	SC015	frozen	M	immature (14.0 months)	160	57	100.18	508	W	Cu	0.125	Dentsply
Struthio camelus	TLG (LNR)	SC030	frozen	U	immature (~11.0 months)	170	81	117.93	500	W	Cu	0.125	MICRO
Struthio camelus	TLG (LNR)	SC063	frozen	M	immature (15.0 months)	165	333	117.51	267	W	Cu	0.125	MICRO
Struthio camelus	TLG (PBZ)	SC080 (26013)	frozen	M	adult (~19.5–21.5 years)	165	300	119.06	267	W	None	N/A	MICRO
Struthio camelus	TLG (CG)	SC004	skeleton	M	adult (≥ 20.0 years)	120	100	90.89	200	W	None	N/A	AMNH

Appendix A. cont… *Additional Specimen Sample*

Species	Institution Code	Specimen #	Specimen Type	Sex	Relative Age
Casuarius casuarius	TLG (CCP)	C046	fixed in formalin	U	embryonic (~HH23)
Casuarius casuarius	TLG (CCP)	C048	fixed in formalin	U	embryonic (~HH28)
Casuarius casuarius	TLG (GPZ)	C035	fixed in formalin	U	embryonic (~HH39)
Casuarius casuarius	TLG (CCP)	C012	skeleton	U	embryonic (~HH42)
Casuarius casuarius	TLG (CCP)	C005	frozen	U	embryonic (~HH43)
Casuarius casuarius	TLG (CCP)	C028	frozen	U	embryonic (~HH45)
Casuarius casuarius	TLG (CCP)	C009	skeleton	U	immature (1 day)
Casuarius casuarius	TLG (CCP)	C014	skeleton	M	immature (1 day)
Casuarius casuarius	TLG (CCP)	C045	frozen	U	immature (7 days)
Casuarius casuarius	TLG (CCP)	C036	frozen	U	immature (12 days)
Casuarius casuarius	TLG (CCP)	C041	frozen	U	immature (21 days)
Casuarius casuarius	NHMUK	1899.11.10.3	skeleton	U	immature (~5.0–7.0 months)
Casuarius casuarius	NHMUK	S/1972.1.11	skeleton	U	immature (~8.0–11.0 months)
Casuarius casuarius	NHMUK	1899.11.10.1	skeleton	U	immature (~10.0–12.0 months)
Casuarius casuarius	AMNH	SKEL 1106	skeleton	U	immature (~24.0–36.0 months)
Casuarius casuarius	AMNH	SKEL 3200	skeleton	U	immature (~24.0–36.0 months)
Casuarius casuarius	AMNH	SKEL 1517	skeleton	U	adult (≥ 4.0 years)
Casuarius casuarius	AMNH	SKEL 1695	skeleton	U	adult (≥ 4.0 years)
Casuarius casuarius	AMNH	SKEL 1717	skeleton	U	adult (≥ 4.0 years)
Casuarius casuarius	AMNH	SKEL 3870	skeleton	U	adult (≥ 4.0 years)
Casuarius casuarius	AMNH	SKEL 14823	skeleton	U	adult (≥ 4.0 years)
Casuarius casuarius	MV	B13452	skeleton	F	adult (≥ 4.0 years)
Casuarius casuarius	QM	O.31137	skeleton	U	adult (≥ 4.0 years)
Casuarius casuarius	AMNH	SKEL 1519	skeleton	U	adult (≥ 4.0 years)
Casuarius casuarius	NHMUK	1939.12.9.1052	skeleton	U	adult (≥ 4.0 years)
Casuarius casuarius	NHMUK	1972.1.12	skeleton	U	adult (≥ 4.0 years)
Casuarius casuarius	NHMUK	S/2010.1.20	skeleton	U	adult (≥ 4.0 years)
Casuarius casuarius	MV	B12907	skeleton	F	adult (≥ 4.0 years)
Casuarius casuarius	QM	O.30105	skeleton	U	adult (≥ 4.0 years)
Casuarius casuarius	QM	O.30604	skeleton	U	adult (≥ 4.0 years)
Casuarius casuarius	QM	O.31352	skeleton	F	adult (≥ 4.0 years)
Dromaius novaehollandiae	TLG (DAER)	E088	fixed in ethanol	U	embryonic (~HH43)
Dromaius novaehollandiae	TLG (DAER)	E085	fixed in ethanol	U	embryonic (~HH45)
Dromaius novaehollandiae	TLG (WEL)	E057	skeleton	F	adult (~4.0–5.0 years)
Dromaius novaehollandiae	TLG (RCER)	E053	skeleton	F	adult (≥ 20.0 years)
Dromaius novaehollandiae	TLG (RCER)	E083	skeleton	M	adult (≥ 20.0 years)
Dromaius novaehollandiae	TLG (PBZ)	E140 (900104)	skeleton	M	adult (30.5 years)
Struthio camelus	TLG (LNR)	SC033	fixed in formalin	U	embryonic (~HH36)
Struthio camelus	TLG (LNR)	SC040	frozen	U	immature (2 days)
Struthio camelus	TLG (LNR)	SC043	frozen	U	immature (2.0 months)
Struthio camelus	TLG (LNR)	SC081	frozen	M	immature (2.7 months)
Struthio camelus	TLG (KSM)	SC059	frozen	F	immature (~18.0–24.0 months)

Appendix B. The following R code was used from Chapter III analyses.

```
#####################################################################
#Ch III Ontogenetic allometry and functional implications of the#
####################southern cassowary casque#####################
###################(c) 2020 Todd L. Green##########################
#####################written in R 3.4.3############################
#####################################################################


############Directory setting and package loading#################


#find current working directory
getwd()
#set working directory
setwd('YOUR FOLDER LOCATION')
#list the files in the current working directory
list.files(getwd())
#Load packages used throughout script
#smatr package
library(smatr)
#package for D'Agostino K-squared test and kurtosis
#quantification
library(moments)
#Package for outlier testing
library(outliers)
##Package containing Shapiro-Wilks and Breusch-Pagal test
library(lmtest)
#package for power analysis
library(pwr)
#lmodel2 package
library(lmodel2)
```

```
#####################################################################
##################Bony Casques Data Inspection#####################
#####################################################################

#read in data
bcass_dat<-read.csv('Bony_Casques_ALL_SPECIMENS.csv',header=T)
head(bcass_dat)

#########Individual Measurements for Skewness & Kurtosis#########

#Measurement of skewness and kurtosis
agostino.test(bcass_dat$Log_Casque_Height_mm)
kurtosis(bcass_dat$Log_Casque_Height_mm,na.rm=T)
agostino.test(bcass_dat$Log_Casque_Length_mm)
kurtosis(bcass_dat$Log_Casque_Length_mm,na.rm=T)
agostino.test(bcass_dat$Log_Skull_Length_mm)
kurtosis(bcass_dat$Log_Skull_Length_mm,na.rm=T)
agostino.test(bcass_dat$Log_Skull_Width_mm)
kurtosis(bcass_dat$Log_Skull_Width_mm,na.rm=T)

########################Outlier Testing############################

#outlier testing (box plots)(ALL INDIVIDUAL MEASUREMENTS)
boxplot(bcass_dat$Log_Casque_Height_mm)
chisq.out.test(bcass_dat$Log_Casque_Height_mm,
variance=var(bcass_dat$Log_Casque_Height_mm,na.rm=T), opposite=F)
boxplot(bcass_dat$Log_Casque_Length_mm)
chisq.out.test(bcass_dat$Log_Casque_Length_mm,
variance=var(bcass_dat$Log_Casque_Length_mm,na.rm=T), opposite=F)
boxplot(bcass_dat$Log_Skull_Length_mm)
chisq.out.test(bcass_dat$Log_Skull_Length_mm,
variance=var(bcass_dat$Log_Skull_Length_mm,na.rm=T), opposite=F)
boxplot(bcass_dat$Log_Skull_Width_mm)
chisq.out.test(bcass_dat$Log_Skull_Width_mm,
variance=var(bcass_dat$Log_Skull_Width_mm,na.rm=T), opposite=F)
```

```
#################Normality: Shapiro-Wilks Tests##################

##Shapiro-Wilks test (ALL INDIVIDUAL MEASUREMENTS)
shapiro.test(bcass_dat$Log_Casque_Height_mm)
shapiro.test(bcass_dat$Log_Casque_Length_mm)
shapiro.test(bcass_dat$Log_Skull_Length_mm)
shapiro.test(bcass_dat$Log_Skull_Width_mm)

############Log Casque Height vs. Log Skull Length###############

#OLS model
cH_v_sL<-
sma(Log_Casque_Height_mm~Log_Skull_Length_mm,data=bcass_dat,metho
d=c('OLS'))
cH_v_sL
plot(cH_v_sL)

#####################################################################

#Linearity test (residuals plot)
plot(cH_v_sL,which='residual')

#####################################################################

#normality testing
##Q-Q plot
plot(cH_v_sL,which='qq')

#####################################################################

#heteroscedasticity testing (Breusch-Pagan test)
plot(cH_v_sL,which='residual')
bptest(bcass_dat$Log_Casque_Height_mm~bcass_dat$Log_Skull_Length_
mm)
```

```
#####################################################################

#statistical power analysis
#u(degrees of freedom), v(sample size), f2(effect size)
#significance level set to 0.01
#f2=R^2/(1-R^2)=effect size
#power function for general linear models
pwr.f2.test(u= 1, v=21, f2=(0.7764123/(1-
0.7764123)),sig.level=0.01)

#############Log Casque Height vs. Log Skull Width###############

#OLS model
cH_v_sW<-
sma(Log_Casque_Height_mm~Log_Skull_Width_mm,data=bcass_dat,method
=c('OLS'))
cH_v_sW
plot(cH_v_sW)

#####################################################################

#Linearity test (residuals plot)
plot(cH_v_sW,which='residual')

#####################################################################

#normality testing
##Q-Q plot
plot(cH_v_sW,which='qq')

#####################################################################

#heteroscedasticity testing (Breusch-Pagan test)
plot(cH_v_sW,which='residual')
bptest(bcass_dat$Log_Casque_Height_mm~bcass_dat$Log_Skull_Width_m
m)
```

```
#####################################################################

#statistical power analysis
#u(degrees of freedom), v(sample size), f2(effect size)
#significance level
#f2=R^2/(1-R^2)=effect size
#power function for
pwr.f2.test(u= 1, v=22, f2=(0.7316602/(1-
0.7316602)),sig.level=0.01)

############Log Casque Length vs. Log Skull Length##############

#OLS model
cL_v_sL<-
sma(Log_Casque_Length_mm~Log_Skull_Length_mm,data=bcass_dat,metho
d=c('OLS'))
cL_v_sL
plot(cL_v_sL)

#####################################################################

#Linearity test (residuals plot)
plot(cL_v_sL,which='residual')

#####################################################################

#normality testing
##Q-Q plot
plot(cL_v_sL,which='qq')

#####################################################################

#heteroscedasticity testing (Breusch-Pagan test)
plot(cL_v_sL,which='residual')
```

```
bptest(bcass_dat$Log_Casque_Length_mm~bcass_dat$Log_Skull_Length_
mm)

#####################################################################

#statistical power analysis

#u(degrees of freedom), v(sample size), f2(effect size)

#significance level

#f2=R^2/(1-R^2)=effect size

#power function for

pwr.f2.test(u= 1, v=25, f2=(0.9257049/(1-
0.9257049)),sig.level=0.01)



#############Log Casque Length vs. Log Skull Width###############


#OLS model

cL_v_sW<-
sma(Log_Casque_Length_mm~Log_Skull_Width_mm,data=bcass_dat,method
=c('OLS'))

cL_v_sW

plot(cL_v_sW)


#####################################################################


#Linearity test (residuals plot)

plot(cL_v_sW,which='residual')


#####################################################################


#normality testing

##Q-Q plot

plot(cL_v_sW,which='qq')


#####################################################################
```

```
#heteroscedasticity testing (Breusch-Pagan test)
plot(cL_v_sW,which='residual')
bptest(bcass_dat$Log_Casque_Length_mm~bcass_dat$Log_Skull_Width_m
m)

#####################################################################

#statistical power
#u(degrees of freedom), v(sample size), f2(effect size)
#significance level
#f2=R^2/(1-R^2)=effect size
#power function for
pwr.f2.test(u= 1, v=25, f2=(0.9141979/(1-
0.9141979)),sig.level=0.01)



#####################################################################
##############Keratin Casques Data Inspection#####################
#####################################################################

#read in data
kcass_dat<-
read.csv('Keratinized_Casques_ALL_SPECIMENS.csv',header=T)
head(kcass_dat)

#########Individual Measurements for Skewness & Kurtosis#########

#skewness and kurtosis
agostino.test(kcass_dat$Log_Casque_Height_mm,na.rm=T)
kurtosis(kcass_dat$Log_Casque_Height_mm,na.rm=T)
agostino.test(kcass_dat$Log_Casque_Length_mm,na.rm=T)
kurtosis(kcass_dat$Log_Casque_Length_mm,na.rm=T)
agostino.test(kcass_dat$Log_Head_Length_mm,na.rm=T)
kurtosis(kcass_dat$Log_Head_Length_mm,na.rm=T)
agostino.test(kcass_dat$Log_Head_Width_mm,na.rm=T)
kurtosis(kcass_dat$Log_Head_Width_mm,na.rm=T)
```

```
#########################Outlier Testing#########################

#outlier testing (box plots)(ALL INDIVIDUAL MEASUREMENTS)
boxplot(kcass_dat$Log_Casque_Height_mm)
chisq.out.test(kcass_dat$Log_Casque_Height_mm,
variance=var(kcass_dat$Log_Casque_Height_mm,na.rm=T), opposite=F)
boxplot(kcass_dat$Log_Casque_Length_mm)
chisq.out.test(kcass_dat$Log_Casque_Length_mm,
variance=var(kcass_dat$Log_Casque_Length_mm,na.rm=T), opposite=F)
boxplot(kcass_dat$Log_Head_Length_mm)
chisq.out.test(kcass_dat$Log_Head_Length_mm,
variance=var(kcass_dat$Log_Head_Length_mm,na.rm=T), opposite=F)
boxplot(kcass_dat$Log_Head_Width_mm)
chisq.out.test(kcass_dat$Log_Head_Width_mm,
variance=var(kcass_dat$Log_Head_Width_mm,na.rm=T), opposite=F)

##################Normality: Shapiro-Wilks Tests#################

##Shapiro-Wilks test (ALL INDIVIDUAL MEASUREMENTS)
shapiro.test(kcass_dat$Log_Casque_Height_mm)
shapiro.test(kcass_dat$Log_Casque_Length_mm)
shapiro.test(kcass_dat$Log_Head_Length_mm)
shapiro.test(kcass_dat$Log_Head_Width_mm)

############Log Casque Height vs. Log Head Length################

#OLS model
cH_v_hL<-
sma(Log_Casque_Height_mm~Log_Head_Length_mm,data=kcass_dat,method
=c('OLS'))
cH_v_hL
plot(cH_v_hL)

################################################################
```

```
#Linearity test (residuals plot)
plot(cH_v_hL,which='residual')

#####################################################################

#normality testing
##Q-Q plot
plot(cH_v_hL,which='qq')

#####################################################################

#heteroscedasticity testing (Breusch-Pagan test)
plot(cH_v_hL,which='residual')
bptest(kcass_dat$Log_Casque_Height_mm~kcass_dat$Log_Head_Length_m
m)

#####################################################################

#statistical power
#u(degrees of freedom), v(sample size), f2(effect size)
#significance level
#f2=R^2/(1-R^2)=effect size
#power function for
pwr.f2.test(u= 1, v=47, f2=(0.819653/(1-
0.819653)),sig.level=0.01)

############Log Casque Height vs. Log Head Width################

#OLS model
cH_v_hW<-
sma(Log_Casque_Height_mm~Log_Head_Width_mm,data=kcass_dat,method=
c('OLS'))
cH_v_hW
plot(cH_v_hW)
```

```
#####################################################################

#Linearity test (residuals plot)
plot(cH_v_hW,which='residual')

#####################################################################

#normality testing
##Q-Q plot
plot(cH_v_hW,which='qq')

#####################################################################

#heteroscedasticity testing (Breusch-Pagan test)
plot(cH_v_hW,which='residual')
bptest(kcass_dat$Log_Casque_Height_mm~kcass_dat$Log_Head_Width_mm
)

#####################################################################

#statistical power
#u(degrees of freedom), v(sample size), f2(effect size)
#significance level
#f2=R^2/(1-R^2)=effect size
#power function for
pwr.f2.test(u= 1, v=49, f2=(0.7104859/(1-
0.7104859)),sig.level=0.01)

##############Log Casque Length vs. Log Head Length##############

#OLS model
cL_v_hL<-
sma(Log_Casque_Length_mm~Log_Head_Length_mm,data=kcass_dat,method
=c('OLS'))
cL_v_hL
plot(cL_v_hL)
```

```
#####################################################################

#Linearity test (residuals plot)
plot(cL_v_hL,which='residual')

#####################################################################

#normality testing
##Q-Q plot
plot(cL_v_hL,which='qq')

#####################################################################

#heteroscedasticity testing (Breusch-Pagan test)
plot(cL_v_hL,which='residual')
bptest(kcass_dat$Log_Casque_Length_mm~kcass_dat$Log_Head_Length_m
m)

#####################################################################

#statistical power
#u(degrees of freedom), v(sample size), f2(effect size)
#significance level
#f2=R^2/(1-R^2)=effect size
#power function for
pwr.f2.test(u= 1, v=49, f2=(0.915323/(1-
0.915323)),sig.level=0.01)

############Log Casque Length vs. Log Head Width################

#OLS model
cL_v_hW<-
sma(Log_Casque_Length_mm~Log_Head_Width_mm,data=kcass_dat,method=
c('OLS'))
cL_v_hW
```

```
plot(cL_v_hW)

#####################################################################

#Linearity test (residuals plot)
plot(cL_v_hW,which='residual')

#####################################################################

#normality testing
##Q-Q plot
plot(cL_v_hW,which='qq')

#####################################################################

#heteroscedasticity testing (Breusch-Pagan test)
plot(cL_v_hW,which='residual')
bptest(kcass_dat$Log_Casque_Length_mm~kcass_dat$Log_Head_Width_mm
)

#####################################################################

#statistical power
#u(degrees of freedom), v(sample size), f2(effect size)
#significance level
#f2=R^2/(1-R^2)=effect size
#power function for
pwr.f2.test(u= 1, v=52, f2=(0.8553816/(1-
0.8553816)),sig.level=0.01)



#####################################################################
#####ANCOVAs of male and female linear cranial measurements######
#####################################################################
```

```
#######Keratin_Log_Casque_Height_vs_Log_Head_Length_#############


#read in data

cass_KCHvHL<-
read.csv('ANCOVA_NO_OUTLIERS_KERAT_CSQ_HT_vs_HD_LH_SEX.csv',
header=T)

head(cass_KCHvHL)

modelKCHvHL<-aov(Log_Casque_Height_mm~Log_Head_Length_mm + Sex,
data=cass_KCHvHL)

summary(modelKCHvHL)

modelKCHvHL


##########Keratin_Log_Casque_Length_vs_Log_Head_Length###########


#read in data

cass_KCLvHL<-
read.csv('ANCOVA_NO_OUTLIERS_KERAT_CSQ_LH_vs_HD_LH_SEX.csv',
header=T)

head(cass_KCLvHL)

modelKCLvHL<-aov(Log_Casque_Length_mm~Log_Head_Length_mm + Sex,
data=cass_KCLvHL)

summary(modelKCLvHL)

modelKCLvHL



#################################################################
########ANCOVA of maturity level and cranial measurements########
#################################################################


#read in data

cass_KCHvHL<-
read.csv('ANCOVA_NO_OUTLIERS_KERAT_CSQ_HT_vs_HD_LH_SEX.csv',
header=T)

head(cass_KCHvHL)

model_maturity<-aov(Log_Casque_Height_mm~Log_Head_Length_mm +
Relative_Age, data=cass_KCHvHL)

summary(model_maturity)

model_maturity
```

```
#####################################################################
###############Bony Casques OLS Regressions#######################
#####################################################################

#################Casque_Height_vs_Skull_Length#################


#read in csv file
bcass_dat<-read.csv('Bony_Casques_ALL_SPECIMENS.csv',header=T)
head(bcass_dat)
modBCHvSL<-
lmodel2(Log_Casque_Height_mm~Log_Skull_Length_mm,data=bcass_dat,
nperm=99)
modBCHvSL
plot(modBCHvSL, method='OLS', pch=16, cex=1.5, main="", xlab="Log
Skull Length (mm)", ylab="Log Casque Height (mm)", font=2)


##isometry line, used as reference in all the OLS plots
iso_x<-c(0,1)
iso_y<-iso_x-1
iso_mod<-lm(iso_y~iso_x)
abline(iso_mod)



#################Casque_Height_vs_Skull_Width#################


modBCHvSW<-
lmodel2(Log_Casque_Height_mm~Log_Skull_Width_mm,data=bcass_dat,np
erm=99)
modBCHvSW
plot(modBCHvSW, method='OLS', pch=16, cex=1.5, main="", xlab="Log
Skull Width (mm)", ylab="Log Casque Height (mm)", font=2)


abline(iso_mod)
```

```
##################Casque_Length_vs_Skull_Length##################


bcass_dat

modBCLvSL<-
lmodel2(Log_Casque_Length_mm~Log_Skull_Length_mm,data=bcass_dat,n
perm=99)

modBCLvSL

plot(modBCLvSL, method='OLS', pch=16, cex=1.5, main="", xlab="Log
Skull Length (mm)", ylab="Log Casque Length (mm)", font=2)


abline(iso_mod)



##################Casque_Length_vs_Skull_Width###################


bcass_dat

modBCLvSW<-
lmodel2(Log_Casque_Length_mm~Log_Skull_Width_mm,data=bcass_dat,np
erm=99)

modBCLvSW

plot(modBCLvSW, method='OLS', pch=16, cex=1.5, main="", xlab="Log
Skull Width (mm)", ylab="Log Casque Length (mm)", font=2)


abline(iso_mod)



#################################################################
##############Keratin Casques OLS Regressions####################
#################################################################


##################Casque_Height_vs_Head_Length###################


#read in csv file

kcass_dat<-
read.csv('Keratinized_Casques_ALL_SPECIMENS.csv',header=T)

head(kcass_dat)
```

```
modCHvHL<-
lmodel2(Log_Casque_Height_mm~Log_Head_Length_mm,data=kcass_dat,np
erm=99)

modCHvHL

plot(modCHvHL, method='OLS', pch=16, cex=1.5, main="", xlab="Log
Head Length (mm)", ylab="Log Casque Height (mm)", font=2)


abline(iso_mod)



###################Casque_Height_vs_Head_Width###################


modCHvHW<-
lmodel2(Log_Casque_Height_mm~Log_Head_Width_mm,data=kcass_dat,npe
rm=99)

modCHvHW

plot(modCHvHW, method='OLS', pch=16, cex=1.5, main="", xlab="Log
Head Width (mm)", ylab="Log Casque Height (mm)", font=2)


abline(iso_mod)



###################Casque_Length_vs_Head_Length#################


modCLvHL<-
lmodel2(Log_Casque_Length_mm~Log_Head_Length_mm,data=kcass_dat,np
erm=99)

modCLvHL

plot(modCLvHL, method='OLS', pch=16, cex=1.5, main="", xlab="Log
Head Length (mm)", ylab="Log Casque Length (mm)", font=2)


abline(iso_mod)



###################Casque_Length_vs_Head_Width###################
```

```
modCLvHW<-
lmodel2(Log_Casque_Length_mm~Log_Head_Width_mm,data=kcass_dat,npe
rm=99)

modCLvHW

plot(modCLvHW, method='OLS', pch=16, cex=1.5, main="", xlab="Log
Head Width (mm)", ylab="Log Casque Length (mm)", font=2)


abline(iso_mod)
```

Appendix C. The following R code was used from Chapter IV analyses.

```
#####################################################################
#####Ch IV Adult casque disparity in the genus Casuarius and#####
##################implications for visual display#################
##############(c)2020 Todd L. Green & David Ian Kay##############
######################written in R3.6.3############################
#####################################################################

############################PACKAGES#################################

##read in Momocs, a morphometrics package. we are using v1.3.0
library(Momocs)
#read in tibble to coerce dataframes to tibble type for momocs
library(tibble)
#read in ggplot2 for plots not associated with Momocs functions
library(ggplot2)
#packages necessary for the PCO and non-Momocs LDA analyses
library(MASS)
library(vegan)

#####################################################################
#####################################################################
###################RIGHT/LEFT SPECIFICITY ANALYSIS###################
#####################################################################
#####################################################################

######################Workspace save/load############################

#save workspace
save.image("cass_test.RData")
#load workspace
load("cass_test.RData")

##############Data read-in and outline creation#################
```

```
#Set working directory to the folder of the binary mask images
getwd()
setwd("cass_test")
#list all files in current folder to double check the folder
#contents
list.files(getwd())
#read in the factors list to categorize specimens
cass_info<-as_tibble(read.csv("test_info.csv", header=T,
row.names=1))
#create an object containing the filesnames to reference them for
#import
lf <- list.files(getwd(), full.names=TRUE)
#import the binary mask jpegs using the file list
cass_test<-import_jpg(lf)
#convert them to outline, simultaneously adding factors to the
#objects
cass_outline<-Out(cass_test, fac=cass_info)
#plot all of them to make sure they appear correct, you can color
#them by variables with the fac input
panel(cass_outline, fac='side', name=T)
panel(cass_outline, fac='side')
#mosaic function allows for a legend
mosaic(cass_outline,'side',legend=T)

######################Procustes alignment#######################
#in order to be able to run a Procrustes alignment the outlines
must
#have the same number of points. Check the number of average
#points
#and interpolate all outlines to that average
cass_outline
#interpolating to average number of points
cass_outline_int<-coo_interpolate(cass_outline,5388)
#plot the outlines on top of each other to observe current
#alignment
stack(cass_outline_int)
#procrustes alignment, this can take as long as ~35 minutes
cass_pro<-fgProcrustes(cass_outline_int)
#stacked plot of aligned outlines
```

```
stack(cass_pro)


##################Elliptical Fourier
transformation##################
#calibrate harmonics needed to capture 99.9% shape variance
cass_test_harm<-calibrate_harmonicpower_efourier(cass_pro,
nb.h=20, plot=T)
##16 captures 99.9%
#altered graph to show more than just 10 harmonics
cass_test_harm$gg+theme_minimal()+
coord_cartesian(xlim=c(0.5,17),ylim=c(0,100))+
ggtitle('Harmonic calibration')
#calibrate the reconstructions
calibrate_reconstructions_efourier(cass_pro,range=1:16)
#elliptical fourier transformation with the number of harmonics
#previously chosen from the calibration
cass_test_e_trans<-efourier(cass_pro,nb.h=16,norm=F)
#need to access harmonics data to then send to the principal
#coordinate analysis
#analysis, which can be done by calling the $coe part of the
#fourier transformed data
cass_test_e_trans$coe
#write the Fourier coefficients to a csv
cass_test_e_trans<-
write.csv(file='cass_test_e_trans.csv',cass_test_e_trans$coe)


##################Principal coordinate analysis##################
#using the capland function in vegan package
#to set up a PCO, the "formula" portion of the function call is
#the data~1
#We chose euclidean distance to construct the dissimilarity
#matrix
cass_pco<-capscale(cass_harm_dat~1,distance="euclidean")
#look at output
summary(cass_pco)
str(cass_pco)
#create an ordination plot,
ordiplot(cass_pco)
```

```
##Setting up pco results for running the MANOVA/LDA
#read in the information matrix in the default dataframe (vegan
#doesn't work well with tibble)
cass_info<-read.csv("test_info.csv",header=T,row.names=1)
#extract the first two principal coordinates (first two site
#scores)
cass_pco_MDS<-scores(cass_pco,display=c('sites'))
#assign the side information to this dataframe
cass_pco_MDS_fac<-cbind(cass_pco_MDS, cass_info)
#colnames(cass_pco_MDS_fac)[3]<-'side'  #line to rename a column,
#we added the whole factor list
cass_pco_MDS_fac
#write it to a csv, double check that everything is correct
write.csv(cass_pco_MDS_fac,file='cass_pco_MDS_fac.csv')

##############################MANOVA################################
cass_pco_MANOVA<-aov(MDS1+MDS2~side,data=cass_pco_MDS_fac)

##############################LDA################################
#Just the "principle coordinates" (first two site scores)
cass_pco_lda<-lda(side ~ MDS1 + MDS2,data=cass_pco_MDS_fac)
#use the predict function to test the LDA, but establish the pco
#data as a DATAFRAME
cass_lda_predict<-
predict(cass_pco_frame_lda,newdata=as.data.frame(cass_pco_MDS))
#check the predicted portion for a % correct
cass_lda_predict$class
#build a cross validation (CV) table
CV.fac<-cass_lda_predict$class
CV.tab<-table(cass_pco_MDS_fac[,3],CV.fac)
names(dimnames(CV.tab))<-c('actual','classified')
CV.correct<-sum(diag(CV.tab))/sum(CV.tab)
tab <- CV.tab
  ce <- sapply(seq_along(1:nrow(tab)),
               function(i) 1-(sum(tab[i, -i])/sum(tab[i, ])))
  names(ce) <- rownames(tab)
#correct classification rate
ce
```

```
#classification table
tab
#site scores capturing 99% variance
#extract first 6 site scores (principal coordinates)
cass_pco_MDS_all<-
scores(cass_pco,choices=c(1:6),display=c('sites'))
#assign the side and sex information to this dataframe
cass_pco_MDS_all_fac<-cbind(cass_pco_MDS_all, cass_info)
#colnames(cass_pco_MDS_all_fac)[7]<-'side'
cass_pco_MDS_all_fac
#write it to a csv, double check that everything is correct
write.csv(cass_pco_MDS_all_fac, file='cass_pco_MDS_all_fac.csv')

################################MANOVA#################################
cass_pco_MANOVA_all<-
aov(MDS1+MDS2+MDS3+MDS4+MDS5+MDS6~side,data=cass_pco_MDS_all_fac)

################################LDA#####################################
#of all 6 site scores
cass_pco_all_lda<-lda(side ~
MDS1+MDS2+MDS3+MDS4+MDS5+MDS6,data=cass_pco_MDS_all_fac)
#use the predict function to test the LDA, but establish the pco
#data as a dataframe
cass_all_lda_predict<-
predict(cass_pco_all_lda,newdata=as.data.frame(cass_pco_MDS_all))
#check the predicted portion for a % correct
cass_all_lda_predict$class
#build a CV table
CV.fac_all<-cass_all_lda_predict$class
CV.tab_all<-table(cass_pco_MDS_all_fac[,7],CV.fac_all)
names(dimnames(CV.tab_all))<-c('actual','classified')
CV.correct_all<-sum(diag(CV.tab_all))/sum(CV.tab_all)
tab_all <- CV.tab_all
  ce_all <- sapply(seq_along(1:nrow(tab_all)),
               function(i) 1-(sum(tab_all[i, -i])/sum(tab_all[i,
]")))
  names(ce_all) <- rownames(tab_all)
#correct classification rate
```

```
ce_all
#classification table
tab_all

#####################################################################
#####################################################################
#######GEOMETRIC MORPHOMETRIC ANALYSIS OF CASQUE OUTLINES########
#####################################################################
#####################################################################

#####################################################################
#########################CC SEX ANALYSIS#############################
#LATERAL ASPECT

######################Workspace save/load##########################

#save workspace
save.image("all_cc_sex_lat.RData")
#load workspace
load("all_cc_sex_lat.RData")

############################Data input#################################
#read in the factors list to categorize specimens using tibble
CC_lat_info<-
as_tibble(read.csv("CC_sexes_lat_fac.csv",header=T,row.names=1))
#Set working directory to the folder containing the binary masks
getwd()
setwd("ALL_CC_SEXES_LAT")
#list files in current folder to double check the folder contents
list.files(getwd())
#create a dataframe containing the filesnames to easily reference
#them
lf<-list.files(getwd(), full.names=TRUE)
#import the binary mask jpegs using the file list
CC_lat_binary<-import_jpg(lf)
#convert to outlines, simultaneously adding factors to the
#objects
CC_lat_out<-Out(CC_lat_binary,fac=CC_lat_info)
```

```
#plot all of them to make sure they appear correct, you can color
#them by variables with the fac input
panel(CC_lat_out, fac='sex', name=TRUE)
panel(CC_lat_out, fac='sex')#red is male
#The mosaic command allows for a legend to be created
mosaic(CC_lat_out,CC_lat_out$sex,legend=TRUE)
#plot the outlines on top of each other
stack(CC_lat_out)

######################Procrustes alignment#########################
#call the Coe object to see the number of points in the outlines
CC_lat_out
#to use the procrustes alignment, the outlines must have the
#same number of coordinates, so interpolate the points to average
#number of points.
CC_lat_out_int<-coo_interpolate(CC_lat_out,n=5034)
#plot out the unaligned
stack(CC_lat_out_int)
#procrustes alignment
CC_lat_pro<-fgProcrustes(CC_lat_out_int)
#examine the alignment
stack(CC_lat_pro)

################Elliptical Fourier Transformation################
#calibrate harmonics needed to capture 99.9% shape variance
cal_CC_lat<-
calibrate_harmonicpower_efourier(CC_lat_pro,nb.h=20,plot=T)
#code to alter the harmonic calibration graph
cal_CC_lat$gg+theme_minimal()+
coord_cartesian(xlim=c(0.5,17),ylim=c(0,100))+
ggtitle('Harmonic calibration')
#calibrate the reconstructions, as a visualization
cal_CC_lat_recon<-
calibrate_reconstructions_efourier(CC_lat_pro,range=1:16)
#EFA with the number of harmonics previously chosen from the
#calibration. I do not normalize the coefficients because of
#possible alignment inconsistencies
CC_lat_ef<-efourier(CC_lat_pro,nb.h=16,norm=F)
```

```
################################PCA#################################
cc_sex_lat_PCA<-PCA(CC_lat_ef,fac='sex')
#plot out the results
plot_PCA(cc_sex_lat_PCA)
svg('cc_sex_lat_PCA_001.svg')
plot_PCA(cc_sex_lat_PCA)
dev.off()
#plot with the shapes
plot_PCA(cc_sex_lat_PCA,'sex')
svg('cc_sex_lat_PCA_002.svg')
plot_PCA(cc_sex_lat_PCA,'sex')
dev.off()
#plot with the shapes filled in
plot_PCA(cc_sex_lat_PCA,'sex',chullfilled=T)
svg('cc_sex_lat_PCA_003.svg')
plot_PCA(cc_sex_lat_PCA,'sex',chullfilled=T)
dev.off()

############################MANOVA#################################
CC_lat_MANOVA<-MANOVA(cc_sex_lat_PCA,fac='sex')
CC_lat_MANOVA
#MANOVA showing the results of the pairwise comparisons
CC_lat_PW_MANOVA<-MANOVA_PW(cc_sex_lat_PCA,fac='sex')
CC_lat_PW_MANOVA

################################LDA#################################
CC_lat_LDA<-LDA(cc_sex_lat_PCA,'sex')
CC_lat_LDA
#create an LDA plot
plot_LDA(CC_lat_LDA,'sex')
#plot CV table
plot_CV(CC_lat_LDA)


#####################################################################
#ANTERIOR/ROSTRAL ASPECT
```

```
######################Workspace save/load#########################

#save workspace
save.image("all_cc_sex_ant.RData")
#load workspace
load("all_cc_sex_ant.RData")

############################Data input#############################
#read in the factors list to categorize specimens using tibble
CC_ant_info<-
as_tibble(read.csv("CC_sexes_ant_fac.csv",header=T,row.names=1))
#Set working directory to the folder containing the binary masks
getwd()
setwd("ALL_CC_SEXES_ANT")
#list files in current folder to double check the folder contents
list.files(getwd())
#create a dataframe containing the filesnames to easily reference
#them
lf<-list.files(getwd(), full.names=TRUE)
#import the binary mask jpegs using the file list
CC_ant_binary<-import_jpg(lf)
#convert to outlines, simultaneously adding factors to the
#objects
CC_ant_out<-Out(CC_ant_binary,fac=CC_ant_info)
#plot all of them to make sure they appear correct, you can color
#them by variables with the fac input



panel(CC_ant_out, fac='sex', name=TRUE)
panel(CC_ant_out, fac='sex')
#The mosaic command allows for a legend to be created
mosaic(CC_ant_out,CC_ant_out$sex,legend=TRUE)
#plot the outlines on top of each other
stack(CC_ant_out)

####################Procrustes alignment#########################
#call the Coe object to see the number of points in the outlines
CC_ant_out
```

```
#to use the procrustes alignment, the outlines must have the
#same number of coordinates, so interpolate the points to average
#number of points.
CC_ant_out_int<-coo_interpolate(CC_ant_out,n=3668)
#plot out the unaligned outlines
stack(CC_ant_out_int)
#procrustes alignment
CC_ant_pro<-fgProcrustes(CC_ant_out_int)
#examine the alignment
stack(CC_ant_pro)

################Elliptical Fourier Transformation################
#calibrate harmonics needed to capture 99.9% shape variance
cal_CC_ant<-
calibrate_harmonicpower_efourier(CC_ant_pro,nb.h=20,plot=T)
#code to alter the harmonic calibration graph
cal_CC_ant$gg+theme_minimal()+
coord_cartesian(xlim=c(0.5,17),ylim=c(0,100))+
ggtitle('Harmonic calibration')
#calibrate the reconstructions, as a visualization
cal_CC_ant_recon<-
calibrate_reconstructions_efourier(CC_ant_pro,range=1:14)
#EFA with the number of harmonics previously chosen from the
#calibration. I do not normalize the coefficients because of
#possible alignment inconsistencies
CC_ant_ef<-efourier(CC_ant_pro,nb.h=14,norm=F)
#can access harmonic data by calling the $coe part of the fourier
#transformed data object
CC_ant_ef$coe

################################PCA################################
cc_sex_ant_PCA<-PCA(CC_ant_ef,fac='sex')
#plot out the results
plot_PCA(cc_sex_ant_PCA)
svg('cc_sex_ant_PCA_001.svg')
plot_PCA(cc_sex_ant_PCA)
dev.off()
#plot with the shapes
```

```
plot_PCA(cc_sex_ant_PCA,'sex')
svg('cc_sex_ant_PCA_002.svg')
plot_PCA(cc_sex_ant_PCA,'sex')
dev.off()
#plot with the shapes filled in
plot_PCA(cc_sex_ant_PCA,'sex',chullfilled=T)
svg('cc_sex_ant_PCA_003.svg')
plot_PCA(cc_sex_ant_PCA,'sex',chullfilled=T)
dev.off()

################################MANOVA#################################
CC_ant_MANOVA<-MANOVA(cc_sex_ant_PCA,fac='sex')
CC_ant_MANOVA
#MANOVA showing the results of the pairwise comparisons
CC_ant_PW_MANOVA<-MANOVA_PW(cc_sex_ant_PCA,fac='sex')
CC_ant_PW_MANOVA

################################LDA#################################
CC_ant_LDA<-LDA(cc_sex_ant_PCA,'sex')
CC_ant_LDA
#create an LDA plot
plot_LDA(CC_ant_LDA,'sex')
#plot a CV table
plot_CV(CC_ant_LDA)


#####################################################################
##################GEOGRAPHY CASQUE ANALYSIS##########################
#####################################################################
#CC LATERAL ASPECT

######################Workspace save/load##########################
#save the workspace image
save.image("CC_lat_geo.RData")
#load the workspace image
load("CC_lat_geo.RData")
```

```
############################Data input##############################
#read in the factors list to categorize specimens using tibble
CC_lat_geo_info<-
as_tibble(read.csv("all_cc_geo_lat_fac.csv",header=T,row.names=1)
)
#Set working directory to the folder containing the binary masks
getwd()
setwd("ALL_CC_GEO_LAT")
#list files in current folder to double check the folder contents
list.files(getwd())
#create a dataframe containing the filesnames to easily reference
#them
lf<-list.files(getwd(), full.names=TRUE)
#import the binary mask jpegs using the file list
CC_lat_geo_binary<-import_jpg(lf)
#convert to outlines, simultaneously adding factors to the
#objects
CC_lat_geo_out<-Out(CC_lat_geo_binary,fac=CC_lat_geo_info)
#plot all of them to make sure they appear correct, you can color
#them by variables with the fac input
panel(CC_lat_geo_out, fac='geo', name=TRUE)
panel(CC_lat_geo_out, fac='geo')
#The mosaic command allows for a legend to be created
mosaic(CC_lat_geo_out,CC_lat_geo_out$geo,legend=T)
#plot the outlines on top of each other
stack(CC_lat_geo_out)

#####################Procrustes alignment#######################
#call the Coe object to see the number of points in the outlines
CC_lat_geo_out
#to use the procrustes alignment, the outlines must have the
#same number of coordinates, so interpolate the points to average
#number of points.
CC_lat_geo_out_int<-coo_interpolate(CC_lat_geo_out,n=5175)
#plot out the unaligned
stack(CC_lat_geo_out_int)
#procrustes alignment
CC_lat_geo_pro<-fgProcrustes(CC_lat_geo_out_int)
#examine the alignment
```

```
stack(CC_lat_geo_pro)

################Elliptical Fourier Transformation################
#calibrate harmonics needed to capture 99.9% shape variance
cal_CC_lat_geo<-
calibrate_harmonicpower_efourier(CC_lat_geo_pro,nb.h=20,plot=T)
#code to alter the harmonic calibration graph
cal_CC_lat_geo$gg+theme_minimal()+
coord_cartesian(xlim=c(0.5,17),ylim=c(0,100))+
ggtitle('Harmonic calibration')
#calibrate the reconstructions, as a visualization
cal_CC_lat_geo_recon<-
calibrate_reconstructions_efourier(CC_lat_geo_pro,range=1:16)
#EFA with the number of harmonics previously chosen from the
#calibration. I do not normalize the coefficients because of
#possible alignment inconsistencies
CC_lat_geo_ef<-efourier(CC_lat_geo_pro,nb.h=16,norm=F)

################################PCA################################
CC_lat_geo_PCA<-PCA(CC_lat_geo_ef,fac='geo')
#plot out the results
plot_PCA(CC_lat_geo_PCA)
svg('CC_lat_geo_PCA_001.svg')
plot_PCA(CC_lat_geo_PCA)
dev.off()
#plot with the shapes
plot_PCA(CC_lat_geo_PCA,'geo',legend=T)
svg('CC_lat_geo_PCA_002.svg')
plot_PCA(CC_lat_geo_PCA,'geo',morphospace=T)
dev.off()
#plot with the shapes filled in
plot_PCA(CC_lat_geo_PCA,'geo',chullfilled=T)
svg('CC_lat_geo_PCA_003.svg')
plot_PCA(CC_lat_geo_PCA,'geo',chullfilled=T)
dev.off()

############################MANOVA############################
CC_lat_geo_MANOVA<-MANOVA(CC_lat_geo_PCA,fac='geo')
```

```
CC_lat_geo_MANOVA
#MANOVA showing the results of the pairwise comparisons
CC_lat_geo_PW_MANOVA<-MANOVA_PW(CC_lat_geo_PCA,fac='geo')
CC_lat_geo_PW_MANOVA

################################LDA################################
#The idea here is to take the PC scores from the PCA model,
#remove the points without the geographic data, then run an LDA
#with the predict function on these data
test<-CC_lat_geo_PCA$x[,1:13]
test2<-CC_lat_geo_PCA$fac[,2]
test3<-cbind(test,test2)
test4<-na.omit(test3)
CC_lat_geo_LDA<-
MASS::lda(geo~PC1+PC2+PC3+PC4+PC5+PC6+PC7+PC8+PC9+PC10+PC11+PC12+
PC13,data=test4)
CC_lat_geo_LDA_pred<-predict(CC_lat_geo_LDA,test4[,1:13])
CC_lat_geo_LDA_pred$class
#build a CV table
CV.fac<-MASS::lda(test4[,1:13],grouping=test4[,14],tol=1e-
05,CV=T)$class
CV.tab<-table(test4[,14],CV.fac)
names(dimnames(CV.tab))<-c('actual','classified')
CV.correct<-sum(diag(CV.tab))/sum(CV.tab)

tab <- CV.tab
  ce <- sapply(seq_along(1:nrow(tab)),
               function(i) 1-(sum(tab[i, -i])/sum(tab[i, ])))
  names(ce) <- rownames(tab)
ce
tab



#####################################################################
#CC ANTERIOR GEO

######################Workspace save/load#########################
#save the workspace image
```

```
save.image("CC_ant_geo.RData")
#load the workspace image
load("CC_ant_geo.RData")

############################Data input##############################
#read in the factors list to categorize specimens using tibble
CC_ant_geo_info<-
as_tibble(read.csv("all_cc_geo_ant_fac.csv",header=T,row.names=1)
)
#Set working directory to the folder containing the binary masks
getwd()
setwd("ALL_CC_GEO_ANT")
#list files in current folder to double check the folder contents
list.files(getwd())
#create a dataframe containing the filesnames to easily reference
#them
lf<-list.files(getwd(), full.names=TRUE)
#import the binary mask jpegs using the file list
CC_ant_geo_binary<-import_jpg(lf)
#convert to outlines, simultaneously adding factors to the
#objects
CC_ant_geo_out<-Out(CC_ant_geo_binary,fac=CC_ant_geo_info)
#plot all of them to make sure they appear correct, you can color
#them by variables with the fac input
panel(CC_ant_geo_out, fac='geo', name=TRUE)
panel(CC_ant_geo_out, fac='geo')
#The mosaic command allows for a legend to be created
mosaic(CC_ant_geo_out,CC_ant_geo_out$geo)

#####################Procrustes alignment#########################
#call the Coe object to see the number of points in the outlines
CC_ant_geo_out
#to use the procrustes alignment, the outlines must have the
#same number of coordinates, so interpolate the points to average
#number of points.
CC_ant_geo_out_int<-coo_interpolate(CC_ant_geo_out,n=3623)
stack(CC_ant_geo_out_int)
#procrustes alignment
CC_ant_geo_pro<-fgProcrustes(CC_ant_geo_out_int)
```

```
#examine the alignment
stack(CC_ant_geo_pro)

################Elliptical Fourier Transformation################
#calibrate harmonics needed to capture 99.9% shape variance
cal_CC_ant_geo<-
calibrate_harmonicpower_efourier(CC_ant_geo_pro,nb.h=20,plot=T)
#code to alter the harmonic calibration graph
cal_CC_ant_geo$gg+theme_minimal()+
coord_cartesian(xlim=c(0.5,15),ylim=c(0,100))+
ggtitle('Harmonic calibration')
#calibrate the reconstructions, as a visualization
cal_CC_ant_geo_recon<-
calibrate_reconstructions_efourier(CC_ant_geo_pro,range=1:14)
#EFA with the number of harmonics previously chosen from the
#calibration. I do not normalize the coefficients because of
#possible alignment inconsistencies
CC_ant_geo_ef<-efourier(CC_ant_geo_pro,nb.h=14,norm=F)

################################PCA################################
CC_ant_geo_PCA<-PCA(CC_ant_geo_ef,fac='geo')
#plot out the results
plot_PCA(CC_ant_geo_PCA)
#plot with the shapes
plot_PCA(CC_ant_geo_PCA,'geo')
#plot with the shapes filled in
plot_PCA(CC_ant_geo_PCA,'geo',chullfilled=T)

############################MANOVA############################
CC_ant_geo_MANOVA<-MANOVA(CC_ant_geo_PCA,fac='geo')
CC_ant_geo_MANOVA
#MANOVA showing the results of the pairwise comparisons
CC_ant_geo_PW_MANOVA<-MANOVA_PW(CC_ant_geo_PCA,fac='geo')
CC_ant_geo_PW_MANOVA

############################LDA############################
```

```
#The idea here is to take the PC scores from the PCA model,
#remove the points without the geographic data, then run an LDA
#with the predict function on these data
test<-CC_ant_geo_PCA$x[,1:14]
test2<-CC_ant_geo_PCA$fac[,2]
test3<-cbind(test,test2)
test4<-na.omit(test3)
CC_ant_geo_LDA<-
MASS::lda(geo~PC1+PC2+PC3+PC4+PC5+PC6+PC7+PC8+PC9+PC10+PC11+PC12+
PC13+PC14,data=test4)
CC_ant_geo_LDA_pred<-predict(CC_ant_geo_LDA,test4[,1:14])
CC_ant_geo_LDA_pred$class
#build a CV table
CV.fac<-MASS::lda(test4[,1:14],grouping=test4[,15],tol=1e-
05,CV=T)$class
CV.tab<-table(test4[,15],CV.fac)
names(dimnames(CV.tab))<-c('actual','classified')
CV.correct<-sum(diag(CV.tab))/sum(CV.tab)

tab <- CV.tab
  ce <- sapply(seq_along(1:nrow(tab)),
               function(i) 1-(sum(tab[i, -i])/sum(tab[i, ])))
  names(ce) <- rownames(tab)
ce
tab



#####################################################################
#######################ALL SPECIES ANALYSIS#########################
#####################################################################
#LATERAL ASPECT

######################Workspace save/load##########################
#save the workspace image
save.image("all_lat.RData")
#load the workspace image
load("all_lat.RData")
```

```
############################Data input##############################
#read in the factors list to categorize specimens using tibble
all_lat_info<-
as_tibble(read.csv("all_lat_fac.csv",header=T,row.names=1))
#Set working directory to the folder containing the binary masks
getwd()
setwd("ALL_SP_LAT")
#list files in current folder to double check the folder contents
list.files(getwd())
#create a dataframe containing the filesnames to easily reference
#them
lf<-list.files(getwd(), full.names=TRUE)
#import the binary mask jpegs using the file list
all_lat_binary<-import_jpg(lf)
#convert to outlines, simultaneously adding factors to the
#objects
all_lat_out<-Out(all_lat_binary,fac=all_lat_info)
#plot all of them to make sure they appear correct, you can color
#them by variables with the fac input
panel(all_lat_out, fac='sex',names=T)#red is uknown, blue is
female, #yellow male
svg('panel_all_lat_sex.svg')
panel(all_lat_out, fac='sex')
dev.off()
panel(all_lat_out, fac='species')
svg('panel_all_lat_species.svg')
panel(all_lat_out, fac='species')
dev.off()
#mosaic plots (with a legend)
mosaic(all_lat_out, f='species',legend=TRUE)
svg('mosaic_all_lat_species.svg')
mosaic(all_lat_out, f='species',legend=TRUE)
dev.off()
#mosaic plots (with a legend)
mosaic(all_lat_out, f='sex',legend=TRUE)
svg('mosaic_all_lat_sex.svg')
mosaic(all_lat_out, f='sex',legend=TRUE)
dev.off()
```

```
######################Procrustes alignment#########################
#call the Coe object to see the number of points in the outlines
all_lat_out
#to use the procrustes alignment, the outlines must have the
#same number of coordinates, so interpolate the points to average
#number of points.
all_lat_out_int<-coo_interpolate(all_lat_out,n=5127)
#plot out the unaligned
stack(all_lat_out_samp)
#procrustes alignment
all_lat_pro<-fgProcrustes(all_lat_out_int)
#examine the alignment
stack(all_lat_pro)

################Elliptical Fourier Transformation################
#calibrate harmonics needed to capture shape
cal_all_lat<-
calibrate_harmonicpower_efourier(all_lat_pro,nb.h=20,plot=T)
#code to alter the harmonic calibration graph
cal_all_lat$gg+theme_minimal()+
coord_cartesian(xlim=c(0.5,17),ylim=c(0,100))+
ggtitle('Harmonic calibration')
#calibrate the reconstructions, as a visualization
cal_all_lat_recon<-
calibrate_reconstructions_efourier(all_lat_pro,range=1:15)
#EFA with the number of harmonics previously chosen from the
#calibration. I do not normalize the coefficients because of
#possible alignment inconsistencies
all_lat_ef<-efourier(all_lat_pro,nb.h=15,norm=F)

################################PCA################################
all_lat_PCA<-PCA(all_lat_ef,fac='species')
#plot out the results
plot_PCA(all_lat_PCA)
svg('all_lat_PCA_001.svg')
plot_PCA(all_lat_PCA)
dev.off()
```

```
#plot with the shapes
plot_PCA(all_lat_PCA,'species')
svg('all_lat_PCA_002.svg')
plot_PCA(all_lat_PCA)
dev.off()
#plot with the shapes filled in
plot_PCA(all_lat_PCA,'species',chullfilled=T)
svg('all_lat_PCA_003.svg')
plot_PCA(all_lat_PCA,'species',chullfilled=T)
dev.off()

################################MANOVA################################
all_lat_MANOVA<-MANOVA(all_lat_PCA,fac='species')
all_lat_MANOVA
#MANOVA showing the results of the pairwise comparisons
all_lat_PW_MANOVA<-MANOVA_PW(all_lat_PCA,fac='species')
all_lat_PW_MANOVA

################################LDA################################
all_lat_LDA<-LDA(all_lat_PCA,'species')
all_lat_LDA
#create an LDA plot
plot_LDA(all_lat_LDA)
#create a cross-validation table
plot_CV(all_lat_LDA)


#####################################################################
#All SPECIES ANTERIOR ASPECT

######################Workspace save/load########################

#save workspace
save.image("all_ant.RData")
#load workspace
load("all_ant.RData")
```

```
############################Data input##############################
#read in the factors list to categorize specimens using tibble
all_ant_info<-
as_tibble(read.csv("all_ant_fac.csv",header=T,row.names=1))
#Set working directory to the folder containing the binary masks
getwd()
setwd("ALL_SP_ANT")
#list files in current folder to double check the folder contents
list.files(getwd())
#create a dataframe containing the filesnames to easily reference
#them
lf<-list.files(getwd(), full.names=TRUE)
#import the binary mask jpegs using the file list
all_ant_binary<-import_jpg(lf)
#convert to outlines, simultaneously adding factors to the
#objects
all_ant_out<-Out(all_ant_binary,fac=all_ant_info)
#plot all of them to make sure they appear correct, you can color
#them by variables with the fac input
panel(all_ant_out, fac='sex', name=TRUE)
panel(all_ant_out, fac='sex')
panel(all_ant_out, fac='species', name=TRUE)
panel(all_ant_out, fac='species')
#The mosaic command allows for a legend to be created
mosaic(all_ant_out,all_ant_out$species,legend=TRUE)
mosaic(all_ant_out,all_ant_out$sex,legend=TRUE)

######################Procrustes alignment#########################
#call the Coe object to see the number of points in the outlines
all_ant_out
#to use the procrustes alignment, the outlines must have the
#same number of coordinates, so interpolate the points to average
#number of points.
all_ant_out_int<-coo_interpolate(all_ant_out,n=3488)
#plot out the unaligned
stack(all_ant_out_int)
#procrustes alignment
all_ant_pro<-fgProcrustes(all_ant_out_int)
```

```
#examine the alignment
stack(all_ant_pro)

################Elliptical Fourier Transformation################
#calibrate harmonics needed
cal_all_ant<-
calibrate_harmonicpower_efourier(all_ant_pro,nb.h=20,plot=T)
#code to alter the harmonic calibration graph
cal_all_ant$gg+theme_minimal()+
coord_cartesian(xlim=c(0.5,17),ylim=c(0,100))+
ggtitle('Harmonic calibration')
#calibrate the reconstructions, as a visualization
cal_all_ant_recon<-
calibrate_reconstructions_efourier(all_ant_pro,range=1:15)
#EFA with the number of harmonics previously chosen from the
#calibration. I do not normalize the coefficients because of
#possible alignment inconsistencies
all_ant_ef<-efourier(all_ant_pro,nb.h=15,norm=F)

################################PCA################################
all_ant_PCA<-PCA(all_ant_ef,fac='species')
#plot out the results
plot_PCA(all_ant_PCA)
svg('all_ant_PCA_001.svg')
plot_PCA(all_ant_PCA)
dev.off()
#plot with the shapes
plot_PCA(all_ant_PCA,'species')
svg('all_ant_PCA_002.svg')
plot_PCA(all_ant_PCA,'species')
dev.off()
#plot with the shapes filled in
plot_PCA(all_ant_PCA,'species',chullfilled=T)
svg('all_ant_PCA_003.svg')
plot_PCA(all_ant_PCA,'species',chullfilled=T)
dev.off()

################################MANOVA################################
```

```
all_ant_MANOVA<-MANOVA(all_ant_PCA,fac='species')
all_ant_MANOVA
#MANOVA showing the results of the pairwise comparisons
all_ant_PW_MANOVA<-MANOVA_PW(all_ant_PCA,fac='species')
all_ant_PW_MANOVA

################################LDA################################
all_ant_LDA<-LDA(all_ant_PCA,'species')
all_ant_LDA
#create an LDA plot
plot_LDA(all_ant_LDA)
plot_CV(all_ant_LDA)

####################################################################
####################################################################
####################OUTLIER IDENTIFICATION#########################
####################################################################
####################################################################
#########################C. casuarius###############################

#LATERAL

######################Workspace save/load#########################
#load the workspace image from the geographical analysis, as it
contains all the aligned/transformed data and PCA
load("CC_lat_geo.RData")

####################Outlier identification#########################
#Use which_out to specify which specimens in the list are
#outliers based on a chosen confidence level
CC_lat_outlier<-which_out(CC_lat_geo_PCA$x[, 1:13], 0.01)
CC_lat_outlier
CC_lat_geo_PCA$x[c(17,23,35,61,88,89,93,94),1:2]
#assign colors to the points, then the outliers
cols <- rep("black", nrow(CC_lat_geo_PCA$x))
outliers <- which_out(CC_lat_geo_PCA$x[,1:13], 0.01)
outliers2<-c(17,23,35,61,88,89,93,94)
```

```
cols[outliers2] <- "red"
#plot the aligned stack to make sure it isn't just rotation
#problems
stack(CC_lat_geo_pro,cols=cols)
plot(CC_lat_geo_PCA, col=cols,cex=0.9,zoom=0.9)
# remove them for Coe, rePCA, replot
CC_lat_geo_ef %>% slice(-outliers) %>% PCA %>%
plot(zoom=0.9,cex=0.9)



#####################################################################
#ANTERIOR/ROSTRAL

######################Workspace save/load#########################
#load the workspace image from the geographical analysis, as it
contains all the aligned/transformed data and PCA
load("CC_ant_geo.RData")

#####################Outlier identification#######################
#Use which_out to specify which specimens in the list are
#outliers based on a chosen confidence level
CC_ant_outlier<-which_out(CC_ant_geo_PCA$x[, 1:14], 0.01)
CC_ant_outlier
CC_ant_geo_PCA$x[c(14,16,19,59),1:2]
#assign colors to the points, then the outliers
cols <- rep("black", nrow(CC_ant_geo_PCA$x))
outliers <- which_out(CC_ant_geo_PCA$x[,1:14], 0.01)
outliers2<-c(14,16,19,59)
cols[outliers2] <- "red"
#plot the aligned stack to make sure it isn't just rotation
#problems
stack(CC_ant_geo_pro,cols=cols)
plot(CC_ant_geo_PCA, col=cols,cex=0.9,zoom=0.9)
# remove them for Coe, rePCA, replot
CC_ant_geo_ef %>% slice(-outliers) %>% PCA %>%
plot(zoom=0.9,cex=0.9)
```

```
#####################################################################
############################C. bennetti##############################
#LATERAL
#####################################################################
#save workspace image
save.image("CB_lat_outlier.RData")
#load workspace image
load("CB_lat_outlier.RData")

############################Data input###############################
#set working directory
getwd()
setwd("CB_LAT")
getwd()
#double check the file names
list.files(getwd())
#create a dataframe containing the filesnames to easily reference
#them
lf<-list.files(getwd(), full.names=TRUE)
#read in the csv file of sexes
CB_lat_fac<-read.csv("CB_lat_fac.csv",header=T,row.names=1)
#import the binary mask jpegs using the file list
CB_lat_binary<-import_jpg(lf)
#convert to outlines, simultaneously adding factors to the
#objects
CB_lat_out<-Out(CB_lat_binary,fac=CB_lat_fac)
#plot all of them to make sure they appear correct, you can color
#them by variables with the fac input
panel(CB_lat_out, fac='sex', name=TRUE)
panel(CB_lat_out, fac='sex')
#The mosaic command allows for a legend to be created
mosaic(CB_lat_out,CB_lat_out$sex,legend=T)
#plot the outlines on top of each other
stack(CB_lat_out)

#####################Procrustes alignment########################
#call the Coe object to see the number of points in the outlines
CB_lat_out
```

```
#to use the procrustes alignment, the outlines must have the
#same number of coordinates, so interpolate the points to average
#number of points.
CB_lat_out_int<-coo_interpolate(CB_lat_out,n=5139)
stack(CB_lat_out_int)
#procrustes alignment
CB_lat_pro<-fgProcrustes(CB_lat_out_int)
#examine the alignment
stack(CB_lat_pro)

################Elliptical Fourier Transformation################
#calibrate harmonics needed to capture 99.9% shape variance
cal_CB_lat<-
calibrate_harmonicpower_efourier(CB_lat_pro,nb.h=20,plot=T)
#code to alter the harmonic calibration graph
cal_CB_lat$gg+theme_minimal()+
coord_cartesian(xlim=c(0.5,15),ylim=c(0,100))+
ggtitle('Harmonic calibration')
#calibrate the reconstructions, as a visualization
cal_CB_lat_recon<-
calibrate_reconstructions_efourier(CB_lat_pro,range=1:14)
#EFA with the number of harmonics previously chosen from the
#calibration. I do not normalize the coefficients because of
#possible alignment inconsistencies
CB_lat_ef<-efourier(CB_lat_pro,nb.h=14,norm=F)
#can access harmonic data by calling the $coe part of the fourier
#transformed data object
CB_lat_ef$coe

################################PCA################################
CB_lat_PCA<-PCA(CB_lat_ef,fac='sex')
#plot out the results
plot_PCA(CB_lat_PCA)
#plot with the shapes
plot_PCA(CB_lat_PCA,'sex')
#plot with the shapes filled in
plot_PCA(CB_lat_PCA,'sex',chullfilled=T)
```

```
#####################Outlier identification#######################
#Use which_out to specify which specimens in the list are
#outliers based on a chosen confidence level
CB_lat_outlier<-which_out(CB_lat_PCA$x[, 1:8], 0.01)
CB_lat_outlier
CB_lat_PCA$x[c(8),1:2]
#assign colors to the points, then the outliers
cols <- rep("black", nrow(CB_lat_PCA$x))
outliers <- which_out(CB_lat_PCA$x[,1:8], 0.01)
outliers2<-c(8)
cols[outliers2] <- "red"
#plot the aligned stack to make sure it isn't just rotation
#problems
stack(CB_lat_pro,cols=cols)
plot(CB_lat_PCA, col=cols,cex=0.9,zoom=0.9)
# remove them for Coe, rePCA, replot
CB_lat_ef %>% slice(-outliers) %>% PCA %>% plot(zoom=0.9,cex=0.9)


#####################################################################
##ANTERIOR/ROSTRAL

#######################Workspace save/load#########################
#save workspace image
save.image("CB_ant_outlier.RData")
#load workspace image
load("CB_ant_outlier.RData")

############################Data input#############################
#set working directory
getwd()
setwd("CB_ANT")
getwd()
#double check the file names
list.files(getwd())
#create a dataframe containing the filesnames to easily reference
#them
lf<-list.files(getwd(), full.names=TRUE)
```

```
#read in the csv file of sexes
CB_ant_fac<-read.csv("CB_ant_fac.csv",header=T,row.names=1)
#import the binary mask jpegs using the file list
CB_ant_binary<-import_jpg(lf)
#convert to outlines, simultaneously adding factors to the
#objects
CB_ant_out<-Out(CB_ant_binary,fac=CB_ant_fac)
#plot all of them to make sure they appear correct, you can color
#them by variables with the fac input
panel(CB_ant_out, fac='sex', name=TRUE)
panel(CB_ant_out, fac='sex')
#The mosaic command allows for a legend to be created
mosaic(CB_ant_out,CB_ant_out$sex,legend=T)

######################Procrustes alignment#########################
#call the Coe object to see the number of points in the outlines
CB_ant_out
#to use the procrustes alignment, the outlines must have the
#same number of coordinates, so interpolate the points to average
#number of points.
CB_ant_out_int<-coo_interpolate(CB_ant_out,n=3170)
#plot out the unaligned
stack(CB_ant_out_int)
#procrustes alignment
CB_ant_pro<-fgProcrustes(CB_ant_out_int)
#examine the alignment
stack(CB_ant_pro)

################Elliptical Fourier Transformation################
#calibrate harmonics needed to capture 99.9% shape variance
cal_CB_ant<-
calibrate_harmonicpower_efourier(CB_ant_pro,nb.h=20,plot=T)
#code to alter the harmonic calibration graph
cal_CB_ant$gg+theme_minimal()+
coord_cartesian(xlim=c(0.5,17),ylim=c(0,100))+
ggtitle('Harmonic calibration')
#calibrate the reconstructions, as a visualization
```

```
cal_CB_ant_recon<-
calibrate_reconstructions_efourier(CB_ant_pro,range=1:16)
cal_CB_ant_recon
#EFA with the number of harmonics previously chosen from the
#calibration. I do not normalize the coefficients because of
#possible alignment inconsistencies
CB_ant_ef<-efourier(CB_ant_pro,nb.h=16,norm=F)

################################PCA################################
CB_ant_PCA<-PCA(CB_ant_ef,fac='sex')
#plot out the results
plot_PCA(CB_ant_PCA)
#plot with the shapes
plot_PCA(CB_ant_PCA,'sex')
#plot with the shapes filled in
plot_PCA(CB_ant_PCA,'sex',chullfilled=T)

####################Outlier identification#####################
#Use which_out to specify which specimens in the list are
#outliers based on a chosen confidence level
CB_ant_outlier<-which_out(CB_ant_PCA$x[, 1:12], 0.01)
CB_ant_outlier
CB_ant_PCA$x[c(2,9,12),1:2]
#assign colors to the points, then the outliers
cols <- rep("black", nrow(CB_ant_PCA$x))
outliers <- which_out(CB_ant_PCA$x[,1:12], 0.01)
outliers2<-c(2,9,12)
cols[outliers2] <- "red"
#plot the aligned stack to make sure it isn't just rotation
#problems
stack(CB_ant_pro,cols=cols)
plot(CB_ant_PCA, col=cols,cex=0.9,zoom=0.9)
# remove them for Coe, rePCA, replot
CB_ant_ef %>% slice(-outliers) %>% PCA %>% plot(zoom=0.9,cex=0.9)



#################################################################
####################C. unappendiculatus#########################
```

```
##LATERAL

######################Workspace save/load#########################
#save workspace image
save.image("CU_lat_outlier.RData")
#load workspace image
load("CU_lat_outlier.RData")

############################Data input#############################
#set working directory
getwd()
setwd("CU_LAT")
getwd()
#double check the file names
list.files(getwd())
#create a dataframe containing the filesnames to easily reference
#them
lf<-list.files(getwd(), full.names=TRUE)
#read in the csv file of sexes
CU_lat_fac<-read.csv("CU_lat_fac.csv",header=T,row.names=1)
#import the binary mask jpegs using the file list
CU_lat_binary<-import_jpg(lf)
#convert to outlines, simultaneously adding factors to the
#objects
CU_lat_out<-Out(CU_lat_binary,fac=CU_lat_fac)
#plot all of them to make sure they appear correct, you can color
#them by variables with the fac input
panel(CU_lat_out, fac='sex', name=TRUE)
panel(CU_lat_out, fac='sex')
#The mosaic command allows for a legend to be created
mosaic(CU_lat_out,CU_lat_out$sex,legend=T)
#plot the outlines on top of each other
stack(CU_lat_out)

######################Procrustes alignment#######################
#call the Coe object to see the number of points in the outlines
CU_lat_out
```

```
#to use the procrustes alignment, the outlines must have the
#same number of coordinates, so interpolate the points to average
#number of points.
CU_lat_out_int<-coo_interpolate(CU_lat_out,n=4835)
#plot out the unaligned
stack(CU_lat_out_int)
#procrustes alignment
CU_lat_pro<-fgProcrustes(CU_lat_out_int)
#examine the alignment
stack(CU_lat_pro)

################Elliptical Fourier Transformation################
#calibrate harmonics needed to capture 99.9% shape variance
cal_CU_lat<-
calibrate_harmonicpower_efourier(CU_lat_pro,nb.h=20,plot=T)
cal_CU_lat
#code to alter the harmonic calibration graph
cal_CU_lat$gg+theme_minimal()+
coord_cartesian(xlim=c(0.5,15),ylim=c(0,100))+
ggtitle('Harmonic calibration')
#calibrate the reconstructions, as a visualization
cal_CU_lat_recon<-
calibrate_reconstructions_efourier(CU_lat_pro,range=1:14)
cal_CU_lat_recon
#EFA with the number of harmonics previously chosen from the
#calibration. I do not normalize the coefficients because of
#possible alignment inconsistencies
CU_lat_ef<-efourier(CU_lat_pro,nb.h=14,norm=F)

################################PCA################################
CU_lat_PCA<-PCA(CU_lat_ef,fac='sex')
#plot out the results
plot_PCA(CU_lat_PCA)
#plot with the shapes
plot_PCA(CU_lat_PCA,'sex')
#plot with the shapes filled in
plot_PCA(CU_lat_PCA,'sex',chullfilled=T)
```

```
####################Outlier identification#######################
#Use which_out to specify which specimens in the list are
#outliers based on a chosen confidence level
CU_lat_outlier<-which_out(CU_lat_PCA$x[, 1:9], 0.01)
CU_lat_outlier
CU_lat_PCA$x[c(8),1:2]
#assign colors to the points, then the outliers
cols <- rep("black", nrow(CU_lat_PCA$x))
outliers <- which_out(CU_lat_PCA$x[,1:9], 0.01)
outliers2<-c(8)
cols[outliers2] <- "red"
#plot the aligned stack to make sure it isn't just rotation
#problems
stack(CU_lat_pro,cols=cols)
plot(CU_lat_PCA, col=cols,cex=0.9,zoom=0.9)
# remove them for Coe, rePCA, replot
CU_lat_ef %>% slice(-outliers) %>% PCA %>% plot(zoom=0.9,cex=0.9)


##ANTERIOR/ROSTRAL

#####################Workspace save/load#########################
#save workspace image
save.image("CU_ant_outlier.RData")
#load workspace image
load("CU_ant_outlier.RData")

############################Data input#############################
#set working directory
getwd()
setwd("CU_ANT")
getwd()
#double check the file names
list.files(getwd())
#create a dataframe containing the filesnames to easily reference
#them
lf<-list.files(getwd(), full.names=TRUE)
#read in the csv file of sexes
```

```
CU_ant_fac<-read.csv("CU_ant_fac.csv",header=T,row.names=1)
#import the binary mask jpegs using the file list
CU_ant_binary<-import_jpg(lf)
#convert to outlines, simultaneously adding factors to the
#objects
CU_ant_out<-Out(CU_ant_binary,fac=CU_ant_fac)
#plot all of them to make sure they appear correct, you can color
#them by variables with the fac input
panel(CU_ant_out, fac='sex', name=TRUE)
panel(CU_ant_out, fac='sex')
#The mosaic command allows for a legend to be created
mosaic(CU_ant_out,CU_ant_out$sex,legend=T)

######################Procrustes alignment#########################
#call the Coe object to see the number of points in the outlines
CU_ant_out
#to use the procrustes alignment, the outlines must have the
#same number of coordinates, so interpolate the points to average
#number of points.
CU_ant_out_int<-coo_interpolate(CU_ant_out,n=3437)
#plot out the unaligned
stack(CU_ant_out_int)
#procrustes alignment
CU_ant_pro<-fgProcrustes(CU_ant_out_int)
#examine the alignment
stack(CU_ant_pro)

################Elliptical Fourier Transformation################
#calibrate harmonics needed to capture 99.9% shape variance
cal_CU_ant<-
calibrate_harmonicpower_efourier(CU_ant_pro,nb.h=20,plot=T)
cal_CU_ant
#code to alter the harmonic calibration graph
cal_CU_ant$gg+theme_minimal()+
coord_cartesian(xlim=c(0.5,16),ylim=c(0,100))+
ggtitle('Harmonic calibration')
#calibrate the reconstructions, as a visualization
```

```
cal_CU_ant_recon<-
calibrate_reconstructions_efourier(CU_ant_pro,range=1:15)
cal_CU_ant_recon
#EFA with the number of harmonics previously chosen from the
#calibration. I do not normalize the coefficients because of
#possible alignment inconsistencies
CU_ant_ef<-efourier(CU_ant_pro,nb.h=15,norm=F)

################################PCA################################
CU_ant_PCA<-PCA(CU_ant_ef,fac='sex')
#plot out the results
plot_PCA(CU_ant_PCA)
#plot with the shapes
plot_PCA(CU_ant_PCA,'sex')
#plot with the shapes filled in
plot_PCA(CU_ant_PCA,'sex',chullfilled=T)

####################Outlier identification#######################
#Use which_out to specify which specimens in the list are
#outliers based on a chosen confidence level
CU_ant_outlier<-which_out(CU_ant_PCA$x[, 1:7], 0.01)
CU_ant_outlier
CU_ant_PCA$x[c(8),1:2]
#assign colors to the points, then the outliers
cols <- rep("black", nrow(CU_ant_PCA$x))
outliers <- which_out(CU_ant_PCA$x[,1:7], 0.01)
outliers2<-c(8)
cols[outliers2] <- "red"
#plot the aligned stack to make sure it isn't just rotation
#problems
stack(CU_ant_pro,cols=cols)
plot(CU_ant_PCA, col=cols,cex=0.9,zoom=0.9)
# remove them for Coe, rePCA, replot
CU_ant_ef %>% slice(-outliers) %>% PCA %>% plot(zoom=0.9,cex=0.9)
```

VITA

TODD LANDON GREEN

Candidate for the Degree of

Doctor of Philosophy

Dissertation: ONTOGENY, DISPARITY, AND FUNCTION OF THE ENIGMATIC CASQUES OF CASSOWARIES (*CASUARIUS*): A CASE STUDY OF CRANIAL ORNAMENTATION IN ARCHOSAURS

Major Field: Biomedical Sciences

Biographical:

Education:

Completed the requirements for the Doctor of Philosophy in Biomedical Sciences at Oklahoma State University, Stillwater, Oklahoma in December, 2020.

Completed the requirements for the Master of Science in Zoology at Colorado State University, Fort Collins, Colorado in 2012.

Completed the requirements for the Bachelor of Science in Biology; Zoology at Colorado State University, Fort Collins, Colorado in 2008.

Experience:

Graduate Research Associate at Oklahoma State University Center for Health Sciences in 2015 and 2018–2020.

Graduate Teaching Associate for Clinical Anatomy, BIOM 5116 at Oklahoma State University Center for Health Sciences from 2016–2018.

Department Associate in Earth Sciences at Denver Museum of Nature and Science from 2013–2016

Professional Memberships:

American Association for Anatomy, American Emu Association, Sigma Xi, Society for Integrative and Comparative Biology, Society of Vertebrate Paleontology, Western Interior Paleontological Society